PAMAM Dendrimer Modified Microporous PVDF Membranes for Protein Separation

Zitong Xu

uOttawa

Thesis submitted to the University of Ottawa

in partial fulfillment of the requirements for the degree of

Doctor of Philosophy in Chemical Engineering

Department of Chemical and Biological Engineering

Faculty of Engineering

University of Ottawa

November 2024

Abstract

In this PhD thesis, the process of protein separation using PAMAM dendrimer-modified PVDF membranes was systematically studied. By selecting different KOH alkaline solutions, PAMAM was immobilized either on the surface of the PVDF membrane (treated with KOH aqueous solution) or simultaneously on both the surface and inside the pores of the PVDF membrane (treated with KOH isopropanol solution). The effects of different alkaline treatments on the surface properties of PVDF membranes and on the filtration of whey protein and casein were also systematically investigated. Additionally, the Donnan-steric pore model with dielectric exclusion (DSPM-DE) was used to analyze the separation processes of PVDF membranes and PAMAM dendrimer modified membranes. The study on PAMAM dendrimer modified PVDF membranes revealed that immobilizing PAMAM on both the surface and inside the pores of PVDF membranes significantly enhanced the rejection of whey protein but notably reduced the permeate flux. After immobilizing generation 3 PAMAM dendrimer, with carboxyl functional groups, the rejection for whey protein increased from 58.9% (PVDF membrane) to 98.8%, while the permeate flux decreased from 15.3 LMH (PVDF membrane) to 2.3 LMH. When the PAMAM dendrimer was immobilized only on the surface of the PVDF membrane, both the rejection for whey protein and permeate flux increased. After immobilizing generation 3 PAMAM dendrimer, with carboxyl functional groups, on the membrane surface, the rejection and permeate flux for whey protein increased to 79.0% and 30.3 LMH, respectively.

Simultaneously modifying the membrane surface and interior results in decreased bulk porosity and increased Donnan potential, leading to a significant increase in whey protein rejection. However, the smaller bulk porosity also causes a decrease in the permeate flux. Modifying only the membrane surface increases the pore size and generates a negative

Donnan potential. This modification results in both higher whey protein rejection and permeate flux. However, due to the larger pore size, weaker Donnan potential, and the absence of charges within the pores (resulting in a weaker dielectric exclusion), the whey protein rejection of surface modified membranes is lower than that of membranes modified on both the surface and interior.

Résumé

Dans cette thèse de doctorat, le processus de séparation des protéines utilisant des membranes en PVDF modifiées par des dendrimères PAMAM a été systématiquement étudié. En sélectionnant différentes solutions alcalines de KOH, le PAMAM a été immobilisé soit à la surface de la membrane en PVDF (traitée avec une solution aqueuse de KOH), soit simultanément à la surface et à l'intérieur des pores de la membrane en PVDF (traitée avec une solution de KOH dans l'isopropanol). Les effets de ces différents traitements alcalins sur les propriétés de surface des membranes en PVDF ainsi que sur la filtration des protéines de lactosérum et de la caséine ont également été systématiquement investigués. De plus, le modèle de pore stérique avec exclusion diélectrique (DSPM-DE) a été utilisé pour analyser les processus de séparation des membranes en PVDF et des membranes modifiées par des dendrimères PAMAM. L'étude sur les membranes en PVDF modifiées par des dendrimères PAMAM a révélé que l'immobilisation du PAMAM à la fois sur la surface et à l'intérieur des pores des membranes en PVDF améliorait significativement le rejet des protéines de lactosérum mais réduisait notablement le flux de perméat. Après immobilisation d'un dendrimère PAMAM de génération 3, avec des groupes fonctionnels carboxyle, le rejet des protéines de lactosérum est passé de 58,9 % (membrane en PVDF) à 98,8 %, tandis que le flux de perméat a diminué de 15,3 LMH (membrane en PVDF) à 2,3 LMH. Lorsque le dendrimère PAMAM a été immobilisé uniquement à la surface de la membrane en PVDF, à la fois le rejet des protéines de lactosérum et le flux de perméat ont augmenté. Après immobilisation d'un dendrimère PAMAM de génération 3, avec des groupes fonctionnels carboxyle, à la surface de la membrane, le rejet et le flux de perméat pour les protéines de lactosérum ont augmenté à 79,0 % et 30,3 LMH, respectivement.

La modification simultanée de la surface de la membrane et de son intérieur entraîne une diminution de la porosité en vrac et une augmentation du potentiel Donnan, conduisant à une augmentation significative du rejet des protéines de lactosérum. Cependant, la taille réduite des pores provoque également une diminution du flux de perméat. La modification uniquement de la surface de la membrane augmente la porosité en vrac et génère un potentiel Donnan négatif. Cette modification entraîne à la fois un rejet plus élevé des protéines de lactosérum et un flux de perméat plus important. Cependant, en raison de la plus grande taille des pores, du potentiel Donnan plus faible et de l'absence de charges à l'intérieur des pores (entraînant une exclusion diélectrique plus faible), le rejet des protéines de lactosérum par les membranes modifiées en surface est inférieur à celui des membranes modifiées à la fois sur la surface et à l'intérieur.

Statement of contributions

I solemnly declare that I wrote this thesis, including the design and management of all experiments, characterizations, and performance testing. I personally designed, constructed, and troubleshot all experimental setups for data collection in this project.

My supervisors, Dr. Christopher Q. Lan and Dr. Takeshi Matsuura provided guidance on concept development and experimentation and contributed to data analysis, discussion of results, and reviewing and responding to editors' comments. Dr. Dipak Rana assisted with manuscript revisions and submissions.

Acknowledgement

I would like to express my heartfelt gratitude to my grandfather, Mr. Jianzhong Xu, and my parents, Mr. Tao Xu and Mrs. Haiyun Yang, for their unwavering and selfless support. Their encouragement has allowed me to dedicate myself entirely to my PhD program.

I am also deeply thankful to my supervisors, Dr. Christopher Q. Lan and Dr. Takeshi Matsuura, for their invaluable support, insightful feedback, and guidance throughout my doctoral studies. Their mentorship has been instrumental in my successful completion of the PhD program.

Additionally, I wish to extend my appreciation to Dr. Dipak Rana for his wise and practical advice on my research, and for addressing numerous questions I encountered during my studies.

I would like to acknowledge the financial support that I received from the China Scholarship Council (CSC).

I am grateful to Franco Ziroldo from the Laboratory Support department for his technical assistance with equipment, and to Yun Liu for her support with SEM and XPS measurements. I also want to thank the undergraduate and MEng students who assisted me during my research.

Last but not the least, special appreciation goes to my friends and lab partners, who have been a source of encouragement throughout this journey.

List of published and ongoing manuscripts

1. **Zitong Xu**, Guixuan Ma, Hongying Zhou, Xinyue Wang, Dipak Rana, Takeshi Matsuura, Christopher Q. Lan, A Moderate and effective approach for surface engineering of PVDF membranes: treatment using alkaline isopropanol solution. (In preparation)

2. **Zitong Xu**, Guixuan Ma, Dipak Rana, Takeshi Matsuura, Christopher Q. Lan. Surface modification of polyvinylidene fluoride membranes using KOH/water/alcohol ternary: effects of alcohol and other conditions. (In preparation)

3. **Zitong Xu**, Guixuan Ma, Hongying Zhou, Xinyue Wang, Dipak Rana, Takeshi Matsuura, Christopher Q. Lan. Polyamidoamine dendrimer-modified polyvinylidene fluoride microporous membranes for protein separation. Reactive and Functional Polymers, 2024, 106021. Doi: 10.1016/j.reactfunctpolym.2024.106021.

4. **Zitong Xu**, Guixuan Ma, Dipak Rana, Takeshi Matsuura, Christopher Q. Lan. Engineering polyvinylidene fluoride membranes using charge tunable dendrimer polyamidoamine to enable microporous membranes for protein separation. Separation and Purification Technology, Volume 354, Part 4, 2025, 128887, ISSN 1383-5866. Doi: 10.1016/j.seppur.2024.128887.

5. **Zitong Xu**, Guixuan Ma, Dipak Rana, Takeshi Matsuura, Christopher Q. Lan. Effects of polyamidoamine dendrimer immobilization on protein separation of PVDF membrane: mathematical analysis by Donnan steric pore model with dielectric exclusion (DSPM-DE). (In preparation)

Table of Contents

List of Figures

List of Tables

Chapter 1. Introduction

1.1. Problem statement

Low flux and fouling have been two major challenges in the application of membrane filtration for the separation of bioproducts such as recombinant proteins, monoclonal antibodies, concentrated milk, and lactose-free milk. Therefore, it is of great interest to systematically investigate the effects of dendrimer modification on membrane properties and performance. While membranes have been widely used for the separation of bioproducts, including different proteins, these processes have almost exclusively utilized UF membranes that reject target proteins by sieving (i.e., size rejection).

1.2. Objectives

The objectives of this project are threefold: (1) to develop effective approaches for introducing dendrimers with different charged functional groups into polyvinylidene fluoride (PVDF) membranes; (2) to verify the hypothesis that the mechanism of nanofiltration (NF) for rejecting small ions can be extended to the rejection of ionic polymers and proteins using dendrimer-modified ultrafiltration (UF) membranes with appropriate pore sizes; and (3) to develop charged membranes suited for the production of whey proteins with excellent permeability and antifouling features.

Dendrimers have a relatively small molecular radius and a large, controllable number of sites for anchoring functional molecules. Therefore, grafting dendrimers onto the surface or both inside the pores and on the surface of UF membranes can introduce charged groups while having minimal impact on membrane pore size. This allows the membranes to maintain high permeability while acquiring charges of a selected nature (i.e., positive or

negative) and density. Such charged membranes should be able to reject charged macromolecules, such as proteins, that are smaller than the membrane pores. The permeability of these membranes, while potentially enhanced or reduced during the modification process, would be significantly greater than that of uncharged membranes for the separation of the same macromolecules based on size rejection, which would require a significantly smaller pore size. The charged membranes are also expected to have significantly improved antifouling properties due to the reduction of hydrophobic interactions between the charged membrane surface and macromolecules, which is a major contributor to fouling.

To the best of our knowledge, this will be the first time the concept of using dendrimer modified charged membranes for whey protein separation is tested. Additionally, this study compares, for the first time, the effects of immobilizing dendrimers at different membrane locations, such as on the membrane surface or simultaneously on both the membrane surface and within the membrane pores, on filtration performance.

1.3. Structure of the thesis

Chapter 2 of this thesis introduces the filtration process of microfiltration (MF), UF and NF. This chapter provides a detailed description of the methods for modifying membranes using dendrimers, as well as the synthesis methods of polyamidoamine (PAMAM) dendrimers used in Chapter 5, Chapter 6 and Chapter 7.

Chapter 3 studies the alkaline treatment of PVDF membranes, which is a pretreatment step for PAMAM dendrimer grafting. In this chapter, the PVDF membrane was treated with KOH alkaline isopropanol solution at various treatment temperatures. The surface properties and filtration performance of modified membranes were researched.

Chapter 4 further investigates the effect of alkaline treatment on the hydrophilicity of the membrane surface. The effects of various alkaline treatment parameters were investigated. This chapter provides more details for a better understanding of the effects of different alkaline treatment processes on PVDF membranes.

Chapter 5 analyzes the performance of modified PVDF membranes, which have been grafted with PAMAM dendrimer both within the pores and on the surface, in the separation of whey proteins. In this chapter, the mechanism of grafting PAMAM dendrimer onto PVDF membranes is explored in depth through the investigation of the surface chemical properties of the modified membranes.

Chapter 6 examines the effect of surface PAMAM dendrimer grafting on the filtration performance of PVDF membranes in whey protein separation. In this chapter, the impact of the peripheral functional groups of PAMAM dendrimers with varying charge strength on the performance of the modified membranes is analyzed. Additionally, this chapter compares the properties and filtration performance of membranes grafted with PAMAM dendrimers both within the pores and on the surface, as discussed in Chapter 5.

Chapter 7 investigates the effect of different generations of PAMAM dendrimers on the performance of separation membranes in whey protein separation. This chapter also analyzes the separation processes of the membranes discussed in Chapter 3, Chapter 5, Chapter 6, and Chapter 7 using the Donnan Steric pore model with dielectric exclusion (DSPM-DE).

Finally, Chapter 8 summarizes the conclusions of this study, proposes a strategy for future research, and offers suggestions for areas where further improvements could be made.

Chapter 2. Research Background

Acronyms and Symbols

Abbreviation

BPPO	bromomethylated poly (2,6-dimethyl-1,4-phenylene oxide)
BSA	bovine serum albumin
CNTs	carbon nanotubes
DF	diafiltration
DSPM-DE	Donnan Steric pore model with dielectric exclusion
EDA	ethylenediamine
FO	forward osmosis
GO	graphene oxide
IP	interfacial polymerization
MA	methyl acrylate
MD	membrane distillation
MDA	melamine-based dendrimer amines
MF	microfiltration
MOFs	metal-organic frameworks
PMD	m-phenylenediamine
MWCO	molecular weight cutoff

NF	nanofiltration
PAM	Polyacrylamide
PAMAM	polyamidoamine
PDA	polydopamine
PEBAX	Polyether Block Amide
PEG	Polyethylene glycol
PES	polyether sulfone
PIP	piperazine
PPI	polypropylene imine
PAA	polyacrylic acid
PC	polycarbonate
PSF	polysulfone
PVA	Polyvinyl Alcohol
PVDF	polyvinylidene fluoride
RO	reverse osmosis
TFC	thin-film composite
TMAAM	trimesoyl amide amine
TMC	trimethyl chloride
UF	ultrafiltration
VSEP	vibratory shear enhanced processing

Nomenclature

A	effective area of the membrane
C_M	polarization modulus
$c_{i,f}$	bulk concentration of solute in the feed phase
$c_{i,p}$	bulk concentration of solute in the permeate phase
D_i	solute diffusivity of solute i
$D_{i,\infty}$	diffusion efficient of solute i in the bulk solution
F	Faraday constant
e	electron charge
J	permeate flux
J_C	solute flow caused by convection
J_D	solute flow caused by diffusion
J_i	flux of solute i
J_v	volumetric permeate flux
K	membrane permeability constant
$K_{i,a}$	diffusion hindrance factor
$K_{i,d}$	advection hindrance factor
k_B	Boltzmann constant
L	physical thickness of membranes
L_e	effective membrane thickness

R_i	rejection
R	ideal gas constant
r_i	Stokes radius of solute i
r_p	average pore radius of the membrane
T	solution temperature
t	filtration time
V	permeate volume
$X(x)$	volumetric charge density at position x along the membrane pore
z_i	valance of ion i
γ_i	activity coefficients of ion i
ΔP	hydraulic pressure difference across the membrane
Δw_i	solvation energy difference of ion i
$\Delta \Pi$	transmembrane osmotic pressure difference
$\Delta \phi_0$	Donnan potential across the interface between solution and membrane phase
ε	porosity of the membranes
ε_0	dielectric constant of vacuum
ε_b	dielectric constant of solvent in bulk
ε_p	dielectric constant of solvent in membrane pore
η	dynamic viscosity of the solvent
λ_i	ratio of pore radius and the Stokes radius of solute i

τ	tortuosity of membrane pores
$\phi(x)$	electrical potential at position x along the membrane pore
$\varphi_{D,i}$	Donnan exclusion factor
$\varphi_{DE,i}$	dielectric exclusion factor
$\varphi_{S,i}$	steric exclusion factor

2.1. MF and UF membranes

Membrane separation technology relies on semipermeable membranes that selectively allow different components to pass through, achieving the separation and purification of mixtures. Pressure-driven membrane separation technology has been widely applied in various fields, such as seawater desalination, removal of heavy metal ions from water, and protein purification. This technology utilizes the pressure difference across the membrane to drive the solution through the semipermeable membrane. Pressure-driven membrane filtration processes for liquid processing can be classified as microfiltration (MF), ultrafiltration (UF), nanofiltration (NF), and reverse osmosis (RO), depending on the pore size [1], [2]. Membranes for liquid processing can also be driven by concentration gradients, such as in dialysis, or by electro-force, as in electrodialysis (using ion-exchange membranes), and thermally, as in membrane distillation (MD). MF and UF membranes are pressure-driven separation membranes with pore sizes in the ranges of 0.05-10 μm and 1-100 nm, respectively [3]. The ability of UF membranes to retain fine particles or solute molecules is usually described by the molecular weight cutoff (MWCO), which is the molecular weight of the solute that the membrane can retain 90% of it. The MWCO of UF membranes is usually greater than 10 kDa [4].

In general, MF membranes are used to separate substances of micrometer size, such as soluble macromolecules, including large proteins [5], and suspended particles, such as bacteria, yeast cells, and fungal spores [6]. MF membranes have lower hydrodynamic resistance compared to their UF counterparts due to their relatively large pores, allowing them to achieve higher permeate flux at lower transmembrane hydrostatic pressures (usually 1 to 3 bar). For this reason, the MF process is primarily used as a pretreatment step in water treatment, such as the pretreatment stage before the application of UF in the food/dairy industry, NF in the chlor-alkaline process, and RO in the desalination process.

The separation mechanism of UF is similar to that of MF, primarily based on mechanical sieving, i.e., size exclusion. Due to the smaller pore size, UF membranes can separate macromolecules with a wider range of molecular sizes, including those that cannot be separated by MF membranes. UF membranes can separate protein molecules, starch molecules [7], and emulsions (like water-oil emulsions) [8]. As a result of the smaller pores, UF membranes have lower permeability than MF membranes and require higher operating pressures (usually between 1 and 5 bar).

2.1.1. Characterization of membrane performance

Membrane selectivity

The rejection coefficient, R_i, which is also called rejection, is used to evaluate the selectivity of certain species in the membrane filtration process. It is defined by Equation (2-1).

$$R_i = \frac{c_{i,f} - c_{i,p}}{c_{i,f}} \cdot 100\% \tag{2-1}$$

where $c_{i,f}$ and $c_{i,p}$ are the bulk concentration of solute in the feed phase and permeate phase, respectively.

Membrane flux

The permeate flux, J, of the pressure-driven membrane describes the permeability of the membrane, which can be expressed by Equation (2-2).

$$J = \frac{V}{A \cdot t} \tag{2-2}$$

Where V is the permeate volume. A is the effective area of the membrane. t is the filtration time to obtain the permeate volume V. The flux of a membrane is usually determined by the transmembrane pressure and the properties of membranes, which can be described by Equation (2-3).

$$J = K \cdot \frac{\Delta P - \Delta \Pi}{L_e} \tag{2-3}$$

Where K is the membrane permeability constant. L_e is the membrane thickness, ΔP is the transmembrane pressure. $\Delta \Pi$ is the transmembrane osmotic pressure difference.

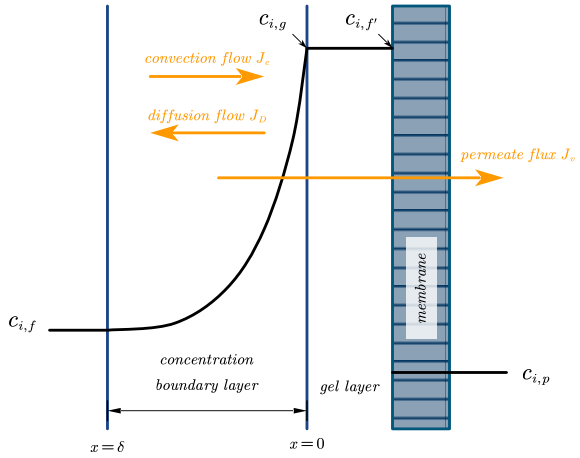

Figure 2.1 Solute concentration distribution in MF or UF process

As Figure 2.1 shows, in a pressure-driven filtration process, the solute continually accumulates near the feed-membrane interface and forms a stable concentration gradient at a steady state, which is called a concentration boundary layer (in some cases, the solute also forms a gel layer between the boundary layer and membrane, and Figure 2.1 corresponds to such as the case). The J_C and J_D are solute flow caused by convection and diffusion, respectively. This accumulation phenomenon is known as concentration polarization. According to the film theory [3], [9], the flux of solute in the boundary layer is the sum of convection flow driven by pressure and the diffusion retro flow caused by the

concentration gradient, which is given by Equation (2-4).

$$J_v \cdot c_{i,f} = D_i \cdot \frac{dc}{dx} + J_v \cdot c_{i,p} \quad (2\text{-}4)$$

Where J_v is the flux of solvent. D_i is the solute diffusivity of specie i at different x coordinates in the boundary layer. $c_{i,f}$ and $c_{i,p}$ are the concentration of solute i at the feed bulk and permeate respectively. Integration of Equation (2-4) over the whole boundary layer x coordinate, from 0 to δ, gives.

$$J_v = k \cdot ln\left(\frac{c_{i,f'} - c_{i,p}}{c_{i,f} - c_{i,p}}\right) \quad (2\text{-}5)$$

$$k = \frac{D}{\delta} \quad (2\text{-}6)$$

Equation (2-4) can be simplified as Equation (2-7) when the rejection is 100%.

$$C_M = \frac{c_{i,f'}}{c_{i,f}} = exp\left(\frac{J_v}{k}\right) \quad (2\text{-}7)$$

Where C_M is the polarization modulus, which is determined by the solvent flux and the diffusivity of solute i.

2.1.2. Mechanism of MF or UF process

MF and UF membranes separate substances in solution primarily by steric hindrance, which is determined by the molecular size of the substance and the pore size of the membrane. Some MF and UF membranes can partially adsorb solutes or particles, which can enhance rejection. Additionally, a fouling cake with a porous structure that forms on the membrane surface can further contribute to the sieving of molecules or particles that are smaller than the membrane pores.

2.2. NF membranes

The pore size of NF membranes is between that of UF membranes and RO membranes, generally not exceeding 2 nm [3]. Unlike other pressure-driven membranes (RO, UF, and MF membranes), the functional groups on the surface of NF membranes can be fully or partially ionized. This ionization causes electrostatic interactions between the NF membranes and ions, allowing NF membranes to selectively reject ions based on their properties, such as the charge sign (positive or negative), charge density (monovalent or multivalent), and ion radius. NF membranes can be used for the pretreatment of RO desalination, treatment of surface or groundwater, and municipal sewage treatment [10]. The most common structure of NF membranes is the thin-film composite (TFC). TFC membranes typically have an ultrathin selective layer, ranging from 10 to 400 nm in thickness, supported by a porous substrate [2].

2.2.1. Separation mechanism of NF process

NF membranes retain uncharged solutes through both steric hindrance from membrane pores and diffusion differences within the membrane matrix. For charged solutes, electrostatic interactions occur between the ions and the NF membrane. Currently, three types of models are widely used to explain the NF process:

Irreversible Thermodynamics Model: This model treats the membrane as a black box, requiring no knowledge of the separation mechanisms [11], [12], [13].

Solution-Diffusion Model: This model typically describes transport through dense membranes, assuming that solutes and solvents permeate only by diffusion and ignoring interactions between solute and solvent [13]. However, this simplification can lead to significant deviations in experimental results at high pressures. Paul et al. [14] improved

this model by introducing the Maxwell-Stefan equation, which relies on force balance among the species in solution. This modification allows the solution-diffusion model to be extended to non-ideal mixture systems.

Pore Flow Model: This model assumes that solutes and solvents pass through the membrane via permeation pathways (pores) larger than the solute or solvent molecules [15]. A specific type of pore flow model, the Donnan Steric Pore Model with Dielectric Exclusion (DSPM-DE), is discussed in the following sections [16], [17].

DSPM-DE Model

The DSPM-DE is one of the widely accepted models for NF membranes. This model considers solute partitioning at the solution-membrane interface via steric exclusion, dielectric exclusion, and Donnan exclusion. It accounts for solute transport along the membrane's pores via diffusion, advection, and electro-migration. To simplify the mathematical model, several assumptions are made in DSPM-DE: (1) Only the active layer of the TFC NF membrane is considered, neglecting the influence of the support layer. (2) The shape and size of the pores are simplified as cylindrical and uniform. (3) Solute molecules are considered spherical. (4) Only flow perpendicular to the membrane surface is considered, ignoring the crossflow of the solute. (5) The model is applied to dilute systems, thus ignoring interactions between solute molecules. (6) The dielectric constant of the solvent in the membrane pore is constant at different positions within the membrane pore. (7) Electro-neutrality is maintained everywhere inside the membrane and at the solution-membrane interface. (8) The NF process is assumed to be in a steady state [17].

The DSPM-DE model describes the relationship between permeate flux, solute rejection, the properties of the membrane, and the properties of the feed solution. It considers the effects of steric rejection, dielectric rejection, and Donnan rejection of solutes during the

filtration process. This comprehensive approach allows for a better understanding of how various factors influence the overall performance of nanofiltration membranes.

Solvent flux

The solvent flux in DSPM-DE can be described by the Hagen-Poiseuille Equation (2-8).

$$J_v = \frac{r_p^2 \cdot (\Delta P - \Delta \pi)}{8 \cdot \eta \cdot L_e} \tag{2-8}$$

Where J_v is the volumetric permeate flux. r_p is the average pore radius of the membrane. η is the dynamic viscosity of the solvent. ΔP is the hydraulic pressure difference across the membrane. L_e is the effective membrane thickness that can be described by Equation (2-9). $\Delta \pi$ is the osmotic pressure difference between feed and permeate solution which can be expressed by Equation (2-10).

$$L_e = \frac{\tau \cdot L}{\varepsilon} \tag{2-9}$$

Where τ is the tortuosity of membrane pores. L is the physical thickness of membranes. ε is the porosity of the membranes.

$$\Delta \pi = R \cdot T \cdot \sum_{i=1}^{N} \left(c_{i,f} - c_{i,p} \right) \tag{2-10}$$

Where R is the ideal gas constant. T is the solution temperature. $c_{i,f}$ and $c_{i,p}$ are the concentration of ion i in feed and permeate respectively.

Solute partitioning at the interface of solution-membrane

Three different exclusion factors are considered in DSPM-DE, for estimating the

partitioning of solute at the solution-membrane interface.

Steric exclusion

Steric exclusion is the exclusion sieving of solute molecules by membrane pores. As Equation (2-11) shows, the solute molecules whose Stokes radius is equal to or bigger than the radius of the membrane pore cannot enter the pore. When the Stokes radius of solute, r_i, is smaller than pore's radius, r_p, the steric exclusion factor, $\varphi_{S,i}$, is determined by the radius of the solute and membrane pore.

$$\varphi_{S,i} = \begin{cases} \left(1 - \frac{r_i}{r_p}\right)^2, \ for\ r_i < r_p \\ 0, \ \ for\ r_i \geq r_p \end{cases} \tag{2-11}$$

Dielectric exclusion

Dielectric exclusion is caused by the dielectric constant of the solvent being different in the bulk solution and inside the narrow membrane pores. The dielectric constant of solvent in the membrane pore is much smaller than it is in the bulk. The solutes, usually ions, are often with high polarity, so they tend to stay in the solvent with a high dielectric constant. Therefore, there is a hindrance to the solute to enter the membrane pore. The dielectric exclusion factor $\varphi_{DE,i}$ can be calculated by Equation (2-12).

$$\varphi_{DE,i} = \exp\left(-\frac{\Delta w_i}{k_B \cdot T}\right) \tag{2-12}$$

Where k_B is Boltzmann constant and Δw_i is the solvation energy difference of ion i which can be calculated by Equation (2-13).

$$\Delta w_i = \frac{z_i^2 \cdot e^2}{8 \cdot \pi \cdot \varepsilon_0 \cdot r_i} \cdot \left(\frac{1}{\varepsilon_b} - \frac{1}{\varepsilon_p}\right) \tag{2-13}$$

Where z_i is the valance of ion i. e is the electron charge. ε_0, ε_b and ε_p are the dielectric constant of vacuum, solvent in bulk, and solvent in membrane pore.

Donnan exclusion

Donnan exclusion is generated by electrostatic repulsion between the membrane surface and the ionic solute. Due to the ionization of the functional group, the membrane surface is charged. The degree of ionization of the functional group depends on the pH of the bulk solution. As Equation (2-14) shows, the Donnan exclusion factor $\varphi_{D,i}$ is related to the temperate, ionic valence and $\Delta\phi_0$, Donnan potential across the interface between the solution and membrane phase.

$$\varphi_{D,i} = \exp\left(-\frac{z_i \cdot e}{k_B \cdot T} \cdot \Delta\phi_0\right) \tag{2-14}$$

Solute partitioning at the solution-membrane interface is determined by the product of steric exclusion factor, dielectric exclusion, and Donna exclusion factor. The solute partitioning on the feed side and the permeate side is described by Equation (2-15) and Equation (2-16) respectively.

$$\frac{\gamma_i(x=0) \cdot c_i(x=0)}{\gamma_{i,f} \cdot c_{i,f}} = \varphi_{S,i} \cdot \varphi_{DE,i} \cdot \varphi_{D,i} \tag{2-15}$$

$$\frac{\gamma_i(x=\delta) \cdot c_i(x=\delta)}{\gamma_{i,p} \cdot c_{i,p}} = \varphi_{S,i} \cdot \varphi_{DE,i} \cdot \varphi_{D,i} \tag{2-16}$$

Where the γ_i is the activity coefficients of ion i.

The solutions across the membrane at steady-state would maintain electro-neutrality, which is shown in Equations (2-17), (2-18), and (2-19) for the feed side, the permeate side, and in the pore, respectively.

$$\sum_{i=1}^{N} z_i \cdot c_{i,f} = 0 \tag{2-17}$$

$$\sum_{i=1}^{N} z_i \cdot c_{i,p} = 0 \tag{2-18}$$

$$\sum_{i=1}^{N} z_i \cdot c_i(x) + X(x) = 0 \tag{2-19}$$

Where $X(x)$ is the volumetric charge density at position x along the membrane pore.

Solute transport along the membrane pore

In DSPM-DE, the solute transport in the membrane pore is described by the extended Nernst-Planck Equation (2-20). On the right side of Equation (2-20), the first term represents diffusive flux, the second term represents advective flux and the third term represents electro-migration.

$$J_i = -K_{i,d} \cdot D_{i,\infty} \cdot \frac{dc_i}{dx} + K_{i,a} \cdot c_i \cdot J_v - \frac{z_i \cdot c_i \cdot K_{i,d} \cdot D_{i,\infty} \cdot F}{R \cdot T} \cdot \frac{d\phi(x)}{dx} \tag{2-20}$$

Where J_i is the flux of solute i. $D_{i,\infty}$ is diffusion efficient of solute i in the bulk solution. $\phi(x)$ is electrical potential at position x along the membrane pore. F is Faraday constant. $K_{i,d}$ and $K_{i,a}$ are the diffusion hindrance factor and advection hindrance factor, respectively. Both $K_{i,d}$ and $K_{i,a}$ are only related to λ_i, the ratio of pore radius and the Stokes radius of solute i, shown in Equation (2-23). The $K_{i,d}$ and $K_{i,a}$ can be calculated by Equation (2-21) and (2-22).

$$K_{i,a} = \frac{1+3.867 \cdot \lambda_i - 1.907 \cdot \lambda_i^2 - 0.834 \cdot \lambda_i^3}{1+1.867 \cdot \lambda_i - 0.741 \cdot \lambda_i^2} \tag{2-21}$$

$$K_{i,d} = \begin{cases} \dfrac{1+\frac{9}{8}\lambda_i \ln \lambda_i - 1.56\lambda_i + 0.53\lambda_i^2 + 1.95\lambda_i^3 - 2.82\lambda_i^4 + 0.27\lambda_i^5 + 1.10\lambda_i^6 - 0.44\lambda_i^7}{(1-\lambda_i)^2}, & \lambda_i \le 0.95 \\ 0.98 \cdot \left(\dfrac{1-\lambda_i}{\lambda_i}\right)^{2.5}, & \lambda_i \le 0.95 \end{cases} \tag{2-22}$$

$$\lambda_i = \frac{r_i}{r_p} \tag{2-23}$$

At the steady-state, the solute flux J_i and the solvent flux J_v have the relationship shown in Equation (2-24), since $J_i \ll J_v$, the total flux is approximately equal to the solvent flux.

$$J_i = J_v \cdot c_{i,p} \tag{2-24}$$

2.3. Modification methods of PVDF membranes

Polyvinylidene fluoride (PVDF) is a very promising membrane material, due to its excellent thermal stability, high chemical resistance against corrosive chemicals, mechanical strength, and membrane-forming ability. However, its strong hydrophobic nature leads to low water permeability and easy fouling by proteins. Through membrane modification, the surface properties of PVDF membranes, such as hydrophilicity, can be significantly altered, thereby enhancing their performance in membrane separation processes.

PVDF membranes can be modified using several techniques to enhance their hydrophilicity, antifouling properties, and overall performance. Surface coating involves dipping the PVDF membrane into a solution containing target chemicals for coating, such as polyvinyl alcohol (PVA), chitosan, and polyether block amide (PEBAX), to improve the antifouling properties of membranes [18], [19]. Typically, the coating layer is not very durable. It may wash away during use. Surface grafting, which forms covalent bonds between the chemical for grafting and the membrane, offers long-term chemical stability. Surface grafting methods include UV photo-grafting, plasma treatment, electron beam grafting, and living/controlled polymerization. However, it may reduce permeability by blocking membrane pores from grafting chemicals.

Surface grafting immobilizes the hydrophilic functional groups, such as carboxyl and amine groups, onto the PVDF membrane surface by covalent bonds through chemical reactions, providing long-term stability and significant hydrophilicity improvement, though the process requires precise control of reaction conditions. Surface grafting can be achieved through plasma treatment [20], [21], [22], [23], UV-photo grafting [24], [25], [26], [27], [28], electron beam irradiation [29], chemical solution treatment [30], [31], [32], [33] and etc.

Blending modification mixes hydrophilic polymers like polyethylene glycol (PEG) and polyacrylamide (PAM) with PVDF resin to create modified membranes via phase inversion. Since the other chemicals are mixed into the PVDF membrane matrix, it may affect the membrane's mechanical properties. Additionally, incorporating other advanced materials, such as graphene oxide (GO) [34], [35], carbon nanotubes (CNTs) [36], [37], [38], [39], metal-organic frameworks (MOFs) [40], [41], MXene [42], [43], SiO_2 nanoparticles [44], and TiO_2 nanoparticles [45], dendrimer, can also improve the filtration performance of PVDF membranes. For instance, Lecaros et al. significantly improved the separation efficiency of PVDF membranes for ethanol/water separation by immobilizing a layer of Ionically cross-linked sodium alginate and polyamidoamine (PAMAM) dendrimer on the membrane surface [46].

2.4. Dendrimer

Dendritic polymers, also known as hyperbranched polymers, are a class of polymers characterized by their abundant side chains, resembling the branch structure of trees or starburst structures. Generally, dendritic polymers are divided into two categories based on the frameworks of molecules: polydisperse and monodisperse (Figure 2.2). Polydisperse dendritic polymers can be further subdivided into hyperbranched polymers, dendrigrafts,

and dendritic-linear hybrids [47]. These polydisperse dendritic polymers are non-uniform and contain chains or side chains of varying lengths. On the other hand, monodisperse dendritic polymers include dendrimers and dendrons, which have uniform and consistent structures.

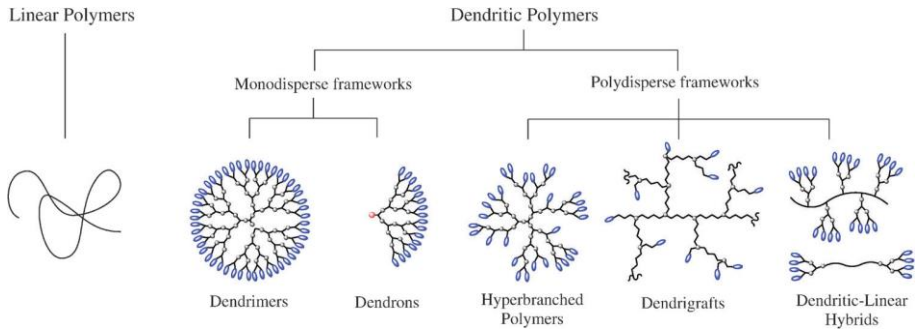

Figure 2.2 Schematic overview of the sub-classes of the family of dendritic polymer [47].

Dendrimers are spherical, branched-like molecules, also known as starburst dendritic macromolecules. In the 1980s, Donald Tomalia first synthesized and reported monodisperse dendrimers, specifically poly(amidoamine), with an NH_3 core, by repeatedly performing Michael addition and amidation reactions [48]. A typical dendrimer has three key features: (1) a central core surrounded or shielded by dendritic wedges, (2) an outer shell consisting of a repeatedly branched structure, and (3) a peripheral outside layer with numerous terminal functional groups. Due to their unique topological structure, dendrimers possess abundant terminal functional groups, large internal cavities, precise molecular structures, high degrees of geometric symmetry, and structural uniformity. Consequently, dendrimers hold great potential for various advanced applications, including targeted drug delivery, gene delivery, sensors, catalysis, wastewater treatment, and filtration membrane modification.

Among the diverse types of dendrimers, PAMAM and polypropylene imine (PPI) are the two most popular and commercially viable. They are widely used in biomedical

applications, catalysis, and industrial processes due to their remarkable biological properties, self-assembling capability, electrostatic interactions, chemical stability, low toxicity, high aqueous solubility, and reactivity [49].

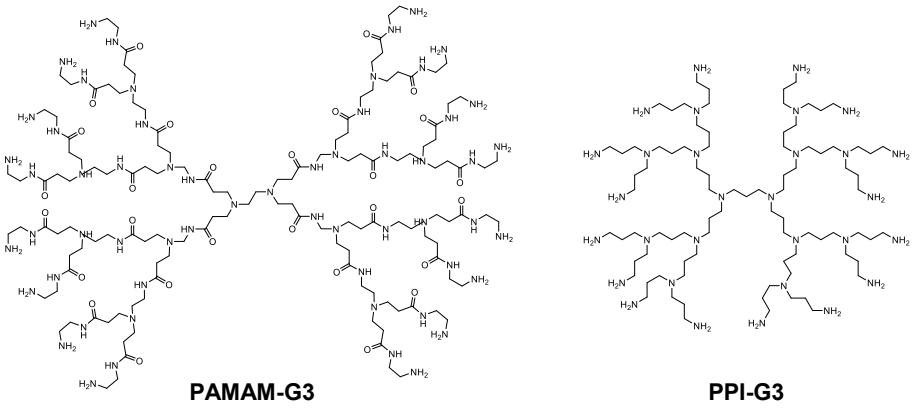

Figure 2.3 Molecular formula of generation 3 PAMAM dendrimer and generation 3 PPI dendrimer.

As shown in Figure 2.3, the structures of PPI and PAMAM dendrimers are very similar, with the primary difference being the presence of carbonyl groups in the branches of PAMAM dendrimers. However, the synthesis of PPI dendrimers is more complex, requiring more toxic chemicals and more cumbersome reaction conditions. Therefore, modifying PVDF membranes with PAMAM dendrimers is more promising and feasible.

2.4.1. Synthesis methods of dendrimer

Unlike traditional polymers prepared by one-pot synthesis, dendrimers are typically synthesized via a stepwise approach, which involves many steps, especially for high-generation dendrimers. Generally, the synthesis methods include the divergent method, the convergent method, the solid-phase method, and the double-stage convergent method (a combination of the divergent and convergent methods). Recently, some advanced strategies have been proposed, such as self-assembly synthesis, one-pot synthesis, orthogonal growth method, chemo-selective growth method, accelerated synthesis, and click chemistry

synthesis [50].

Divergent synthesis

In the divergent method, dendrimers are synthesized from the inside out. Monomer molecules are first attached to the dendrimer core, and then layers are grafted onto the periphery of the dendrimer step by step.

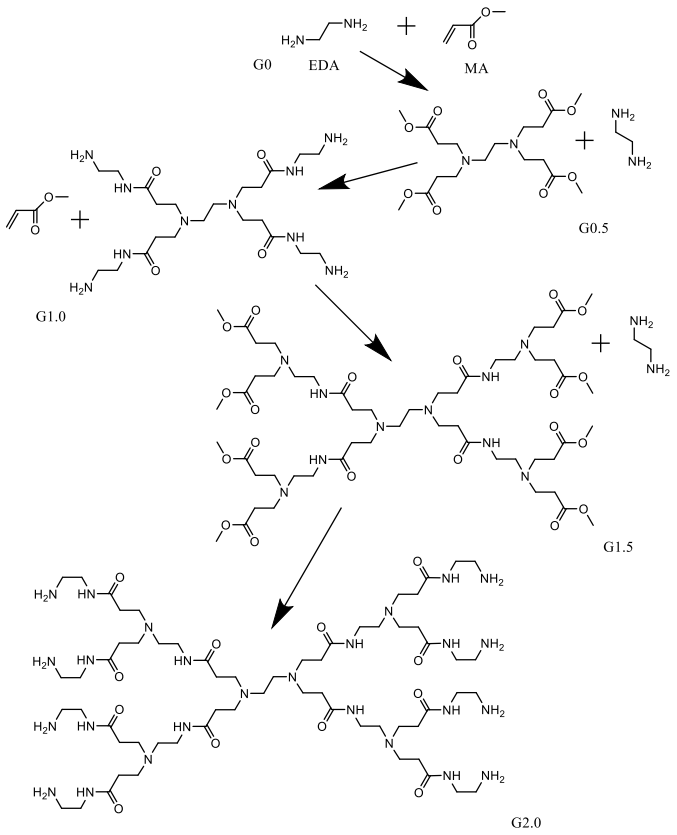

Figure 2.4 Synthesis of PAMAM dendrimer: the divergent approach.

For example, as shown in Figure 2.4, according to Donald Tomalia's strategy [48] for synthesizing PAMAM dendrimers, four methyl acrylate molecules are first added to the two terminal amine groups (-NH_2) of an ethylenediamine (EDA) core through a Michael addition reaction to obtain a half-generation PAMAM dendrimer (PAMAM-G0.5). Next, the four -OCH_3 groups of the terminal methyl ester groups in the PAMAM-G0.5 molecule

are replaced by four EDA molecules via an amidation reaction to generate a full-generation PAMAM dendrimer (PAMAM-G1.0). Subsequently, repeating the Michael addition reaction produces a PAMAM-G1.5 dendrimer, and repeating the amidation reaction generates a PAMAM-G2.0 dendrimer. Higher-generation PAMAM dendrimers can be synthesized by alternating between the Michael addition and amidation reactions.

As the molecular size of dendrimers increases, the probability of defects also rises due to structural crowding. Since the chemical and physical properties of normal and defect dendrimers are similar, separating defect dendrimers from normal ones is challenging, which decreases the mono-dispersity of the product [48], [51]. Additionally, it is necessary to remove excess reactants at every step, as divergent synthesis requires many iterations, and residual reactants from each step can react with those in subsequent steps. However, as dendrimer generation increases, the solution's viscosity also rises, and dendrimers cannot withstand high temperatures for purification. This makes the purification of high-generation dendrimers difficult.

Defect of PAMAM in the divergent synthesis

Due to the complexity of dendrimer structures, especially at high generations, defects can occur during divergent synthesis. These defect structures can result from four types of side reactions: incomplete Michael addition, retro-Michael reaction, intramolecular cyclization, and dendrimer bridging [52].

The incomplete Michael addition occurs when a terminal amine group combines with only one methyl acrylate (MA) molecule instead of two. This is typically due to insufficient reaction time. The retro-Michael reaction, on the other hand, involves the detachment of one or two MA molecules from the amine group of the PAMAM, a process promoted by high temperatures. Both incomplete Michael addition and retro-Michael reactions result in

branch structures missing repeat units. Intramolecular cyclization happens when an EDA molecule reacts with a terminal ester group on the same branch of a PAMAM molecule, forming macrocyclic defects. This side reaction is facilitated by high dilution conditions. Dendrimer bridging occurs when one EDA molecule reacts with two ester groups from different PAMAM molecules, linking them together. This is more likely to happen when EDA is in short supply. Furthermore, water molecules can hydrolyze ester bonds, converting them into carboxyl groups that are non-reactive with the amine groups of EDA. This hydrolysis results in inactive terminal groups, leading to missing repeat unit defects [52]. Residual EDA or MA can act as initiator cores, producing low-generation dendrimers in subsequent syntheses and reducing overall product purity. Given that defective dendrimers and low-generation dendrimer impurities have similar chemical and physical properties, making them difficult to separate, it is essential to minimize the formation of defects and low-generation dendrimers during synthesis.

High temperatures are deleterious to PAMAM dendrimers, both during synthesis and storage. During synthesis, elevated temperatures (i.e., > 80℃) can promote the retro-Michael reaction and intramolecular cyclization, regardless of the EDA concentration. For example, first-generation PAMAM dendrimers can be reversed at temperatures above 120℃, and significant dendrimer bridging occurs when exposed to temperatures higher than 150℃ [48]. Many papers have reported that the reaction temperature should be lower than 30℃, which means the temperature should not be over 120℃.

A large excess of EDA (over 10 times) is necessary for amidation, except for the formation of the first and second-generation dendrimers. Without this excess, serious dendrimer bridging occurs, resulting in a yellow gel-like product. Dendrimers with few bridging defects are homogeneous and appear as pale-yellow syrup, with the color becoming a brilliant yellow as the generation increases. In contrast, a large excess of MA is not required

for the Michael addition; an excess of 1.1 times MA is sufficient to inhibit the retro-Michael reaction.

Incomplete removal of EDA or MA after each synthesis step can lead to the presence of low-generation dendrimers mixed in the final product, which are difficult to separate. While residual MA and EDA can be removed by simple vacuum evaporation, removing trace EDA from high-generation dendrimers is more challenging. This is due to the high viscosity of high-generation dendrimers, the low volatility of EDA, and the vacuum evaporation temperature cannot be higher than 120℃ to avoid damaging the dendrimer structure. To effectively remove trace EDA, azeotropic distillation (e.g., using n-butanol or toluene) and wiped film distillation can be employed at relatively low temperatures. Additionally, using an oil bath during vacuum distillation can help prevent structural damage caused by localized high temperatures [52].

The ester groups in half-generation PAMAM dendrimers are prone to hydrolysis in aqueous solutions or humid environments. Therefore, it is crucial to prevent half-generation PAMAM dendrimers from contacting with water and to store them in a dry environment for long-term storage.

Convergent synthesis

In the convergent approach [51], the dendrimer is synthesized from the outside to the core. The outside unit is synthesized on the sub-outer unit, to form a fragment of the dendrimer. These fragments are progressively combined with inner units to create larger segments. Finally, these larger fragments, known as dendrons, are anchored to the core unit to complete the dendrimer structure.

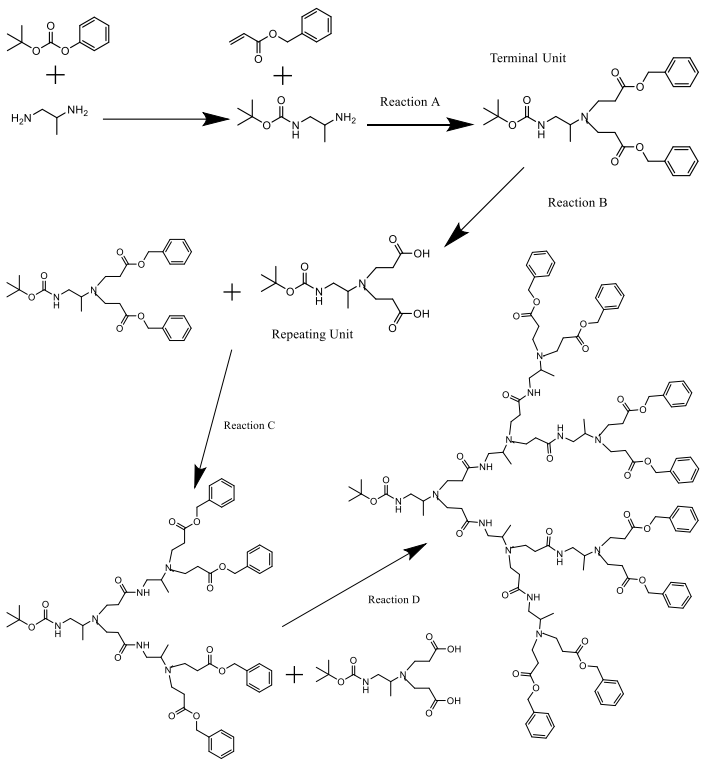

Figure 2.5 Convergent approach to the synthesis of PAMAM dendrimer.

For example, Christensen et al [53]. synthesized a kind of PAMAM dendrimers by a convergent approach. As shown in Figure 2.5, first, they connected two benzyl acrylate molecules on the terminal amine of a (2-Aminopropyl) carbamic acid tert-butyl ester molecule by Michael reaction (reaction A in Figure 2.5), to generate the terminal unit of the dendrimer, whose two-terminal carboxyl groups connect and are deactivated by two benzyl groups respectively. Then they removed the tert-butyl ester group of terminal units to generate the repeating unit with the active amine (reaction B in Figure 2.5). Then, they added two terminal units to one repeating unit by the amidation reaction (reaction C in Figure 2.5). The tert-butyl ester of terminal units was replaced and connected with the carboxyl group of repeating units, to form a dendron, a fragment, or a branch of the dendrimer. Then, a large branch was generated by adding two small branches, synthesized before, to one repeating unit (reaction D in Figure 2.5). By repeating this adding step at different times, the fragment of different generation dendrimers can be generated. In the

final step, all branches were connected to the core unit, 1,2-propane diamine, to form a dendrimer [53].

Compared with the divergent method, the convergent strategy intrinsically decreases the complexity of intermediates, so the risk of structure defect is lower during the synthesis The intermediate of divergent methods and convergent methods are dendrimers and dendrons, respectively. The dendrimer synthesized by convergent methods has fewer impurities, more mono-dispersity, and lower defects because better purification of dendrons is possible before final attachment to the core [52], [54]. However, due to the steric hindrance increase with the increase of dendron size, the reaction efficiency will decrease significantly, for synthesizing high generation dendrimer. Therefore, the synthesis efficiency is limited by convergent methods. In addition, due to steric congestion created in high-generation dendrons., the convergent methods can only produce the dendrimers up to generation 4 [51]. Therefore, extensive research is still needed before the convergent method can be widely adopted.

Solid-Phase synthesis

Solid phase synthesis is a very simplified and efficient method based on divergent synthesis. The difference between those two methods is that in the solid phase method, the core of the dendrimer is anchored on the solid. Then, by divergent iterative a part of dendrimer, dendron, is synthesized. After finishing the synthesis, the core of the dendrimer and the solid are disconnected and the dendrons are connected to form a dendrimer structure [55], [56], [57].

2.5. Dendrimer modified membranes

Currently, lots of dendrimers are applied in the modification of separation membranes,

including MF, UF, NF, RO, forward osmosis (FO), and gas separation membranes. There are three kinds of methods reported for immobilizing dendrimers onto membranes, which are grafting, coating, and blending [58]. The PAMAM molecule is connected with the polymer chains of membranes by covalent bonds via the grafting method. By coating, the PAMAM dendrimer is adsorbed or coated on the surface of the membrane. In the blending method, the PAMAM dendrimer is mixed into the casting solution.

2.5.1. Grafting

Grafting of the dendrimer can be achieved by two different approaches, which are "grafting-to" [59] and "grafting-from". In the grafting-to approach, the dendrimer is first synthesized and then grafted to the membrane, while, in the grafting-from approach, the core of the dendrimer is first grafted on the membrane surface and then, the dendrimer is synthesized. Generally, the way to graft dendrimers on the membrane depends on the chemical properties of the membrane surface. If the membrane contains appropriate groups that can react with the peripheral group of dendrimers, dendrimers can be directly grafted onto the membrane [60]. In some cases, the coupling agent may be used to induce the reaction between dendrimers and membranes [61], [62], [63], [64], [65]. For instance, Amariei et al. reported grafting PAMAM-G3 dendrimer on polyacrylic acid (PAA) / PVA hybrid electrospun membrane by using N, N-dicyclohexylcarbodiimide as the coupling agent [61].

If the dendrimer cannot directly react with the membrane matrix, it needs to introduce active groups by pretreatment before grafting. Active groups are generated during the pretreatment, enabling the formation of a covalent bond with the peripheral group of dendrimers. Generally, there are three ways to introduce an active group, UV irradiation, plasma treatment, and chemical treatment [58].

A variety of solutions have been applied for the chemical pretreatment of PVDF membranes, such as (1) acid aqueous solution of potassium permanganate [66], [66], (2) aqueous alkaline solution (NaOH or KOH) [67], [68], [69], [70], [71], [72], [73], [74], (3) alcoholic alkaline solution (NaOH or KOH) [70], [75], [76], (4) Piranha solution, mixture of sulfuric acid and hydrogen peroxide [30], [77]. In addition, some researchers reported that the amine groups of some organic molecules, such as 2-Amino-2-methyl-1-propanol [69], can directly react and form covalent bonds with PVDF membranes under alkaline condition [78], [79]. This provides a new possible method for grafting dendrimers with amine groups as peripheral functional groups. The alkaline treatment is usually performed with a hot solution (over 60℃) since PVDF has good alkaline resistance at room temperature. It is believed that carboxyl, hydroxyl, or carbonyl groups are formed after the treatment [68], [71], [72]. On the other hand, the alkaline treatment with the alkaline alcoholic solution or an alkaline aqueous solution of amine hydroxide ions dehydrofluorides forms a carbon-carbon double bond in PVDF chains [69], [70], [75], [78], [79]. When the reaction is in an aqueous solution, the double bond will continue to react with water molecules and form carboxyl, hydroxyl, or carbonyl groups on the PVDF backbone. However, when there is a primary amine in the aqueous solution, the double bond will prefer to undergo an addition reaction with a primary amine, forming a carbon-nitrogen bond, rather than with a water molecule [78]. The double bond of the modified PVDF molecule will be kept and treated with the alkaline alcoholic solution.

Some researchers also reported a method in which some agents, precursors, provide anchor sites for graft dendrimers. Usually, they first immobilized precursors on the membrane, and then grafted dendrimer on those precursors. The connection between precursors and membranes and the connection between precursors and dendrimers generally are covalent bonds, which provide good strength to prevent flaking. The PVDF membranes required pretreatment, before immobilizing the precursor. For instance, Li et. al reported the use of

trimethyl chloride (TMC) as the precursor to graft silver-PAMAM dendrimer (the silver nanoparticles are encapsulated inside of PAMAM dendrimer) onto alkaline treated PVDF membranes [76].

The way to graft the core of dendrimers, in the grafting-from approach, is similar to that of the grafting-to approach. In the grafting-from approach, since the dendrimer is built on the surface of the membrane, it is easier to separate dendrimers from the unreacted (excess) chemicals that are used for the synthesis of dendrimers. In the grafting-from approach, dendrimers have no spherical structure anymore. Therefore, it is more accurate to call those molecules dendrons. Zhang et al. [80] reported the grafting-from approach for dendrimer grafting. First, the core of PAMAM dendrimer, EDA was grafted on the bromomethylated poly (2,6-dimethyl-1,4-phenylene oxide) (BPPO) hollow fiber membranes. Then, they repeated the synthesis step of the PAMAM dendrimer by alternately reacting with MA and EDA. Finally, they successfully fabricated the hollow fiber membranes with PAMAM dendrons on their surface.

2.5.2. Coating

Unlike grafting methods, the bonding force between dendrimers and membranes is van der Waals or electrostatic forces in the coating method [58]. The common approaches of the coating method are direct precipitation [81] and interfacial polymerization (IP).

In the precipitation method, the dendrimer is adsorbed on the surface of the membrane. For instance, Savariar et al. [82] reported the coating of PPI dendrimer on membranes, which consists of the adsorption of PAA on the pore wall of polycarbonate (PC) membrane by simple filtration. Then, the PPI dendrimers are adsorbed onto the PAA layer by electrostatic force while PPI is filtered by the PAA/PC membrane.

The common method of the IP process is to perform IP on the surface of the membrane, and then immobilize the dendrimer by grafting or precipitation (adsorption). According to Zhang [83] IP of m-phenylenediamine (MPD) and TMC was first performed to form a polyamide layer on the surface of the polyethersulfone (PES) - PEG blend membrane. Then, PAMAM dendrimers were grafted on the polyamide layer. Some researchers also reported mixing the dendrimers in one of the reactants for IP. For instance, Manna et al. found that permeabilities, selectivity, and anti-fouling ability were increased in the filtration of multi-negatively charged organic dye molecules when trimesoyl amide amine (TMAAM) dendrimers were blended in the solution of piperazine (PIP), and IP is performed with TMC on the PES UF membranes [84]. Some researchers tried to use dendrimers as a reactant of IP. For example, Mansourpanah and Jafari [85] reported IP of PAMAM dendrimer and TMC on the surface of the PES UF membrane could double the NaCl rejection [85].

Dopamine can oxidatively polymerize automatically and form polydopamine (PDA) [86], [87]. This thin PDA layer can stick strongly on the surface where the polymerization takes place. The thin PDA layer cannot only play the role of a selective layer but also provide the sites for the grafting of dendrimers.

2.5.3. Blending

Blending is an economical and easy-to-operate method for embedding PAMAM in the membrane. Blending only needs to mix the dendrimers into the casting solution without additional treatment. For instance, Karimipour et al. blended the melamine-based dendrimer amines (MDA) functionalized GO nanosheets into PES membranes by directly adding them into the casting solution of PES membranes [81]. The anti-fouling performance of the modified PES membrane was significantly improved during bovine serum albumin (BSA).

However, dendrimers immobilized by coating or blending are not as strongly attached as those immobilized by grafting. During long-term use, dendrimers immobilized by coating or blending may be eluted from the membrane.

2.6. Application of membranes in the dairy industry

Normally, the composition of milk is water (87.7%), carbohydrate (4.9%), fat (3.4%), protein (3.3%), minerals (0.7%, referred to as ash), and vitamins [88]. The carbohydrate in milk is lactose, which is water-soluble, and trace amounts of some monosaccharides and oligosaccharides. The composition of milk fat is very complex, which is composed of triglycerides with over 400 individual fatty acids. Most fatty acids of milk fat have straight chains that have 4 to 18 carbons. The triglycerides in milk are in the form of 1 to 10 μm globules that are surrounded by a protein and phospholipid membrane. Milk contains water-soluble vitamins, such as thiamin (vitamin B1), riboflavin (vitamin B2), niacin (vitamin B3), cobalamin (vitamin B12), and a small amount of pantothenic acid (vitamin B5), pyridoxine (vitamin B6), vitamin C, niacin and folate. The mineral in milk includes potassium (0.14%), calcium (0.11%), phosphorous (0.09%), sodium (0.04%), magnesium (0.01%) and a small amount of selenium, zinc-iron, and copper. In milk, approximately 67% of the calcium, 35% of the magnesium, and 44% of the phosphate are salts bound within the casein micelle and the remainder is soluble in the whey phase.

There are two major types of protein in milk. They are casein protein (82%) which contains phosphorus and will precipitate at pH 4.6, and whey protein (18%) which is still dissolved in solution at pH 4.6. There are four types of caseins, α-s1, α-s2, ß, and 6. The caseins are suspended in milk as a micelle, which is a sphere with a diameter of 0.04 to 0.3 μm. Casein micelles are stable and do not precipitate from the solution. Most of the casein protein is separated during cheese production. The remaining solution is whey (serum), in other

words, whey is the byproduct of the cheese industry. The whey protein in the milk mainly includes ß-lactoglobulin (50%), α-lactalbumin (20%), bovine serum albumin (BSA), immunoglobulins, lactoferrin, transferrin, and many minor proteins and enzymes [88].

Table 2.1 Composition of different whey and UF permeate in the dairy industry [88].

Composition	Milk	Sweet whey	Acid whey		UF permeate
		cheddar	HCl	Lactic	cheddar
pH	6.7	6.1	4.7	4	6.1
Solids (%)	13	6.6	5.1	6	5.5
Lactose (%)	4.9	4.8	3.7	3.9	4.7
Protein (%)	3.3	0.9	0.73	0.72	0.01
Ash (%)	0.7	0.59	0.6	0.72	0.53
Lactic acid (%)	/	0.13	0	0.6	0
Fat (%)	3.4	0.06	0.05	0.003	0
Calcium (ppm)	1130	430	1200	1140	375
Phosphorus (ppm)	910	440	680	900	275
Potassium (ppm)	1430	1460	1200	1530	1450
Sodium (ppm)	400	430	270	400	430
Chloride ppm	/	970	2600	910	940

As mentioned above, whey is the byproduct of the cheese industry. Therefore, the composition of whey depends on the type of cheese produced. There are two types of whey, acid whey, and sweet whey. The sweet whey is from the production of rennet cheese and its pH is over 5.6. The acid whey is from the manufacturing of fresh cheese produced by lactic acid fermentation. The pH of acid whey is smaller than 5.1. The composition of different types of whey is shown in Table 2.1 [89]. Table 2.2 shows the properties of the proteins in whey. As Table 2.2 shows, about 70% of whey proteins have molecular weights of more than 14 kDa [90] and about 90% of whey proteins have isoelectric points smaller than pH 6.7, which is the pH of the sweet whey. Therefore, most protein in sweet whey is negatively charged.

Usually, MF membranes with a pore size of 0.1 to 2 μm are used for removing bacteria,

fungi spores, somatic cells, and fat globules from milk [91]. Ceramic membranes with a size below 0.1 μm could retain most casein in the retention phase [92], [93], [94], [95]. However, to retain all casein, the UF membranes of MWCO no more than 20 kDa are used [95].

Table 2.2 Protein composition in sweet whey [90].

Whey protein	Concentration (g/L)	Proportion of protein (%)	Isoelectric point (pH)	Molecular weight (kDa)
β-Lactoglobulin	3	50	5.3-5.3	18.3
α-Lactalbumin	0.7	12	4.2-4.5	14
Proteose peptones	1.4	23	/	4.1-40.8
Bovine serum albumins	0.3	5	5.1	69
Immunoglobulins	0.6	10	5.5-8.3	15-1000
Lactoferrin	0.05	0.8	9	81-84
Lactoperoxidase	0.03	0.5	9.6	89
Glycomacropeptide	/	/	4.2	7

Several membrane filtration systems have been researched for whey protein recovery, such as diafiltration (DF), vibratory shear enhanced processing (VSEP), integrated membrane systems of FO/RO and UF/NF, air injection enhanced UF, and biocatalysis coupled UF process [96]. The literature shows that the UF membranes with MWCO of 10 or 25 kDa could concentrate the whey to a very concentrated solution. For example, Barba et al. reported that the whey protein could be concentrated to 99.5 % by a 10 kDa polysulfone (PSF) membrane [97]. Yee et al., using a 10 kDa PES membrane concentrated the whey protein to 80 % [98], [99]. A membrane with MWCO of 10 kDa could reject most of the whey protein. Only some peptides and amino acids leaked [96]. Fouling is a serious challenge in the membrane filtration process of whey or milk. Hydrophilic membranes with smoother surfaces usually show better anti-fouling properties for proteins in the dairy industry. Meng et al. also reported that the zwitterionic layer helped to reduce the protein fouling of polyacrylonitrile membranes [100]. Using a rotating disk system or vibrating

system also can reduce protein fouling [101].

2.7. Conclusions

The review shows that enhancing the permeability, selectivity, and antifouling properties of separation membranes by immobilizing dendrimers has been extensively studied. Researchers have explored various methods of modifying separation membranes with dendrimers. These include directly incorporating dendrimers into the membrane matrix, grafting dendrimers onto the membrane surface, and fabricating a selective layer of membrane through the polymerization of dendrimers with other materials. Additionally, advanced materials functionalized with dendrimers have been used to modify separation membranes, such as dendrimer-functionalized GO, dendrimer-functionalized SiO_2 nanoparticles, and dendrimer-encapsulated Ag nanoparticles.

Dendrimer-modified membranes exhibit excellent performance, showing great potential in applications such as removing heavy metal ions from water and separating and purifying proteins. In the field of protein separation, dendrimer modified PVDF membranes can significantly improve separation efficiency and selectivity while reducing membrane fouling issues, thereby extending membrane lifespan and lowering operational costs. This holds significant importance for industries such as biopharmaceuticals, food processing, and biotechnology.

Currently, numerous studies have reported on the application of dendrimer-modified PVDF membranes in metal ion separation. However, there are fewer studies on the application of dendrimer-modified PVDF membranes in protein separation, especially in dairy protein separation. Protein separation is a complex process that involves factors such as molecular size, shape, charge, and hydrophilicity. The unique structure and multifunctional groups of

dendrimers offer distinct advantages in regulating the surface properties and pore structure of membranes, enabling efficient protein separation. Developing more efficient and stable dendrimer-modified membrane materials can not only enhance the purity of protein separation but also provide new ideas and methods for the application of membrane separation technology in more fields.

2.8. References

[1] R. W. Baker, *Membrane Technology and Applications*. John Wiley & Sons, 2012.

[2] Z. Yang *et al.*, "A Critical Review on Thin-Film Nanocomposite Membranes with Interlayered Structure: Mechanisms, Recent Developments, and Environmental Applications," *Environ. Sci. Technol.*, vol. 54, no. 24, pp. 15563–15583, Dec. 2020, doi: 10.1021/acs.est.0c05377.

[3] R. Singh, "Introduction to Membrane Technology," in *Membrane Technology and Engineering for Water Purification*, Elsevier, 2015, pp. 1–80. doi: 10.1016/B978-0-444-63362-0.00001-X.

[4] U. W. R. Siagian *et al.*, "High-Performance Ultrafiltration Membrane: Recent Progress and Its Application for Wastewater Treatment," *Curr Pollution Rep*, vol. 7, no. 4, pp. 448–462, Dec. 2021, doi: 10.1007/s40726-021-00204-5.

[5] S. F. Anis, R. Hashaikeh, and N. Hilal, "Microfiltration membrane processes: A review of research trends over the past decade," *Journal of Water Process Engineering*, vol. 32, p. 100941, Dec. 2019, doi: 10.1016/j.jwpe.2019.100941.

[6] C. Charcosset, *Membrane processes in biotechnology and pharmaceutics*. Amsterdam ; Boston: Elsevier, 2012.

[7] S. Al Aani, T. N. Mustafa, and N. Hilal, "Ultrafiltration membranes for wastewater and water process engineering: A comprehensive statistical review over the past decade," *Journal of Water Process Engineering*, vol. 35, p. 101241, Jun. 2020, doi: 10.1016/j.jwpe.2020.101241.

[8] J. Yu, C. Cao, and Y. Pan, "Advances of Adsorption and Filtration Techniques in

Separating Highly Viscous Crude Oil/Water Mixtures," *Adv. Mater. Interfaces*, vol. 8, no. 16, p. 2100061, Aug. 2021, doi: 10.1002/admi.202100061.

[9] V. Chen, A. G. Fane, S. Madaeni, and I. G. Wenten, "Particle deposition during membrane filtration of colloids: transition between concentration polarization and cake formation," *Journal of Membrane Science*, vol. 125, no. 1, pp. 109–122, Mar. 1997, doi: 10.1016/S0376-7388(96)00187-1.

[10] A. W. Mohammad, Y. H. Teow, W. L. Ang, Y. T. Chung, D. L. Oatley-Radcliffe, and N. Hilal, "Nanofiltration membranes review: Recent advances and future prospects," *Desalination*, vol. 356, pp. 226–254, Jan. 2015, doi: 10.1016/j.desal.2014.10.043.

[11] O. Kedem and A. Katchalsky, "Thermodynamic analysis of the permeability of biological membranes to non-electrolytes," *Biochimica et Biophysica Acta*, vol. 27, pp. 229–246, Jan. 1958, doi: 10.1016/0006-3002(58)90330-5.

[12] K. S. Spiegler and O. Kedem, "Thermodynamics of hyperfiltration (reverse osmosis): criteria for efficient membranes," *Desalination*, vol. 1, no. 4, pp. 311–326, Dec. 1966, doi: 10.1016/S0011-9164(00)80018-1.

[13] J. G. Wijmans and R. W. Baker, "The solution-diffusion model: a review," *Journal of Membrane Science*, vol. 107, no. 1–2, pp. 1–21, Nov. 1995, doi: 10.1016/0376-7388(95)00102-I.

[14] D. Paul, "Reformulation of the solution-diffusion theory of reverse osmosis," *Journal of Membrane Science*, vol. 241, no. 2, pp. 371–386, Oct. 2004, doi: 10.1016/j.memsci.2004.05.026.

[15] T. Matsuura and S. Sourirajan, "Reverse osmosis transport through capillary pores under the influence of surface forces," *Ind. Eng. Chem. Proc. Des. Dev.*, vol. 20, no. 2, pp. 273–282, Apr. 1981, doi: 10.1021/i200013a015.

[16] W. R. Bowen and J. S. Welfoot, "Modelling of membrane nanoÿltration—pore size distribution e ects," *Chemical Engineering Science*, p. 15, 2002.

[17] R. Wang and S. Lin, "Pore model for nanofiltration: History, theoretical framework, key predictions, limitations, and prospects," *Journal of Membrane Science*, vol. 620, p. 118809, Feb. 2021, doi: 10.1016/j.memsci.2020.118809.

[18] G. Kang and Y. Cao, “Application and modification of poly(vinylidene fluoride) (PVDF) membranes – A review,” *Journal of Membrane Science*, vol. 463, pp. 145–165, Aug. 2014, doi: 10.1016/j.memsci.2014.03.055.

[19] Y. Subasi and B. Cicek, “Recent advances in hydrophilic modification of PVDF ultrafiltration membranes – a review: part I,” *Membrane Technology*, vol. 2017, no. 10, Art. no. 10, Oct. 2017, doi: 10.1016/S0958-2118(17)30191-X.

[20] M. N. Zainol Abidin, M. M. Nasef, and T. Matsuura, “Fouling Prevention in Polymeric Membranes by Radiation Induced Graft Copolymerization,” *Polymers (Basel)*, vol. 14, no. 1, p. 197, Jan. 2022, doi: 10.3390/polym14010197.

[21] M. Nakata and H. Kumazawa, “Gas permeability and permselectivity of plasma-treated polyethylene membranes,” *Journal of Applied Polymer Science*, vol. 101, no. 1, pp. 383–387, 2006, doi: 10.1002/app.23850.

[22] Y. Han, S. Song, Y. Lu, and D. Zhu, “A method to modify PVDF microfiltration membrane via ATRP with low-temperature plasma pretreatment,” *Applied Surface Science*, vol. 379, pp. 474–479, Aug. 2016, doi: 10.1016/j.apsusc.2016.04.114.

[23] A. Venault *et al.*, “Design of near-superhydrophobic/superoleophilic PVDF and PP membranes for the gravity-driven breaking of water-in-oil emulsions,” *Journal of the Taiwan Institute of Chemical Engineers*, vol. 65, pp. 459–471, Aug. 2016, doi: 10.1016/j.jtice.2016.05.011.

[24] M.-X. Hu, Q. Yang, and Z.-K. Xu, “Enhancing the hydrophilicity of polypropylene microporous membranes by the grafting of 2-hydroxyethyl methacrylate via a synergistic effect of photoinitiators,” *Journal of Membrane Science*, vol. 285, no. 1, pp. 196–205, Nov. 2006, doi: 10.1016/j.memsci.2006.08.023.

[25] Y. Chen *et al.*, “Controlled grafting from poly(vinylidene fluoride) microfiltration membranes via reverse atom transfer radical polymerization and antifouling properties,” *Polymer*, vol. 48, no. 26, Art. no. 26, Dec. 2007, doi: 10.1016/j.polymer.2007.10.043.

[26] H. Hua, Y. Xiong, C. Fu, and N. Li, “pH-sensitive membranes prepared with poly(methyl methacrylate) grafted poly(vinylidene fluoride) via ultraviolet irradiation-induced atom transfer radical polymerization,” *RSC Adv.*, vol. 4, no. 74, Art. no. 74, 2014, doi: 10.1039/C4RA06368F.

[27] S. Golcuk, A. E. Muftuoglu, S. U. Celik, and A. Bozkurt, “Synthesis and characterization of polymer electrolyte membranes based on PVDF and styrene via photoinduced grafting,” *J Polym Res*, vol. 20, no. 5, Art. no. 5, May 2013, doi: 10.1007/s10965-013-0144-2.

[28] Q. Deng, Y. Chen, and W. Sun, “Preparation of polymer brushes from poly(vinylidene fluoride) surfaces by UV irradiation pretreatment,” *Surf. Rev. Lett.*, vol. 14, no. 01, Art. no. 01, Feb. 2007, doi: 10.1142/S0218625X07009013.

[29] F. Liu, B.-K. Zhu, and Y.-Y. Xu, “Improving the hydrophilicity of poly(vinylidene fluoride) porous membranes by electron beam initiated surface grafting of AA/SSS binary monomers,” *Applied Surface Science*, vol. 253, no. 4, pp. 2096–2101, Dec. 2006, doi: 10.1016/j.apsusc.2006.04.007.

[30] S. Al-Gharabli, J. Kujawa, M. O. Mavukkandy, and H. A. Arafat, “Functional groups docking on PVDF membranes: Novel Piranha approach,” *European Polymer Journal*, vol. 96, pp. 414–428, Nov. 2017, doi: 10.1016/j.eurpolymj.2017.09.029.

[31] S. Zhang, Y. Li, Y. Yuan, L. Jiang, H. Wu, and Y. Dong, “Biomimetic hydrophilic modification of poly (vinylidene fluoride) membrane for efficient oil-in-water emulsions separation,” *Separation and Purification Technology*, vol. 329, p. 125227, Jan. 2024, doi: 10.1016/j.seppur.2023.125227.

[32] S. Zhang, J. Shen, X. Qiu, D. Weng, and W. Zhu, “ESR and vibrational spectroscopy study on poly(vinylidene fluoride) membranes with alkaline treatment,” *Journal of Power Sources*, vol. 153, no. 2, Art. no. 2, Feb. 2006, doi: 10.1016/j.jpowsour.2005.05.020.

[33] H. Lei, H. Yu, Y. Lu, X. Lu, and Z. Xu, “A facile approach for the surface modification of poly(vinylidene fluoride) membrane via surface-initiated atom transfer radical polymerization,” *Chinese J. Polym. Sci.*, vol. 26, no. 01, Art. no. 01, 2008, doi: 10.1142/S0256767908002728.

[34] M. S. Sri Abirami Saraswathi, D. Rana, N. J. Kaleekkal, K. Divya, and A. Nagendran, “Investigating the efficacy of PVDF membranes customized with sulfonated graphene oxide nanosheets for enhanced permeability and antifouling,” *Journal of Environmental Chemical Engineering*, vol. 8, no. 5, p. 104426, Oct. 2020, doi: 10.1016/j.jece.2020.104426.

[35] K. Ko, Y. Yu, M.-J. Kim, J. Kweon, and H. Chung, “Improvement in fouling resistance of silver-graphene oxide coated polyvinylidene fluoride membrane prepared by pressurized filtration,” *Separation and Purification Technology*, vol. 194, pp. 161–169, Apr. 2018, doi: 10.1016/j.seppur.2017.11.016.

[36] J. Zhao *et al.*, “Construction of a multi-layer protection of CS polymer brush grafted DA@CNTs coating on PVDF membrane for effective removal of dye effluent,” *Journal of Hazardous Materials*, vol. 460, p. 132435, Oct. 2023, doi: 10.1016/j.jhazmat.2023.132435.

[37] S. Gholami, J. L. Llacuna, V. Vatanpour, A. Dehqan, S. Paziresh, and J. L. Cortina, “Impact of a new functionalization of multiwalled carbon nanotubes on antifouling and permeability of PVDF nanocomposite membranes for dye wastewater treatment,” *Chemosphere*, vol. 294, p. 133699, May 2022, doi: 10.1016/j.chemosphere.2022.133699.

[38] S. Wu, K. Li, W. Shi, and J. Cai, “Chitosan/polyvinylpyrrolidone/polyvinyl alcohol/carbon nanotubes dual layers nanofibrous membrane constructed by electrospinning-electrospray for water purification,” *Carbohydrate Polymers*, vol. 294, p. 119756, Oct. 2022, doi: 10.1016/j.carbpol.2022.119756.

[39] R. Zhou, D. Rana, T. Matsuura, and C. Q. Lan, “Effects of multi-walled carbon nanotubes (MWCNTs) and integrated MWCNTs/SiO_2 nano-additives on PVDF polymeric membranes for vacuum membrane distillation,” *Separation and Purification Technology*, vol. 217, pp. 154–163, Jun. 2019, doi: 10.1016/j.seppur.2019.02.013.

[40] S. Shen, H. Li, Y. Shen, R. Bai, and G. Zhang, “Modification of PVDF membrane by post-modified NH_2-MIL-88B(Fe) showing improved permeability and oil/water separation performance,” *Journal of Environmental Chemical Engineering*, vol. 11, no. 3, Art. no. 3, Jun. 2023, doi: 10.1016/j.jece.2023.109621.

[41] I. Gupta, E. T. Farinas, and S. Mitra, “Development of carbon nanotube-metal organic framework (MOF) hybrid antiviral microfiltration membrane,” *Separation and Purification Technology*, vol. 315, p. 123766, Jun. 2023, doi: 10.1016/j.seppur.2023.123766.

[42] “Ultrathin 2D Ti_3C_2Tx MXene membrane for effective separation of oil-in-water emulsions in acidic, alkaline, and salty environment - ScienceDirect.” Accessed: Jul.

16, 2024. https://www.sciencedirect.com/science/article/pii/S0021979719313931

[43] S. Chen, T. Wang, X. Zhuo, Y. Wang, and L. Wu, "PVDF mixed matrix membranes by incorporation of ionic liquid and MXene for enhancing permeation and antifouling performance," *Journal of Environmental Chemical Engineering*, vol. 10, no. 3, p. 108027, Jun. 2022, doi: 10.1016/j.jece.2022.108027.

[44] S. Ding, L. Zhang, Y. Li, and L. Hou, "Fabrication of a novel polyvinylidene fluoride membrane via binding SiO_2 nanoparticles and a copper ferrocyanide layer onto a membrane surface for selective removal of cesium," *Journal of Hazardous Materials*, vol. 368, pp. 292–299, Apr. 2019, doi: 10.1016/j.jhazmat.2019.01.065.

[45] Z. Li, D. Rana, Z. Wang, T. Matsuura, and C. Q. Lan, "Synergic effects of hydrophilic and hydrophobic nanoparticles on performance of nanocomposite distillation membranes: An experimental and numerical study," *Separation and Purification Technology*, vol. 202, pp. 45–58, Aug. 2018, doi: 10.1016/j.seppur.2018.03.032.

[46] R. L. G. Lecaros *et al.*, "Ionically cross-linked sodium alginate and polyamidoamine dendrimers for ethanol/water separation through pervaporation," *Separation and Purification Technology*, vol. 275, p. 119125, Nov. 2021, doi: 10.1016/j.seppur.2021.119125.

[47] M. V. Walter and M. Malkoch, "Simplifying the synthesis of dendrimers: accelerated approaches," *Chem. Soc. Rev.*, vol. 41, no. 13, pp. 4593–4609, Jun. 2012, doi: 10.1039/C2CS35062A.

[48]D. A. Tomalia *et al.*, "A New Class of Polymers: Starburst-Dendritic Macromolecules," *Polym J*, vol. 17, no. 1, pp. 117–132, Jan. 1985, doi: 10.1295/polymj.17.117.

[49] B. Devadas, A. P. Periasamy, and K. Bouzek, "A review on poly(amidoamine) dendrimer encapsulated nanoparticles synthesis and usage in energy conversion and storage applications," *Coordination Chemistry Reviews*, vol. 444, p. 214062, Oct. 2021, doi: 10.1016/j.ccr.2021.214062.

[50] R. Y. Patle and J. S. Meshram, "The advanced synthetic modifications and applications of multifunctional PAMAM dendritic composites," *React. Chem. Eng.*, vol. 7, no. 1, Art. no. 1, 2022, doi: 10.1039/D1RE00074H.

[51] Z. Lyu, L. Ding, A. Y.-T. Huang, C.-L. Kao, and L. Peng, "Poly(amidoamine)

dendrimers: covalent and supramolecular synthesis," *Materials Today Chemistry*, vol. 13, pp. 34–48, Sep. 2019, doi: 10.1016/j.mtchem.2019.04.004.

[52] V. Gupta and S. Nayak, "Dendrimers: A Review on Synthetic Approaches," *J App Pharm Sci*, pp. 117–122, 2015, doi: 10.7324/JAPS.2015.50321.

[53] M. Pittelkow and J. B. Christensen, "Convergent synthesis of internally branched PAMAM dendrimers," *ORGANIC LETTERS*, vol. Vol. 7, no. No. 7, pp. 1295–1298, Jan. 2005.

[54] A. W. Bosman, H. M. Janssen, and E. W. Meijer, "About Dendrimers: Structure, Physical Properties, and Applications," *Chem. Rev.*, vol. 99, no. 7, pp. 1665–1688, Jul. 1999, doi: 10.1021/cr970069y.

[55] A. Basso, N. Pegg, B. Evans, and M. Bradley, "Solid-Phase Synthesis of Amidine-Based GP IIb-IIIa Antagonists on Dendrimer Resin Beads," *Eur. J. Org. Chem.*, vol. 2000, no. 23, pp. 3887–3891, Dec. 2000, doi: 10.1002/1099-0690(200012)2000:23<3887::AID-EJOC3887>3.0.CO;2-T.

[56] C. Fromont and M. Bradley, "High-loading resin beads for solid phase synthesis using triple branching symmetrical dendrimers," *Chem. Commun.*, no. 4, pp. 283–284, 2000, doi: 10.1039/a906515f.

[57] V. Swali, N. J. Wells, G. J. Langley, and M. Bradley, "Solid-Phase Dendrimer Synthesis and the Generation of Super-High-Loading Resin Beads for Combinatorial Chemistry," *J. Org. Chem.*, vol. 62, no. 15, pp. 4902–4903, Jul. 1997, doi: 10.1021/jo9708654.

[58] O. Karatas, R. Keyikoglu, N. Atalay Gengec, V. Vatanpour, and A. Khataee, "A review on dendrimers in preparation and modification of membranes: progress, applications, and challenges," *Materials Today Chemistry*, vol. 23, p. 100683, Mar. 2022, doi: 10.1016/j.mtchem.2021.100683.

[59] X. Bao *et al.*, "Polyamidoamine dendrimer grafted forward osmosis membrane with superior ammonia selectivity and robust antifouling capacity for domestic wastewater concentration," *Water Research*, vol. 153, pp. 1–10, Apr. 2019, doi: 10.1016/j.watres.2018.12.067.

[60] T. A. Otitoju, R. A. Saari, and A. L. Ahmad, "Progress in the modification of reverse

osmosis (RO) membranes for enhanced performance," *Journal of Industrial and Engineering Chemistry*, vol. 67, pp. 52–71, Nov. 2018, doi: 10.1016/j.jiec.2018.07.010.

[61] G. Amariei *et al.*, "Dendrimer-functionalized electrospun nanofibres as dual-action water treatment membranes," *Science of The Total Environment*, vol. 601–602, pp. 732–740, Dec. 2017, doi: 10.1016/j.scitotenv.2017.05.243.

[62] A. M. Saenz de Jubera *et al.*, "Development and Performance Characterization of a Polyamide Nanofiltration Membrane Modified with Covalently Bonded Aramide Dendrimers," *Environ. Sci. Technol.*, p. 130711065921008, Jul. 2013, doi: 10.1021/es400765q.

[63] J. Ledesma-García, G. Orozco, R. Antaño, and L. A. Godínez, "Preparation and study of cellulose acetate membranes modified with linear polymers covalently bonded to Starburst polyamidoamine dendrimers," *Journal of Applied Polymer Science*, vol. 110, no. 5, pp. 2898–2906, 2008, doi: 10.1002/app.28833.

[64] G. Amariei, K. Boltes, P. Letón, I. Iriepa, I. Moraleda, and R. Rosal, "Poly(amidoamine) dendrimers grafted on electrospun poly(acrylic acid)/poly(vinyl alcohol) membranes for host–guest encapsulation of antioxidant thymol," *J. Mater. Chem. B*, vol. 5, no. 33, pp. 6776–6785, 2017, doi: 10.1039/C7TB01498H.

[65] M. Li *et al.*, "Positively Charged Nanofiltration Membrane with Dendritic Surface for Toxic Element Removal," *ACS Sustainable Chem. Eng.*, vol. 5, no. 1, pp. 784–792, Jan. 2017, doi: 10.1021/acssuschemeng.6b02119.

[66] S. Wang, J. Li, J. Suo, and T. Luo, "Surface modification of porous poly(tetrafluoraethylene) film by a simple chemical oxidation treatment," *Applied Surface Science*, vol. 256, no. 7, pp. 2293–2298, Jan. 2010, doi: 10.1016/j.apsusc.2009.10.055.

[67] M. Grasselli and N. Betz, "Making porous membranes by chemical etching of heavy-ion tracks in β-PVDF films," *Nuclear Instruments and Methods in Physics Research Section B: Beam Interactions with Materials and Atoms*, vol. 236, no. 1–4, pp. 501–507, Jul. 2005, doi: 10.1016/j.nimb.2005.04.027.

[68] M. Kamaz, A. Sengupta, A. Gutierrez, Y.-H. Chiao, and R. Wickramasinghe, "Surface Modification of PVDF Membranes for Treating Produced Waters by Direct Contact

Membrane Distillation," *IJERPH*, vol. 16, no. 5, p. 685, Feb. 2019, doi: 10.3390/ijerph16050685.

[69] C. Sun and X. Feng, "Enhancing the performance of PVDF membranes by hydrophilic surface modification via amine treatment," *Separation and Purification Technology*, vol. 185, pp. 94–102, Sep. 2017, doi: 10.1016/j.seppur.2017.05.022.

[70] E. Boyraz, F. Yalcinkaya, J. Hruza, and J. Maryska, "Surface-Modified Nanofibrous PVDF Membranes for Liquid Separation Technology," *Materials*, vol. 12, no. 17, p. 2702, Aug. 2019, doi: 10.3390/ma12172702.

[71] G. Zhao and W.-N. Chen, "Enhanced PVDF membrane performance via surface modification by functional polymer poly(N-isopropylacrylamide) to control protein adsorption and bacterial adhesion," *Reactive and Functional Polymers*, vol. 97, pp. 19–29, Dec. 2015, doi: 10.1016/j.reactfunctpolym.2015.10.001.

[72] A. Qin, X. Li, X. Zhao, D. Liu, and C. He, "Engineering a Highly Hydrophilic PVDF Membrane via Binding TiO_2 Nanoparticles and a PVA Layer onto a Membrane Surface," *ACS Appl. Mater. Interfaces*, vol. 7, no. 16, pp. 8427–8436, Apr. 2015, doi: 10.1021/acsami.5b00978.

[73] W. Zhang, Y. Lu, J. Liu, X. Li, B. Li, and S. Wang, "Preparation of re-entrant and anti-fouling PVDF composite membrane with omniphobicity for membrane distillation," *Journal of Membrane Science*, vol. 595, p. 117563, Feb. 2020, doi: 10.1016/j.memsci.2019.117563.

[74] G. J. Ross, J. F. Watts, M. P. Hill, and P. Morrissey, "Surface modification of poly(vinylidene fluoride) by alkaline treatment1. The degradation mechanism," *Polymer*, vol. 41, no. 5, pp. 1685–1696, Mar. 2000, doi: 10.1016/S0032-3861(99)00343-2.

[75] X. Wang, Z. Wang, Z. Wang, Y. Cao, and J. Meng, "Tethering of hyperbranched polyols using PEI as a building block to synthesize antifouling PVDF membranes," *Applied Surface Science*, vol. 419, pp. 546–556, Oct. 2017, doi: 10.1016/j.apsusc.2017.05.037.

[76] G. Li, L. Shen, Y. Luo, and S. Zhang, "The effect of silver-PAMAM dendrimer nanocomposites on the performance of PVDF membranes," *Desalination*, vol. 338, pp. 115–120, Apr. 2014, doi: 10.1016/j.desal.2014.02.001.

[77] S. Al-Gharabli and J. Kujawa, “Molecular activation of fluoropolymer membranes via base piranha treatment to enhance transport and mitigate fouling – new materials for water purification,” *Journal of Membrane Science*, vol. 624, p. 119105, Apr. 2021, doi: 10.1016/j.memsci.2021.119105.

[78] G. Vitola, R. Mazzei, E. Fontananova, and L. Giorno, “PVDF membrane biofunctionalization by chemical grafting,” *Journal of Membrane Science*, vol. 476, pp. 483–489, Feb. 2015, doi: 10.1016/j.memsci.2014.12.004.

[79] C.-H. Kuo, G.-J. Chen, Y.-K. Twu, Y.-C. Liu, and C.-J. Shieh, “Optimum Lipase Immobilized on Diamine-Grafted PVDF Membrane and Its Characterization,” *Ind. Eng. Chem. Res.*, vol. 51, no. 14, pp. 5141–5147, Apr. 2012, doi: 10.1021/ie300011q.

[80] Q. Zhang, N. Wang, L. Zhao, T. Xu, and Y. Cheng, “Polyamidoamine Dendronized Hollow Fiber Membranes in the Recovery of Heavy Metal Ions,” *ACS Appl. Mater. Interfaces*, vol. 5, no. 6, pp. 1907–1912, Mar. 2013, doi: 10.1021/am400155b.

[81] H. Karimipour, A. Shahbazi, and V. Vatanpour, “Fouling decline and retention increase of polyethersulfone membrane by incorporating melamine-based dendrimer amine functionalized graphene oxide nanosheets (GO/MDA),” *Journal of Environmental Chemical Engineering*, vol. 9, no. 1, Art. no. 1, Feb. 2021, doi: 10.1016/j.jece.2020.104849.

[82] E. N. Savariar, M. M. Sochat, A. Klaikherd, and S. Thayumanavan, “Functional Group Density and Recognition in Polymer Nanotubes,” *Angew. Chem. Int. Ed.*, vol. 48, no. 1, pp. 110–114, Jan. 2009, doi: 10.1002/anie.200804136.

[83] W.-P. Zhu, J. Gao, S.-P. Sun, S. Zhang, and T.-S. Chung, “Poly(amidoamine) dendrimer (PAMAM) grafted on thin film composite (TFC) nanofiltration (NF) hollow fiber membranes for heavy metal removal,” *Journal of Membrane Science*, vol. 487, pp. 117–126, Aug. 2015, doi: 10.1016/j.memsci.2015.03.033.

[84] L.-F. Liu *et al.*, “Modification of polyamide TFC nanofiltration membrane for improving separation and antifouling properties,” *RSC Adv.*, vol. 8, no. 27, pp. 15102–15110, 2018, doi: 10.1039/C8RA01374H.

[85] Y. Mansourpanah and Z. Jafari, “Efficacy of different generations and concentrations of PAMAM–NH_2 on the performance and structure of TFC membranes,” *Reactive and Functional Polymers*, vol. 93, pp. 178–189, Aug. 2015, doi:

10.1016/j.reactfunctpolym.2015.04.010.

[86] Z.-L. Qiu *et al.*, “Ionic Dendrimer Based Polyamide Membranes for Ion Separation,” *ACS Nano*, vol. 15, no. 4, pp. 7522–7535, Apr. 2021, doi: 10.1021/acsnano.1c00936.

[87] H. Wang, C. Wu, Z. Wei, C. Li, and Q. Liu, “Surface chemistry, topology and desalination performance controlled positively charged NF membrane prepared by polydopamine-assisted graft of starburst PAMAM dendrimers,” *RSC Adv.*, vol. 6, no. 6, pp. 4673–4682, 2016, doi: 10.1039/C5RA25047A.

[88] “Nutrient Content of Milk Varieties | MilkFacts.info.” Accessed: Jun. 17, 2022. http://milkfacts.info/Nutrition%20Facts/Nutrient%20Content.htm

[89] K. Waldron, *Handbook of waste management and co-product recovery in food processing*. 2007.

[90] K. R. Marshall, “Industrial isolation of milk proteins: whey proteins.,” *Developments in Dairy Chemistry*, vol. 1, pp. 339–373, 1982.

[91] K. Soodam and T. P. Guinee, “The case for milk protein standardisation using membrane filtration for improving cheese consistency and quality,” *Int J Dairy Technol*, vol. 71, no. 2, pp. 277–291, May 2018, doi: 10.1111/1471-0307.12502.

[92] C. E. Jørgensen, R. K. Abrahamsen, E.-O. Rukke, A.-G. Johansen, R. B. Schüller, and S. B. Skeie, “Optimization of protein fractionation by skim milk microfiltration: Choice of ceramic membrane pore size and filtration temperature,” *Journal of Dairy Science*, vol. 99, no. 8, pp. 6164–6179, Aug. 2016, doi: 10.3168/jds.2016-11090.

[93] P. Punidadas and S. S. H. Rizvi, “Separation of milk proteins into fractions rich in casein or whey proteins by cross flow filtration,” *Food Research International*, vol. 31, no. 4, pp. 265–272, May 1998, doi: 10.1016/S0963-9969(98)00088-X.

[94] O. Le Berre and G. Daufin, “Skimmilk crossflow microfiltration performance versus permeation flux to wall shear stress ratio,” *Journal of Membrane Science*, vol. 117, no. 1, pp. 261–270, Aug. 1996, doi: 10.1016/0376-7388(96)00076-2.

[95] C. E. Jørgensen, R. K. Abrahamsen, E.-O. Rukke, T. K. Hoffmann, A.-G. Johansen, and S. B. Skeie, “Processing of high-protein yoghurt – A review,” *International Dairy Journal*, vol. 88, pp. 42–59, Jan. 2019, doi: 10.1016/j.idairyj.2018.08.002.

[96] W. Wen-qiong, W. Yun-chao, Z. Xiao-feng, G. Rui-xia, and L. Mao-lin, “Whey protein membrane processing methods and membrane fouling mechanism analysis,” *Food Chemistry*, vol. 289, pp. 468–481, Aug. 2019, doi: 10.1016/j.foodchem.2019.03.086.

[97] D. BARBA, F. BEOLCHINI, and F. VEGLIÓ, “Minimizing Water Use in Diafiltration of Whey Protein Concentrates,” *Separation Science and Technology*, vol. 35, no. 7, pp. 951–965, Jan. 2000, doi: 10.1081/SS-100100204.

[98] K. W. K. Yee, D. E. Wiley, and J. Bao, “Whey protein concentrate production by continuous ultrafiltration: Operability under constant operating conditions,” *Journal of Membrane Science*, vol. 290, no. 1, pp. 125–137, Mar. 2007, doi: 10.1016/j.memsci.2006.12.026.

[99] K. W. K. Yee, A. Alexiadis, J. Bao, and D. E. Wiley, “Effects of multiple-stage membrane process designs on the achievable performance of automatic control,” *Journal of Membrane Science*, vol. 320, no. 1, pp. 280–291, Jul. 2008, doi: 10.1016/j.memsci.2008.04.010.

[100] H. Meng, Q. Cheng, and C. Li, “Polyacrylonitrile-based zwitterionic ultrafiltration membrane with improved anti-protein-fouling capacity,” Applied Surface Science, vol. 303, pp. 399–405, Jun. 2014, doi: 10.1016/j.apsusc.2014.03.015.

[101] M. Y. Jaffrin, “Dynamic shear-enhanced membrane filtration: A review of rotating disks, rotating membranes and vibrating systems,” Journal of Membrane Science, vol. 324, no. 1–2, pp. 7–25, Oct. 2008, doi: 10.1016/j.memsci.2008.06.050.

Chapter 3. A Moderate and Effective Approach for Surface Engineering of PVDF Membranes: Treatment Using Alkaline Isopropanol Solution

Abstract

Due to the excellent chemical resistance, the modification of PVDF membranes typically necessitates implementation under more rigorous conditions, accompanied by an extended processing time. A moderate and effective approach requiring low alkaline concentration and short contact time was demonstrated for the surface engineering of microporous membranes made of polyvinylidene fluoride (PVDF), a commonly used polymer for membrane fabrication. This approach involved treating the membranes with a 0.5 M KOH isopropanol solution at specific temperatures (20℃, 30℃, 40℃, 50℃, and 60℃) to achieve the desired effects. The alkaline treatment resulted in the generation of abundant hydroxyl groups, carboxyl groups, alkenyl, and carbonyl groups on the PVDF membrane matrix. For the membranes treated at 60℃, the contact angle decreased from 89.9° for the PVDF membranes to 57.7°, indicating increased hydrophilicity. Additionally, the surface Zeta potential (at pH 10.0) decreased from -44.1 mV to -64.2 mV, further confirming the modification of the membrane surface. The alkaline treatment significantly enhanced the rejection of various substances such as poly (acrylic acid) (PAA), poly (ethylene oxide) (PEO), casein protein, and whey protein, without substantially changing membrane permeability.

Acronyms and Symbols

Abbreviation

ATR-FTIR	attenuated total reflectance-Fourier transform infrared
BSA	bovine serum albumin
CNTs	carbon nanotubes
DI	deionized
DMAc	*N*, *N*-dimethylacetamide
DOS	degree of substitution
FRR	flux recovery ratio
MF	microfiltration
MOFs	metal-organic frameworks
NF	nanofiltration
NIPS	non-solvent induced phase separation
NPs	nanoparticles
SEM	scanning electron microscopy
PAA	polyacrylic acid
PAMAM	polyamidoamine
PEG	polyethylene glycol
PEI	polyethyleneimine

PES	polyether sulfone
PEO	polyethylene oxide
PSF	polysulfone
PVDF	polyvinylidene fluoride
RO	reverse osmosis
TMC	trimesoyl chloride
UF	ultrafiltration
XPS	X-ray photoelectron spectroscopy

Nomenclature

A	effective area of the membranes
A_{sample}	area of the membrane sample during porosity measurement
c_f	concentration of feed
c_p	concentration of permeate
$DOS_i\%$	degree of substitution of the membrane alkaline treated at i℃
F_0	elemental content of fluorine at the surface of the base membrane
F_i	elemental content of fluorine at the surface of membrane alkaline treated at i℃
l	thickness of the dry membrane sample
R	solute rejection
t	filtration time

v	volume of the permeate
w_d	bulk porosity
w_w	weight of the wet membrane sample
ε	weight of the dry membrane sample
$\rho_{butanol}$	density of n-butanol

3.1. Introduction

The performance of pressure-driven membranes, including microfiltration (MF) membranes, ultrafiltration (UF), nanofiltration (NF), and reverse osmosis (RO) membranes relies heavily on the properties of membrane surface including pore size and size distribution as well as roughness and hydrophilicity. Therefore, modification of the membrane surface has been a widely adopted method for the enhancement of membrane performance. Of particular relevance, some hydrophobic polymers such as polyvinylidene fluoride (PVDF) have been widely used in fabricating membranes for their mechanical strength, processibility, and chemical and temperature resistance [1]. The research related to PVDF membranes has had a notable increase during the last decade [2]. Different approaches have been adopted for the modification of PVDF membrane surface, including physical approaches and chemical modification.

The most common physical approach for membrane surface engineering is blending, which involves mixing the primary polymer, e.g., PVDF, with inorganic or organic additives in the casting solution for membrane fabrication. For instance, inorganic materials such as nanoparticles (NPs) of SAPO-34 zeolite [3], TiO_2 [4], SiO_2 [5], graphene oxide [6], and multi-walled carbon nanotubes [7] and functional agents such as choline chloride and 1,5-diphenylcarbazide [8] have been demonstrated to be able to significantly increase the membrane surface hydrophilicity and porosity, and therefore membrane permeability. This approach does not involve chemical reactions and is easy to carry out. However, the additives are usually quite expensive, and the structure of the entire membrane matrix is affected. Furthermore, leakage of NPs and small molecule organic additives during prolonged membrane operations could cause deterioration of membrane performance and environmental hazards.

Common chemical methods for membrane surface modification include interfacial polymerization, surface precipitation, and grafting. In interfacial polymerization, the two monomers used for interfacial polymerization are dissolved in two mutually immiscible solvents. After the membrane is wetted with one of the two monomer solutions, the other solution is added, and polymerization occurs at the interface where the two solutions come into contact to form a very thin polymeric layer. Qui et al. fabricated a selective layer on the surface of the polysulfone (PSF) membrane through the interfacial polymerization of polyamidoamine (PAMAM) and trimesoyl chloride (TMC). By changing the peripheral functional groups of PAMAM dendrimer, the membrane showed a higher selectivity for positive or negative multivalent metal ions [9]. Surface precipitation involves forming an additional thin layer of nanomaterials such as the metal-organic frameworks (MOFs) on the membrane surface, which is often fortified by on-site polymerization. For instance, Shen et al. precipitated a mixture of polyethyleneimine (PEI) and NH_2-MIL-88B(Fe) MOFs on PVDF membranes, which was followed by grafting perfluoroalkyl poly ethoxy acetic acid through a condensation reaction. The modified membranes exhibited a significant sevenfold increase in permeate flux compared to PVDF membranes in oil/water separation [10]. Abdolmaleki et al. achieved a 900% permeate flux increase and 50% to 90% flux recovery rate improvement by blending PVDF with sulfonated polyether sulfone (PES) and subsequent grafting of hyperbranched polyethyleneimine onto the sulfonyl group of sulfonated PES after membrane fabrication. [11]. Yue et al. achieved self-cleaning ability and improved flux recovery ratio (FRR) through precipitating and crosslinking sodium alginate onto the PVDF membrane matrix to create a crosslinked layer with pH-dependent porosity [12]. Zheng et al. achieved surface immobilization of Cu-MOF-74 using polymerized dopamine [13]. The grafting method usually requires pretreatment to activate the PVDF molecule so that it can react with other modifying reagents. The pretreatment for grafting includes plasma treatment, UV light treatment, and chemical

treatments. For instance, Al-Gharabli et al. activated PVDF membranes using acidic or alkaline H_2O_2 solutions, followed by grafting amino-functionalized silane and carbon nanotubes (CNTs) [14]. Kamaz et al. treated PVDF membranes with NaOH aqueous solution and acidic $KMnO_4$ aqueous solution, followed by grafting benzophenone (hydrophilic polymers) through UV light [15].

PVDF is a chemically inert polymer containing C-C, C-H, and C-F bonds that are difficult to react with other materials and therefore, need activation for effective chemical modification of PVDF membrane surface. Pretreatment such as plasma [16], [17], UV irradiation [18], [19], [20], [21], and in particular chemical treatment [14], [15] have been the most common approaches used to activate the PVDF membranes. Chemical reagents used for the activation of PVDF membranes are the mixture of hydrogen peroxide and sulfuric acid or ammonium hydroxide [22], $KMnO_4$ and alkaline aqueous solution [15].

Most alkaline treatments of PVDF membranes [10], [15], [23], [24], [25] were executed in the aqueous solution, which requires a high alkaline concentration (8 M or higher), high treatment temperature (about 80℃) and long contact time, rendering it high chemical costs, the requirement of high chemical resistant equipment, and long residence time. For instance, Ross et al. [26] reported that the content of fluorine did not have a significant change in the first 4 hours when using 12 M NaOH aqueous solution to treat PVDF membranes at 80℃. The fluorine content only had a noticeable reduction when the treatment time was over 8 hours. Alternatively, alkaline treatment by the isopropanol solution of potassium hydroxide has been shown to work quite effectively at low temperatures, low alkaline concentrations, and short treatment times [23] [26], suggesting its potential to become a cost-effective approach for PVDF membrane activation. In this study, we systematically investigated the effects of temperature on the effectiveness of treating PVDF membranes with potassium hydroxide in the isopropanol solution for

activation. Data indicate that the treatment successfully caused defluorination and introduced charged groups onto the membrane surface by replacing fluorine with -OH or -COOH. The filtration of polyacrylic acid (PAA), polyethylene oxide (PEO) casein, and whey protein solutions by the activated PVDF membranes were also tested.

3.2. Experimental

3.2.1. Materials

PVDF, Kynar® 740 (Pellet, M_w = 410 kDa), kindly supplied by Arkema Inc. (Philadelphia, PA) was used in this experiment as the host polymers. The pore former agent polyethylene glycol (PEG) (M_w = 1 kDa) was purchased from Sigma-Aldrich Inc. (St. Louis, MO). Anhydrous *N*, *N*-dimethylacetamide (DMAc) with a purity of 99.8%, potassium hydroxide, and isopropanol with a purity of 99.5% were purchased from Sigma-Aldrich Inc. (St. Louis, MO). The PAA (M_w = 100 kDa), PEO (M_w = 100 kDa), casein protein, and whey protein for filtration were purchased from Sigma-Aldrich Inc. (St. Louis, MO). Barium chloride with a purity of 99.9%, hydrochloric acid, iodine, and potassium iodide for PEO concentration analysis was purchased from Sigma-Aldrich Inc. (St. Louis, MO). The Bradford Reagent for whey and casein protein analysis was purchased from Sigma-Aldrich Inc. (St. Louis, MO). The PAA (M_w = 450 kDa), and potassium nitrate for surface zeta potential measurement were purchased from Sigma-Aldrich Inc. (St. Louis, MO).

3.2.2. Membrane fabrication

In this research, the PVDF membranes were prepared using the non-solvent induced phase separation (NIPS) method. The cast solution was created by mixing 15 wt% of PVDF, 3 wt% of PEG, and 82 wt% of DMAc in a shaker at 180 rpm and 60°C for 24 hours.

Afterward, the resulting mixture was cooled to room temperature before casting the membranes. The mixture solution was then cast onto a glass plate using a uniform-speed automatic film applicator (model AFA-II, Beijing, China) to achieve a thickness of 100 μm. Before immersion, the cast film was left exposed to air for 1 minute to enhance uniformity. Subsequently, the film was immersed in distilled water at 25℃ along with a glass plate, initiating the phase inversion process. Following this, the membrane was carefully peeled off the glass plate and left in the water bath for 24 hours. The water in the bath was replaced every 6 hours to ensure the complete removal of residual PEG and DMAc. To prevent damage from water pervaporation, the wet membrane was washed three times with ethanol before being dried and stored at room temperature. After this step, the membranes were dried by air sweeping at room temperature for another 24 hours before being subjected to subsequent modifications and testing.

3.2.3. Alkaline modification of PVDF membranes

Firstly, the PVDF membranes were washed twice with deionized (DI) water and twice with ethanol. Subsequently, the membranes were dried at room temperature for 2 hours to eliminate residual ethanol before the modification process. Next, the PVDF membrane was immersed in a 0.5 M KOH isopropanol solution at various temperatures for 1 minute. Due to the thin and porous structure of the PVDF membrane used for alkaline treatment, it is highly susceptible to being quickly wetted by isopropanol and the modification reactions took place rapidly. When the PVDF membrane was immersed in the alkaline solution, the temperature within the membrane rapidly reached that of the solution. For instance, when treating the PVDF membrane with a 60℃ alkaline solution, the membrane's color changed from white to dark brown within 2 seconds. Nevertheless, given that the membrane matrix temperature could be remarkably different from the pretreatment temperature, pre-heating of membranes is recommended for future studies. After the alkaline treatment, the

membrane was rapidly transferred to 5℃ isopropanol, which quickly lowered the membrane's temperature and halted the reaction. The treatment temperatures used were 10℃, 20℃, 30℃, 40℃, 50℃, and 60℃, and they were labeled as Alk10, Alk20, Alk30, Alk40, Alk50, and Alk60, respectively. Following the modification step, the membranes were again washed twice with ethanol and twice with DI water to remove any residual chemicals. After this, the modified membranes were left to dry at room temperature for 24 hours in preparation for the subsequent tests.

3.2.4. Membrane filtration

The filtration performance of both the PVDF membranes and the alkaline-modified membranes was evaluated using the dead-end filtration setup, as described in our previous research [28]. The setup for dead-end filtration is shown in Figure 3.1. Here is a brief overview of the setup and procedure: (1) Setup: The membrane was positioned at the bottom of the feed chamber, which contains 200 mL of the respective feed solution. The effective area of the membranes used in the experiment is 0.00159 m^2. Filtration was conducted under a pressure of 60 psig (4.14 bar), supplied by nitrogen gas from a nitrogen cylinder. The entire process was carried out at room temperature. (2) Feed Solutions: Four different solutions were subjected to filtration, namely PAA, PEO, casein protein, and whey protein solutions. Each feed solution has a concentration of 100 ppm. (3) pH Adjustment: Since casein protein has limited solubility in DI water at pH 6, the pH of feed solution was adjusted to 10 using NaOH solution and HNO_3 before filtration test. To ensure that filtration tests for different substances are conducted under the same conditions, the pH of whey protein, PAA, and PEO solutions was also adjusted to 10 using the same method. (4) Pre-filtration: To enhance the accuracy of the experiment, an initial 10 mL of permeate is discarded before sample collection. All filtration tests were carried out in triplicate using three new coupons fabricated from different batches. The flux of the membranes is

calculated using Equation (3-1) in the following.

$$Flux = \frac{v}{t \cdot A} \tag{3-1}$$

Where v is the volume (L) of the permeate collected during the time t (hour) and the A is the effective area of the membranes (m^2).

The polymer salt rejection and the protein rejection R were calculated by the Equation (3-2) below:

$$R = \frac{c_f - c_p}{c_f} \times 100\% \tag{3-2}$$

Where c_f and c_p are the concentration of the feed and permeate, respectively.

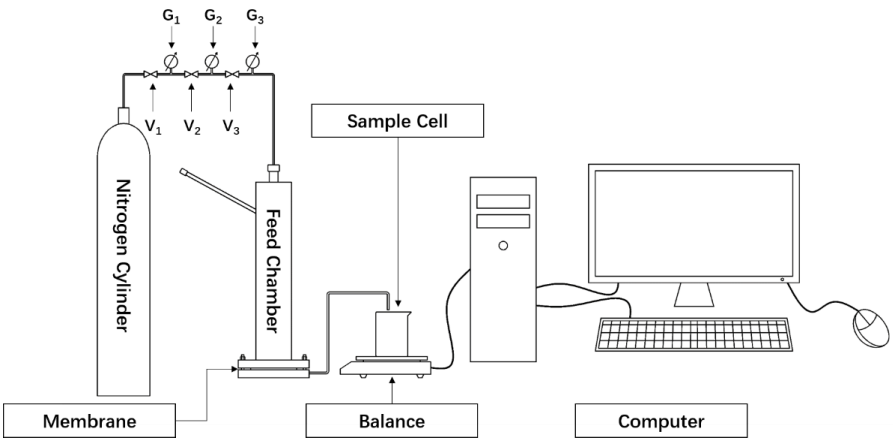

Figure 3.1 Setup for dead-end filtration [28].

In this research, the concentrations of various components in the feed and samples were determined using UV-Vis spectrophotometry. The specific methods for each component are as follows: (a) PAA Concentration Measurement: The UV light absorption at 205 nm of standard solutions containing 20, 40, 60, 80, and 100 ppm PAA was measured to create a standard curve. The UV light absorption of the samples at 205 nm was then measured.

The PAA concentration in the samples was calculated by fitting the sample's UV light absorption data into the standard curve. (b) PEO Concentration Measurement: The permeate samples containing PEO were diluted 10 times with DI water. To 0.8 mL of the diluted samples, 0.1 mL of a barium chloride solution (5wt% $BaCl_2$ solution containing 1 M HCl) and 0.1 mL of an iodine solution (solution containing 1.3wt% I and 5 wt% KI) were added. The mixture was gently shaken and stood still for 15 minutes. The UV light absorption of the mixture at 535 nm was measured using the UV-Vis spectrophotometer. A standard curve of light absorption versus PEO concentration was generated by measuring the absorption intensity at 535 nm of the feed with various dilution ratios using the same method. The concentration of PEO in the samples was calculated by comparing the UV light absorption at 535 nm of the samples with the standard curve. (c) Casein and whey protein concentration measurement: A permeate sample, 0.5 mL of the permeate sample was mixed with 0.5 mL of Bradford Reagent and stood still for 15 minutes. The UV light absorption of the mixture solution at 595 nm was measured using the UV-Vis spectrophotometer. A standard curve was generated by measuring the UV absorption of the standard bovine serum albumin (BSA) solutions of various concentrations following the same method. The protein concentration in the samples was calculated by fitting the UV absorption data of the samples into the standard curve.

3.2.5. Membrane characterization

ATR-FTIR

The functional groups of the membrane's surface were determined by the attenuated total reflectance-Fourier transform infrared (ATR-FTIR) using the Agilent Tech-Cary 630 (Agilent, Canada) spectrometer. The membrane samples were washed with DI water and dried before the measurement.

XPS

The surface properties of the PVDF and alkaline-modified membranes, including the elemental composition ratio, and functional groups, were quantified by X-ray photoelectron spectroscopy (XPS) using an Al X-ray source on a Kratos Axis Nova spectrometer (Kratos Analytical, Ltd., UK). According to XPS data, the degree of substitution, $DOS_i\%$, of fluorine was calculated by the following equation:

$$DOS_i\% = \frac{(F_0 - F_i)}{F_i} \times 100\% \quad (3\text{-}3)$$

Where F_0 is the elemental content of fluorine at the surface of the base membrane, and $DOS_i\%$ and F_i are the degree of substitution and the elemental content of fluorine at the surface of the membrane treated at i°C (i = 20, 40, and 60), respectively.

SEM

The morphology of the membrane's top surface and cross-section was investigated using scanning electron microscopy (SEM) (JSM-7500F FESEM, JEOL, Japan). An accelerating voltage of 3 kV and a working distance of 10 mm was utilized. To generate the cross-sectional image of the membranes, the samples were immersed in liquid nitrogen for 1 minute and then carefully stretched with tweezers to induce fracture. To prepare the samples for SEM analysis, the surface or cross-section of each membrane was coated with a 10 nm layer of gold-palladium using a low vacuum coater (Leica EM ACE200, Germany). Subsequently, the surface porosity, average pore size, maximum pore size, and pore number density were analyzed using the software Image J. The pore size here is the diameter of the pore.

Contact angle

The water contact angle of the membranes was measured by the sessile method using the VCA Optima Surface Analysis System (AST Product, Inc. Billerica, MA, US) at 25℃. 1 μL deionized water droplet was placed on the surface of the dry membrane to measure the contact angle. The measurement was made at 5 random spots of the membrane surface and the average value was reported.

Bulk porosity

The porosity of the membrane was measured by the wet-dry method [29]. Briefly, the membrane was cut into three 1x1 cm^2 square samples and the thickness of each sample was measured by a Vernier caliper. Then, the sample was immersed in n-butanol for 24 h, ensuring that n-butanol completely wetted the membrane pores. N-butanol on the surface of the membrane sample was wiped by a rubber scraper, followed by weighing the wet membrane sample. After drying the membrane sample in an oven for 24 h at 50℃ to completely evaporate the n-butanol, the dry sample was weighed. The overall porosity of membranes can be calculated by the following equation.

$$\varepsilon = \frac{w_w - w_d}{A_{sample} \cdot l \cdot \rho_{butanol}} \quad (3\text{-}4)$$

Where ε is the bulk porosity, w_w and w_d are the weight (g) of the wet membrane sample and the weight (g) of the membrane sample after drying, respectively. A_{sample} is the area of the membrane sample (cm^2), l is the thickness (cm) of the dry membrane sample and $\rho_{butanol}$ is the density ($g \cdot cm^{-3}$) of n-butanol. Three samples were used for the measurement and the average value was reported.

Surface Zeta potential

The surface charge property of the PVDF and alkaline treated membranes was analyzed by the surface zeta potential test, using the surface Zeta potential cell (ZEN1020) which is the accessory kit for the Zetasizer Nano Z (Malvern Panalytical, Worcestershire, UK). First, a membrane sample was cut into size 3x5 mm^2 and glued to the sample holder with double-sided tape. Then the sample was put into the sample cuvette (DTS0012) containing 1 mL electrolytic solution (1 mM KNO_3 aqueous solution containing 0.5 wt% of PAA with a molecular weight of 450 kDa as tracer particles) with varied pH values (pH 2.6 to 11.2). The pH of the electrolytic solution was controlled by adding 5 wt% HNO_3 or 0.5 M KOH solution.

3.3. Results and discussion

3.3.1. Membrane characterization

Effect on surface hydrophilicity of membranes

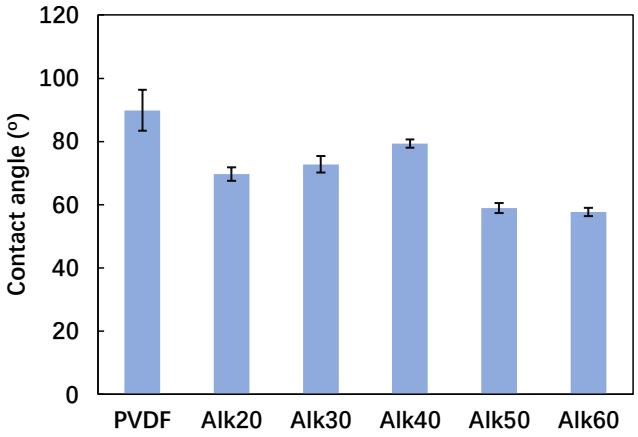

Figure 3.2 Contact angle of the PVDF membranes and alkaline treated membranes at different temperatures.

Figure 3.2 shows the contact angle of the PVDF membranes and the alkaline-treated membranes at different temperatures. The contact angle of the PVDF membranes was found to be 89.9°, indicating their hydrophobic nature. However, after alkaline treatment, the membranes exhibited an increased tendency towards hydrophilicity, leading to a decrease in the contact angle. The membranes tend to be more hydrophilic when treating temperature increases from 20℃ to 60℃. The contact angle reduces obviously when the treating temperature increases from 40℃ to 50℃. Continually increase the treating temperature to 60℃, and the contact angle slightly decreases to 57.7°. The observed increase in hydrophilicity can be attributed to the replacement of hydrogen and fluorine atoms on the PVDF molecules at the membrane surface with hydrophilic hydroxyl and carbonyl groups during the alkaline treatment. This chemical transformation enhances the membrane's hydrophilic properties and consequently lowers the contact angle. XPS data (Figure 3.5) that will be shown later indeed confirmed the replacement of some fluorine and hydrogen atoms by hydroxyl and carboxyl groups on the membrane surface. The rates of these reactions were influenced to different extents by changes in temperature, highlighting the significance of temperature as a crucial factor affecting the reaction kinetics.

Effect on surface zeta potential of membranes

Figure 3.3 illustrates the surface Zeta potential of PVDF membranes and the Alk20, Alk40, and Alk60 membranes at various pH levels ranging from pH 2.6 to pH 11.5. The surface Zeta potential of the PVDF membrane decreased from -5.4 mV at pH 2.6 to -42.2 mV at pH 6.3, after which it remained relatively constant. When comparing the surface Zeta potentials of different membranes at the same temperature, the order of the observed was PVDF ≈ Alk20 ≈ Alk40 > Alk60. As an example, at pH 10.0, which is within the level-off regime, the surface Zeta potentials for the membranes were -44.1 mV, -42.4 mV, -41.7 mV,

and -64.2 mV for PVDF, Alk20, Alk40, and Alk60, respectively. One plausible reason for the rise in negative Zeta potential on the membrane surface after alkaline treatment is the formation of more negatively charged functional groups (such as -OH) within the membrane matrix following exposure to an alkaline solution, which will be discussed in section 3.3.1. This indicates that the surface zeta potential of the membrane is significantly reduced only at higher treatment temperatures. Importantly, it is worth noting that membranes with lower surface Zeta potential exhibit lower contact angles, suggesting that the functional groups responsible for the high surface potential also enhance the hydrophilicity of the membranes.

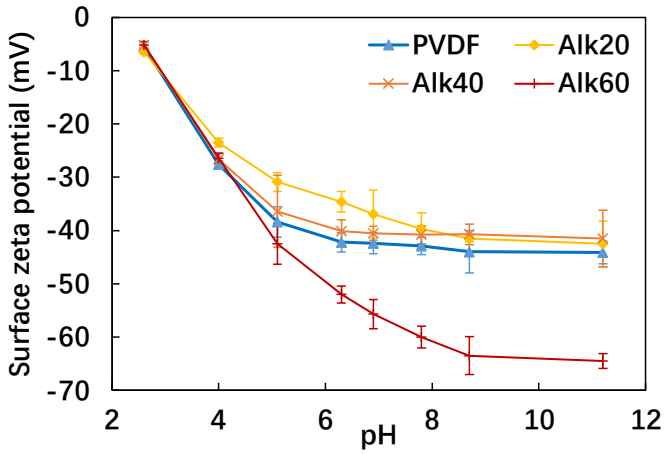

Figure 3.3 Surface zeta potential of the PVDF membranes and alkaline treated membranes at different treating temperatures, Alk20, Alk40, and Alk60 represent alkaline treatment at 20℃, 40℃, and 60℃ respectively.

Effect on the surface chemistry of the membranes

Figure 3.4 shows the FTIR spectra of the PVDF membrane and the alkaline-treated membranes, labeled as base, Alk20, Alk40, and Alk60, corresponding to PVDF membranes and the membranes treated at 20℃, 40℃, and 60℃, respectively. All the membranes exhibit double absorbance peaks at 840 cm^{-1} and 875 cm^{-1}, attributed to C-C backbone vibrations, a broad peak at 1180 cm^{-1} resulting from C-F bond stretching vibrations, and a

peak at 1400 cm^{-1} related to the asymmetrical bending vibration of C-H bonds. Following alkaline treatment, the membranes' surface changes from white to brown, indicating the occurrence of chemical reactions at the membrane's surface. However, no new peaks appear or disappear during alkaline treatment at 20℃ or 40℃. While FTIR did not detect the peaks of functional groups generated during alkaline treatment, XPS analysis, discussed in the following section, confirms the formation of new functional groups. The lack of detection in FTIR may be attributed to the instrument's sensitivity, which might not be sufficient to identify the newly formed chemical groups. Raising the treatment temperature to 60℃ results in the appearance of new peaks in the FTIR spectra, which are the peaks at 1580 cm^{-1}, 1650 cm^{-1}, and a broad peak at 3300 cm^{-1}. These are attributed to the C=C bond stretching vibration, the C=O bond stretching vibration, and the O-H stretching vibration, respectively. This observation suggests the formation of carbon-carbon double bonds, carboxyl groups, and hydroxyl groups after the 60℃ alkaline treatments.

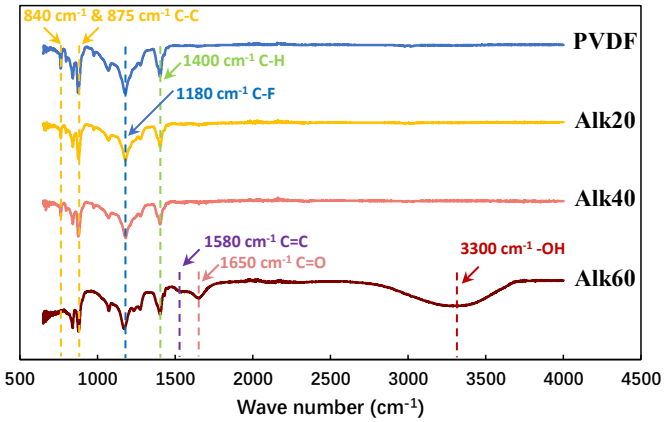

Figure 3.4 FTIR spectrum of the PVDF membranes and alkaline treated membranes at different treating temperatures, Alk20, Alk40, and Alk60 represent alkaline treated at 20℃, 40℃, and 60℃ respectively.

Table 3.1 presents the elemental composition and DOS value of the PVDF membrane and the alkaline-modified membranes, based on the XPS analysis. As the treating temperature increased, the extent of alkaline treatment also increased, resulting in a reduction of

fluorine (F) content from 45.11 at.% in the PVDF membrane to 29.92 at.% in the membrane treated at 60℃. Correspondingly, the DOS value of the film rose to 50.77%, meaning that more than half of the fluorine atoms were substituted. Conversely, the oxygen (O) content on the membrane surface increased from 0.74 at.% in the PVDF membrane to 6.18 at.% in the membrane treated at 60℃. These findings suggest that the significant number of fluorine (F) atoms on the membrane surface were replaced by oxygen-containing functional groups, likely the hydroxyl group (-OH) and the carboxyl group (-COOH). Additionally, the data also revealed that with the decrease of fluorine (F) from the membrane, the carbon (C) atoms have not been removed in large quantities, leading to an increase in surface carbon content from 54.15 at.% in the base membrane to 63.89 at.% in the membrane treated at 60℃. These changes indicate the successful incorporation of oxygen-containing functional groups and the subsequent increase in carbon content, demonstrating the effectiveness of the alkaline treatment process.

Table 3.1 Effect of temperature on membrane surface elemental composition and the DOS.

Element	PVDF (at.%)	Alk20 (at.%)	Alk40 (at.%)	Alk60 (at.%)
C 1s	54.15	57.88	60.19	63.89
O 1s	0.74	2.83	4.12	6.18
F 1s	45.11	39.29	35.69	29.92
DOS_i	0.00	14.81	26.39	50.77

Figure 3.5 shows the XPS spectrum of PVDF membranes and the membranes treated with the alkaline solution at various temperatures. Table 3.2 lists the functional group composition of the surface of PVDF membranes and alkaline-treated membranes. There are two peaks of strong intensity in the C 1s spectrum, the C-C peak (284.8 eV) and the C-F_2 peak (289.3 eV). In addition, the presence of C-OH groups (285.2 eV for C 1s, 531.6 eV for O 1s) and C-O-C groups (529.6 eV) was detected in the PVDF membrane. This could be attributed to the residual pore-forming agent (PEG) we used in membrane

fabrication. The sample also contained a small number of C-F_3 groups (687.6 eV) and C-HF clusters (686 eV), which could be attributed to either measurement error or defective PVDF molecules in the membranes, or both.

Table 3.2 Composition of functional groups of PVDF and alkaline modified membranes related with C 1s, O 1s, and F 1s.

Element	Core level	Bond	Binding energy (eV)	Functional group composition (at.%)			
				PVDF	Alk20	Alk40	Alk60
C	1s	C=C	283.5	/	11.5	11.4	11.9
		C-C	284.8	41.8	43.6	46.8	50.0
		CH_3	284.1	11.2	/	/	/
		C-OH	285.2	/	0.9	1.3	0.8
		C=O	286.4	0.6	2.1	2.9	5.3
		C-HF	287.8	6.2	3.1	6.1	5.7
		C-F_2	289.3	37.7	37.7	27.9	22.6
		CF_3	290.0	2.3	1.0	2.3	1.5
	sp^3	C-C sp^3	291.9	/	/	1.1	1.6
	1s	K^+ ions absorb	294.6	/	/	0.3	0.6
O	1s	C-O-C	529.5	16.0	/	/	/
		C=O	530.1	/	31.1	30.1	13.7
		C-OH	531.6	84.0	68.9	69.9	86.3
F	1s	C-HF	685.7	13.5	7.5	16.7	19.1
		C-F_2	686.3	81.6	90.2	76.9	75.8
		C-F_3	687.5	4.9	2.4	6.4	5.0

After alkaline treatment, the content of C-F_2 decreased, and the decrease in C-F_2 content increased significantly with increasing treatment temperature. However, the C-F_3 and C-HF content did not show significant changes. The mechanism of the alkaline treating process of PVDF has been previously reported and different views exist on the subsequent reactions. Some researchers suggested that hydroxide ions deprotonate the -CH_2- structure in the PVDF molecule, forming a -CF_2-CH^-- structure. Subsequently, the -CH^-- causes the adjacent -CF_2- to lose a fluorine (F) atom and reacts with a water molecule to form a -CHF-CHOH- structure when the PVDF membranes are treated with KOH or NaOH aqueous

solutions [25], [30]. On the other hand, other researchers propose that -CH$^-$-causes the adjacent -CF_2- to lose a fluorine atom, resulting in a -CH=CF- structure. The -CH=CF- then reacts with the hydroxide to form -CH$^-$-CFOH- [23], [26], [27], [31], [32].

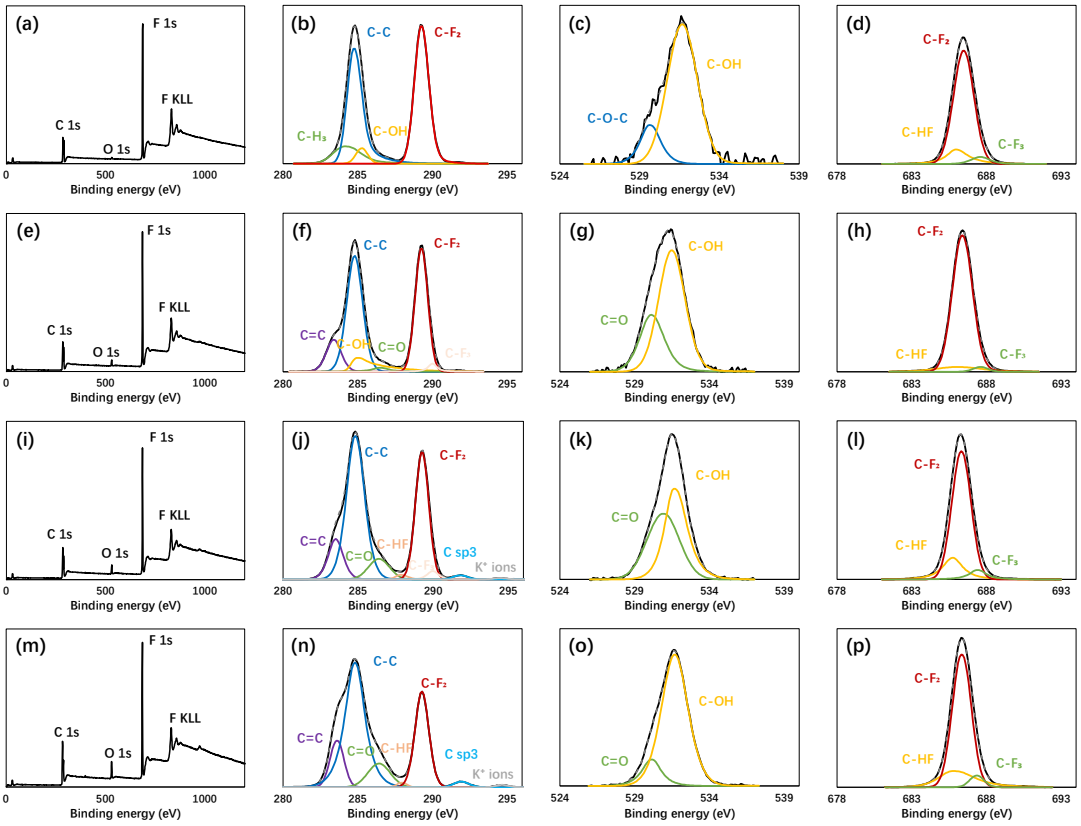

Figure 3.5 XPS survey spectra, C 1s peaks, O 1s peaks, and F 1s peaks of PVDF membranes, i.e., (a), (b), (c), and (d), respectively; of membranes treated at 20°C, i.e., (e), (f), (g) and (h), respectively; at 40°C, i.e., (i), (j), (k) and (l), respectively; at 60°C, i.e., (m), (n), (o) and (p), respectively.

In our research, the content of C-HF bonds did not show significant changes after alkaline treatment, indicating that the -CH=COH- or -CH$^-$-CFOH- structures were formed, rather than the -CHF-CHOH- structure. At the same time, the alkaline treatment introduced C-OH bonds (285.2 eV), C=O bonds (286.4 eV), and C=C bonds (283.5 eV). In a word, the defluorination process of PVDF molecules is divided into three steps, which are described by Equations (3-5), (3-6) and (3-7). The first step is that OH^- deprotonates -CH_2- to form a negatively charged -CH$^-$- structure. Then -CH$^-$-will remove a fluorine atom from adjacent

-CF_2- to form -CH=CF-. Finally, part of -CH=CF- undergoes an addition reaction with water molecules to form a -CH_2-CFOH- structure. As the degree of defluorination further increases, -CH_2-CFOH- is kept deprotonated by OH^- to form -CH^--CFOH-, which then defluorinated to form an unstable -CH=COH- structure. Subsequently the -CH=COH- rearranges into a -CH_2-CO- structure, as Equations (3-8), (3-9) and (3-10) are shown. After alkaline treatment, the content of C=C bonds significantly increased, rising from 0% in the PVDF membrane to 11.5% in the membrane treated at 20°C. However, further increases in treatment temperature had little effect on the content of C=C bonds. The content of C=O bonds linearly increased with increasing treatment temperature, and the C-OH bonds reached their maximum when the treatment temperature was 40°C. The ratio of C-OH bonds to C=O bonds was 0.45, 0.43, and 0.16 for treatment temperatures of 20°C, 40°C, and 60°C, respectively, indicating that higher treatment temperatures favored the formation of C=O bonds.

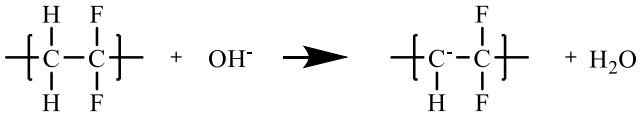

(3-5)

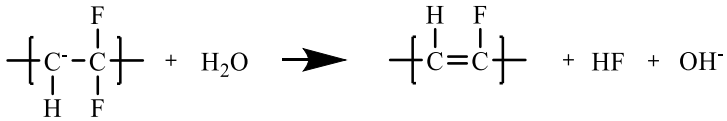

(3-6)

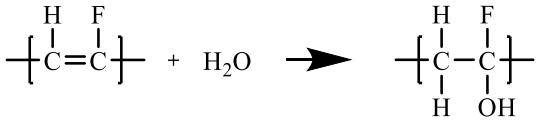

(3-7)

When the treatment temperature reached 40°C, the peaks of K^+ (294.6 eV) and C-C sp^3 (291.9 eV) appeared, and their intensity increased with increasing temperature. Despite thorough washing of the samples before testing, these K^+ ions were adsorbed on the membrane surface by negatively charged functional groups during the treatment of the PVDF membrane with KOH solution. Moreover, as the degree of alkaline treatment

increased, more K^+ ions were adsorbed on the membrane, indicating an increase in the number of negatively charged functional groups on the membrane surface that leads to a stronger surface charge. Consequently, more K^+ ions were adsorbed, and due to the strong electrostatic interaction, it was difficult to remove them by washing.

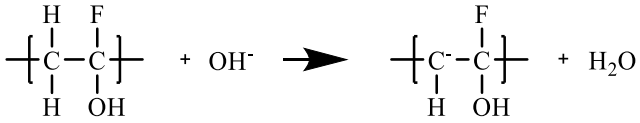

(3-8)

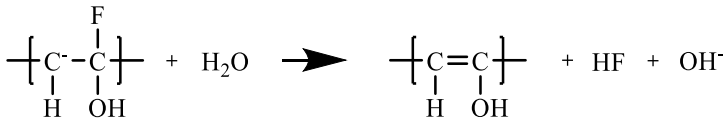

(3-9)

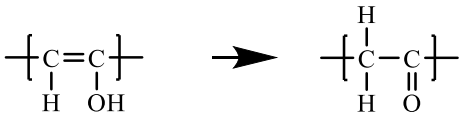

(3-10)

In addition, the decrease in surface zeta potential of the membranes is related to the ratio of -OH groups to -C=O groups on the surface. The ratios of -OH (531.6 eV) and -C=O (530.1 eV) on the surface of Alk20 and Alk40 membranes are 68.9:31.1 and 69.9:30.1 respectively. However, this ratio is 86.3:13.7 on the surface Alk60 membranes, which indicates the amount of -OH groups significant increase. The surface zeta potential of the corresponding membranes dropped from around -42 mV to -64.2 mV at pH 10. This shows that the surface zeta potential of the membrane is related to the -OH groups content on the membrane surface.

SEM and porosity

Figure 3.6 shows the SEM cross-sectional images of the PVDF membrane and the membrane treated at 60°C. They were very similar to each other being composed of a finger-like layer and a sponge-like layer, which is typical of microporous PVDF

membranes [29], [33]. These micrographs show that after alkaline treatment, alkaline treatment has no significant effect on the morphology of the finger-like layer or sponge-like layer. The skin layer at the top of the MF or UF membrane acts as the selective layer with fine pores. The thickness of the skin layer was estimated by analyzing the cross-sectional SEM image of the membranes using Image-J software to be approximately 0.3 μm. This was compatible with the literature data, which are typically in the range of 0.2-3.0 μm [34].

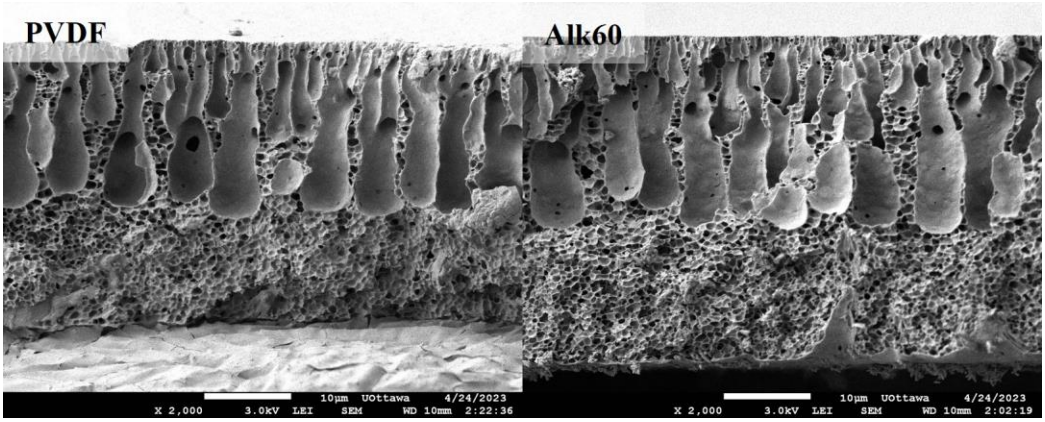

Figure 3.6 Cross-sectional SEM images of the PVDF membranes and the membrane alkaline treated at 60°C.

Table 3.3 lists the bulk porosity, surface porosity, maximum pore size, average pore size, and the pore numbers density of the PVDF membranes and the alkaline-treated membranes at different 20°C, 40°C, and 60°C. The analysis excluded pores with an area less than 500 nm^2, focusing on those with a diameter larger than 25nm. The terms "new" and "used" refer to measurements conducted before and after a whey filtration test, respectively. At treating temperatures of 20°C and 40°C, the bulk porosity of the membrane matrix is approximately 79%, which is nearly the same as the PVDF membranes. However, the porosity of the membranes slightly decreases from 79% to 71% when treated with 60°C alkaline solutions. This minor difference may be attributed to experimental errors. The surface porosity of the membranes increased with treatment temperature, which was 2.0%, 2.1%, 2.6%, and 2.9%

for the base membrane, Alk20, Alk40, and Alk60 respectively.

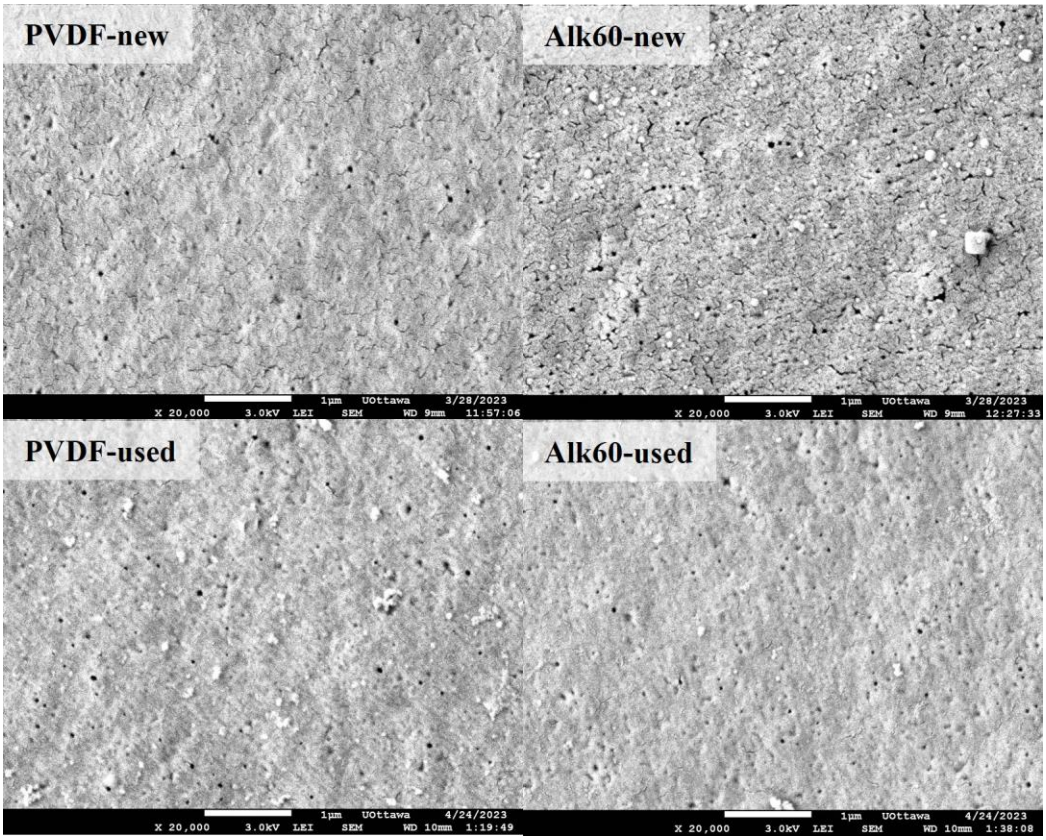

Figure 3.7 Surface SEM images of the PVDF membranes and the membranes alkaline-treated at different temperatures; Alk20, Alk40, and Alk60 represent alkaline treatment at 20°C, 40°C and 60°C respectively; new and used represent the membranes before and after whey filtration respectively.

Notably, all alkaline-treated membranes exhibited higher surface porosity than the PVDF membrane, and the surface porosity increased incrementally with the increase of treatment temperature. The surface porosity is defined as the proportion of membrane surface area occupied by pores. Meanwhile, as shown in Table 3.3, the maximum pore diameter and average pore diameter of different membranes were nearly the same with some exceptions, which were 80 nm and 40 nm for maximum and average diameter, respectively. The surface pore number density was approximately the same for the base membranes and the membranes treated at 20°C and 40°C, at around 12.6 per μm^2. While the pore number density increased to 19.1 per μm^2 when the membranes were treated at 60°C, this is most

likely an outliner since it is unlikely that the alkaline treatment could etch the skin of the membrane to generate new pores.

Table 3.3 Bulk porosity, surface porosity, the maximum, average pore size, and surface pore number density of PVDF membranes and alkaline treated membranes at different temperatures; Alk20, Alk40, and Alk60 represent alkaline treated at 20°C, 40°C and 60°C respectively; new and used represent the membranes before and after whey filtration respectively. (Note: Only data for new membranes is presented in the table for bulk porosity.)

Membrane	Bulk porosity (%)	Surface porosity (%)	Max pore diameter (nm)	Average pore diameter (nm)	Pore number density (pores per·μm^2)
PVDF-new	79±1.3	2.0±0.15	71.4±3.7	40.3±0.5	13.0±0.25
Alk20-new	79±0.8	2.1±0.07	71.4±4.2	37.4±0.2	12.9±0.52
Alk40-new	80±0.6	2.6±0.21	87.4±1.6	46.0±1.3	12.6±0.31
Alk60-new	71±1.1	2.9±0.06	71.4±2.7	39.2±0.8	19.1±0.44
PVDF-used	NA	1.8±0.08	79.8±2.3	42.4±1.3	12.9±0.21
Alk20-used	NA	2.0±0.04	71.4±3.9	45.1±0.7	12.7±0.51
Alk40-used	NA	2.3±0.11	71.4±1.5	38.3±0.9	21.5±0.32
Alk60-used	NA	2.5±0.13	71.4±0.9	39.0±0.4	23.4±0.11

Comparing the micrographs of different new membranes (membranes before any filtration tests) shown in Figure 3.7, it can be observed that the edges of the pores become blurred after the filtration test. As presented in Table 3.3, while the bulk porosity and maximum pore size of all the membranes were similar for all temperatures, except for a few outliers, the surface porosity of the treated membranes increased with temperature significantly. Specifically, the surface porosity of the base membrane was 2.0%, while that of the membranes treated at 20°C, 40°C, and 60°C were 2.1%, 2.6%, and 2.9%, respectively. These values correspond to increases of 5%, 30%, and 45% over the base membrane, respectively. These findings suggest that while the treatment did not substantially change the bulk structure of the membrane, it effectively modified the surface properties of the membrane. Even though the potassium hydroxide solution in isopropanol solution could penetrate the membrane pores, it did not significantly alter the overall membrane structure.

However, it led to noticeable changes in the surface properties, resulting in increased surface porosity.

Comparing the micrographs of the same membranes before and after whey protein filtration tests, as shown in Figure 3.7, the edges of the pores become blurred after the filtration test. This observation aligns with the slight decrease in surface porosity after filtration (Table 3.3). These findings suggest that, after filtration, some proteins remained adsorbed in the membrane pores, indicating that rinsing with deionized water was insufficient to completely remove the adsorbed proteins. Furthermore, the pore density of the Alk40 and Alk60 increased by 70.1% (21.5 per μm^2) and 22.6% (23.4 per μm^2), respectively. This implies that the transmembrane pressure might have caused irreversible deformation of the membrane pores during the filtration process. Consequently, some originally small membrane pores were enlarged enough to be detected by SEM, resulting in a higher number density of detectable membrane pores. Simultaneously, due to the blockage of larger membrane pores by proteins during the filtration process, although the number density of membrane pores increased, the surface porosity decreased. However, it is worth noting that the surface porosity and the maximum and average pore sizes of the same membranes were not significantly affected by the filtration, except for a couple of outliers. This indicates that the overall structure of the membranes remained relatively unchanged after the filtration process, with the observed alterations primarily confined to the surface properties and pore edges.

3.3.2. Rejection of charged and noncharged macromolecules

The molecular weights of PAA and PEO used for filtration are both 100 kDa. However, their monomer molecular weights are 72 g/mol and 44 g/mol, respectively. As a result, PEO molecules form much longer chains than PAA molecules when they have the same

molecular weight. PAA is an anionic polymer due to the presence of negatively charged carboxyl groups, while PEO is a noncharged polymer at neutral pH as it lacks charged groups. There are four main types of casein proteins, namely α-s1 casein, α-s2 casein, β-casein, and κ-casein, with molecular weights ranging from 19 kDa to 25 kDa. Their isoelectric points fall between pH 4.1 and pH 5.8, indicating they carry a negative charge at pH 10 [35]. Whey proteins are composed of various types of proteins, including β-Lactoglobulin, α-Lactalbumin, proteose peptones, bovine serum albumins, and immunoglobulins. These proteins have a wide molecular weight distribution, ranging from 4.1 kDa to 1000 kDa, with the majority falling between 4.1 kDa and 40.8 kDa. Most of their isoelectric points are between pH 4.2 and pH 5.3. Importantly, all of these proteins have isoelectric points below pH 10, and therefore carry negative charges at pH 10 as well [36].

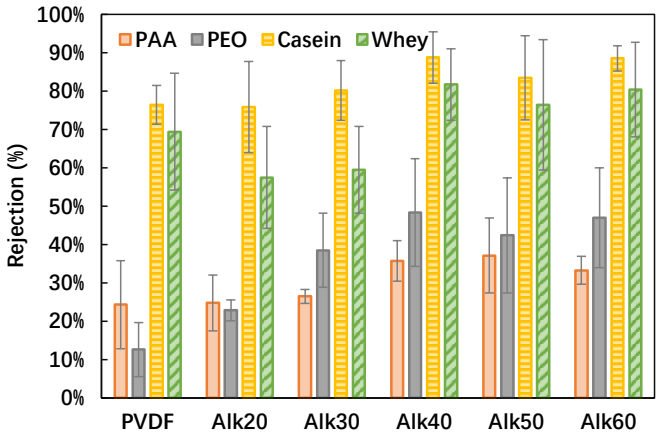

Figure 3.8 Rejection of the PVDF membranes and alkaline treated membranes (Alk20, Alk30, Alk40, Alk50, and Alk60) at different treating temperatures in PAA, PEO, Casein protein, and whey protein filtration. (The pH of the feed solution for PAA, PEO, casein protein, and whey protein filtrations is at pH 10.)

Figure 3.8 presents the rejection of two linear macromolecules, negatively charged PAA, and noncharged PEO, along with two different proteins, i.e., casein protein, and whey proteins, using various membranes. The data demonstrate that alkaline treatment enhances

the rejection of the four macromolecules and the rejection improvements increase with treatment temperature in the range of 20-40℃ and reach plateaus beyond 40℃. The only exception is the PVDF membrane for whey protein filtration, which has a rejection larger than that of the Alk20 and Alk30 membranes, which seems to be an outliner. Furthermore, this trend could be partially explained by the increase of the surface zeta potential of the membrane with the alkaline treatment temperature.

It is worth noting that the rejection of both proteins, which have tertiary structures due to the folding of peptide chains, is much larger than both the linear polymers, i.e., PAA and PEO, even though the molecular weights of the proteins are much smaller than the two linear molecules. These data suggest the effective diameter of macromolecules has a larger impact on their rejection by a given membrane than the molecular weight.

It is also of interest to compare the rejections of the two linear polymers. The PAA has a pendent carboxyl group for every two carbon atoms in the carbon chain, which is negatively charged in the buffer pH and therefore has a very high charge density. However, PAA has a rejection smaller than the noncharged PEO of the same molecular weight when the filtration of these two polymers is tested with the PVDF membrane. Furthermore, the alkaline treatment seems to have a greater impact on the PEO rejection compared to the PAA rejection. For example, the PEO rejection of PVDF membranes is 12.6%, but after alkaline treatment, it increases to 22.8% at 20℃ and plateaus at 48.4% at 40℃ and beyond. Whereas the PAA rejection of PVDF membranes is 24.3%, and after alkaline treatment, the PAA rejection is 24.5% at 20℃ and plateaus at approximately 37.1% at 40℃ and beyond. This indicates that the surface Zeta potential has a stronger influence on the rejection of the noncharged PEO rejection than the heavily charged PAA. These counterintuitive observations could be tentatively explained as follows.

While the PEO molecule does not have charged pendant functional groups, it still has partial negative charges due to the fact that the oxygen atom has a larger electronegativity (3.44) than the carbon atom (2.55) and there is one oxygen atom for every two carbon atoms in the PEO linear molecule. Furthermore, the PAA has a large pendant group of -COOH whereas PEO has no pendant group. According to the additivity rule [37], PAA has 0.35 nm^2 and PEO 0.27 nm^2 of cross-sectional area. Consequently, the PEO molecules would be substantially longer than the PAA molecules of the same molecular weight. Therefore, the long PEO molecules may form entanglements. On the other hand, the PAA molecules may not be able to form entanglements due to primarily the strong expelling forces between a large number of its negatively charged pendant carboxyl groups. In other words, the PEO may pass through the membrane pores as entanglements and the PAA as linear molecules. The entanglements of PEO would have a much larger diameter than its linear chain of PAA. Therefore, the electrostatic rejection by the negative charges on the pore walls of the membrane would be much stronger on the PEO entanglements than the PAA linear chain. This is because the electrostatic interaction between two charges increases quadratically as the distance decreases and linearly with the increase of the charge intensity. This reasoning is based on the hypothesis that the treatment of membranes with alkaline isopropanol solution also introduces charged groups to the pore walls. This is reasonable since the isopropanol solution could completely wet the membrane and therefore the reactions that lead to the substitution of fluorine and hydrogen atoms on the bulk membrane surface should also happen on the pore surface. Indeed, the mechanical strength of the membrane is significantly weakened by the treatment, indicating that the polymer chains are interrupted not only on the membrane surface but also in the membrane matrices.

The variation trend of casein rejection and whey protein rejection with treating temperature follows a similar pattern to that of PAA and PEO rejection discussed earlier. Between 20°C

and 40℃, the rejection of both casein and whey proteins increases with the rise in treatment temperature. However, once the treatment temperature exceeds 40℃, the rejection levels off, and further temperature increases do not lead to significant changes in rejection. For casein rejection, after alkaline treatment at temperatures above 40℃, there is a notable increase. The casein rejection of PVDF membranes is 76.4%, while after 40℃ alkaline treatments, it reaches 88.8%. On the other hand, for whey protein rejection, PVDF membranes have a rejection of 69.4%. After alkaline treatment at 20℃ or 30℃, the whey protein rejection decreases to 57.5% and 59.5%, respectively, both of which are lower than the rejection of PVDF membranes. However, when the treating temperature is 40℃, the whey protein rejection increases to 81.7%, higher than that of PVDF membranes. As discussed earlier, alkaline treatment increases the surface zeta potential of the membrane and generates new micropores while enlarging the size of the existing smaller pores. This results in some protein leakage. Since whey contains many small molecular proteins, such as protease peptones (molecular weight between 4.1 to 40.8 kDa) and glycomacropeptide (molecular weight of 7 kDa), as well as casein proteins with molecular weights between 19 and 25 kDa, the negative impact of this leakage on protein rejection is more significant than the positive impact of the membrane's surface zeta potential. Therefore, at 20℃ and 30℃ treatment temperatures, the whey protein rejection is lower than that of PVDF membranes. However, as the treatment temperature increases, the effect of the surface zeta potential becomes more pronounced, leading to an increase in whey protein rejection. In summary, the rejection behavior of casein and whey proteins with increasing alkaline treatment temperature is consistent with the trend observed for PAA and PEO rejection.

3.3.3. Flux

Figure 3.9 illustrates the flux of both PVDF membranes and alkaline-treated membranes. The pure water flux of the PVDF membranes was 107.4 LMH. However, the alkaline

treatment at all temperatures reduced the pure water flux of the membranes and the extent of flux decrease increased with treatment temperature, with the pure water flux being 70.2 LMH and 49.1 LMH at treating temperature 20℃ and 60℃, respectively. This result was unexpected considering the SEM image analysis, which indicated an increase in membrane surface porosity with the rise in treatment temperature. Typically, the pure water flux of a membrane increases with the growth of surface porosity. One possible explanation for the decrease in pure water flux after alkaline treatment is that it led to a reduction in the elasticity and mechanical strength of the membrane matrix. Consequently, under the applied pressure during filtration, the pores of the membrane may have undergone deformation and shrinkage, causing a decrease in pure water flux. This effect appeared to be more significant than the increase in flux expected from the rise in surface porosity. The shrinkage of PVDF membranes after alkaline treatment has been previously reported by [38].

Regarding the PAA flux, the PVDF membrane had a flux of 36.1 LMH. Except for the treatment at 20℃, which seemed to have no significant effect, all other alkaline-treated membranes exhibited a PAA flux smaller than that of the PVDF membrane. When the treating temperature increased from 20℃ to 40℃, the PAA flux continuously decreased from 38.5 LMH to 27.2 LMH, but then slightly increased to 29.5 LMH with 60℃ treatments. The increase in surface negative charge after alkaline treatment led to higher electrostatic interaction between the membranes and PAA molecules, resulting in an increased flow resistance for the PAA solution and a notable decrease in PAA flux. However, with the treating temperature increase, more pores were generated due to the etching by the alkaline solution, leading to an increase in surface porosity and a reduction in flow resistance. This decrease in flow resistance caused by the increased pore size dominated the flux behavior when the treating temperature increased from 40℃ to 60℃, resulting in a slight increase in PAA flux.

For the PEO flux, it initially decreased (20℃ to 30℃) and then increased (30℃ to 60℃) as the alkaline treatment temperature rose. The PEO flux of the alkaline-treated membranes was lower than the flux of the PVDF membranes, which was 20.5 LMH. The extent of the PEO flux decrease was less significant compared to the PAA flux decrease. This is because the molecular chain of PEO is longer than that of PAA, leading to higher viscosity for the PEO solution and higher flow resistance. Consequently, the resistance created by electrostatic interactions had a smaller effect on the overall flow resistance, resulting in a less pronounced decrease in PEO flux. Moreover, with the treating temperature increase, more micropores were formed on the membrane surface, leading to an increase in PEO flux when the treating temperature exceeded 30℃.

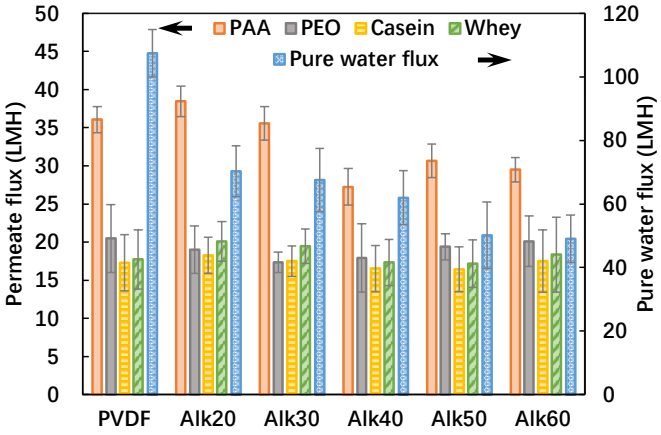

Figure 3.9 Flux of the PVDF membranes and alkaline treated membranes (Alk20, Alk30, Alk40, Alk50, and Alk60) at different treating temperatures in PAA, PEO, Casein protein, and whey protein filtration. Pure water filtration was conducted at pH 7, while PAA, PEO, casein protein, and whey protein filtration were performed at pH 10.

The flux behavior for both casein and whey filtration followed a similar trend. As the treating temperature increased, the flux decreased between 20℃ and 40℃ and then is stable between 40℃ and 50℃. Finally, the flux increased between 50℃ and 60℃. Based on the earlier hypothesis, both the resistance caused by electrostatic interactions and the increase in flux due to surface porosity affected the membrane flux. When the treating

temperature was between 20℃ and 40℃, the effect of electrostatic interactions dominated the flux behavior, leading to a decrease in flux with the increase in temperature. However, when the temperature was between 50℃ and 60℃, the effect of increased porosity dominated the flux, increasing flux.

In summary, the unexpected reduction in pure water flux after alkaline treatment can be explained by the decrease in membrane matrix elasticity and mechanical strength, leading to pore deformation and shrinkage during filtration. The flux behavior for PAA, PEO, casein, and whey proteins was influenced by both electrostatic interactions and changes in surface porosity, with different temperature ranges leading to different dominant effects on the flux behavior.

3.4. Conclusions

In this research, PVDF membranes were modified using a KOH isopropanol solution to enhance the surface negative charge. Compared to modifying PVDF with an alkaline aqueous solution, when using an alkaline propanol solution for modification, a lower alkaline concentration, lower processing temperature, and shorter processing time are required. This approach allows the reaction to take place under milder conditions, resulting in higher processing efficiency. Alkaline treatment of PVDF membranes introduces several functional groups, including carbon-carbon double bonds, hydroxyl groups, and carboxyl groups. Alkaline treatment did not have a significant influence on the morphology of the PVDF membranes. However, after modification, the surface Zeta potential of the membranes increased from -44.1 mV to -64.2 mV at pH 10. The rejection for PAA, PEO, casein protein, and whey protein with PVDF membranes was 24.3%, 12.6%, 76.4%, and 69.4%, respectively. The results of the filtration tests showed that alkaline treatment effectively increased the rejection of PAA, PEO, casein protein, and whey protein. The

membranes achieved their best rejection for PEO, casein protein, and whey protein separation when the treating temperature was 40℃, with rejection percentages of 48.4%, 88.8%, and 81.7%, respectively. The PAA filtration test had a maximum rejection of 37.1% when the treating temperature was 50℃. The rejection of membranes treated at 60℃ is a little lower than the maximum rejection for all feed solutions, but the flux of membranes treated at 60℃ is relatively large. Specifically, the flux of the membrane treated at 60℃ was 29.5 LMH for PAA, 20.1 LMH for PEO, 17.5 LMH for casein protein, and 18.4 LMH for whey protein. Comparatively, the flux of PVDF membranes was 36.1 LMH for PAA, 20.5 LMH for PEO, 17.3 LMH for casein protein, and 17.7 LMH for whey protein. Therefore, the membrane treated at 60℃ exhibited the best filtration performance. Alkaline treatment of the membranes not only increased their negative surface charge but also enlarged the membrane pores and formed new microporous structures on the membrane surface. Both the rejection and flux performance of the membranes were influenced by the membrane surface charge, surface porosity, and the presence of new microporous structures. These research findings demonstrate that alkaline treatment can significantly enhance the filtration performance of PVDF membranes, with the best overall results achieved at a treating temperature of 60℃. The combination of increased negative surface charge, surface porosity, and new microporous structures contributes to the improved rejection and flux characteristics of the treated membranes.

3.5. References

[1] J. Teixeira, V. F. Cardoso, G. Botelho, A. M. Morão, J. Nunes-Pereira, and S. Lanceros-Mendez, “Effect of Polymer Dissolution Temperature and Conditioning Time on the Morphological and Physicochemical Characteristics of Poly(Vinylidene Fluoride) Membranes Prepared by Non-Solvent Induced Phase Separation,” *Polymers*, vol. 13, no. 23, p. 4062, Nov. 2021, doi: 10.3390/polym13234062.

[2] D. Zou and Y. M. Lee, “Design strategy of poly(vinylidene fluoride) membranes for

water treatment," *Progress in Polymer Science*, vol. 128, p. 101535, May 2022, doi: 10.1016/j.progpolymsci.2022.101535.

[3] V. Vatanpour, M. E. Yekavalangi, and M. Safarpour, "Preparation and characterization of nanocomposite PVDF ultrafiltration membrane embedded with nanoporous SAPO-34 to improve permeability and antifouling performance," *Separation and Purification Technology*, vol. 163, pp. 300–309, May 2016, doi: 10.1016/j.seppur.2016.03.011.

[4] N. A. M. Nor *et al.*, "Effects of heat treatment of TiO_2 nanofibers on the morphological structure of PVDF nanocomposite membrane under UV irradiation," *Journal of Water Process Engineering*, vol. 20, pp. 193–200, Dec. 2017, doi: 10.1016/j.jwpe.2017.11.007.

[5] H. Mahdavi, N. Zeinalipour, M. A. Kerachian, and A. A. Heidari, "Preparation of high-performance PVDF mixed matrix membranes incorporated with PVDF-g-PMMA copolymer and GO@SiO_2 nanoparticles for dye rejection applications," *Journal of Water Process Engineering*, vol. 46, p. 102560, Apr. 2022, doi: 10.1016/j.jwpe.2022.102560.

[6] M. L. Tran, C.-C. Fu, T.-H. Wei, C.-T. Hsieh, and R.-S. Juang, "Surface coating of titania and graphene oxide onto plasma-activated polymer membranes as efficient photocatalysts for organics removal from water," *Journal of Water Process Engineering*, vol. 37, p. 101488, Oct. 2020, doi: 10.1016/j.jwpe.2020.101488.

[7] Y. Zhao *et al.*, "Effect of graphite oxide and multi-walled carbon nanotubes on the microstructure and performance of PVDF membranes," *Separation and Purification Technology*, vol. 103, pp. 78–83, Jan. 2013, doi: 10.1016/j.seppur.2012.10.012.

[8] A. Asadi, F. Gholami, S. Nazari, and M. Dolatshah, "Improved filtration performance of polyvinylidene fluoride nanocomposite membranes embedded with deep eutectic solvent: Application towards MBR," *Desalination*, vol. 543, p. 116088, Dec. 2022, doi: 10.1016/j.desal.2022.116088.

[9] Z.-L. Qiu *et al.*, "Ionic Dendrimer Based Polyamide Membranes for Ion Separation," *ACS Nano*, vol. 15, no. 4, pp. 7522–7535, Apr. 2021, doi: 10.1021/acsnano.1c00936.

[10] S. Shen, H. Li, Y. Shen, R. Bai, and G. Zhang, "Modification of PVDF membrane by post-modified NH_2-MIL-88B(Fe) showing improved permeability and oil/water

separation performance," *Journal of Environmental Chemical Engineering*, vol. 11, no. 3, p. 109621, Jun. 2023, doi: 10.1016/j.jece.2023.109621.

[11] H. R. Abdolmaleki, S. A. Mousavi, and H. Heydari, "Novel positively charged PVDF/SPES membranes surface grafted by hyperbranched polyethyleneimine (HBPEI): Fabrication, characterization, antifouling properties, and performance on the removal of cationic E-coat paint," *Polymer Testing*, vol. 122, p. 108020, May 2023, doi: 10.1016/j.polymertesting.2023.108020.

[12] C. Yue and G. Zhang, "Calcium ion crosslinked sodium alginate coated PVDF membrane for improved smart pH-responsive properties," *Journal of Environmental Chemical Engineering*, vol. 10, no. 6, p. 108684, Dec. 2022, doi: 10.1016/j.jece.2022.108684.

[13] H. Zheng *et al.*, "Surface modified by green synthetic of Cu-MOF-74 to improve the anti-biofouling properties of PVDF membranes," *Chemical Engineering Journal*, vol. 411, p. 128524, May 2021, doi: 10.1016/j.cej.2021.128524.

[14] S. Al-Gharabli and J. Kujawa, "Molecular activation of fluoropolymer membranes via base piranha treatment to enhance transport and mitigate fouling – new materials for water purification," *Journal of Membrane Science*, vol. 624, p. 119105, Apr. 2021, doi: 10.1016/j.memsci.2021.119105.

[15] M. Kamaz, A. Sengupta, A. Gutierrez, Y.-H. Chiao, and R. Wickramasinghe, "Surface Modification of PVDF Membranes for Treating Produced Waters by Direct Contact Membrane Distillation," *IJERPH*, vol. 16, no. 5, p. 685, Feb. 2019, doi: 10.3390/ijerph16050685.

[16] A. Venault *et al.*, "Design of near-superhydrophobic/superoleophilic PVDF and PP membranes for the gravity-driven breaking of water-in-oil emulsions," *Journal of the Taiwan Institute of Chemical Engineers*, vol. 65, pp. 459–471, Aug. 2016, doi: 10.1016/j.jtice.2016.05.011.

[17] Y. Han, S. Song, Y. Lu, and D. Zhu, "A method to modify PVDF microfiltration membrane via ATRP with low-temperature plasma pretreatment," *Applied Surface Science*, vol. 379, pp. 474–479, Aug. 2016, doi: 10.1016/j.apsusc.2016.04.114.

[18] Y. Chen *et al.*, "Controlled grafting from poly(vinylidene fluoride) microfiltration membranes via reverse atom transfer radical polymerization and antifouling

properties," *Polymer*, vol. 48, no. 26, pp. 7604–7613, Dec. 2007, doi: 10.1016/j.polymer.2007.10.043.

[19] H. Hua, Y. Xiong, C. Fu, and N. Li, "pH-sensitive membranes prepared with poly(methyl methacrylate) grafted poly(vinylidene fluoride) via ultraviolet irradiation-induced atom transfer radical polymerization," *RSC Adv.*, vol. 4, no. 74, pp. 39273–39279, 2014, doi: 10.1039/C4RA06368F.

[20] S. Golcuk, A. E. Muftuoglu, S. U. Celik, and A. Bozkurt, "Synthesis and characterization of polymer electrolyte membranes based on PVDF and styrene via photoinduced grafting," *J Polym Res*, vol. 20, no. 5, p. 144, May 2013, doi: 10.1007/s10965-013-0144-2.

[21] Q. Deng, Y. Chen, and W. Sun, "Preparation of polymer brushes from poly(vinylidene fluoride) surfaces by UV irradiation pretreatment," *Surf. Rev. Lett.*, vol. 14, no. 01, pp. 23–30, Feb. 2007, doi: 10.1142/S0218625X07009013.

[22] S. Al-Gharabli, J. Kujawa, M. O. Mavukkandy, and H. A. Arafat, "Functional groups docking on PVDF membranes: Novel Piranha approach," *European Polymer Journal*, vol. 96, pp. 414–428, Nov. 2017, doi: 10.1016/j.eurpolymj.2017.09.029.

[23] C. Sun and X. Feng, "Enhancing the performance of PVDF membranes by hydrophilic surface modification via amine treatment," *Separation and Purification Technology*, vol. 185, pp. 94–102, Sep. 2017, doi: 10.1016/j.seppur.2017.05.022.

[24] E. Boyraz, F. Yalcinkaya, J. Hruza, and J. Maryska, "Surface-Modified Nanofibrous PVDF Membranes for Liquid Separation Technology," *Materials*, vol. 12, no. 17, p. 2702, Aug. 2019, doi: 10.3390/ma12172702.

[25] A. Qin, X. Li, X. Zhao, D. Liu, and C. He, "Engineering a Highly Hydrophilic PVDF Membrane via Binding Tio Nanoparticles and a PVA Layer onto a Membrane Surface," *ACS Appl. Mater. Interfaces*, vol. 7, no. 16, pp. 8427–8436, Apr. 2015, doi: 10.1021/acsami.5b00978.

[26] G. J. Ross, J. F. Watts, M. P. Hill, and P. Morrissey, "Surface modification of poly(vinylidene fluoride) by alkaline treatment1. The degradation mechanism," *Polymer*, vol. 41, no. 5, pp. 1685–1696, Mar. 2000, doi: 10.1016/S0032-3861(99)00343-2.

[27] X. Wang, Z. Wang, Z. Wang, Y. Cao, and J. Meng, “Tethering of hyperbranched polyols using PEI as a building block to synthesize antifouling PVDF membranes,” *Applied Surface Science*, vol. 419, pp. 546–556, Oct. 2017, doi: 10.1016/j.apsusc.2017.05.037.

[28] Z. Xu, S. Gu, D. Rana, T. Matsuura, and C. Q. Lan, “Chemical precipitation enabled UF and MF filtration for lead removal,” *Journal of Water Process Engineering*, vol. 41, p. 101987, Jun. 2021, doi: 10.1016/j.jwpe.2021.101987.

[29] Z. Li, D. Rana, Z. Wang, T. Matsuura, and C. Q. Lan, “Synergic effects of hydrophilic and hydrophobic nanoparticles on performance of nanocomposite distillation membranes: An experimental and numerical study,” *Separation and Purification Technology*, vol. 202, pp. 45–58, Aug. 2018, doi: 10.1016/j.seppur.2018.03.032.

[30] C.-H. Kuo, G.-J. Chen, Y.-K. Twu, Y.-C. Liu, and C.-J. Shieh, “Optimum Lipase Immobilized on Diamine-Grafted PVDF Membrane and Its Characterization,” *Ind. Eng. Chem. Res.*, vol. 51, no. 14, pp. 5141–5147, Apr. 2012, doi: 10.1021/ie300011q.

[31] B. D. Mather, K. Viswanathan, K. M. Miller, and T. E. Long, “Michael addition reactions in macromolecular design for emerging technologies,” *Progress in Polymer Science*, vol. 31, no. 5, pp. 487–531, May 2006, doi: 10.1016/j.progpolymsci.2006.03.001.

[32] G. Vitola, R. Mazzei, E. Fontananova, and L. Giorno, “PVDF membrane biofunctionalization by chemical grafting,” *Journal of Membrane Science*, vol. 476, pp. 483–489, Feb. 2015, doi: 10.1016/j.memsci.2014.12.004.

[33] R. Zhou, D. Rana, T. Matsuura, and C. Q. Lan, “Effects of multi-walled carbon nanotubes (MWCNTs) and integrated MWCNTs/SiO_2 nano-additives on PVDF polymeric membranes for vacuum membrane distillation,” *Separation and Purification Technology*, vol. 217, pp. 154–163, Jun. 2019, doi: 10.1016/j.seppur.2019.02.013.

[34] R. Singh, “Introduction to Membrane Technology,” in *Membrane Technology and Engineering for Water Purification*, Elsevier, 2015, pp. 1–80. doi: 10.1016/B978-0-444-63362-0.00001-X.

[35] W. N. Eigel *et al.*, “Nomenclature of Proteins of Cow’s Milk: Fifth Revision1,” *Journal of Dairy Science*, vol. 67, no. 8, pp. 1599–1631, Aug. 1984, doi:

10.3168/jds.S0022-0302(84)81485-X.

[36] K. R. Marshall, “Industrial isolation of milk proteins: whey proteins.,” *Developments in Dairy Chemistry*, vol. 1, pp. 339–373, 1982.

[37] C. Verdun, P. Couvreur, H. Vranckx, V. Lenaerts, and M. Roland, “Development of a nanoparticle controlled-release formulation for human use,” *Journal of Controlled Release*, vol. 3, no. 1, pp. 205–210, Jan. 1986, doi: 10.1016/0168-3659(86)90081-7.

[38] G. Wen *et al.*, “Preparation of alkali-resistant PVDF membranes via immobilization of sodium lauryl sulfate (SDS) on surface,” *Appl Water Sci*, vol. 11, no. 3, p. 55, Mar. 2021, doi: 10.1007/s13201-021-01377-6.

Chapter 4. Surface Modification of Polyvinylidene Fluoride Membranes Using KOH/water/alcohol Ternary: Effects of Alcohol and Other Conditions

Abstract

Alkaline treatment is a cost-effective and easy-to-operate method that can effectively alter the hydrophilicity of polyvinylidene fluoride (PVDF) membranes. It makes the surface of PVDF membranes chemically active by introducing hydrophilic groups, e.g., hydroxyl and carboxyl groups, and therefore could be used as an effective pretreatment for membrane surface engineering including the grafting of other target chemical molecules onto to membrane surface. This treatment enhances the hydrophilicity of the membrane surface and could therefore also improve membrane permeability and reduce fouling. In this research, we systematically studied the alkaline treatment using KOH/alcohol/water ternaries at different conditions. Results indicate that the inclusion of alcohol in the reaction system could impact the efficiency of membrane surface modification through altering the chemical reaction mechanism as well as affecting the reacting mixture's properties such as OH^- activity and membrane wettability. The effectiveness of different alcohols was in the order of methanol > ethanol > isopropanol, which is in accordance with the orders of their polarity and reactivity. While the membrane wettability of the ternaries increased with the proportion of alcohol (in particular, isopropanol) in a ternary, the extent of membrane surface modification decreased due to the consequent reduction of OH^- activity. Increase of KOH concentration and treatment time both led to the monotonic increase of the extent of surface modification in the tested ranges as measured by the decrease of membrane contact angle.

Acronyms and Symbols

Abbreviation

ATR-FTIR	attenuated total reflectance-Fourier transform infrared
DMAc	*N*, *N*-dimethylacetamide
NIPS	non-solvent induced phase separation
PA	polyamide
PAN	polyacrylonitrile
PC	polycarbonate
PE	polyethylene
PEG	polyethylene glycol
PEI	polyetherimide
PES	polyethersulfone
PP	polypropylene
PSF	polysulfone
PTFE	polytetrafluoroethylene
PVC	polyvinyl chloride
PVDF	polyvinylidene fluoride

Nomenclature

A	pre-exponential factor (frequency factor)

A_φ	Debye-Hückel constant or limiting law constant ($mol^{-1/2} \cdot L^{3/2}$)
a_i	ionic activity of ion i
B	Debye-Hückel parameter or distance parameter ($nm^{-1} \cdot mol^{-1/2} \cdot L^{3/2}$)
b	empirical parameter in the Pitzer model
C^φ	ternary interaction parameter, describing interactions involving three ions
c_i	molar concentration of ion i (M)
E_a	activation energy
f	fraction of the droplet that is actually in contact with the surface of the membrane
I	molar ionic strength (M)
k	reaction rate constant
m_j	molar fraction of ion j
n	reaction order
R	ideal gas constant
r	roughness ratio
r_i	Stokes radius of ion i
T	temperature (K)
v	reaction rate
z_i	charge number of that ion i

α	parameter related to the distance of the closest approach of ions in the Pitzer model
$\beta_{i,j}^{(0)}$	first virial coefficient, the short-range interactions between ions i and j
$\beta_{i,j}^{(1)}$	second virial coefficient, accounting for additional interaction effects
γ_i	activity coefficient
ϵ	dielectric constant
θ_{air}	contact angle between the air and the droplet
θ_{CB}	heterogeneous contact angle
θ_W	contact angle on a rough surface
θ_Y	contact angle on a smooth surface

4.1. Introduction

Membrane filtration is a very efficient separation method, which is widely used in many fields, such as protein purification, heavy metal removal, gas separation, and water purification. Materials used to make separation membranes come from a wide range of sources, such as metal, metal oxide, ceramic[1], and polymer [2]. Compared with other materials, using polymers to fabricate filtration membranes has many significant advantages. These advantages have led to the widespread use and development of polymer membranes in various filtration applications [3]. These advantages include: (1) There are many types of polymers. By selecting different polymers, separation membranes with specific properties can be produced. For example, by adjusting preparation conditions (such as polymer concentration, additives, gel bath components, etc.), the pore size of the membrane can be precisely controlled to achieve different degrees of separation such as microfiltration (MF), ultrafiltration (UF), nanofiltration (NF), and reverse osmosis (RO) [4]. (2) Membranes made of polymers are easy to modify and their surface properties can be engineered through different modification methods to better cope with different separation needs. For example, the surface hydrophilicity and hydrophobicity of polymer membranes can be adjusted through various modification methods (such as plasma treatment, chemical grafting, etc.) to adapt to different filtration needs [5]. (3) Polymers usually have good mechanical strength and toughness. Not easy to break during use [6]. (4) The preparation process of polymer membranes is relatively simple, such as the phase inversion method, solution casting method, electrospinning method, etc., and can achieve large-scale production [7]. Common materials used to make filtration membranes include polyvinylidene fluoride (PVDF), polytetrafluoroethylene (PTFE), polyethersulfone (PES), polysulfone (PSU), polyacrylonitrile (PAN), nylon (polyamide, PA), polycarbonate (PC), polyethylene (PE), polypropylene (PP), polyetherimide (PEI), polyvinyl chloride (PVC),

cellulose esters (such as cellulose acetate), etc. [7].

Among them, PVDF membrane is widely used in fields such as water treatment, gas separation, and biomedicine due to its excellent chemical stability, mechanical strength, and thermal stability [8]. However, PVDF membranes are inherently hydrophobic, which limits their antifouling performance and permeability in water treatment applications. The boundary layer between the membrane interface of a hydrophobic membrane and water has almost no hydrogen bonding interactions. The repulsion of water molecules from the hydrophobic membrane surface is a spontaneous process accompanied by an increase in entropy, so pollutant molecules tend to adsorb to the membrane surface and occupy the boundary layer. Hydrophobic membranes will hinder the passage of water molecules, resulting in reduced membrane flux, and are more likely to adsorb organic and biological pollutants, increasing the risk of membrane fouling [9], [10]. To improve the hydrophilicity of PVDF membranes, a variety of surface modification methods have been developed in recent years, such as plasma treatment [11], [12], ultraviolet (UV) radiation [13], [14], [15], [16], ozone treatment [17] and chemical treatment [18], [19], [20], [21]. Plasma treatment uses high-energy plasma to introduce oxygen or nitrogen-containing functional groups on the surface of the PVDF membrane to increase hydrophilicity. High-energy UV radiation can break and reorganize PVDF molecules. Thereby generating active free radicals on the surface of the PVDF membrane. In contrast, chemical treatment, especially alkaline solution treatment, has become an important modification method because of its simple operation and significant effect.

Alkaline solution treatment uses alkaline solution, such as KOH solution and NaOH solution, to treat the PVDF membrane. It can introduce hydrophilic functional groups, such as hydroxyl and carboxyl groups, on to the membrane surface, thereby significantly improve the hydrophilicity of the membrane. The reaction conditions of alkaline solution

treatment are mild, the treatment process is easy to control, and it does not require expensive equipment, making it suitable for large-scale industrial production. Studies have shown that alkaline solution treatment can improve the surface hydrophilicity of PVDF membrane and reduce the membrane surface free energy [22]. Hydrophilic membranes have high surface tension and can form hydrogen bonds with surrounding water molecules, thereby forming a thin water boundary layer between the membrane and the solution. The water boundary layer reduces the potential energy barrier for water molecules when passing through the membrane, so it is easier for water molecules to pass through the membrane and improve the permeability of the membrane. At the same time, the water boundary layer can prevent pollutants from contacting the membrane and improve the anti-fouling performance of the membrane [9], [10]. In addition, alkaline treatment can increase the chemical activity of PVDF membranes, making them easier to be modified by other advanced materials, such as graphene oxide (GO) [23], [24], carbon nanotubes (CNTs) [25], MXene [26] and dendrimer [27], [27]. In summary, This modification method improves the performance of the membrane and provides strong support for the widespread applications of PVDF membranes [28].

Studies have shown that the hydrophilicity of PVDF membranes can be improved by treatment with alkaline solutions. However, most of these studies focus on the influence of a single treatment parameter, such as treatment time, temperature, or alkaline concentration. Although these single-parameter studies have provided fundamental insights, they have not fully revealed the complex interaction mechanisms during alkaline solution treatment. There is a lack of systematic research on the types and contents of solvents in solutions, which limits the in-depth understanding and optimization of the modification process. Alcoholic solvents can play an important role in alkaline solution processing. In this study, we examined the effects of alkaline treatment on the efficiency of surface modification of PVDF membranes using contact angle (hydrophilicity) and color change as the primary

indicators. Various parameters were investigated, including treatment time, treatment temperature, isopropanol proportion, KOH concentration, and types of mixed alcohols in alkaline solution.

4.2. Experimental

4.2.1. Materials

The polymer of membranes, PVDF, Kynar® 740 (Pellet, M_w = 410 kDa), was kindly supplied by Arkema Inc. (Philadelphia, PA). The pore former agent, polyethylene glycol (PEG) (M_w = 1 kDa), and the solvent for casting solution, anhydrous *N*, *N*-dimethylacetamide (DMAc) with a purity of 99.8% were purchased from Sigma-Aldrich Inc. (St. Louis, MO). Potassium hydroxide, methanol with a purity of 99.5%, ethanol with a purity of 99%, isopropanol with a purity of 99.5%, and n-butanol with a purity of 99.5% were purchased from Sigma-Aldrich Inc.

4.2.2. PVDF membrane fabrication

In this chapter, the PVDF membrane was fabricated using the non-solvent phase separation (NIPS) method, as discussed in detail in Chapter 3. The casting solution used for membrane fabrication consisted of 82 wt% DMAc, 15 wt% PVDF, and 3 wt% PEG.

4.2.3. Alkaline treatment of PVDF membranes

The PVDF membrane was treated with an alkaline solution under various conditions, as detailed below:

Effects of Treatment Time

The membrane was treated with an aqueous solution containing 0.5 M KOH and 25 vol% isopropanol at 60°C for different durations: 2 minutes, 5 minutes, 10 minutes, 30 minutes, 60 minutes, and 180 minutes.

Effects of Treatment Temperature

To study the effects of treatment temperature, the membrane was treated with an aqueous solution of 0.5 M KOH and 25 vol% isopropanol for 30 minutes at various temperatures, ranging from 20°C to 80°C in 10°C intervals.

Effects of Isopropanol Concentration

The membrane was treated with an aqueous solution of 0.5 M KOH containing varying proportions of isopropanol at 60°C for 30 minutes. The proportions of isopropanol used were 0 vol%, 5 vol%, 10 vol%, 15 vol%, 20 vol%, 25 vol%, 50 vol%, 75 vol%, 90 vol%, 95 vol%, and 100 vol%.

Effects of KOH Concentration

The effect of KOH concentration was investigated by treating the PVDF membrane with an aqueous solution containing 25 vol% isopropanol and different concentrations of KOH at 60°C for 30 minutes. The KOH concentrations used were 0.1 M, 0.5 M, 1 M, and 2 M.

Effects of Different Alcohols

The effect of different alcohols was studied by treating the PVDF membrane with an aqueous solution of 0.5 M KOH containing 25 vol% of different alcohols at 60°C for 30 minutes. The alcohols used for treatment were methanol, ethanol, isopropanol, and n-butanol.

For the alkaline treatment, the membrane was immersed in the KOH solution with the selected layer facing down. After the treatment, the membrane was washed twice with ethanol and three times with water at room temperature. Finally, the membrane was dried by blowing with compressed air at room temperature.

4.2.4. Membrane characterization

ATR-FTIR

The chemical properties on the membrane's surface were analyzed using attenuated total reflectance-Fourier transform infrared (ATR-FTIR) spectroscopy, employing the Agilent Tech-Cary 630 spectrometer (Agilent, Canada).

Contact angle

The water contact angle of the membrane samples was measured using the sessile drop method with the VCA Optima Surface Analysis System (AST Product, Inc., Billerica, MA, US) at room temperature. A 1 μL deionized water droplet was carefully placed on the surface of the dry sample to measure the contact angle. Measurements were taken with 3 replicated samples, at 5 random spots on each sample. The average value of these measurements was then reported.

4.2.5. Activity of the hydroxide ions

Ionic strength

The process of KOH dissolving in aqueous solution can be expressed by Equation (4-1). The molar ionic strength (I) can be calculated by Equation (4-2).

$$KOH \rightarrow K^+ + OH^- \tag{4-1}$$

$$I = 0.5 \sum_{i=1}^{n} c_i \cdot z_i^2 \tag{4-2}$$

Where c_i is the molar concentration of ion i (M), z_i is the charge number of that ion i. Since KOH is completely dissolved in water, the concentration of K^+ or the concentration of OH^- is equal to the concentration of KOH. Therefore, the molar ionic strength of the KOH solution can be calculated by Equation (4-3).

$$I = c_{KOH} \tag{4-3}$$

Dielectric constant

The dielectric constant (ϵ) of the mixed solution is determined by taking the volume-weighted average of the dielectric constants of its components as Equation (4-4) is shown. The dielectric constants of pure water, methanol, ethanol, isopropanol, and n-butanol are 80.1, 32.7, 24.5, 17.9, and 17.1, respectively [29].

$$\epsilon = alcohol\ vol\% \cdot \epsilon_{alcohol} + (1 - alcohol\ vol\%) \cdot \epsilon_{water} \tag{4-4}$$

Activity coefficient

There are two models for activity coefficient calculations, the Debye-Hückel model and the Pitzer model. By the Debye-Hückel model [30], the activity coefficient (γ_i) of ion i can be calculated by Equation (4-5).

$$\log \gamma_i = -\frac{A_\varphi \cdot z_i^2 \cdot \sqrt{I}}{1 + B \cdot a_i \cdot \sqrt{I}} \tag{4-5}$$

Where a_i is Stokes radius of ion i. Debye-Hückel constant (or limiting law constant) A_φ

($mol^{-1/2}·L^{3/2}$) and Debye-Hückel parameter (or distance parameter) B ($nm^{-1}·mol^{-1/2}·L^{3/2}$) are related with the dielectric constant and the temperature, which can be calculated by Equations (4-6) and (4-7), respectively.

$$A_\varphi = \frac{1.824\times10^6}{(\epsilon\cdot T)^{3/2}} \tag{4-6}$$

$$B = \frac{50.29\sqrt{\epsilon}}{T} \tag{4-7}$$

The Debye-Hückel model is suitable for low-concentration solution systems. For a high-concentration solution system, the activity coefficient (γ_i) of ion i can be calculated by the Pitzer model. For a monovalent solution containing only one salt (or base), the Pitzer model can be simplified as Equation (4-8) [31].

$$\ln(\gamma_i) = -A_\varphi \cdot z_i^2 \cdot \sqrt{I} \cdot \left(1 + \frac{\sqrt{I}}{1+b\cdot\sqrt{I}}\right) + \sum_j m_j \cdot \left(2 \cdot \beta_{i,j}^{(0)} + 2 \cdot \beta_{i,j}^{(1)} \cdot exp\left(-\alpha \cdot \sqrt{I}\right)\right) + m_j \cdot C^\varphi \tag{4-8}$$

Where the first item is the deformation of the Debye-Hückel model. A_φ can be calculated by Equation (4-6). m_j is the molar fraction of ion j. $\beta_{i,j}^{(0)}$ is the first virial coefficient, representing the short-range interactions between ions i and j (here is K^+ and OH^-). $\beta_{i,j}^{(1)}$ is the second virial coefficient, accounting for additional interaction effects, including some specific ion-pair formation. C^φ is a ternary interaction parameter, describing interactions involving three ions, which becomes significant at higher concentrations. The $\beta_{i,j}^{(0)}$, $\beta_{i,j}^{(1)}$, and C^φ for KOH are 0.1298, 0.32, and 0.0041, respectively [32]. b an empirical parameter with a value of 1.2. α is a parameter related to the distance of the closest approach of ions and affects the Debye-Hückel limiting law term in the model. It commonly is 2 for aqueous solution. The ionic activity of ion i, a_i, can be described by Equation (4-9).

$$a_i = \gamma_i \cdot c_i \tag{4-9}$$

4.2.6. Reaction rate

As Equations (3-5), (3-6), and (3-7) are shown, OH^- reacts with the PVDF molecule, removing a fluorine atom on the PVDF molecule and introducing a -OH group [22], [33], [34].

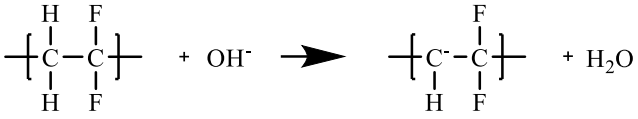

(4-10)

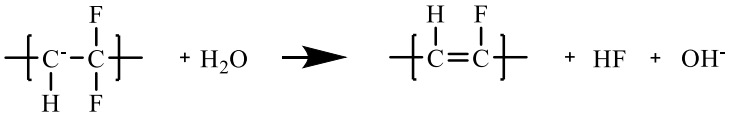

(4-11)

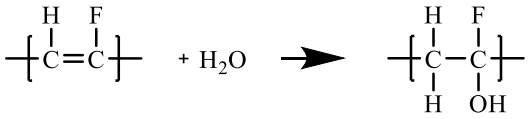

(4-12)

By combining Equations (3-5), (3-6), and (3-7), we obtain the Equation (4-13).

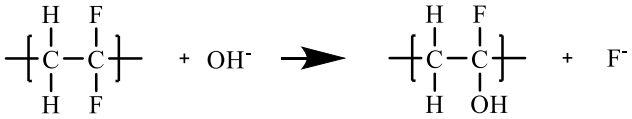

(4-13)

As the reaction proceeds, OH^- will further remove another fluorine atom from the PVDF molecule and introduce a ketone group, which was shown by Equations (4-14), (4-15), and (3-10).

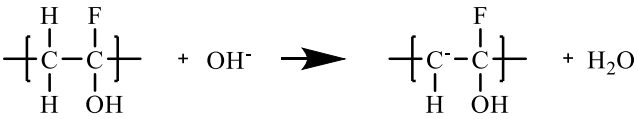

(4-14)

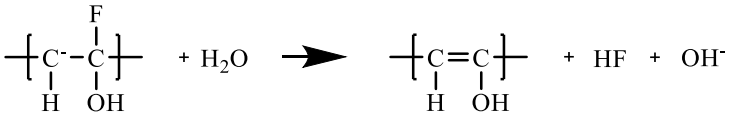

(4-15)

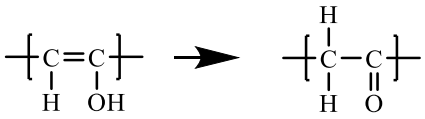

(4-16)

By combining Equations (4-14), (4-15), and (3-10), we obtain the Equation (4-17).

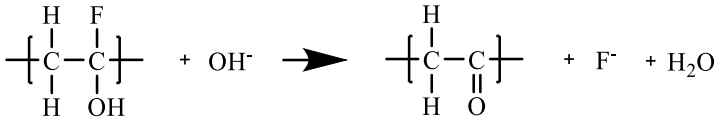

(4-17)

The reaction rate (v) of the alkaline treatment of the PVDF membranes can be described as the function of OH^- activity, as Equation (4-18) shown.

$$v = k \cdot a_{OH^-}^{n} \tag{4-18}$$

Where a_{OH^-} and n are the activity of OH^- and the reaction order (n is 1, since it is first order reaction). k is the rate constant. The PVDF defluorination in an alkaline solution (or the alkaline treatment reaction) is a first-order kinetic reaction [33]. Therefore Equation (4-18) can be written as Equation (4-19).

$$v = k \cdot a_{OH_0^-} \tag{4-19}$$

The rate constant k, is the function of the temperature (T), as Equation (4-20) is shown.

$$k = A \cdot exp\left(\frac{-E_a}{R \cdot T}\right) \tag{4-20}$$

Where A and E_a are the pre-exponential factor (frequency factor) and activation energy, respectively. R is the gas constant (8.314 $J \cdot mol^{-1} \cdot K^{-1}$). Combining Equation (4-20) and

Equation (4-18), the reaction rate can be described by Equation (4-21).

$$v = A \cdot exp\left(\frac{-E_a}{R \cdot T}\right) \cdot a_{OH_0^-} \quad (4\text{-}21)$$

4.2.7. KOH concentration in aqueous or alcoholic phase

Under some conditions, the KOH alcohol-aqueous solution will separate into two phases. The concentration of KOH in the aqueous or alcoholic phase was measured as follows. 10 mL of the upper (aqueous phase) or lower liquid (alcoholic phase) was taken and placed in an evaporating dish and heated the evaporating dish to 200℃ on a hot plate until all the liquid evaporated. Then the evaporating dish was placed in an oven at 70℃ for 24 h. Weigh the mass of the clean dry dish before loading the sample and after drying with the sample to obtain the mass of residual solid (KOH) in it. The concentration of KOH in the liquid phase can be calculated using Equation (4-22).

$$c_{KOH} = \frac{m - m_0}{v_s} \quad (4\text{-}22)$$

where, c_{KOH} is the KOH concentration in the aqueous or alcoholic phase, m_0 and m the masses of the evaporating dish before loading the sample (i.e., the clean dry dish) and after drying with the sample, respectively; and v_s the volume of the liquid added into the evaporating dish, which was 10 mL here.

4.3. Results and discussion

4.3.1. Effect of treatment time

Figure 4.1 shows the effect of alkaline treatment time on the contact angle of the membranes. The alkaline treatment causes PVDF molecules to lose hydrophobic fluorine

atoms while introducing hydrophilic hydroxyl groups, thereby making the membrane more hydrophilic. Longer alkaline treatment results in more hydrophilic hydroxyl groups being introduced on the membranes. Consequently, the contact angle decreases with increased treatment time. As shown in Figure 4.1, within the first 30 minutes of the alkaline treatment, the contact angle decreased slightly. For example, after 30 minutes of treatment, the contact angle decreased by only 1%. However, beyond 30 minutes, the contact angle decreased significantly with a further increase in treatment time. When the membrane was treated for 180 minutes, the contact angle decreased by 15%.

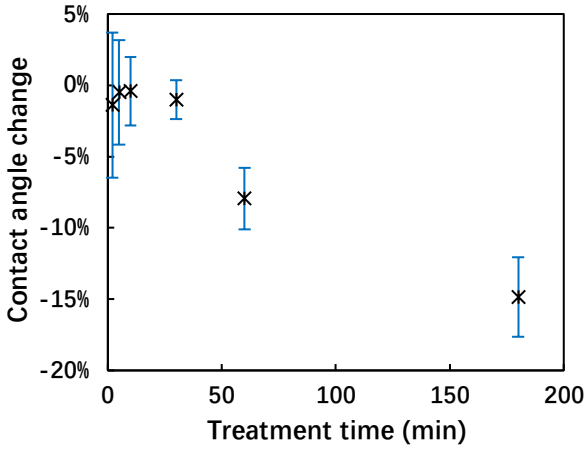

Figure 4.1 Contact angle change of membranes treated by the 0.5 M KOH alkaline solution containing 25 vol% isopropanol at 60°C for different treatment times.

4.3.2. Effect of treatment temperature

Figure 4.2 shows the surface images of the membranes treated by the 0.5 M KOH alkaline solution containing 25 vol% isopropanol for 30 min at different treatment temperatures. The surface of the pristine PVDF membrane was whitish. After being treated with an alkaline solution, the color of the membrane surface changed to light brown or brown. As the alkaline treatment temperature increased, the color of the treated membrane surface becomes darker, which indicates that the degree of alkaline treatment increased with the

increase of treatment temperature.

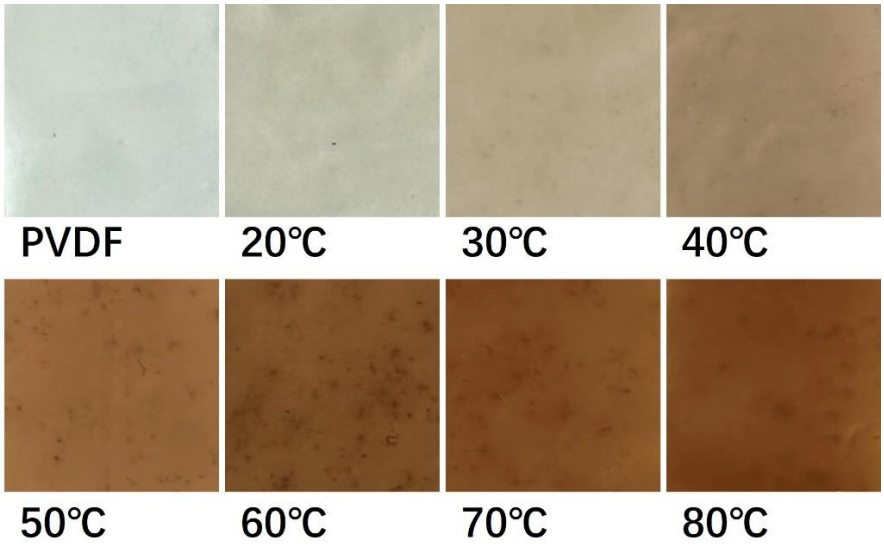

Figure 4.2 Surface images of the PVDF membrane and membranes treated by the 0.5 M KOH alkaline solution containing 25 vol% isopropanol for 30 min at different treatment temperatures.

Figure 4.3 shows the effect of alkaline treatment temperature on the contact angle of the membranes. According to Equations (4-19) and (4-20), the temperature affects the reaction rate in two ways, i.e., via the reaction rate constant and the activity coefficient. Since the activation energy of reaction is positive, increased temperature led to an increase of reaction rate. The OH^- activity also increases with temperature as shown in Table 4.1. Therefore, it is expected that the contact angle decreases monotonically as the temperature increases. However, the experimental data show an unexpected sudden jump in contact angle when treatment temperature increased from 50℃ to 60℃, which is quite counterintuitive. It can be concluded from Figure 4.2 that the degree of alkaline treatment increases with the increase of treatment temperature. Therefore, the change of the contact angle of the membrane surface is not only affected by the degree of alkaline treatment.

According to Equation (4-22), the rate of the chemical reactions in the alkaline treatment were expected to increase monotonically with the increase of the reaction temperature due

to two reasons: (1) an exponential increase of reaction rate constant with temperature, as shown in Equation (4-20). (2) the mild increase of OH^- activity (Table 4.1). Therefore, sudden reduction in contact angle change at 60℃ in comparison to that at 50℃ indicate that there might be some other factors than the surface chemistry that affected the measurement of contact angle.

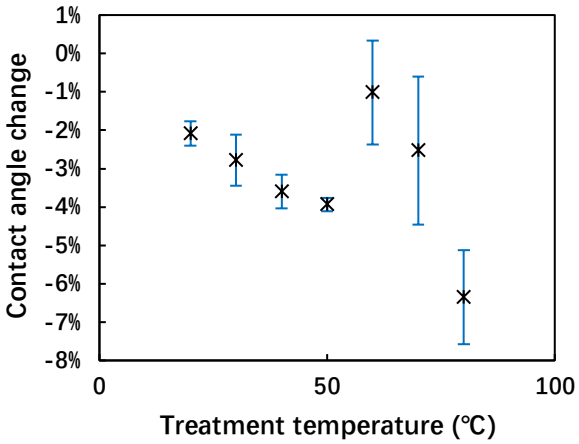

Figure 4.3 Relationship of alkaline treatment temperature on the contact angle change of the membranes treated by the 0.5 M KOH alkaline solution containing 25 vol% isopropanol for 30 min.

As an illustrative example, the formation of air pockets at membrane surface is one of the factors beside the surface chemistry that may affect the measured contact angle. The membrane is not entirely wetted by the liquid during contact angle measurement unless the contact angle approaches zero. In such a scenario, air pockets can form at the interface between the membrane matrix and the droplet. This results in the measured contact angle, θ_{CB}, being greater than the actual contact angle on rough surface θ_w. In some cases, this can lead to the measured contact angle on hydrophilic membrane surfaces falling within the hydrophobic range [35]. This relationship is described by Cassie-Baxter equation, i.e., Equation (4-23) [36].

Table 4.1 OH^- activity of the alkaline treatment at different treatment conditions.

Variable	Level	OH^- activity (M)
Temperature (°C) (25 vol% iso-PrOH, 0.5 M KOH)	20	0.311
	30	0.321
	40	0.332
	50	0.341
	60	0.350
	70	0.359
	80	0.367
KOH concentration (M) (25 vol% iso-PrOH, 60°C)	0.1	0.108
	0.5	0.350
	1	0.514
	2	0.668
Alcohol type (0.5M KOH, 25 vol% alcohol 60°C)	MeOH	0.367
	EtOH	0.358
	iso-PrOH	0.350
	n-BtOH	0.349

MeOH: methanol; EtOH: ethanol; iso-PrOH: isopropanol; n-BtOH: n-butanol.

Where f is fraction of the droplet that is actually in contact with the surface of membrane. θ_{air} is the contact angle between the air and the droplet. The increase of treatment temperature might cause an increase in the surface porosity of the membrane, which might increase the fraction of membrane surface occupied by air pockets and therefore, according to Equation (4-23), an increase in porosity results in an increase of contact angle. This, however, still cannot explain the sudden reduction of the extent of contact angle change when treatment temperature increased from 50°C to 60°C, while temperature increase in other ranges, i.e., from 30°C to 50°C and from 60°C to 90°C, caused the increase of contact angle change.

$$cos(\theta_{CB}) = f \cdot cos(\theta_W) + (1 - f) \cdot cos(\theta_{air}) \quad (4\text{-}23)$$

Another factor that could contribute to the measured contact angle is surface roughness,

which cause the measured contact angle to change in opposite directions when they change monotonically, depending on the value of the intrinsic contact angle, according to the Wenzel equation, i.e., Equation (4-24) [37].

$$cos(\theta_W) = r \cdot cos(\theta_Y) \tag{4-24}$$

The measured contact angle on a rough surface, θ_W, is the product of the roughness factor r and the intrinsic contact angle, θ_Y. Since the roughness factor is always larger than 1, the decrease of membrane roughness, and therefore r, would cause the overestimation of the contact angle of a hydrophilic surface and the underestimation of the contact angle of a hydrophobic surface. Therefore, one possible explanation is that the hydrophobic PVDF membrane had an intrinsic contact angle above 90°, which would decrease after the alkaline treatment. As the extent of surface modification by the alkaline treatment increased with temperature, the intrinsic contact angle would become less than 90° and being transformed into a hydrophilic surface. If the alkaline treatment caused the surface roughness to decrease, then, it would cause the underestimation of the contact angle when the treatment temperature was 50℃ or low but an overestimation of the contact angle when the treatment temperature was 60℃ or higher.

The above explanation, however, has a difficulty, i.e., the measured contact angle of PVDF membranes, both those reported by our group [38] and other researchers [39], [40] have often been smaller than 90°. This contradiction could be hypothetically explained by the existence of factor(s) that would result in the underestimation of the measured contact angle of hydrophobic membranes, although we do not have data to allow an informed speculation on the nature of such factor(s) at present.

4.3.3. Effects of KOH concentration

Figure 4.4 shows the influence of KOH concentration in the alkaline solution on the contact angle of the membranes. After treatment with the 0.1 M KOH solution, the contact angle of the membranes increased by 1.7%. As the KOH concentration increases, the contact angle decreases monotonically. The contact angle decreased by 12.5% when the KOH concentration reached 2 M. This trend coincides with the increase in OH^- activity, as shown in Table 4.1. According to Equation (4-19), the reaction rate increased with the increase of OH^- activity.

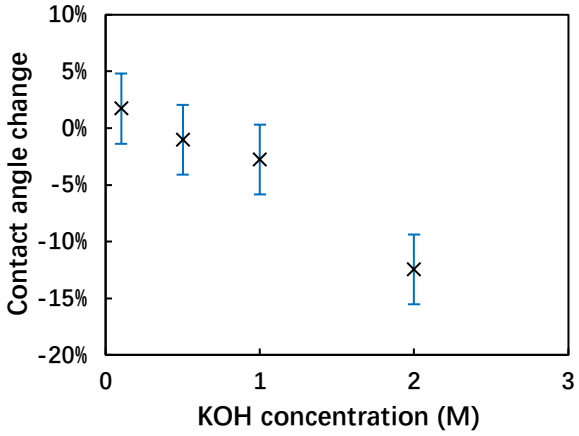

Figure 4.4 Effect of the KOH concentration on the contact angle change of the membrane. The membranes were treated by the KOH alkaline solution containing 25 vol% isopropanol at 60℃ for 30 min.

It's worth noting that the solution separated into two phases when the KOH concentration was 2 M or above. The concentrations of KOH in the alcoholic phase and aqueous phase are 0.317 M and 2.561 M, respectively, when the overall concentration was 2.0 M. In the case of phase separation, the membrane sits at the interface of the two phases and the side facing down, i.e., facing the aqueous phase, was subjected to contact angle measurement after the treatment was completed. It can be seen from Figure 4.4 that the slope of the contact angle versus KOH concentration curve was much smaller from 0.1 M to 1.0 M than

from 1.0 M to 2.0 M. The disproportional increase in the contact angle decrease due to alkaline treatment at 2.0 M seems to reflect the fact that the actual KOH concentration in the aqueous phase was 28% higher than the overall KOH, i.e., 2.0 M.

4.3.4. Effect of isopropanol concentration

Figure 4.5 shows the surface images of the membranes treated by the 0.5 M KOH alkaline solution containing different isopropanol concentration at 60℃ for 30 min. After being treated with an alkaline solution without isopropanol (0 vol% isopropanol), the membrane surface exhibited a slight yellowish discoloration. As the isopropanol content in the alkaline solution increased, the membrane's surface color deepened to a darker brown. This indicates that the degree of alkaline treatment intensified with higher isopropanol concentrations in the solution.

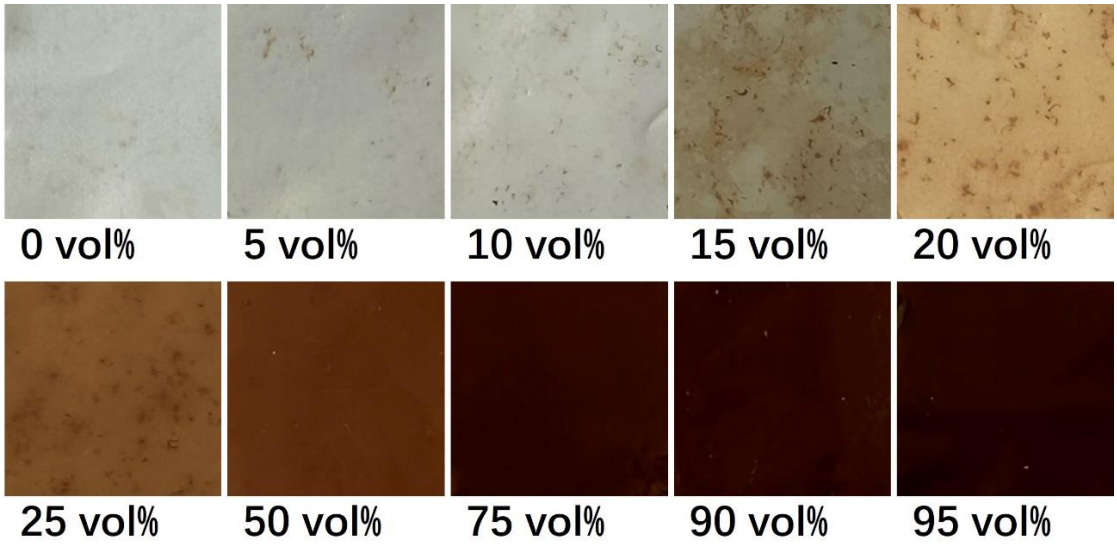

Figure 4.5 Surface images of the membranes treated by the 0.5 M KOH alkaline solution containing different isopropanol concentration at 60℃ for 30 min.

Notably, when the isopropanol concentration ranged from 0 vol% to 25 vol%, the membrane surface color was not uniform, with many darker spots appearing. This may be

due to residual pore former agent, hydrophilic PEG molecules, within the PVDF membrane matrix. Since the alkaline solution cannot immerse the PVDF membrane at lower isopropanol concentrations (0 vol% to 25 vol%), the membrane does not come into proper contact with the solution, reducing the effectiveness of the alkaline treatment. However, these residual PEG molecules may decrease the local hydrophobicity of the membrane's surface, improving its contact with the alkaline solution. Consequently, these localized areas undergo more intense alkaline treatment, resulting in darker spots on the membrane surface.

Figure 4.6 (a) illustrates the influence of the concentration of isopropanol in the KOH/isopropanol/water ternary on the contact angle change of the membrane. When the isopropanol concentration was 0 vol%, the contact angle changed by -27.2%. As the isopropanol concentration increased the extent of contact angle reduction decreased monotonically until 50 vol% isopropanol, indicating a continued reduction of the rate of the surface modifying reactions. However, when the isopropanol proportion exceeds 50 vol%, the trend was reversed and the degree of contact angle reduction increased with increasing isopropanol concentration. At 100 vol% isopropanol, the contact angle decreased by 36.1%, which was the largest contact angle reduction. In the previous discussion of Figure 4.5, it was concluded that the degree of alkaline treatment increased with the rising isopropanol content. However, this trend does not align with the relationship between the contact angle change and the isopropanol content. This suggests that multiple reactions may be occurring simultaneously during the alkaline treatment and that the reactions responsible for the color change on the membrane surface require the participation of alcohol. As will discuss later, there is evidence showing that these alcohols involving reactions may also contribute to the reactions affecting the membrane's surface hydrophilicity.

Since the pristine PVDF membrane is hydrophobic and may expel the polar aqueous solution of KOH, adding isopropanol may increase the wettability of membrane surface and therefore increase the contact angle reduction of membrane surface. However, the experimental data of contact angle change does not support this hypothesis. As shown in Figure 4.6 (b), the contact angle of the single-phase ternary on to the pristine PVDF membrane surface decreased monotonically with the increase of the alcohol concentration, corresponding to the increase of membrane surface wettability but is opposite to the decrease of the extent of surface modification, i.e., membrane contact angle reduction, as indicated in Figure 4.6 (a). Apparently, the contribution of the membrane wettability to the surface modifying reactions, if any, was not sufficient to balance the rate reduction due to the decrease of OH^- activity caused by the increase of alcohol concentration.

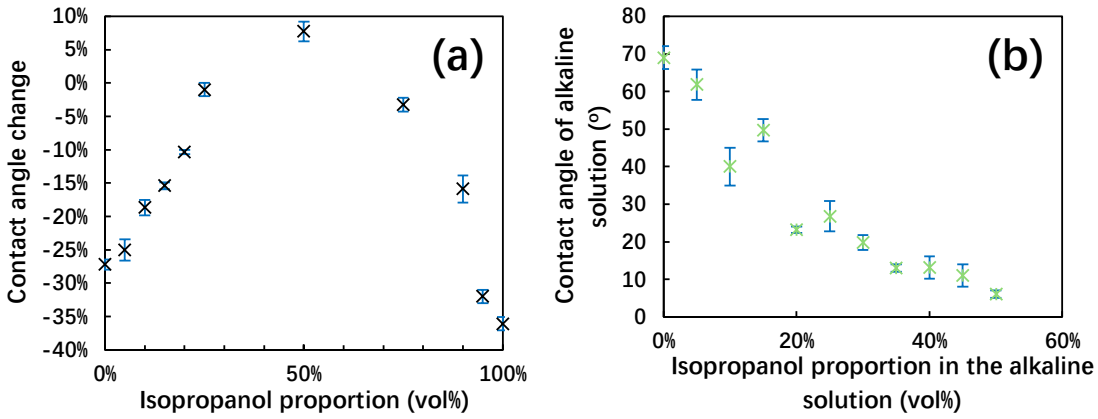

Figure 4.6 Effect of the isopropanol proportion on the contact angle change of the membranes (a). The membranes were treated by the 0.5 M KOH alkaline solution at 60℃ for 30 min. Contact angle of pristine PVDF with 0.5 M KOH solution containing different isopropanol contents (b).

Depicts the FTIR spectrum (Figure 4.7) of the PVDF membranes and the membranes treated with alkaline solutions of different isopropanol concentrations. The peak at 1180 cm^{-1} corresponds to the stretching vibrations of the C-F bond. When the isopropanol concentration increases from 0 vol% to 75 vol%, there is no significant influence on the peak at 1180 cm^{-1}. However, when the concentration of isopropanol exceeds 75 vol%, an

increase in isopropanol concentration significantly weakens the peak at 1180 cm^{-1}. This suggests that a large number of fluorine atoms are removed when the isopropanol content is over 75 vol%. Additionally, a peak at around 1600 cm^{-1} appears at the isopropanol concentration equal to and above 90 vol%. This peak is attributed to either the stretching vibration of the C=C bond (1580 cm^{-1}) or the C=O bond (1650 cm^{-1}).

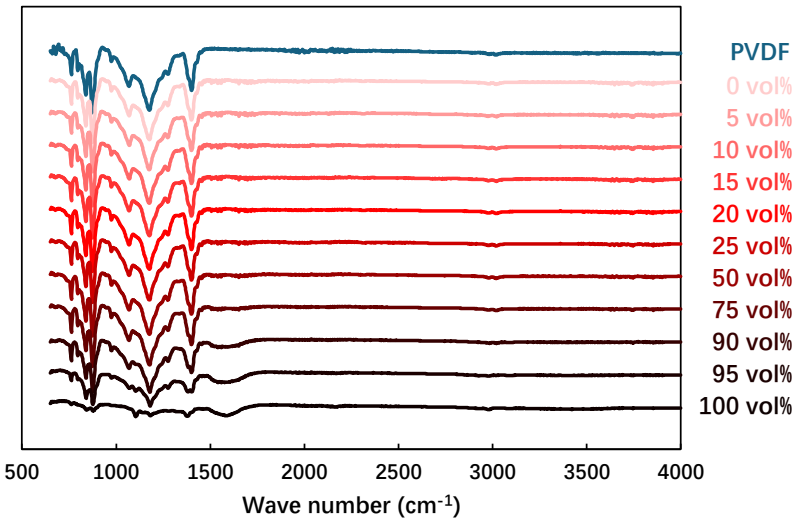

Figure 4.7 FTIR spectrum of the PVDF membranes and the membranes treated by alkaline solution with different proportions of the isopropanol.

The sharp contrast of the treatments by 0.5 M KOH solutions containing 50 vol% or less isopropanol and 75 vol% or more isopropanol coincided with the transform of the ternary from a single-phase to a two-phase system. The ternary was a single-phase system with 50 vol% or less isopropanol but became a two-phase system when containing 75% or more isopropanol. These two phases are the alcohol phase at the top and the aqueous phase at the bottom. The membrane treated in such a two-phase system located at the interface with the treated surface facing the aqueous phase.

As shown in Table 4.2, the OH^- activity of the aqueous phase of a two-phase system was much higher than that in the single-phase system and it increased with the proportion of

isopropanol in the ternary. This is because the solubility of KOH in isopropanol is magnitudes lower than that in water and majority of KOH was dissolved in the aqueous phase (Table 4.2). Therefore, when the overall KOH concentration in the ternary system was constant (0.5 M), the KOH concentration in the aqueous phase would increase with the increase of isopropanol phase and consequently the decrease of water in the system.

Table 4.2 OH^- activity of KOH/ isopropanol /water ternary at different concentration of isopropanol (vol%) with 0.5 M KOH at 60℃.

Isopropanol concentration (vol%)	OH- activity of single-phase system (M)	OH^- concentration/activity [b] of two-phase system (M)	
	Single phase [a]	Alcohol phase	Aqueous phase
0	0.410		
5	0.399		
10	0.389		
15	0.377		
20	0.364		
25	0.350		
50	0.262		
75		0.064/0.027	1.809/0.899
90		0.040/0.023	4.638/1.256
95		0.079/0.028	8.496/1.300

a: The OH- concentration in single phase was 0.5 M.

b: The assumptions were made during activity calculation: (1) the alcohol phase contains no water; (2) the aqueous phase contains no isopropanol.

It is interesting to notice that, when the PVDF membrane was treated with an alkaline solution containing 15 vol% isopropanol, which was a single-phase system with an OH^- activity of 0.35 M, the contact angle of membrane decreased by 15.4%. This reduction is close to the contact angle (15.9%) of the membrane treated with an alkaline solution containing 90 vol% isopropanol, which was a two-phase system with its reacting phase, i.e., the aqueous phase, having a vastly larger OH^- activity of 1.256 M. Apparently, the 25% isopropanol in the single-phase system, which was the reacting phase, contributed to the surface modifying reactions and the contribution of isopropanol was able to balance the

effects of its low OH^- activity, which was only 7.5% that of the reacting phase of the two-phase system containing 90% isopropanol.

4.3.5. Effect of alcohols: wettability, polarity, and reactivity

Figure 4.8 (a) shows the contact angle of membranes treated with 0.5 M alkaline solutions containing 25 vol% methanol, ethanol, isopropanol, or n-butanol at 60℃. Compared to the contact angle of the original PVDF membrane, that of the membrane treated with the alkaline solution containing 25 vol% methanol decreased by 27%, which was the most significant decrease, while the contact angle decreases of membrane treated with 0.5 M KOH in 25 vol% isopropanol aqueous solution was only 1%. For the alkaline solution system containing n-butanol, phase separation occurs, and it will be discussed later. Excluding n-butanol, the extent of contact angle change followed the order of methanol > ethanol > > isopropanol, which shows a linear relationship with the polarity of alcohol as shown in Figure 4.8 (b) and the OH^- activities of the ternaries containing different alcohols are similar to each other (Table 4.1). While the polarity was related to the membrane wettability of the ternaries as shown in Figure 4.8 (c), the afore discussed data of ternaries containing different concentrations of isopropanol already showed that wettability did not contribute to the contact angle change of membrane surface. Considering that the reactivities of these alcohols follow the order of methanol > ethanol > isopropanol, it seems evident that the alcohol in the ternary participated in the surface modifying reactions, the rate of which depends on the reactivity of the alcohol, in addition to the OH^- activity, of reacting phase [41].

As shown in Table 4.1, the OH^- activities of 0.5 M KOH in 25 vol% aqueous solutions of different alcohols are similar to each other. The decrease in contact angle could be hypothetically related to the polarity of the alcohol added to the solution. The polarity index

of water, methanol, ethanol, isopropanol, and n-butanol are 10.2, 5.1, 4.3, 3.9, and 3.9 respectively [42]. As the polarity of the alcohol in the alkaline solution increased, the contact angle of the membrane decreased, as shown in Figure 4.8 (c). The OH^- activity in solution decreased with decrease of polarity of the alcohol added in the solution. For example, the activity of OH^- in a KOH aqueous solution is 0.410 M. If the solution contains 25 vol% methanol or isopropanol, the activity of OH^- decreases to 0367 M or 0.350 M, respectively. As a result of OH^- activity decrease, the reaction rate decreased, leading to a decrease in the degree of contact angle change.

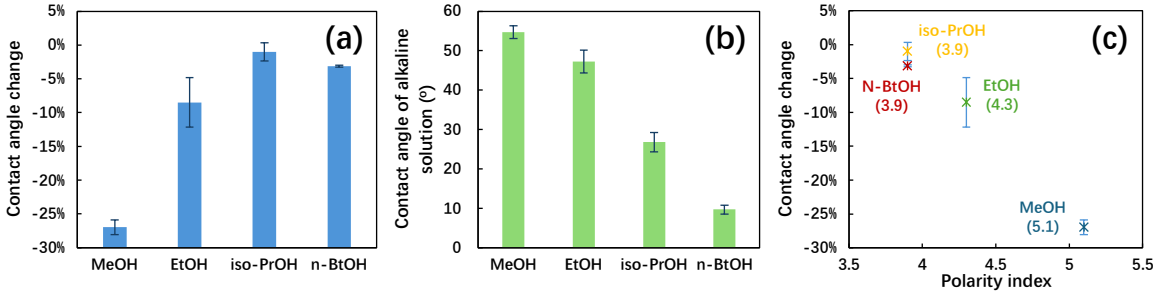

Figure 4.8 Contact angle change of membrane treated by the alkaline solution containing 25 vol% methanol, ethanol, isopropanol, or n-butanol with 0.5 M KOH at 60℃ for 30 min (a). Contact angles of pristine PVDF with alkaline solutions containing 25 vol% methanol, ethanol, isopropanol, or n-butanol (b). Contact angle change of the membrane treated by the alkaline solution containing the alcohol with different polarity index (c). The number below the label is the polarity index of alcohol.

It's worth noting that KOH in n-butanol aqueous solution of 25 vol% or above is separated into two phases and KOH is partitioned between the two phases. The alkaline solution containing n-butanol separated into two phases, which might be the reason for the greater reduction in contact angle. Even though the polarity index of n-butanol is the same as that of isopropanol, treatment with the n-butanol solution resulted in a 3% decrease in contact angle. In contrast, the membrane treated with the isopropanol solution, which did not separate into two phases, only showed a 1% decrease in contact angle. In the KOH aqueous n-butanol solution, the concentrations of KOH in the alcohol phase and aqueous phase are 0.026 M and 0.658 M, respectively. After phase separation, the concentration of KOH in

the aqueous phase increased, which enhanced the OH^- activity and thus strengthened its ability to modify the membrane surface.

Figure 4.8 (b) shows the wetting ability of alkaline solutions containing 25 vol% methanol, ethanol, isopropanol, or n-butanol on the PVDF membrane. The wetting ability of the alkaline solution on the PVDF membrane gradually increased from methanol to n-butanol. However, the membrane treated with the methanol alkaline solution, which had the weakest wetting ability, exhibited the greatest decrease in contact angle. This indicates that when the solution contains 25 vol% alcohol, the wetting ability of the alkaline solution has a minimal impact on the alkaline treatment process for the PVDF membrane.

4.4. Conclusions

In this research, the impact of alkaline treatment on the hydrophilicity of the membranes was investigated. The hydrophilicity of the treated membrane demonstrated an increase with longer alkaline treatment times, higher treatment temperatures, and increased KOH activity. Moreover, hydrophilicity was found to be significantly influenced by the addition of alcohol in the reaction mixture, and in particular the OH^- activity of the ternary, polarity and reactivity of the alcohol, and the alcohol concentration. On one hand, the addition of an alcohol to form a KOH/alcohol/water ternary would reduce the OH^- activity of the tertiary and therefore the extent of membrane modification. On the other hand, the added alcohol apparently participated in the reactions, which cause the color change of the membrane and increased extent of membrane surface modification when compared with alcohol-free binary at the same OH^- activity. The ternary may have phase separation to become a two-phase system when KOH or alcohol concentration reaches a certain threshold. In such a scenario, most KOH would be dissolved in the aqueous phase, which would acquire a KOH concentration and therefore OH^- activity higher than the overall

concentration, resulting in higher extent of surface modification than a single-phase system at similar overall KOH concentration. When comparing between different alcohols, the extent of membrane modification follows the order of methanol > ethanol > iso-propanol, which is consistent with the orders of the polarity and reactivity of these alcohols. The addition of alcohol in the reaction mixture might also cause color change of the treatment membrane and severe conditions, e.g., high temperature and large alcohol in ternary may lead to weakening of membrane mechanical strength.

4.5. References

[1] R. Singh, "Introduction to Membrane Technology," in *Membrane Technology and Engineering for Water Purification*, Elsevier, 2015, pp. 1–80. doi: 10.1016/B978-0-444-63362-0.00001-X.

[2] Y. Peng, F. Guo, Q. Wen, F. Yang, and Z. Guo, "A novel polyacrylonitrile membrane with a high flux for emulsified oil/water separation," *Sep. Purif. Technol.*, vol. 184, pp. 72–78, Aug. 2017, doi: 10.1016/j.seppur.2017.04.036.

[3] P. Saxena and P. Shukla, "A comprehensive review on fundamental properties and applications of poly(vinylidene fluoride) (PVDF)," *Adv. Compos. Hybrid Mater.*, vol. 4, no. 1, Art. no. 1, Mar. 2021, doi: 10.1007/s42114-021-00217-0.

[4] H. Strathmann, "Membrane separation processes," *J. Membr. Sci.*, vol. 9, no. 1–2, pp. 121–189, 1981, doi: 10.1016/S0376-7388(00)85121-2.

[5] D. J. Miller, D. R. Dreyer, C. W. Bielawski, D. R. Paul, and B. D. Freeman, "Surface Modification of Water Purification Membranes," *Angew. Chem. Int. Ed.*, vol. 56, no. 17, Art. no. 17, 2017, doi: 10.1002/anie.201601509.

[6] D. Zou and Y. M. Lee, "Design strategy of poly(vinylidene fluoride) membranes for water treatment," *Prog. Polym. Sci.*, vol. 128, p. 101535, May 2022, doi: 10.1016/j.progpolymsci.2022.101535.

[7] D. L. Oatley-Radcliffe, M. Walters, T. J. Ainscough, P. M. Williams, A. W. Mohammad, and N. Hilal, "Nanofiltration membranes and processes: A review of

research trends over the past decade," *J. Water Process Eng.*, vol. 19, pp. 164–171, Oct. 2017, doi: 10.1016/j.jwpe.2017.07.026.

[8] G. Kang and Y. Cao, "Application and modification of poly(vinylidene fluoride) (PVDF) membranes – A review," *J. Membr. Sci.*, vol. 463, pp. 145–165, Aug. 2014, doi: 10.1016/j.memsci.2014.03.055.

[9] Y. Subasi and B. Cicek, "Recent advances in hydrophilic modification of PVDF ultrafiltration membranes – a review: part I," *Membr. Technol.*, vol. 2017, no. 10, Art. no. 10, Oct. 2017, doi: 10.1016/S0958-2118(17)30191-X.

[10] Y. Subasi and B. Cicek, "Recent advances in hydrophilic modification of PVDF ultrafiltration membranes – a review: part II," *Membr. Technol.*, vol. 2017, no. 11, Art. no. 11, Nov. 2017, doi: 10.1016/S0958-2118(17)30233-1.

[11] A. Venault *et al.*, "Design of near-superhydrophobic/superoleophilic PVDF and PP membranes for the gravity-driven breaking of water-in-oil emulsions," *J. Taiwan Inst. Chem. Eng.*, vol. 65, pp. 459–471, Aug. 2016, doi: 10.1016/j.jtice.2016.05.011.

[12] Y. Han, S. Song, Y. Lu, and D. Zhu, "A method to modify PVDF microfiltration membrane via ATRP with low-temperature plasma pretreatment," *Appl. Surf. Sci.*, vol. 379, pp. 474–479, Aug. 2016, doi: 10.1016/j.apsusc.2016.04.114.

[13] Y. Chen *et al.*, "Controlled grafting from poly(vinylidene fluoride) microfiltration membranes via reverse atom transfer radical polymerization and antifouling properties," *Polymer*, vol. 48, no. 26, Art. no. 26, Dec. 2007, doi: 10.1016/j.polymer.2007.10.043.

[14] H. Hua, Y. Xiong, C. Fu, and N. Li, "pH-sensitive membranes prepared with poly(methyl methacrylate) grafted poly(vinylidene fluoride) via ultraviolet irradiation-induced atom transfer radical polymerization," *RSC Adv*, vol. 4, no. 74, Art. no. 74, 2014, doi: 10.1039/C4RA06368F.

[15] S. Golcuk, A. E. Muftuoglu, S. U. Celik, and A. Bozkurt, "Synthesis and characterization of polymer electrolyte membranes based on PVDF and styrene via photoinduced grafting," *J. Polym. Res.*, vol. 20, no. 5, Art. no. 5, May 2013, doi: 10.1007/s10965-013-0144-2.

[16] Q. Deng, Y. Chen, and W. Sun, "Preparation of polymer brushes from poly(vinylidene

fluoride) surfaces by UV irradiation pretreatment," *Surf. Rev. Lett.*, vol. 14, no. 01, Art. no. 01, Feb. 2007, doi: 10.1142/S0218625X07009013.

[17] Y.-L. Liu, G.-C. Lin, and C.-S. Wu, "Facile approach to functionalizing polymers with specific chemical groups by an ozone treatment: Preparation of crosslinkable poly(vinylidene fluoride) possessing benzoxazine pendent groups," *J. Polym. Sci. Part Polym. Chem.*, vol. 45, no. 5, pp. 949–954, 2007, doi: 10.1002/pola.21925.

[18] S. Zhang, Y. Li, Y. Yuan, L. Jiang, H. Wu, and Y. Dong, "Biomimetic hydrophilic modification of poly (vinylidene fluoride) membrane for efficient oil-in-water emulsions separation," *Sep. Purif. Technol.*, vol. 329, p. 125227, Jan. 2024, doi: 10.1016/j.seppur.2023.125227.

[19] S. Zhang, J. Shen, X. Qiu, D. Weng, and W. Zhu, "ESR and vibrational spectroscopy study on poly(vinylidene fluoride) membranes with alkaline treatment," *J. Power Sources*, vol. 153, no. 2, Art. no. 2, Feb. 2006, doi: 10.1016/j.jpowsour.2005.05.020.

[20] H. Lei, H. Yu, Y. Lu, X. Lu, and Z. Xu, "A facile approach for the surface modification of poly(vinylidene fluoride) membrane via surface-initiated atom transfer radical polymerization," *Chin. J. Polym. Sci.*, vol. 26, no. 01, Art. no. 01, 2008, doi: 10.1142/S0256767908002728.

[21] S. Al-Gharabli, J. Kujawa, M. O. Mavukkandy, and H. A. Arafat, "Functional groups docking on PVDF membranes: Novel Piranha approach," *Eur. Polym. J.*, vol. 96, pp. 414–428, Nov. 2017, doi: 10.1016/j.eurpolymj.2017.09.029.

[22] G. J. Ross, J. F. Watts, M. P. Hill, and P. Morrissey, "Surface modification of poly(vinylidene fluoride) by alkaline treatment1. The degradation mechanism," *Polymer*, vol. 41, no. 5, Art. no. 5, Mar. 2000, doi: 10.1016/S0032-3861(99)00343-2.

[23] H. Mahdavi, N. Zeinalipour, M. A. Kerachian, and A. A. Heidari, "Preparation of high-performance PVDF mixed matrix membranes incorporated with PVDF-g-PMMA copolymer and GO@SiO_2 nanoparticles for dye rejection applications," *J. Water Process Eng.*, vol. 46, p. 102560, Apr. 2022, doi: 10.1016/j.jwpe.2022.102560.

[24] M. L. Tran, C.-C. Fu, T.-H. Wei, C.-T. Hsieh, and R.-S. Juang, "Surface coating of titania and graphene oxide onto plasma-activated polymer membranes as efficient photocatalysts for organics removal from water," *J. Water Process Eng.*, vol. 37, p. 101488, Oct. 2020, doi: 10.1016/j.jwpe.2020.101488.

[25] R. Zhou, D. Rana, T. Matsuura, and C. Q. Lan, “Effects of multi-walled carbon nanotubes (MWCNTs) and integrated MWCNTs/SiO_2 nano-additives on PVDF polymeric membranes for vacuum membrane distillation,” *Sep. Purif. Technol.*, vol. 217, pp. 154–163, Jun. 2019, doi: 10.1016/j.seppur.2019.02.013.

[26] S. Chen, T. Wang, X. Zhuo, Y. Wang, and L. Wu, “PVDF mixed matrix membranes by incorporation of ionic liquid and MXene for enhancing permeation and antifouling performance,” *J. Environ. Chem. Eng.*, vol. 10, no. 3, p. 108027, Jun. 2022, doi: 10.1016/j.jece.2022.108027.

[27] Z. Xu *et al.*, “Polyamidoamine (PAMAM) dendrimer surface grafting polyvinylidene fluoride (PVDF) membranes to enable microporous membranes for protein separation,” *React. Funct. Polym.*, doi: Under review after major revision.

[28] B. S. Lalia, V. Kochkodan, R. Hashaikeh, and N. Hilal, “A review on membrane fabrication: Structure, properties and performance relationship,” *Desalination*, vol. 326, pp. 77–95, Oct. 2013, doi: 10.1016/j.desal.2013.06.016.

[29] J. G. Speight and N. A. Lange, Eds., *Lange’s Handbook of Chemistry*, 16t. ed., 70th anniversary ed. in McGraw-Hill standard handbooks. New York: McGraw-Hill, 2005.

[30] J.-L. Burgot, “Debye–Hückel Theory,” in *The Notion of Activity in Chemistry*, J.-L. Burgot, Ed., Cham: Springer International Publishing, 2017, pp. 479–506. doi: 10.1007/978-3-319-46401-5_46.

[31] Igor. E. S. Lins, Natan. S. Cruz, Gloria. M. N. Costa, and Silvio. A. B. Vieira de Melo, “Correlation and prediction of surface tension in single and mixed aqueous electrolyte solutions based on the mean ionic activity coefficient: A comparative analysis of Pitzer, E-NRTL and E-UNIQUAC models,” *Fluid Phase Equilibria*, vol. 516, p. 112618, Jul. 2020, doi: 10.1016/j.fluid.2020.112618.

[32] K. S. Pitzer and G. Mayorga, “Thermodynamics of electrolytes. II. Activity and osmotic coefficients for strong electrolytes with one or both ions univalent,” *J. Phys. Chem.*, vol. 77, no. 19, pp. 2300–2308, Sep. 1973, doi: 10.1021/j100638a009.

[33] Y. Morita, Y. Saito, S. Kumagai, T. Kameda, T. Shiratori, and T. Yoshioka, “Fluorine recovery through alkaline defluorination of polyvinylidene fluoride,” *J. Mater. Cycles Waste Manag.*, vol. 26, no. 2, pp. 669–678, Mar. 2024, doi: 10.1007/s10163-023-01749-x.

[34] S. Li and J. Zhu, “Leaching kinetics of fluorine during the aluminum removal from spent Li-ion battery cathode materials,” *J. Environ. Sci.*, vol. 138, pp. 312–325, Apr. 2024, doi: 10.1016/j.jes.2023.03.017.

[35] B. J. Ryan and K. M. Poduska, “Roughness effects on contact angle measurements,” *Am. J. Phys.*, vol. 76, no. 11, pp. 1074–1077, Nov. 2008, doi: 10.1119/1.2952446.

[36] A. B. D. Cassie and S. Baxter, “Wettability of porous surfaces,” *Trans. Faraday Soc.*, vol. 40, no. 0, pp. 546–551, Jan. 1944, doi: 10.1039/TF9444000546.

[37] R. N. Wenzel, “RESISTANCE OF SOLID SURFACES TO WETTING BY WATER,” *Ind. Eng. Chem.*, vol. 28, no. 8, pp. 988–994, Aug. 1936, doi: 10.1021/ie50320a024.

[38] M. Baghbanzadeh, D. Rana, T. Matsuura, and C. Q. Lan, “Effects of hydrophilic CuO nanoparticles on properties and performance of PVDF VMD membranes,” *Desalination*, vol. 369, pp. 75–84, Aug. 2015, doi: 10.1016/j.desal.2015.04.032.

[39] A. Kaynak, T. Mehmood, X. J. Dai, K. Magniez, and A. Kouzani, “Study of Radio Frequency Plasma Treatment of PVDF Film Using Ar, O_2 and (Ar + O_2) Gases for Improved Polypyrrole Adhesion,” *Materials*, vol. 6, no. 8, Art. no. 8, Aug. 2013, doi: 10.3390/ma6083482.

[40] Z. Guo, X. Xu, Y. Xiang, S. Lu, and S. P. Jiang, “New anhydrous proton exchange membranes for high-temperature fuel cells based on PVDF–PVP blended polymers,” *J. Mater. Chem. A*, vol. 3, no. 1, pp. 148–155, Dec. 2014, doi: 10.1039/C4TA04952G.

[41] X. He, Q. Wang, R. Fernandes, and B. Shu, “Investigation on the autoignition characteristics of propanol and butanol isomers under diluted lean conditions for stratified low temperature combustion,” *Combust. Flame*, vol. 237, p. 111818, Mar. 2022, doi: 10.1016/j.combustflame.2021.111818.

[42] “Summary of Key Physical Data for Solvents.” Accessed: Jun. 24, 2024. [Online]. Available: https://www.fishersci.co.uk/gb/en/scientific-products/technical-tools/summary-key-physical-data-solvents.html

Chapter 5. Polyamidoamine Dendrimer Modified Polyvinylidene Fluoride Microporous Membranes for Protein Separation

The content of this chapter has been published in: Reactive and Functional Polymers, 2024, 106021. Doi: 10.1016/j.reactfunctpolym.2024.106021.

Abstract

The separation efficiency of pressure-driven filtration membranes is primarily dictated by the membrane pore size. Membranes with larger pores typically demonstrate high flux but low or zero rejection when it comes to separating small molecules. In protein separation, ultrafiltration (UF) membranes with pore sizes smaller than the molecular dimensions of target proteins are commonly used for size rejection. Taking inspiration from the separation mechanism of nanofiltration (NF) membranes, we hypothesize that introducing charged groups into membranes of appropriate pore sizes could significantly enhance the electrostatic interaction between membrane charges and protein charges. This enhancement, occurring at the nanoscale distance when protein molecules approach or pass through charged nanoscale membrane channels, may enable the rejection of proteins substantially smaller than the pore size. Using membranes with relatively large pore sizes could lead to an increase in flux. To test this hypothesis, we conducted experiments involving the modification of polyvinylidene fluoride (PVDF) membranes with suitable pore sizes, using polyamidoamine (PAMAM) dendrimers to introduce negative charges to the membranes. The performance of the PVDF membranes and the modified membranes were investigated in the separation of whey proteins. To evaluate the contribution of steric and electrostatic

hindrance to the solute separation, filtration experiments were performed using polyethylene oxide (PEO) and polyacrylic acid (PAA). The membranes were characterized using techniques such as attenuated total reflectance-Fourier transform infrared (ATR-FTIR), X-ray photoelectron spectroscopy (XPS), and scanning electron microscopy (SEM). The results indicate that the modification enhances the rejection efficiency of whey proteins. The whey protein rejection and permeate flux for PVDF membranes were 58.9% and 15.3 LMH, respectively. Following alkaline treatment (Alk60) or PAMAM-G3.5 dendrimer modification (G3PA), the whey protein rejection increased to 97.3% and 98.8%, respectively. However, alkaline treatment (Alk60) and PAMAM-G3.5 dendrimer modification (G3PA) resulted in a reduction of permeate flux to 5.6 LMH and 2.3 LMH, respectively. This suggests that increasing membrane charge effectively enhances the separation ability of filtration membranes in charged macromolecule separation.

Acronyms and Symbols

Abbreviation

ATR-FTIR	attenuated total reflectance-Fourier transform infrared
BSA	bovine serum albumin
CNTs	carbon nanotubes
DMAc	*N*, *N*-dimethylacetamide
EDA	ethylenediamine
GO	graphene oxide
HA	humic acid
MA	methyl acrylate
MF	microfiltration
MOFs	metal-organic frameworks
MWCO	molecular weight cutoff
NF	nanofiltration
NIPS	non-solvent induced phase separation
PAA	polyacrylic acid
PAMAM	polyamidoamine
PCTFE	polychlorotrifluoroethylene
PEG	polyethylene glycol

PEO	polyethylene oxide
PES	polyether sulfone
PVDF	polyvinylidene fluoride
RO	reverse osmosis
SEM	scanning electron microscopy
UF	ultrafiltration
WP	whey protein
XPS	X-ray photoelectron spectroscopy

Nomenclature

A	effective area of the membrane
A_{sample}	area of the membrane sample during porosity measurement
$c_{i,f}$	concentration of the feed
$c_{i,p}$	concentration of the permeate
CN_{PAMAM}	elemental composition of nitrogen in the PAMAM dendrimer
CN_{memb}	elemental composition of nitrogen on the surface of the membrane
L	loading of the PAMAM dendrimer on the surface of the membrane
l	thickness of the dry membrane sample
M	molecular weight of the polymer
N_{C-N}	numbers of nitrogen atoms in C-N bonds

N_{C-NH}	numbers of nitrogen atoms in C-NH bonds
N_{C-NH_2}	numbers of nitrogen atoms in C-NH_2 bonds
R_i	rejection of solute i
r_s	Stokes radius of polymer
t	filtration time
v	volume of the permeate
w_d	weight of the dry membrane sample
w_w	weight of the wet membrane sample
$[\eta]$	intrinsic viscosity of the polymer
ε	bulk porosity
$\rho_{butanol}$	density of n-butanol

5.1. Introduction

Membrane filtration technology, as a novel separation method, boasts several advantages, including high separation efficiency, simple separation devices, and ease of operation. Various fabrication processes can produce filtration membranes with a wide range of pore sizes, ranging from micrometers to nanometers. This wide range enables the separation of molecules across a broad size spectrum, encompassing fine particles, macromolecules like bacteria, viruses, and proteins [1], [2], [3], as well as small molecules or ions such as metal ions [4]. These versatile capabilities make membrane filtration technology widely applicable across various fields. According to the pore size of the filtration membranes, they are classified as microfiltration (MF), ultrafiltration (UF), nanofiltration (NF), and reverse osmosis (RO) membranes. In the dairy industry, MF and UF membranes play a prominent role. MF membranes are typically employed for separating impurity particles, fat globules, and bacteria in milk [5], [6]. However, due to their relatively large pore size, MF membranes are hard to effectively separate proteins in milk. On the other hand, UF membranes feature a smaller pore size compared to MF membranes. Consequently, UF membranes not only serve to separate bacteria and fat globules in milk but also facilitate the separation of proteins in dairy products, such as whey protein [7]. However, the smaller pore size of UF membranes results in a reduced flux compared to MF membranes, leading to a slower separation speed.

MF and UF membranes primarily separate substances in a solution through steric hindrance, which is governed by both the molecular size of the substance and the pore size of the membrane. NF membranes also employ the mechanisms to retain uncharged solutes, involving steric hindrance from membrane pores and diffusion differences in the membrane matrix [8]. However, due to the charged surface of NF membranes, an electrostatic interaction arises between the charged solute or multivalent ions and the NF

membrane [9]. Consequently, NF membranes can reject charged solutes that are considerably smaller than the membrane pores. Drawing inspiration from the NF membrane separation mechanism, we propose a hypothesis that introducing charged groups into membranes with appropriate pore sizes could significantly enhance the electrostatic interaction between membrane charges and protein charges. This enhancement occurs at the nanoscale distance when protein molecules approach or pass through charged nanoscale membrane channels. As a result, it may enable the rejection of proteins substantially smaller than the pore size, and the use of membranes with relatively large pore sizes could potentially lead to an increase in flux.

Polyvinylidene fluoride (PVDF), a polymer, exhibits exceptional mechanical strength, particularly in resistance to creep and fatigue. Additionally, it has several other outstanding properties, such as high thermal stability, enabling its use across a temperature range from -100 to 300°C. PVDF demonstrates good chemical resistance, radiation resistance, and UV resistance, remaining unaffected by sunlight [9]. Given these remarkable attributes, PVDF finds widespread applications in various fields, including sensors, spin valve devices, energy harvesting and storage, as well as membrane filtration. PVDF is widely used in the fabrication of various types of filtration membranes, such as hollow fibers, tubular membranes, and flat sheets. Over the past decade, there has been a notable increase in the number of published research articles related to PVDF membranes [10]. In the pursuit of enhancing PVDF membrane performance, numerous studies on PVDF membrane modification have been published. These modification methods include blending, copolymerization, coating, and grafting [10], [11], [12].

In the blending approach, additives are introduced into the casting solution of membranes. The addition of different additives can alter the hydrophilicity, modify morphology, or decorate the pores of membranes. Various additives have been reported for PVDF

membrane modification, including (1) inorganic nanoparticles such as SiO_2 [13], TiO_2 [14], (2) graphene oxide (GO) [15], (3) carbon nanotubes (CNTs) [16], (4) metal-organic frameworks (MOFs), (5) Ti_3C_2Tx (MXene), (6) surfactant [17], and (7) polymer [10]. Some polymers can be utilized to modify PVDF membranes not only through blending but also through copolymerization [9]. For example, Zheng et al., using poly(vinylidene fluoride-co-chlorotrifluoroethylene) (PVDF-CTFE) copolymer, fabricated filtration membranes via the non-solvent induced phase separation (NIPS) method, achieving more hydrophobic membranes than traditional PVDF membranes [13]. In copolymerization, the copolymer is synthesized before membrane fabrication. Strictly speaking, PVDF copolymer membranes are no longer classified as PVDF membranes. In surface coating, chemically active monomers, polymers, nanoparticles, or other agents for modification are immobilized on the surface of PVDF membranes. No chemical reaction occurs between the coating layer and the PVDF membrane matrix, and the bonding of the coating layer with the PVDF membrane matrix is achieved through van der Waals or electrostatic forces [18]. Some researchers have explored pretreating PVDF membranes via high-energy radiation or chemical reactions to enhance the adsorption to the coating layer [19], [20]. Coating methods include direct precipitation, which involves the direct precipitation of molecules or nanoparticles on the surface of PVDF membranes, followed by curing through heating or a cross-linking process. Surface polymerization is another coating method, where monomers polymerize on the membrane surface, and additives may be added and embedded in the polymerized layer. In the grafting method, molecules or nanoparticles are anchored on the surface of PVDF membranes through chemical bonds. Due to the good chemical stability of PVDF membranes, pretreatment such as alkaline treatment [21], UV-irradiation [22], and plasma [23] is necessary before grafting.

Dendrimers, characterized by a hyperbranched polymer structure resembling the branches of trees or starburst formations [24], possess precise molecular weight and structure,

abundant peripheral sites for functional groups, and a large internal cavity capable of encapsulating drugs or catalysts [25]. Due to these unique properties, dendrimers are widely used in drug delivery, catalysis, sensors, and energy storage [26]. As research on dendrimers progresses, an increasing number of researchers are exploring their applications in modifying filtration membranes. For example, Karmipour et al. incorporated a melamine-based dendrimer with peripheral amine groups bonded to GO into polyether sulfone (PES) membranes. This modification resulted in a membrane with high flux (pure water flux increased from 19.9 LMH for PES membrane to 53.9 LMH for modified membrane at 0.3 MPa), super hydrophilicity, and improved anti-fouling properties during divalent metal ions filtration [27]. Zhu et al. grafted polyamidoamine dendrimers (PAMAM) onto PES hollow fiber membranes, which significantly enhanced the pure water flux and the rejection of various multivalent heavy metal ions [28]. Li et al. immobilized PAMAM dendrimers, which were decorated with silver nanoparticles, on the surface of PVDF membranes, leading to improved hydrophilicity, antibacterial performance, and anti-fouling ability against bovine serum albumin (BSA) or humic acid (HA) [29].

In this study, we attempted to graft the PAMAM-G3.0 dendrimer onto PVDF membranes, with further modification to the PAMAM-G3.5 dendrimer. Before dendrimer grafting, a simple alkaline pretreatment was employed. The performance of both PVDF and PAMAM dendrimer-modified membranes was assessed by whey protein filtration. Furthermore, filtration experiments were conducted using polyacrylic acid (PAA) and polyethylene oxide (PEO) as the solutes to assess the effects of the steric and electrostatic hindrance in membrane filtration.

5.2. Experimental

5.2.1. Materials

Polyvinylidene fluoride (PVDF), Kynar® 740 (Pellet, M_w = 410 kDa), kindly supplied by Arkema Inc. (Philadelphia, PA) were used in this experiment as host polymers. The pore former agent polyethylene glycol (PEG) (M_w = 1 kDa) was purchased from Sigma-Aldrich Inc. (St. Louis, MO). Anhydrous *N*, *N*-dimethylacetamide (DMAc) with a purity of 99.8%, potassium hydroxide, methanol, and isopropanol with a purity of 99.5% were purchased from Sigma-Aldrich Inc. (St. Louis, MO). The ethylenediamine (EDA), with a purity of 99%, and methyl acrylate (MA), with a purity of 99% for PAMAM dendrimer synthesis were purchased from Sigma-Aldrich Inc. (St. Louis, MO). The polyacrylic acid (PAA) (M_w = 100 kDa), polyethylene oxide (PEO) (M_w = 100 kDa), and whey protein for filtration were purchased from Sigma-Aldrich Inc. (St. Louis, MO). Barium chloride, hydrochloric acid, iodine, and potassium iodide for PEO concentration analysis were purchased from Sigma-Aldrich Inc. (St. Louis, MO). The Bradford Reagent for whey protein analysis was purchased from Sigma-Aldrich Inc. (St. Louis, MO). The PAA (M_w = 450 kDa), and potassium nitrate for surface zeta potential measurement were purchased from Sigma-Aldrich Inc. (St. Louis, MO).

5.2.2. PAMAM dendrimer synthesis

The PAMAM dendrimer was synthesized in this research using the divergent method, starting from the EDA core and building one generation at a time, as Figure 5.1 shows. The synthesis process involved the sequential generation of PAMAM dendrimers. The initial step involved the synthesis of the 0.5 generation PAMAM dendrimer through a Michael addition between MA and EDA. Specifically, 15.74 g of MA (with a 10% excess) was

slowly added dropwise to a mixture of 2.5 g of EDA in 10 mL of methanol within a flask at room temperature. Subsequently, the flask was purged off the air with a nitrogen gas stream, and the neck was sealed. The flask was placed in a shaker and shaken at a speed of 160 rpm for 48 hours at 10°C. Following the reaction, the flask was transferred to an oil bath and connected to a vacuum to remove methanol and residual MA for vacuum evaporation.

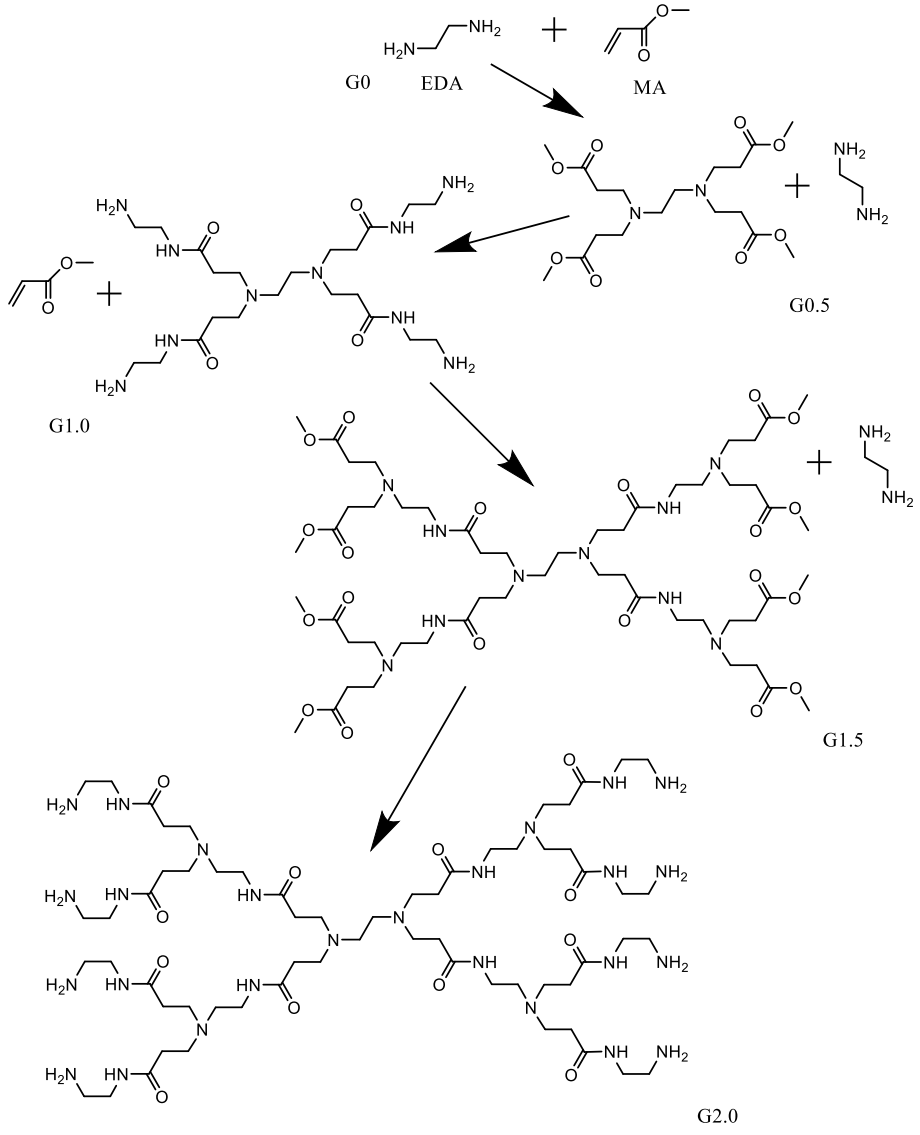

Figure 5.1 Synthesis route of generation 2.0 PAMAM dendrimer.

During vacuum distillation, the solution was stirred by a magnetic rotor at 100 rpm to facilitate gasification. It was crucial to evenly heat the flask to avoid local high temperatures that could lead to serious structural defects in the PAMAM dendrimer. The temperature during vacuum distillation was maintained below 120℃. The vacuum distillation was terminated once the temperature reached 120℃. The residual material in the flask constituted the 0.5 generation PAMAM dendrimer, designated as PAMAM-G0.5. This product appeared as a pale-yellow syrup-like substance at 120℃, solidifying at room temperature. The theoretical weight of the product was 16.82 g.

Table 5.1 Theoretically required and actual amounts of EDA and MA for the synthesis of PAMAM with different generations.

Reaction	Weight of EDA or full-generation PAMAM (g)		Weight of MA or half-generation PAMAM (g)	
	Theoretical	Actual (excess wt %)	Theoretical	Actual (excess wt %)
G0.0 → G0.5	G0.0: 2.50	-	MA: 14.31	15.74 (10%)
G0.5 → G1.0	EDA: 9.98	10.98 (10%)	G0.5: 16.82	-
G1.0 → G1.5	G1.0: 5.00	-	MA: 6.66	7.33 (10%)
G1.5 → G2.0	EDA: 4.65	5.12 (10%)	G1.5: 11.66	-
G2.0 → G2.5	G2.0: 5.00	-	MA: 4.81	5.29 (10%)
G2.5 → G3.0	EDA: 3.36	36.96 (1000%)	G2.5: 9.82	-

Notice: PAMAM-G0.0 is the core of the PAMAM molecule, which is EDA

The synthesis of the generation 1.0 PAMAM dendrimer (PAMAM-G1.0) involves the amidation of PAMAM-G0.5. To achieve this, 16.82 g of PAMAM-G0.5 was dissolved in 15 mL of methanol, and 10.98 g of EDA (with a 10% excess) was slowly added dropwise to the solution mixture at room temperature. Subsequently, the container (flask) was sealed with nitrogen gas and shaken for 48 hours at a speed of 160 rpm at 10℃. The purification step for PAMAM-G1.0 was the same as that for PAMAM-G0.5, involving vacuum distillation. The synthesis of generation 2.0 and generation 3.0 PAMAM dendrimers

followed the same procedure as the synthesis of PAMAM-G1.0, involving repeated steps of Michael addition and amidation. It is worth noting that a higher excess of EDA is required to eliminate defects in the PAMAM dendrimer structure, especially in the synthesis of higher-generation PAMAM dendrimers. The necessary and actual amounts of EDA and MA for the synthesis of PAMAM with different generations are detailed in Table 5.1.

5.2.3. Membrane fabrication

In this study, the PVDF membrane was fabricated using the non-solvent phase separation (NIPS) method, which was discussed in detail in Chapter 3. The casting solution used for membrane fabrication consisted of 82 wt% DMAc, 15 wt% PVDF, and 3 wt% PEG.

5.2.4. Alkaline modification of PVDF membranes

The methods for alkaline treatment have been discussed in detail in Chapter 3. Briefly, the PVDF membrane was immersed in a 0.5 M KOH isopropanol solution at different temperatures: 40℃, 50℃, and 60℃, for 1 minute, followed by immersion in ethanol at room temperature. Then, the membrane was subjected to two ethanol and two deionized water washes to eliminate any residual chemicals, preparing it for the subsequent modification with PAMAM dendrimer grafting and filtration processes. The membranes subjected to alkaline treatment at 40℃, 50℃, and 60℃ were labeled as Alk40, Alk50, and Alk60, respectively.

5.2.5. PAMAM dendrimer-modified membranes

The immobilization of PAMAM-G3.0 on the membrane pretreated with the alkaline solution at 60℃ (Alk60) was carried out as follows. The alkaline-pretreated membrane was

immersed in a methanol solution containing 2.5 wt% PAMAM-G3.0 and 0.5 M KOH and shaken for 24 hours at 10℃. Subsequently, the membrane underwent ethanol wash twice and distilled water wash twice. The membrane modified with PAMAM-G3.0 was labeled as G3.0. Since the peripheral groups of PAMAM-G3.0 were amines, an additional step was taken to react carboxyl groups onto the peripheral layer of the PAMAM dendrimer, through a Michael addition. The G3.0 membrane was immersed in a methanol solution containing MA (50 wt%) and shaken at 10℃ for 24 hours, followed by rinsing with ethanol and deionized water and drying at room temperature. Subsequently, the PAMAM-G3.5 grafted membrane was immersed in a 0.5 M NaOH aqueous solution at room temperature for 30 minutes to hydrolyze the ester groups of PAMAM dendrimer on the membrane into carboxyl groups. This modified membrane was labeled as G3PA. The G3.0 membrane possesses amine groups, which are the positively charged functional groups, whereas the G3PA membrane has carboxylic groups, leading to negative surface charges.

5.2.6. Membrane filtration

A dead-end filtration setup was employed for the evaluation of filtration performance, as detailed in our previous work [30]. Briefly, the membrane was positioned beneath the feed chamber, which contained 200 mL of the feed solution. Nitrogen gas from the nitrogen cylinder was utilized to generate a transmembrane pressure of 60 psig (4.14 bar). The effective area of the membranes was 0.00159 m^2 and the filtration was conducted at room temperature. For the filtration of protein solution, a diluted whey solution containing 100 ppm protein was used as feed. To investigate the separation mechanism, two dissolvable polymer solutions, PAA and PEO solutions were used, each with a concentration of 100 ppm. To enhance the accuracy of the experiment, 10 mL of permeate was discarded before sample collection. All filtration tests were carried out in triplicate using three new coupons fabricated from different batches. The flux of the membranes was calculated using

Equation (5-1).

$$Flux = \frac{v}{t \cdot A} \quad (5\text{-}1)$$

Where v is the volume (L) of the permeate collected during the time t (h) and the A is the effective area of the membrane (m^2).

The polymer and the whey protein rejection R_i were calculated by Equation (5-2).

$$R_i = \frac{c_{i,f} - c_{i,p}}{c_{i,f}} \times 100\% \quad (5\text{-}2)$$

Where $c_{i,f}$ and $c_{i,p}$ are the concentration of the feed and permeate respectively.

The solute concentrations both in feed and permeate were determined by UV-Vis spectrophotometry, which were discussed in Chapter 3. The filtration performance of membranes treated with alkaline solutions at different temperatures for whey protein, PAA, and PEO at high pH (pH = 10) has been discussed in Chapter 3. In this section, the filtration performance of PVDF and modified membranes was examined under the natural pH of each feed solution. The pH of the whey protein and PEO feed solutions was approximately 6, while the pH of the PAA feed solution was around 4.

5.2.7. Membrane characterization

ATR-FTIR

The chemical properties on the membrane's surface were determined by the attenuated total reflectance-Fourier transform infrared (ATR-FTIR) using the Agilent Tech-Cary 630 (Agilent, Canada) spectrometer.

XPS

The elemental composition and functional groups of the base PVDF and alkaline-modified membrane surface were quantified using X-ray photoelectron spectroscopy (XPS) using Kratos Axis Nova spectrometer (Kratos Analytical Ltd., UK) with an Al X-ray source.

The loading of the PAMAM, L, which refers to the mole fraction of atoms constituting PAMAM dendrimer molecules among all the atoms on the membrane surface, was determined by Equations (5-3).

$$L = CN_{membrane}/CN_{PAMAM} \tag{5-3}$$

Where CN_{PAMAM} and CN_{memb} are the elemental composition of nitrogen in the PAMAM dendrimer and on the surface of the membrane, respectively. When L is 100%, the membrane surface is completely covered by PAMAM dendrimer. In that case, the nitrogen atoms molar percentage on the membrane surface is equal to the nitrogen atoms percentage in PAMAM.

The proportion of nitrogen atoms in C-NH_2 bonds to the total number of nitrogen atoms is calculated by Equation (5-4).

$$Ratio_{C-NH_2} = \frac{N_{C-NH_2}}{N_{C-NH_2}+N_{C-NH}+N_{C-N}} \tag{5-4}$$

Where $Ratio_{C-NH_2}$ is the proportion of nitrogen atoms in C-NH_2 bonds to the total number of nitrogen atoms on the membrane surface. N_{C-NH_2}, N_{C-NH}, and N_{C-N} are the numbers of nitrogen atoms in C-NH_2 bonds, C-NH bonds, and C-N bonds, respectively.

SEM

The morphology of the membrane's top surface and cross-section was investigated using a JSM-7500F field-emission scanning electron microscope (FESEM) from JEOL, Japan. The details of surface and cross-section SEM measurements were mentioned in Chapter 3. The surface porosity, average pore size, maximum pore size, and pore number density were determined using Image J software. The pore size here is the diameter of the pore.

Contact angle

The water contact angle of the membranes was measured by the sessile method using the VCA Optima Surface Analysis System (AST Product, Inc., Billerica, MA, US) at 25°C. A 1 μL deionized water droplet was carefully placed on the surface of the dry sample to measure the contact angle. Measurements were made at 5 random spots on the sample, and the average value was reported.

Bulk porosity

The porosity of the membrane was determined using the wet-dry method [31], which was mentioned in Chapter 3. The bulk porosity of the membranes (ε) was calculated using Equation (5-5).

$$\varepsilon = \frac{w_w - w_d}{A_{sample} \cdot l \cdot \rho_{butanol}} \tag{5-5}$$

Where w_w and w_d are the weight (g) of the wet membrane sample and the membrane sample after drying, respectively. A_{sample} is the area of the membrane sample (cm^2), l the thickness (cm) of the dry membrane sample and $\rho_{butanol}$ the density (g/cm^3) of n-butanol. Three samples were used for the measurement and the average value was reported.

Surface zeta potential

The surface charge characteristics of the membranes were assessed through the surface zeta potential test, utilizing the surface Zeta potential cell (ZEN1020) with an accessory kit for the Zetasizer Nano Z (Malvern Panalytical, Worcestershire, UK). The details of surface zeta potential measurement were mentioned in Chapter 3.

Particle size and particle zeta potential

The size and zeta potential of PAA (100 kDa), PEO (100 kDa), and whey protein were analyzed by the Zetasizer Nano Z (Malvern Panalytical, Worcestershire, UK). The concentration of polymer or whey protein solution for particle size measurement was 100 ppm which was the same as the feed concentration. The solutions were ultrasonicated for 30 minutes and degassed for 30 minutes, to well dissolve the polymer and eliminate the gas that may affect the measurement. The Stokes radius of the linear polymer, which is PEO and PAA here, can be calculated by Equation (5-6) [32].

$$r_s = 2.122 \times 10^{-8} \cdot (M \cdot [\eta])^{1/3} \quad (5\text{-}6)$$

Where r_s is the Stokes radius with the unit of cm, M is the molecular weight of the polymer with the unit of g/mol, and $[\eta]$ is the intrinsic viscosity of the polymer, whose unit is dL/g. The intrinsic viscosity of PAA and PEO polymer can be calculated by Equations (5-7) and (5-8).

For PAA [33],

$$[\eta] = 12.4 \times 10^{-4} \cdot M^{0.5} \quad (5\text{-}7)$$

For PEO [32],

$$[\eta] = 1.192 \times 10^{-4} \cdot M^{0.76} \quad (5\text{-}8)$$

5.3. Results and discussion

5.3.1. Membrane characterization

Surface chemistry

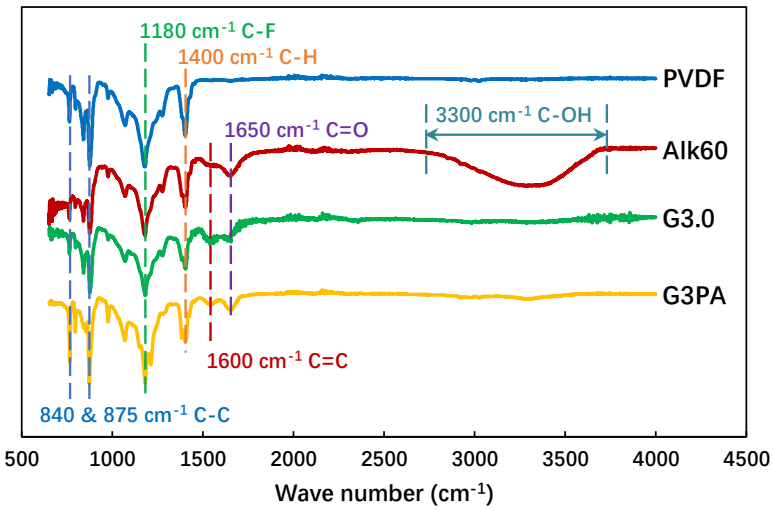

Figure 5.2 FTIR spectrum of the PVDF, Alk60, G3.0, and G3PA membranes.

The alkaline treatment caused the membrane to change color from white to brown and the color became deeper when the extent of the alkaline treatment, which was defined by the alkaline concentration, time, and temperature of treatment, increased. Additionally, alkaline treatment led to a reduction in the membrane's mechanical strength, which also became more severe with the extent of treatment. For instance, extending the alkaline treatment time to 5 minutes at 0.5 M KOH and 60℃ resulted in the modified membrane (either alkali-treated or PAMAM dendrimer-grafted) having such low mechanical strength that filtration experiments cannot be conducted. Considering both the mechanical strength of the membrane and the efficiency of PAMAM dendrimer grafting, the alkaline treatment

time was set to 1 minute. After grafting the PAMAM dendrimer, the color of the membranes did not change significantly and remained brown. As will be discussed more in detail in a later section, the alkaline treatment can cause the formation of C=C double bonds and even the breakup of the carbon chain of PVDF molecules, thereby reducing the mechanical strength of the membrane.

Table 5.2 Membrane surface elemental composition of PVDF (Pristine), alkaline treated (Alk60), PAMAM-G3.0 dendrimer modified (G3.0) and PAMAM-G3.5 dendrimer modified (G3PA) membranes.

Element	PVDF (at. %)	Alk60 (at. %)	G3.0 (at. %)	G3PA (at. %)
C 1s	47.4	59.6	57.6	63.7
N 1s	0	0	7.6	4.2
O 1s	1.0	14.1	13.7	10.0
F 1s	51.5	26.3	21.0	22.2

Figure 5.2 shows the FTIR spectra of the PVDF, Alk60, G3.0, and G3PA membranes. All membranes had double absorption peaks at 840 cm^{-1} and 875 cm^{-1}, caused by C-C backbone vibrations, a broad peak at 1180 cm^{-1}, caused by C-F bond stretching vibrations, and a peak at 1400 cm^{-1}, caused by asymmetrical bending vibration of C-H bonds. After alkaline treatment, three new peaks appeared, a peak at 1600 cm^{-1}, a peak at 1650 cm^{-1}, and a broad peak at 3300 cm^{-1}. These can be attributed to the stretching vibrations of the C=C bond, the C=O bond, and the O-H bond, respectively. In G3.0 with dendrimer grafting, the broad peak at 3300 cm^{-1} disappeared, while the peaks at 1600 cm^{-1} and 1650 cm^{-1}, formed during alkaline treatment, persisted. G3PA also exhibits these two peaks. This suggests that hydroxyl groups react with amine groups of PAMAM dendrimer during PAMAM-G3.0 dendrimer grafting, whereas the C=C bonds or C=O bonds do not react with the PAMAM dendrimer. However, the absorption peak of C-NH_2, 1580 cm^{-1}, is located very close to the absorption peak of C=C, 1600 cm^{-1}, the FTIR spectra cannot directly certify if the dendrimers are immobilized on the membranes. Thus, the surface

chemical properties of membranes were further analyzed by the XPS measurement.

The elemental compositions of carbon, nitrogen, oxygen, and fluorine in the top surface layer of PVDF, Alk60, G3.0, and G3PA membranes are listed in Table 5.5. The experimentally determined ratio of fluorine to carbon content, i.e., 51.5:47.4, is close to the stoichiometric ratio of fluorine to carbon atoms in the PVDF, which is 1:1. The oxygen content of 1% in the PVDF membrane can be attributed to the residue of the pore-forming agent PEG. Alkaline treatment reduces the fluorine content from 51.5% to 26.3% and increases the oxygen content from 1.0% to 14.1% in the membranes. The alkaline treatment replaces fluorine atoms with oxygen-containing groups, i.e., hydroxyl groups (-OH) and carboxyl groups (-COOH). No nitrogen element is detected in the PVDF membrane and Alk60. There is 7.6% and 4.2% nitrogen in the G3.0 and G3PA membranes, respectively. The nitrogen detected in the G3.0 and G3PA membranes is from the PAMAM-G3.0 dendrimer. The decrease of fluorine content from 26.3% of Alk60 to 21.0% in G3.0 and 22.2% in G3PA, respectively, is due to the immersion of Alk60 membranes in a strongly alkaline solution during dendrimer immobilization, which causes further loss of fluorine.

The PAMAM-G3.0 dendrimer contains 228 atoms (excluding hydrogen atoms), with 58 of them being nitrogen atoms. Therefore, the nitrogen composition in PAMAM-G3.0, CN_{PAMAM}, is 25.4%. The XPS data indicates that the nitrogen composition in the G3.0 membrane is 7.6%. Therefore, according to Equation (5-3), the loading (L) of PAMAM-G3.0 dendrimer on membranes is 29.9%. For the PAMAM-G3.5 dendrimer, it contains 420 atoms (excluding hydrogen atoms), including 58 nitrogen atoms. The nitrogen composition in PAMAM-G3.5 is 13.8%. Based on the 4.2% nitrogen content in the G3PA membrane from XPS, the loading rate of the G3PA membrane is 30.4%.

The contents of functional groups related to carbon, nitrogen, oxygen, and fluorine

elements in the PVDF, and modified membranes are listed in Table 5.3. These data are generated by analyzing and fitting the XPS spectrum. Figure 5.3 shows the XPS spectrum for PVDF and the alkaline-treated membrane, while Figure 5.5 shows the XPS spectrum for the PAMAM-G3.0 modified (G3.0) and PAMAM-G3.5 modified (G3PA) membranes. This analysis was conducted using Thermo Advantage software.

Table 5.3 Composition of functional groups of base PVDF, alkaline treated, and dendrimer-modified membranes related with C 1s, N 1s, O 1s, and F 1s.

Element	Core level	Functional group	Binding energy (eV)	Functional group composition (at. %)			
				PVDF	Alk60	G3.0	G3PA
C	1s	C=C	283.5	0	12.0	13.9	11.0
		C-C	284.8	40.8	50.2	50.3	53.6
		$C-H_3$	284.1	10.9	0	0	0
		C-OH	285.2	4.0	0	0	0
		C=O	286.4	0	9.8	11.3	12.9
		C-HF	287.8	0	0.8	0.6	1.6
		$C-F_2$	289.3	44.3	25.0	22.8	20.9
		$C-F_3$	290	0	0	0	0
	sp^3	C-C sp^3	291.9	0	1.6	0.8	0
	1s	K ions absorption	294.6	0	0.6	0.2	0
N	1s	C-N	398.39	NA	NA	82.8	89.0
		C-NH	400.26	NA	NA	10.3	11.0
		$C-NH_2$	405.43	NA	NA	6.9	0
O	1s	C=O	530.1	16.0	13.7	37.1	14.9
		C-OH	531.6	84.0	86.3	62.9	85.1
F	1s	C-HF	685.7	13.5	19.1	2.2	22.2
		$C-F_2$	686.3	81.6	75.8	95.9	77.8
		$C-F_3$	687.5	4.9	5.0	1.9	0

The alkaline treatment not only causes the membrane to contain abundant oxygen-containing functional groups but also introduces many carbon-carbon (C=C) double bonds. Some researchers have reported that the elimination reaction during alkaline treatment can form C=C bonds in PVDF membranes.

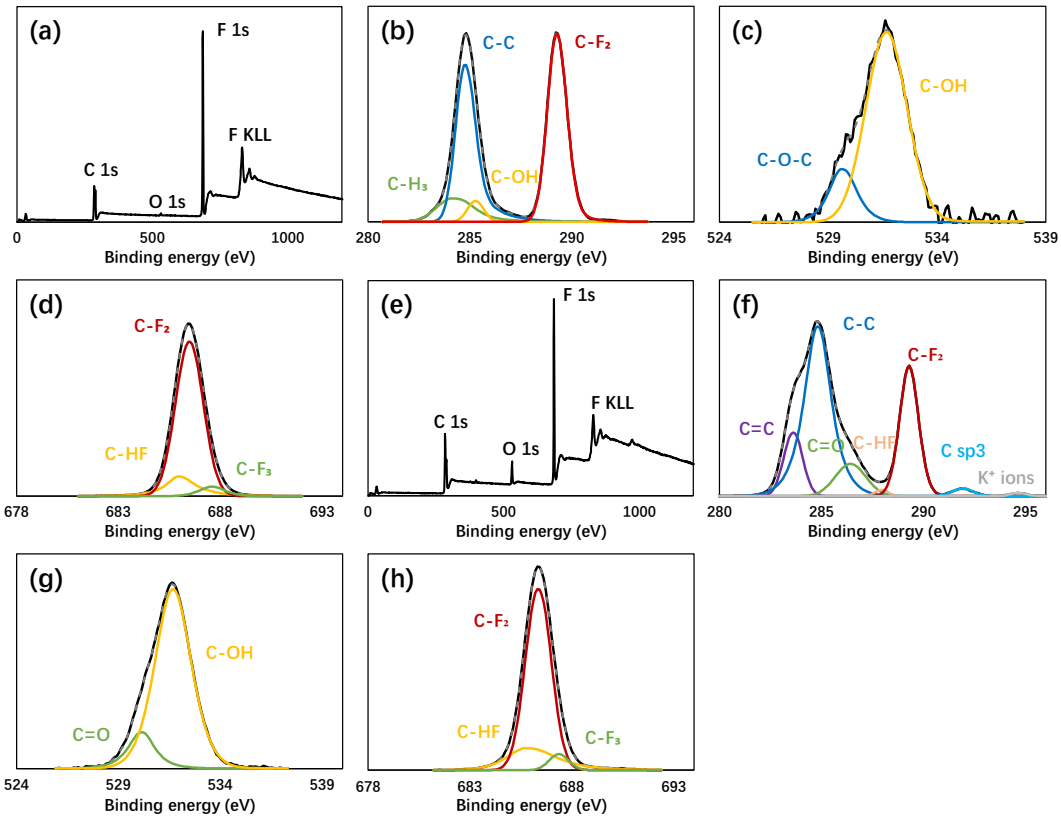

Figure 5.3 XPS whole survey spectra, C 1s peaks, O 1s peaks, and F 1s peaks of the base PVDF membrane {(a), (b), (c), and (d)} and Alk60 {(e), (f), (g) and (h)}.

There are two methods for immobilizing amine-containing molecules on a PVDF membrane. The first method involves directly immersing the membrane in an alkaline solution containing molecules with amine groups [34]. The second method involves initially treating the PVDF membrane with an alkaline solution, followed by immersion in the amine-containing molecule solution [35]. Previous studies have generally found that in an alkaline solution, or an alkaline solution containing molecules with amine groups, PVDF molecules will lose fluorine atoms and form -CH=CF- structures on the carbon chain, as shown by Equations (5-9) and (5-10).

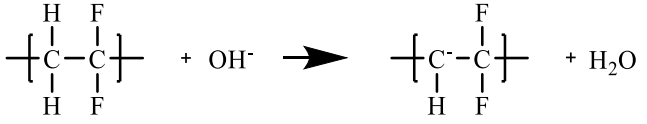

(5-9)

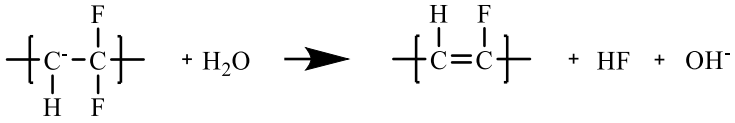

(5-10)

The amine group can react with this structure, forming a C-N bond with the PVDF molecule. In the meantime, the remaining fluorine atom on the carbon can be further removed, resulting in the formation of a -CH=CN- structure [34], [35], [36], [37], as shown in Equation (5-11), (takes the PAMAM dendrimer as an example of amine-containing molecules).

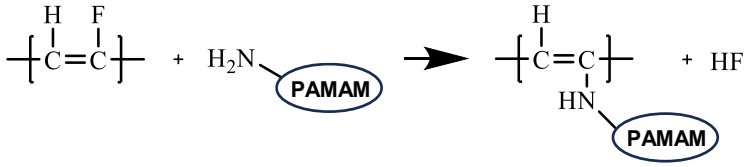

(5-11)

In Table 5.3, the C=C bond composition does not significantly decrease after PAMAM-G3.0 dendrimer grafting. Alk60 contains 12.0% C=C bonds in the C 1s spectrum, while G3.0 and G3PA are 13.9% and 11.0%, respectively, which indicates the PAMAM dendrimer was immobilized on PVDF membranes by -CH=CN- structure, as shown by Equation (5-11). On the other hand, a carbon-carbon double bond can react with water and form a hydroxyl group on the backbone of PVDF molecules, as shown by Equation (5-12).

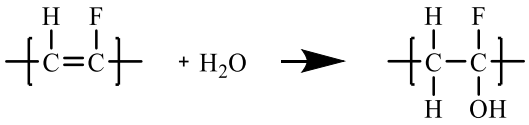

(5-12)

the hydroxyl (C-OH) group content decreased from 86.3% of Alk60 to 62.9% in G3.0 according to the O 1s spectrum, indicating that the hydroxyl groups are consumed during PAMAM dendrimer grafting. Therefore, the peripheral amine group of PAMAM dendrimer also reacts with the hydroxyl (C-OH) group to form a C-O-N structure during dendrimer grafting, as shown in Equation (5-13).

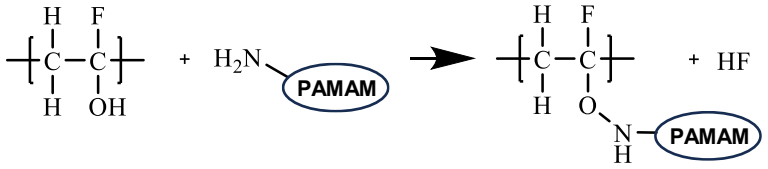

(5-13)

As Figure 5.4 shows, there are 14 C-N bonds, marked green, 28 C-NH bonds, marked orange, and 16 C-NH_2 bonds, marked blue. Therefore, there are a total of 16 + 28 + 14 = 58 nitrogen atoms, among which 16 are from C-NH_2. According to Equation (5-4), the proportion of C-NH_2 bonds to the total number of nitrogen-containing bonds in PAMAM-G3.0 is 16 ÷ 58 = 27.6%.

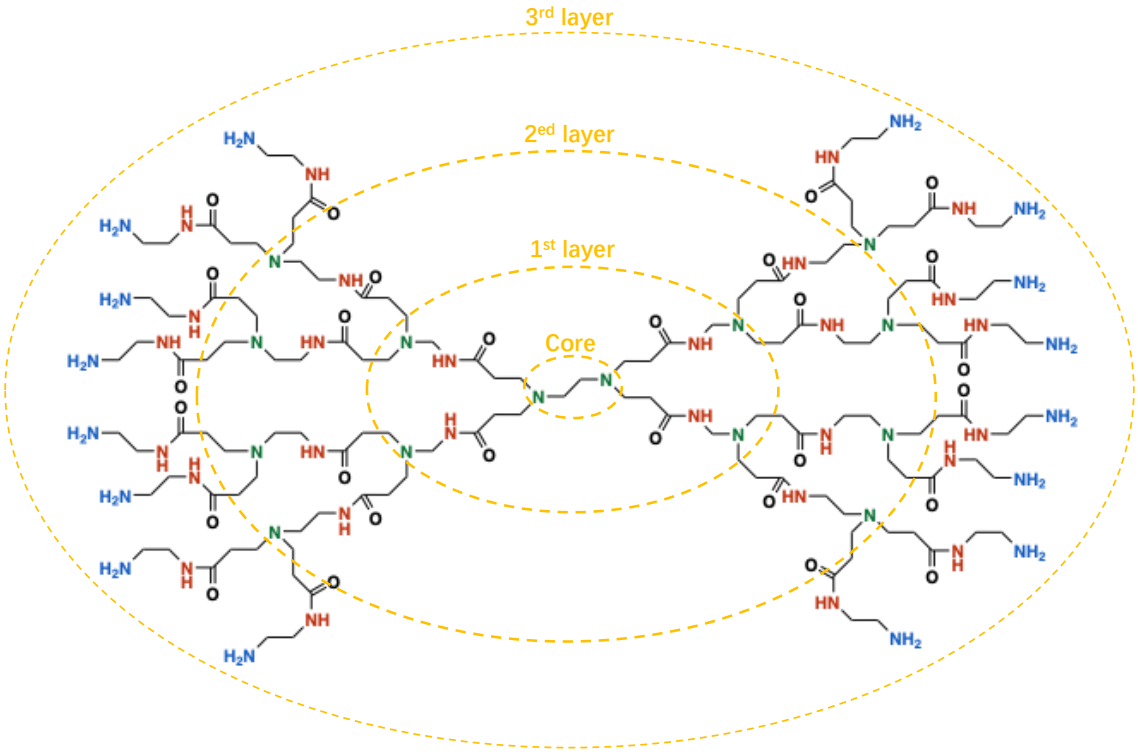

Figure 5.4 Molecular formula of PAMAM-G3.0 dendrimer.

The hydroxyl (C-OH) group content in the G3PA membranes increased to 85.1% when transferring the PAMAM-G3.0 to PAMAM-G3.5, which was contributed by the peripheral carboxyl groups of PAMAM-G3.5 dendrimer.

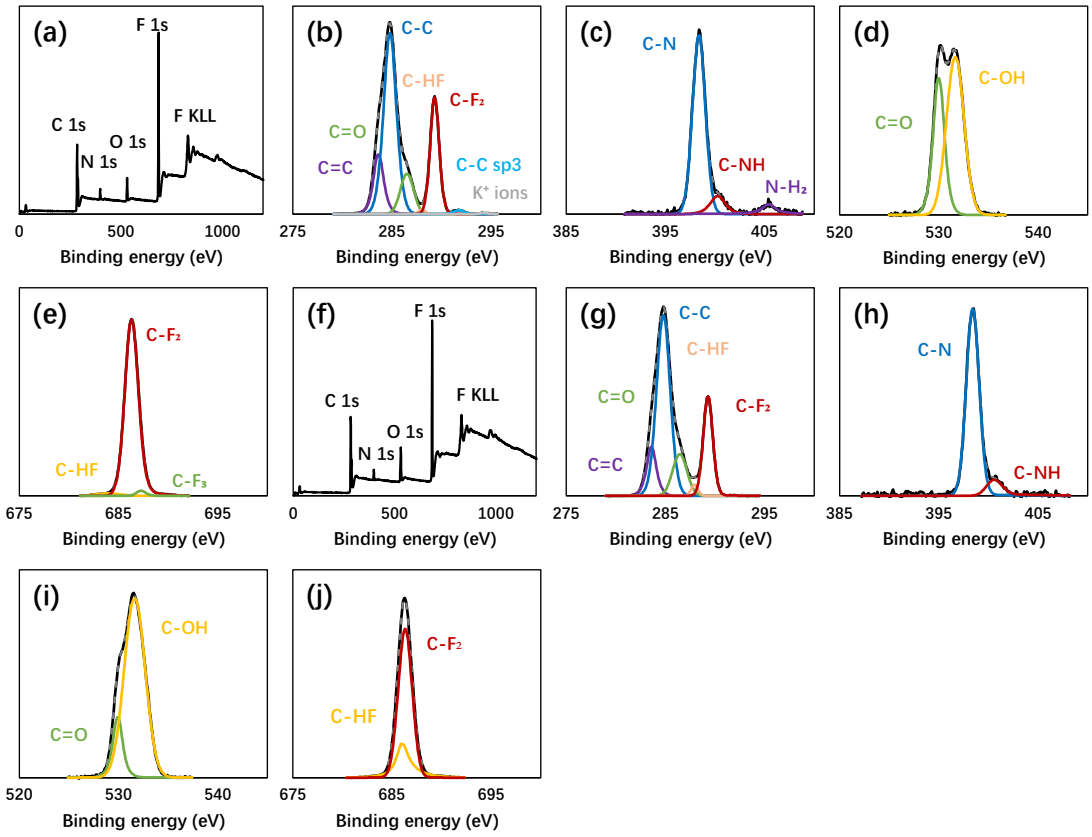

Figure 5.5 XPS whole survey spectra, C 1s peaks, N 1s peaks, O 1s peaks, and F 1s peaks of G3.0 { (a), (b), (c), (d), (e)} and G3PA { (f), (g), (h), (i) and (j)}.

However, the C-NH_2 bonds ratio in the G3.0 membrane is 6.9%, according to the N 1s spectrum. This indicates that about 75% of the C-NH_2 bonds are consumed during grafting. Therefore, one PAMAM-G3.0 dendrimer molecule connects with membranes through 12 amine groups, not just 1 amine group. Since the small PAMAM dendrimer cannot be viewed as rigid spheres, but more like star-like branched molecules (disk-like) [38], the PAMAM-G3.0 dendrimer grafted on the membrane is more like a plate lying on the membrane surface. The 12 peripheral amine groups react with the hydroxyl groups on the membrane surface to form covalent bonds, anchoring the dendrimer on the membrane surface. There are 4 unreacted amine groups for every PAMAM-G3.0 dendrimer, which is immobilized on membranes.

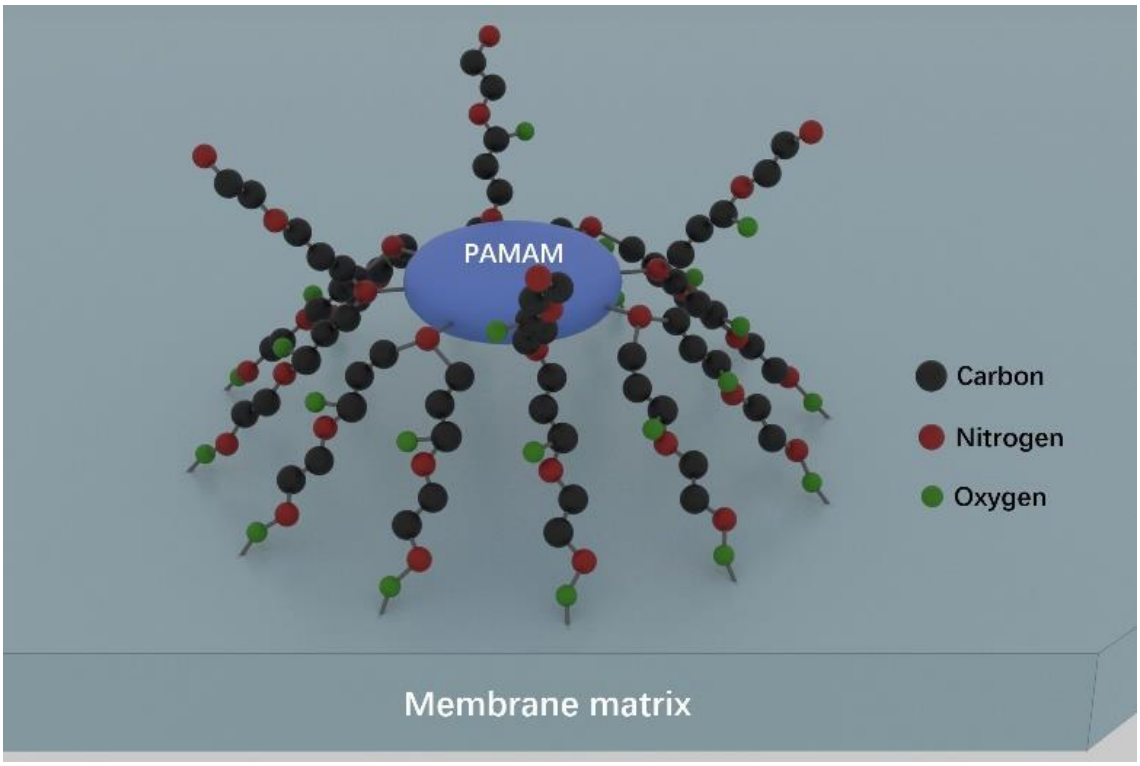

Figure 5.6 Sketch of the connection structure between PAMAM dendrimer and PVDF membrane.

In the schematic diagrams reported on dendrimer-modified filtration membranes, it is often shown that the dendrimers are spherical and protrude from the surface of the membrane. However, our observations suggest that the dendrimer immobilized on the membrane surface is more like a plate lying on the surface of the membranes, as shown in Figure 5.6. Here, we take the mechanism shown in Equation (5-13) as an example.

Surface morphology and porosity

Figure 5.7 displays cross-sectional SEM images of PVDF, Alk60, G3.0, and G3PA membranes. The thickness of both PVDF and modified membranes ranges from 35 to 40 μm, comprising a finger-like layer and a sponge-like layer. The finger-like layer constitutes approximately 60% of the membrane thickness, with smooth pore walls in this layer.

The SEM surface images of PVDF membranes and modified membranes are shown in

Figure 5.8. For all membranes, the surface appears smooth and flat, with a uniformly distributed pore structure. Some cracks are visible on the membrane surfaces, with Alk60 exhibiting the most, followed by the PVDF membrane. In contrast, the G3.0 surface displays the fewest cracks. It is important to note that these cracks are a result of electron beam irradiation during SEM analysis.

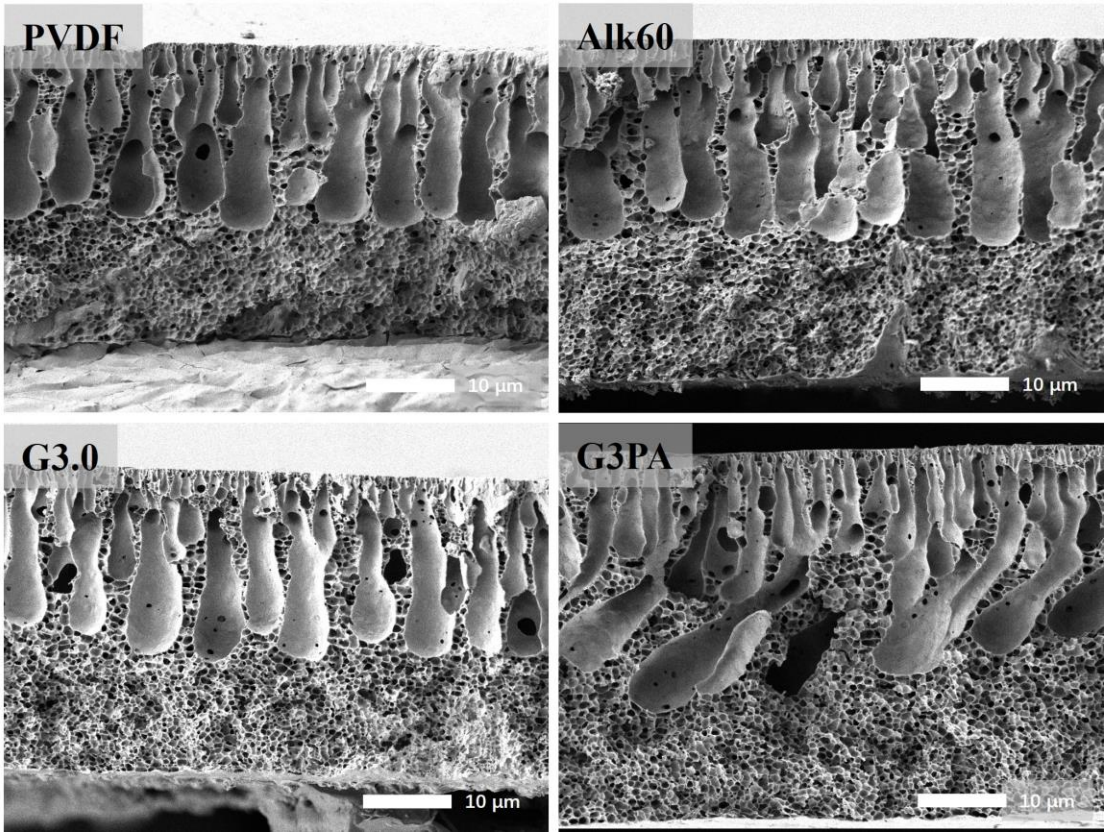

Figure 5.7 Cross-sectional SEM images of the base PVDF membranes, 60°C alkaline treated (Alk60), PAMAM-G3.0 modified (G3.0), and PAMAM-G3.5 modified (G3PA) membranes.

Surface porosity, maximum pore size, average pore size, and surface pore number density were calculated using Image J software and are summarized in Table 5.4. The analysis excluded pores with an area less than 500 nm^2, focusing on those with a diameter larger than 25 nm. The surface porosity of the PVDF membrane is 1.8%. Following 60°C alkaline treatment, membrane surface porosity increases to 2.5% due to the etching effect of the

alkaline solution. Notably, the PAMAM-G3.0 treatment solution containing 0.5 M KOH continues the alkaline etching effect, even at a treatment temperature as low as 10°C. Consequently, surface porosity further increases to 2.8% after PAMAM-G3.0 modification. However, after transferring from G3.0 to G3PA, the surface porosity reduces to 2.5%. This reduction may be attributed to the larger size of the PAMAM-G3.5 dendrimer, occupying more space within the membrane pore.

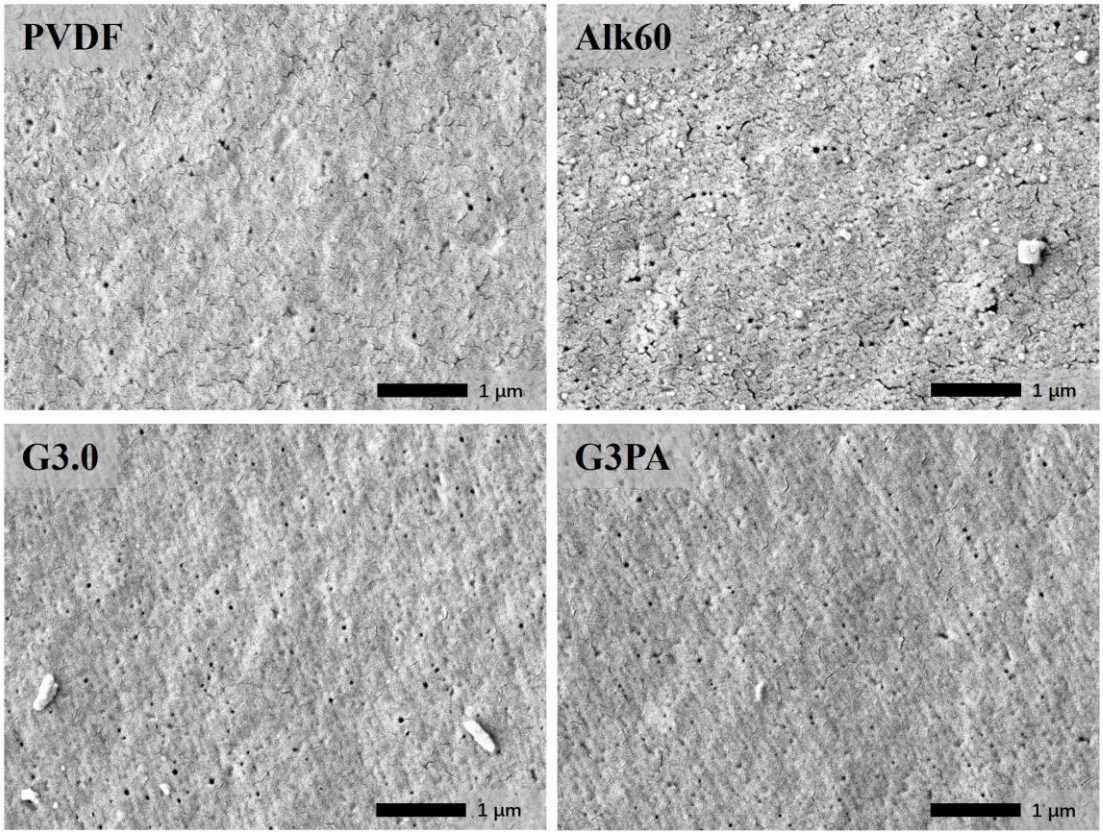

Figure 5.8 Surface SEM images of base PVDF membranes, 60°C alkaline treated (Alk60), PAMAM-G3.0 modified (G3.0), and PAMAM-G3.5 modified (G3PA) membranes.

The maximum pore size of PVDF, Alk60, and G3.0 membrane is consistently around 71 nm. However, the maximum pore size of G3PA slightly deviates at 79.8 nm, which might be out of line. The modification has a minimal impact on the average pore size of membranes, which ranges between 38.6 nm and 41.7 nm for PVDF and modified

membranes. Pore density on the membrane surface is significantly affected by the modification process, particularly during the 60°C alkaline treatment. After alkaline treatment, pore density increases from 13.0 per μm^2 of PVDF membrane to 19.1 per μm^2 for Alk60. The alkaline etching process generates new micropores on PVDF membranes, contributing to the observed increase in pore density. As mentioned earlier, alkaline etching continues during PAMAM-G3.0 treatment, leading to a further increase in pore density to 22.0 per μm^2. However, subsequent transfer from G3.0 to G3PA results in a slight decrease in pore density to 20.2 per μm^2. This reduction can be attributed to the larger size of the PAMAM-G3.5 dendrimer, occupying more space within the membrane pore, and causing the sealing of some small pores.

The alkaline treatment reduces the bulk porosity of the membrane from 79% for PVDF membrane to 71% for Alk60. Subsequent PAMAM-G3.0 and PAMAM-G3.5 treatments further contribute to the reduction in bulk porosity, reaching 67% and 61%, respectively. It is reasonable that G3PA has a lower bulk porosity than G3.0 since the PAMAM-G3.5 dendrimer will occupy more space than the PAMAM-G3.0 dendrimer inside the pores.

Table 5.4 Bulk porosity, surface porosity, the maximum, average pore size, and surface pore number density of the base PVDF membrane, 60°C alkaline treated (Alk60), PAMAM-G3.0 modified (G3.0) and PAMAM-G3.5 modified (G3PA) membranes.

Membrane	Bulk porosity (%)	Surface porosity (%)	Maximum pore diameter (nm)	Average pore diameter (nm)	Pore number density (pores per·μm^2)
PVDF	79 ± 2	1.8 ± 0.1	70.3 ± 4.1	40.3 ± 0.5	13.0 ± 0.1
Alk60	71 ± 1	2.5 ± 0.3	72.4 ± 2.4	39.2 ± 0.3	19.1 ± 0.3
G3.0	67 ± 3	2.8 ± 0.1	71.4 ± 1.5	41.7 ± 0.3	22.0 ± 0.2
G3.5	61 ± 2	2.5 ± 0.1	79.8 ± 2.0	38.6 ± 0.2	20.2 ± 0.2

In summary, alkaline etching of the surface generates new micropores, increasing surface porosity and pore number density. However, alkaline etching inside the membrane matrix

reduces the bulk porosity. The PAMAM-G3.5 dendrimer occupies more space in the pores compared to the PAMAM-G3.0 dendrimer, leading to a decrease in surface porosity, pore number density, and bulk porosity.

Surface hydrophilicity

The contact angles of the PVDF membranes, as well as those treated at 40°C, 50°C and 60°C with alkaline (Alk40, Alk50 and Alk60), PAMAM-G3.0 (G3.0), and PAMAM-G3.5 (G3PA), are illustrated in Figure 5.9. The alkaline treatment introduces numerous hydrophilic hydroxyl and carboxyl groups to the membrane, enhancing its hydrophilicity. The contact angle of the PVDF membrane is 89.9°, and after alkaline treatment at 50°C, the contact angle decreases to 59.0°. Further increases in temperature beyond 50°C have a minimal impact on the density of the polar functional groups. Therefore, when the temperature is raised from 50°C to 60°C, the contact angle only slightly decreases, reaching 57.7°.

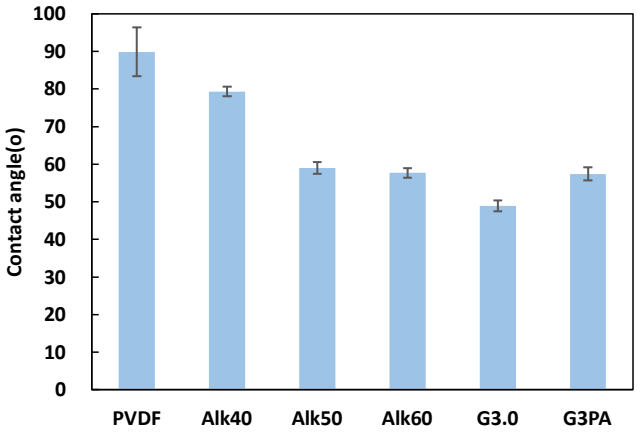

Figure 5.9 Contact angle of the PVDF membranes, 40°C, 50°C, 60°C alkaline treated (Alk40, Alk50 andAlk60), PAMAM-G3.0 modified (G3.0), and PAMAM-G3.5 modified (G3PA) membranes.

Subsequent treatment with PAMAM-G3.0 dendrimer introduces more hydrophilic amine groups on the membrane, further enhancing its hydrophilicity, and the contact angle of the

membrane decreases to 48.9°. However, as the peripheral functional groups of PAMAM-G3.5 dendrimer are carboxyl groups, the hydrophilicity of the membrane decreases when PAMAM-G3.0 on membranes is converted to PAMAM-G3.5. Consequently, the contact angle increases to 57.4°. The contact angles of the membranes treated at 60°C and the PAMAM-G3.5 modified membranes are similar.

Surface zeta potential

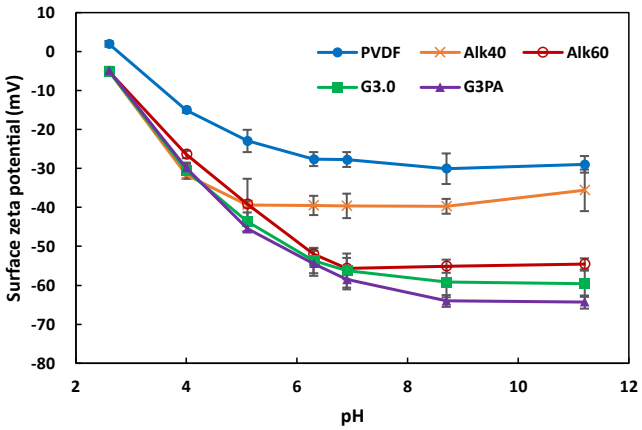

Figure 5.10 Surface zeta potential of the PVDF membranes, 40°C, 60°C alkaline treated (Alk40, Alk60), PAMAM-G3.0 modified (G3.0) and PAMAMG3.5 modified (G3PA) membranes.

The surface zeta potential of the PVDF and modified membranes is illustrated in Figure 5.10. The surface zeta potential tends to decrease with the pH increase. The surface zeta potential of PVDF is -5.4 mV at pH 2.6, reducing to -42.2 mV when the pH increases to 6.3; after pH 6.3, the surface zeta potential of the PVDF membrane enters a plateau stage. The surface zeta potential of Alk40 membranes is slightly lower than that of PVDF membranes. The increase in the alkaline treatment temperature decreases the surface zeta potential of the membrane, which also exhibits a plateau region at the higher pH. For instance, the 40°C alkaline treated membrane enters a plateau area at pH 5.1, with a surface zeta potential of -36.4 mV. In contrast, the membrane alkaline treated at 60°C reaches a surface zeta potential of -55.7 mV at pH 6.9 before entering the plateau region.

Generally, surfaces with amine groups tend to exhibit positive charges. However, in our measurements, the surface charge of the membrane after grafting PAMAM-G3.0 dendrimer slightly increased, e.g., the surface zeta potential of membranes decreases from -59.2 mV for the Alk60 membrane to -61.5 mV for the G3.0 membrane at pH 8.7. This is because alkaline etching continued during dendrimer grafting in the presence of a strong alkaline solution, leading to an increase in the carboxyl group, whose effect surpassed that of the peripheral amine groups of the dendrimer. When transferring the PAMAM-G3.0 on the membranes to PAMAM-G3.5, the negative charge on the membrane surface is further enhanced due to the conversion of the peripheral amine groups to the carboxyl groups. The peripheral functional groups of PAMAM-G3.5 dendrimer are carboxyl groups, which are the same groups present on the 60°C alkaline-treated membranes. However, due to the branch structure of the PAMAM-G3.5 dendrimer, the PAMAM-G3.5 modified membranes have a higher carboxyl group density than that of the 60°C alkaline-treated membranes. Therefore, the G3PA membranes have a lower surface zeta potential of -64.0 mV.

5.3.2. Rejection of solutes of different sizes and charges

Three macromolecules, including two linear polymers, i.e., PAA, which is negatively charged, and PEO, which is noncharged, and whey proteins, were selected strategically in this study to characterize the rejection of membranes. The Stokes radius of PAA and PEO with molecular weight 100 kDa is 7.13 nm and 8.96 nm, respectively, based on Equations (5-6), (5-7) and (5-8). The radius of PAA and PEO measured by the Zetasizer Nano Z instrument were 100.1 nm and 156.6 nm, respectively. The measured radii of PAA and PEO were 14 and 17.5 times their Stokes radius, respectively. Since the concentration of polymers in the solution was low (100 ppm), the interaction between different polymer molecules was weak. Therefore, we cannot use the formation of agglomerates to explain the vast differences between the Stokes radii and their measured radii.

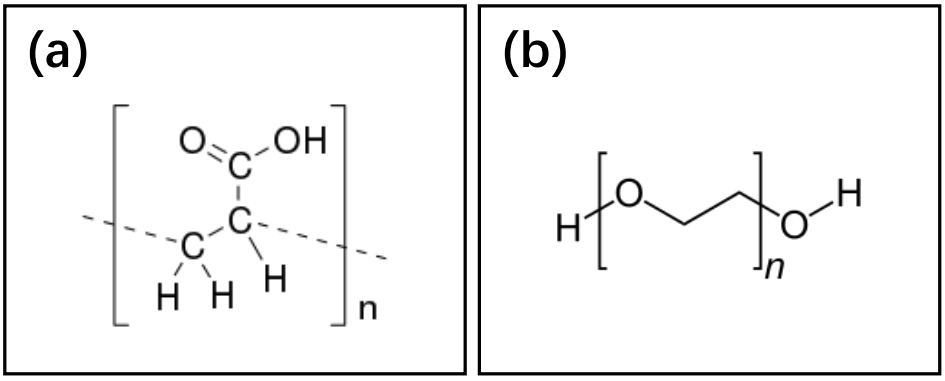

Figure 5.11 Molecular formula of PAA (a) and PEO (b).

As shown in Figure 5.11, the PAA polymer has a carboxyl group as the side group for each monomer, which has a molecular weight of 72 Da. Therefore, a 100 kDa PAA would have approximately 1389 monomers. The fully extended length of PAA would be approximately 340.8 nm. On the other hand, the monomer of PEO has a molecular weight of 44 Da. The fully extended length of 100 kDa PEO is 633.3 nm. The extended lengths of PAA and PEO were 3.4 and 4.0 times their measured radii, respectively. Since the Zetasizer determines the radius of particles by measuring the dynamic light scattering, it appears that the much larger radii of PAA and PEO reported by the Zetasizer than their hydrodynamic radii were caused by the bending and loose folding of the polymer molecules in the solution.

The average measured radius of whey proteins in the feed solution was 99.8 nm. Unlike PAA and PEO polymers, which both have uniform molecular weights of 100 kDa, whey proteins are a mixture of various proteins with molecular weights ranging from 6.7 to 80 kDa [39] and Stokes radii reported to be in the range of 1.0 nm to 6.1 nm [40]. Also, unlike PAA and PEO polymers, which are both linear molecules, each kind of whey protein has its stable and unique nonlinear configuration. Therefore, the much larger average particle size of ~90 nm as reported in Table 5.5 cannot be explained by the loose folding of these protein molecules. The major components of whey proteins, i.e., β-Lactoglobulin and α-Lactalbumin have molecular weights of 18.3 kDa and 14 kDa, respectively, which are 18.3%

and 14.0% of the 100 kDa PAA and PEO, pointing to an average molecular weight several times smaller than that of PAA and PEO. Therefore, at the same mass concentration of 100 ppm, the number of molecules in a whey protein solution would be several times that of PAA and PEO. They hence have a much larger probability of forming agglomerates than PAA or PEO, which was probably the major reason for the ~ 90 nm average radius of whey proteins recorded by the Zetasizer, which was much larger than the aforementioned Stokes radii of all the whey proteins.

Table 5.5 dimensional properties and the zeta potential of PAA, PEO and whey proteins as in feed solution

Material	PAA	PEO	Whey proteins
Molecular weight (kDa)	100	100	6.7 – 80 [39]
The molecular weight of monomer (Da)	72	44	NA
Number of monomers	1388	2272	NA
Fully extended length (nm)	340.8 [41]	633.3 [42]	NA
Measured radius (nm)	100.1	156.6	99.8
Stokes radius	7.13	8.96	1.0-6.0
Feed solution pH	4	6	6
Zeta potential (mV)	-32.4	-3.8	-18.9

The zeta potential of PAA, PEO and whey were -32.4 mV, -3.8 mV and -18.9 mV respectively. The PAA has the lowest zeta potential. The zeta potential of PEO is close to 0 mV.

The rejection of PEO, PAA, and whey protein by PVDF, Alk40, Alk50, Alk60, G3.0 and G3PA membranes is presented in Figure 5.12. Herein PEO rejection as shown in Figure 5.12 (a) is due to the steric hindrance since PEO is electrically neutral. PEO rejection increased progressively with the increase in treatment temperature. While the PEO rejection by the PVDF membrane was 16.4%, it eventually increased to 55.1% by the Alk60 membrane, which had an alkaline treatment temperature of 60℃. It seems that the

alkaline treatment not only introduces charged groups on the membrane surface but also etches the membrane matrix, generating new micropores. This is reflected in the increase of pore number density and surface porosity after alkaline treatment as shown in Table 5.4. However, the maximum and average pore sizes remained almost the same after alkaline treatment.

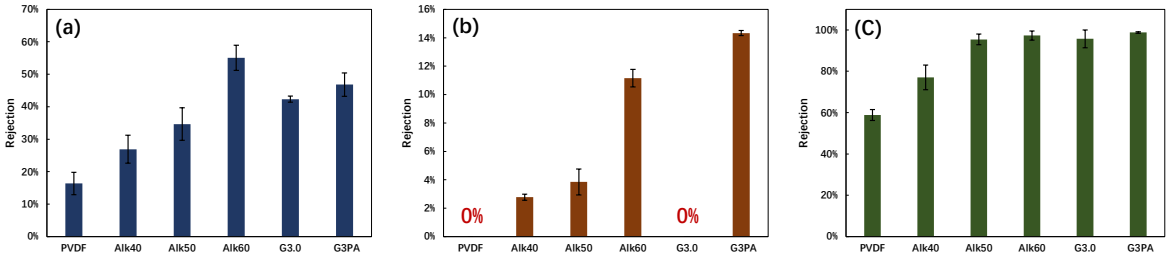

Figure 5.12 Rejection of the PVDF membranes, alkaline treated membranes (Alk40, Alk50, and Alk60) at different treating temperatures, PAMAM-G3.0 modified (G3.0), and PAMAM-G3.5 modified (G3PA) membranes ((a) PEO solute, (b) PAA solute, and (c) whey protein).

Subsequent treatment of the alkaline treated membranes with PAMAM dendrimer grafting reduced the PEO rejection, e.g. PEO rejection of G3.0 is 42.3%. This is probably due to the continuing pore etching that occurs in the strong alkaline environment during the dendrimer grafting, which contributed more to the pore size enlargement than the generation of micropores. Finally, grafting the PAMAM-G3.5 dendrimer onto the membrane surface resulted in a rejection of 46.8%, which is slightly higher than that of G3.0. This is probably because the PAMAM-G3.5 dendrimer occupies more of the space in the pore, reducing the pore size. Based on the PEO rejection data, the order of the membrane pore sizes of different membranes is Alk60<G3PA<G3.0<Alk50<Alk40< PVDF.

As for the PAA rejection, shown in Figure 5.12 (b), the PVDF membrane and G3.0 cannot reject PAA molecules, exhibiting a PAA rejection of 0%. The PAA rejection for alkaline-treated membranes increased from 2.8% of Alk40 to 11.2% of Alk60. G3PA showed the

highest PAA rejection of 14.3%. These results are understandable by considering that PAA rejection is primarily governed by the interactions between the charged PAA molecules and the charges on the surface and inside the pores of a membrane. Electrically neutral PVDF membrane and G3.0, which have positively charged amine groups on the surface, did not exert any electrostatic repulsion on PAA molecules. It is worth noting that the measured size of PAA (Table 5.5) is larger than the pore size of the PVDF or G3.0 membranes (Table 5.4). This phenomenon could be tentatively attributed to the fact that, as afore discussed, the PAA molecules might not have behaved as rigid spheric bodies but rather existed in the form of loosely folded filamentous molecules. Indeed, as aforementioned, the hydrodynamic radius of PAA was much smaller than the average pore radius of membranes. Therefore, the steric exclusion from the membrane cannot effectively prevent PAA molecules, which have a Stokes radius of 7.13 nm, from passing through the membranes (average pore diameter around 40 nm). It is interesting to note that the positively charged G3.0 shows no rejection, while the negatively charged Alk50 has a rejection of 3.8% even though the pore size of G3.0 is smaller. This suggests that the separation by Alk50 is dominated by electrostatic hindrance rather than steric hindrance in PAA filtration. Even though PAA has the same molecular weight as PEO the rejection of PAA was much lower than PEO by electrically neutral PVDF membrane. This could be explained by the larger Stokes radius of PEO (8.96 nm) than that of PAA (7.13 nm).

The whey protein rejection for PVDF membranes, which relied solely on steric hindrance since PVDF carries no charges, was 58.9%. After 40℃ alkaline treatments, the rejection significantly increased to 77.1%. The proteins rejected by the PVDF membrane might be primarily agglomerates that were large enough to be retained by size rejection of the membrane. Further increases in alkaline treatment temperature led to additional rejection enhancement, eventually reaching 97.3% at 60℃. These increases in whey protein rejection are attributed to the increase in surface negative charge. Following PAMAM-G3.0

dendrimer grafting on Alk60 membranes, the whey protein rejection is only slightly reduced to 95.7%, despite the presence of positively charged amine groups in G3.0 and negatively charged carboxylic group in Alk60. The whey protein rejection of G3.0 was only slightly lower than that of G3PA (98.8%), which was the highest rejection observed in this work. Both Alk60 and G3PA are negatively charged but G3PA had a much larger charge density than Alk60, hence, the increased rejection of whey proteins, which are negatively charged at the pH of the feed solution, which is pH6.

As discussed before, when proteins are a mixture of a variety of proteins of different molecular weights and Stokes radii. While relatively large proteins, e.g., Immunoglobulins (75-95 kDa), Bovine serum albumin (66.3 kDa), β-Lactoglobulin (M_w = 18.3 kDa) and α-Lactalbumin (M_w = 14 kDa) are the major proteins in whey, small proteins still account for a significant portion. For instance, glycomacropeptide, which has a molecular weight of only 6.7 kDa, may account for ~24% of whey proteins in some cases [43]. In other words, to have a high rejection of whey proteins as observed with the Alk60 and G3PA membrane, which is 97.3% or higher, a membrane must be able to reject small proteins such as glycomacropeptides, which have Stokes radii of approximately 1.0 nm. Since the membrane radius was approximately 20 nm (pore size 40 nm), the rejection of such small protein molecules would require static electric rejection caused by the negative charges introduced onto the membrane surfaces and pores by the respective treatments. It should be pointed out that the G3.0 membrane was positively charged and the enhanced retention of whey proteins achieved by it in comparison to that of the PVDF membrane was likely achieved by adsorption.

5.3.3. Flux

The pure water flux and permeate flux in PEO, PAA, and whey protein filtration are shown

in Figure 5.13. The pure water flux of the PVDF membrane is 274.1 LMH. Alkaline treatment significantly reduces the pure water flux, with Alk60 exhibiting a flux of 115.7 LMH. Subsequent PAMAM-G3.0 dendrimer grafting further decreases the pure flux to 92.3 LMH. G3PA membrane displays the lowest pure water flux at 60.6 LMH.

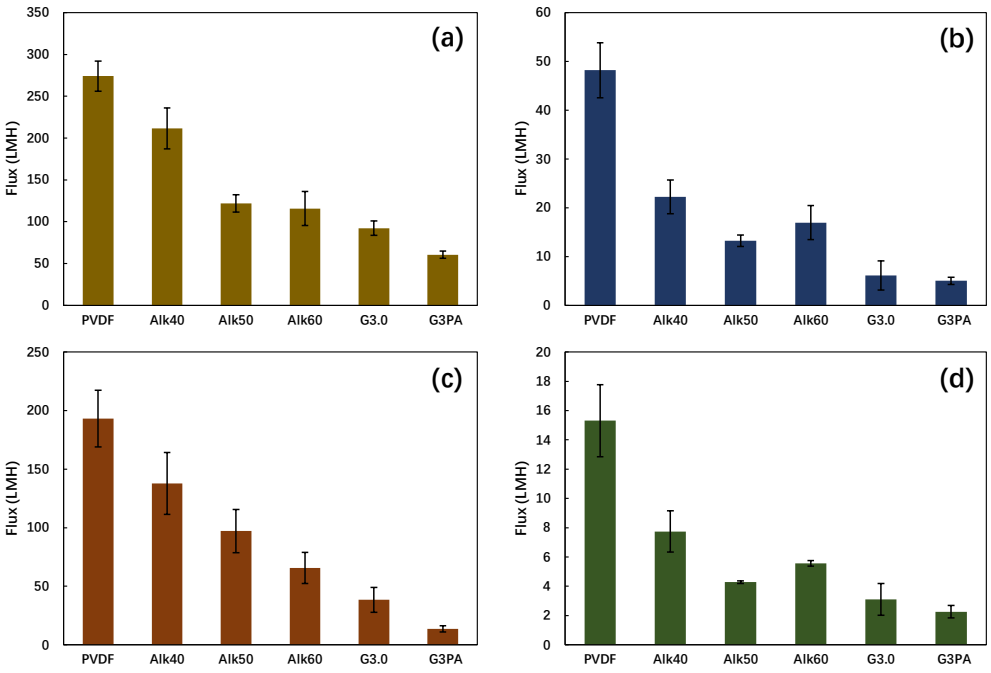

Figure 5.13 Pure water flux (a) and permeate flux of the PVDF membranes, alkaline treated membranes (Alk40, Alk50, and Alk60) at different treating temperatures, PAMAM-G3.0 modified (G3.0), and PAMAM-G3.5 modified (G3PA) membranes in PEO (b), PAA (c), and whey protein (d) filtration.

While alkaline etching increases surface porosity by generating micropores, it affects both the membrane surface and matrix. During the alkaline treatment, the entire PVDF membrane was immersed in an alkaline isopropanol solution, impacting both the surface and internal matrix. As a result, the bulk porosity is decreased (see Table 5.4, second column), leading to a decrease in pure water flux. The transition from G3.0 to G3PA further reduces the bulk porosity and pure water flux due to the bulkiness of the G3.5 dendrimer.

As the same as pure water flux, the alkaline treatment reduced the permeate flux in PEO,

PAA or whey protein filtration. The permeate flux further decreased, after PAMAM-G3.0 dendrimer grafting. The G3PA membrane had the lowest permeate flux in PEO, PAA and whey protein filtration In PEO filtration, the permeate flux of PVDF, Alk60, G3.0, and G3PA was 48.2, 17.0, 6.1, and 5.0 LMH, respectively. In PAA filtration, the PVDF membrane had the highest permeate flux of 193.1 LMH. The permeate flux of Alk60, G3.0, and G3PA membranes is 65.7 LMH, 38.4 LMH, and 13.6 LMH, respectively. During whey protein filtration, the permeate flux of PVDF, Alk60, G3.0, and G3PA membranes is 15.3 LMH, 5.6 LMH, 3.1 LMH, and 2.3 LMH, respectively. For the same membrane, the flux follows the order: of pure water filtration > PAA filtration > PEO filtration > whey protein filtration.

The fluxes of different solutes, when compared for the same membrane, follow the order of pure water > PAA > PEO > whey protein. This phenomenon cannot be attributed to a single factor but may be related to the size, shape, and charge density of molecules that could all affect the texture of the cake layer on the membrane surface formed during filtration, including cake thickness, pore size, porosity, etc. For the two linear polymers, i.e., PAA and PEO, the Zetasizer measured radius of PEO in the solution is 1.56 times of PAA, corresponding to fully extended molecular lengths of 340.8 and 633.3 nm, respectively. The smaller extended length of PAA plus its large density negative charges, may result in more rigid linear molecules than the much longer and electrically neutral PEO molecules and therefore form a cake layer on the membrane surface that is much more porous. On the other hand, the structure of proteins is more complex with quaternary structure, resulting in complex particle shapes and interactions between (including possible agglomeration) and membranes. Furthermore, whey proteins are composed of different proteins of a variety of molecular sizes, with the majority of them being much smaller than PAA and PEO. This may lead to the formation of a dense cake on the membrane surface and hence high flow resistance during filtration.

5.3.4. Comparison with other membranes

As shown in Table 5.6, the research on modified filtration membranes for protein separation has been reported in numerous articles. Most of them use BSA to estimate the filtration performance. For example, Lee et al. fabricated a multiwall carbon nanotube-enhanced membrane (MWCO 12 kDa) and achieved a BSA rejection of 90%. The permeate flux of this membrane was 200 LMH [44]. He et al. synthesized an aluminum oxide membrane whose BSA rejection and permeate flux is 80% and 351 LMH (at 1 bar), respectively [45]. Hartinger et al. estimated the performance of commercial PVDF membranes with 0.1 μm by whey protein filtration. The membrane achieved whey protein rejection of 62% and a permeate flux of 17.5 LMH (at 3 bar) [46].

Table 5.6 Filtration performance of the separation membranes reported in other articles.

Pore radius / MWCO	Modification method	Solute (protein)	Rejection	Permeate flux (LMH)	Ref.
12 kDa	MOF-modified PVDF membrane	BSA	90%	200	[44]
/	Al_2O_3 membrane	BSA	80%	351 @ 1 bar	[45]
100 nm	Commercial PVDF membranes	WP	62%	17.5 @ 3 bar	[46]
98 nm	TiO_2-modified PVDF membrane	BSA	97%	8	[47]
38.6 nm	Alk60	WP	97.3%	5.6 @ 4.14 bar	
38.6 nm	G3PA	WP	98.8%	2.3 @ 4.14 bar	

WP: whey protein

In comparison, the G3PA membrane has the highest whey protein rejection of 98.8% in our research, which is higher than the membranes mentioned above. However, the permeate flux of the G3PA membrane is 2.3 LMH (at 4 bar). In this experiment, the permeate flux

of the modified membrane was significantly lower than that of membranes reported by other researchers. This was partly due to the trade-off between rejection and permeability. Additionally, the flux of the PVDF membrane used for modification was relatively low, which further limited the flux of the modified membrane.

5.4. Conclusions

In this research, the PAMAM dendrimers were successfully grafted onto the PVDF membranes after a simple, one-step alkaline pretreatment. Subsequent modifications involved transferring the peripheral functional groups of the PAMAM dendrimer from positively charged amine groups to negatively charged carboxyl groups.

The alkaline etching on the membrane surface generates new micropores, leading to an increase in surface porosity and pore number density during both alkaline treatment and the PAMAM-G3.0 grafting process. However, alkaline etching inside the membrane matrix reduces the bulk porosity. The PAMAM-G3.5 dendrimer, being larger than PAMAM-G3.0, occupies more space inside membrane pores. Therefore, transferring from PAMAM-G3.0 to PAMAM-G3.5 not only reduces bulk density but also slightly decreases surface porosity and pore number density. The newly formed micropores increased PEO rejection in alkaline-treated and PAMAM-modified membranes, indicating the average pore size decrease. Both alkaline treatment and PAMAM dendrimer modification introduce charges to the PVDF membrane. Negatively charged membranes (alkaline-treated and PAMAM-G3.5 modified (G3PA)) exhibit electrostatic repulsion to the negatively charged PAA polymer, while electrically neutral PVDF membranes and G3.0 membranes, which have positively charged amine groups, cannot reject any PAA polymer. This indicates that the separation process is dominated by electrostatic repulsion rather than steric exclusion during PAA filtration.

All modified membranes exhibit an improvement in whey protein rejection, including the G3.0 membrane, which has positively charged amine groups. The G3PA membrane demonstrates the highest whey protein rejection of 98.8%, while the G3.0 membranes also exhibit a whey protein rejection of 95.7%. In comparison, the whey protein rejection for PVDF membranes is 58.9%. This suggests that steric exclusion dominates whey protein separation. Electrostatic repulsion can also enhance the obstruction of whey protein, but the effect is limited. The separation process is governed by either steric hindrance or electrostatic repulsion. This strongly correlates with the charges carried by the membrane and the target molecules, as well as the relative sizes of membrane pores and target molecules. In our research, the separation process of smaller PAA molecules is predominantly governed by electrostatic repulsion, whereas the separation of larger whey proteins is dominated by steric hindrance. Due to the decrease in bulk porosity, there is a reduction in pure water flux and permeate flux after modification. The pure water flux of PVDF membranes is 274.1 LMH. After modification, the pure water flux decreases to 115.7 LMH, 92.3 LMH, and 60.6 LMH for Alk60, G3.0, and G3PA membranes, respectively. The permeate flux of PVDF membranes during whey protein filtration is 15.4 LMH. After modification, the permeate flux decreases to 5.6 LMH, 3.1 LMH, and 2.3 LMH for Alk60, G3.0, and G3PA membranes, respectively, during whey protein filtration.

In this research, the modification of the membrane enhances the repulsion effect of the membrane on charged macromolecules, increasing the rejection of whey protein. However, alkaline treatment reduces bulk porosity, resulting in a significant decrease in membrane flux.

5.5. References

[1] R. Singh, “Introduction to Membrane Technology,” in *Membrane Technology and Engineering for Water Purification*, Elsevier, 2015, pp. 1–80. doi: 10.1016/B978-0-

444-63362-0.00001-X.

[2] S. F. Anis, R. Hashaikeh, and N. Hilal, “Microfiltration membrane processes: A review of research trends over the past decade,” *Journal of Water Process Engineering*, vol. 32, p. 100941, Dec. 2019, doi: 10.1016/j.jwpe.2019.100941.

[3] U. W. R. Siagian *et al.*, “High-Performance Ultrafiltration Membrane: Recent Progress and Its Application for Wastewater Treatment,” *Curr Pollution Rep*, vol. 7, no. 4, pp. 448–462, Oct. 2021, doi: 10.1007/s40726-021-00204-5.

[4] P. Marchetti, M. F. Jimenez Solomon, G. Szekely, and A. G. Livingston, “Molecular Separation with Organic Solvent Nanofiltration: A Critical Review,” *Chem. Rev.*, vol. 114, no. 21, pp. 10735–10806, Nov. 2014, doi: 10.1021/cr500006j.

[5] K. Soodam and T. P. Guinee, “The case for milk protein standardisation using membrane filtration for improving cheese consistency and quality,” *Int J Dairy Technol*, vol. 71, no. 2, pp. 277–291, May 2018, doi: 10.1111/1471-0307.12502.

[6] H. Eshpari, R. Jimenez-Flores, P. S. Tong, and M. Corredig, “Thermal stability of reconstituted milk protein concentrates: Effect of partial calcium depletion during membrane filtration,” *Food Research International*, vol. 102, pp. 409–418, Dec. 2017, doi: 10.1016/j.foodres.2017.07.058.

[7] W. Wen-qiong, W. Yun-chao, Z. Xiao-feng, G. Rui-xia, and L. Mao-lin, “Whey protein membrane processing methods and membrane fouling mechanism analysis,” *Food Chemistry*, vol. 289, pp. 468–481, Aug. 2019, doi: 10.1016/j.foodchem.2019.03.086.

[8] R. Wang and S. Lin, “Pore model for nanofiltration: History, theoretical framework, key predictions, limitations, and prospects,” *Journal of Membrane Science*, vol. 620, p. 118809, Feb. 2021, doi: 10.1016/j.memsci.2020.118809.

[9] P. Saxena and P. Shukla, “A comprehensive review on fundamental properties and applications of poly(vinylidene fluoride) (PVDF),” *Adv Compos Hybrid Mater*, vol. 4, no. 1, pp. 8–26, Mar. 2021, doi: 10.1007/s42114-021-00217-0.

[10] D. Zou and Y. M. Lee, “Design strategy of poly(vinylidene fluoride) membranes for water treatment,” *Progress in Polymer Science*, vol. 128, p. 101535, May 2022, doi: 10.1016/j.progpolymsci.2022.101535.

[11] Y. Subasi and B. Cicek, “Recent advances in hydrophilic modification of PVDF ultrafiltration membranes – a review: part I,” *Membrane Technology*, vol. 2017, no. 10, pp. 7–12, Oct. 2017, doi: 10.1016/S0958-2118(17)30191-X.

[12] Y. Subasi and B. Cicek, “Recent advances in hydrophilic modification of PVDF ultrafiltration membranes – a review: part II,” *Membrane Technology*, vol. 2017, no. 11, pp. 5–11, Nov. 2017, doi: 10.1016/S0958-2118(17)30233-1.

[13] L. Zheng, J. Wang, D. Yu, Y. Zhang, and Y. Wei, “Preparation of PVDF-CTFE hydrophobic membrane by non-solvent induced phase inversion: Relation between polymorphism and phase inversion,” *Journal of Membrane Science*, vol. 550, pp. 480–491, Mar. 2018, doi: 10.1016/j.memsci.2018.01.013.

[14] Y. Wei, H.-Q. Chu, B.-Z. Dong, X. Li, S.-J. Xia, and Z.-M. Qiang, “Effect of TiO_2 nanowire addition on PVDF ultrafiltration membrane performance,” *Desalination*, vol. 272, no. 1, pp. 90–97, May 2011, doi: 10.1016/j.desal.2011.01.013.

[15] M. Bassyouni, M. H. Abdel-Aziz, M. Sh. Zoromba, S. M. S. Abdel-Hamid, and E. Drioli, “A review of polymeric nanocomposite membranes for water purification,” *Journal of Industrial and Engineering Chemistry*, vol. 73, pp. 19–46, May 2019, doi: 10.1016/j.jiec.2019.01.045.

[16] R. Zhou, D. Rana, T. Matsuura, and C. Q. Lan, “Effects of multi-walled carbon nanotubes (MWCNTs) and integrated MWCNTs/SiO_2 nano-additives on PVDF polymeric membranes for vacuum membrane distillation,” *Separation and Purification Technology*, vol. 217, pp. 154–163, Jun. 2019, doi: 10.1016/j.seppur.2019.02.013.

[17] D. Hou, Z. Yuan, M. Tang, K. Wang, and J. Wang, “Effect and mechanism of an anionic surfactant on membrane performance during direct contact membrane distillation,” *Journal of Membrane Science*, vol. 595, p. 117495, Feb. 2020, doi: 10.1016/j.memsci.2019.117495.

[18] O. Karatas, R. Keyikoglu, N. Atalay Gengec, V. Vatanpour, and A. Khataee, “A review on dendrimers in preparation and modification of membranes: progress, applications, and challenges,” *Materials Today Chemistry*, vol. 23, p. 100683, Mar. 2022, doi: 10.1016/j.mtchem.2021.100683.

[19] X. Li *et al.*, “Enhanced fouling and wetting resistance of composite Hyflon

AD/poly(vinylidene fluoride) membrane in vacuum membrane distillation," *Separation and Purification Technology*, vol. 211, pp. 135–140, Mar. 2019, doi: 10.1016/j.seppur.2018.09.071.

[20] D. Tong *et al.*, "Preparation of Hyflon AD60/PVDF composite hollow fiber membranes for vacuum membrane distillation," *Separation and Purification Technology*, vol. 157, pp. 1–8, Jan. 2016, doi: 10.1016/j.seppur.2015.11.026.

[21] A. Qin, X. Li, X. Zhao, D. Liu, and C. He, "Engineering a Highly Hydrophilic PVDF Membrane via Binding TiO_2 Nanoparticles and a PVA Layer onto a Membrane Surface," *ACS Appl. Mater. Interfaces*, vol. 7, no. 16, pp. 8427–8436, Apr. 2015, doi: 10.1021/acsami.5b00978.

[22] Y. Chen *et al.*, "Controlled grafting from poly(vinylidene fluoride) microfiltration membranes via reverse atom transfer radical polymerization and antifouling properties," *Polymer*, vol. 48, no. 26, pp. 7604–7613, Dec. 2007, doi: 10.1016/j.polymer.2007.10.043.

[23] Y. Han, S. Song, Y. Lu, and D. Zhu, "A method to modify PVDF microfiltration membrane via ATRP with low-temperature plasma pretreatment," *Applied Surface Science*, vol. 379, pp. 474–479, Aug. 2016, doi: 10.1016/j.apsusc.2016.04.114.

[24] T. Baig, J. Nayak, V. Dwivedi, A. Singh, and P. K. Tripathi, "A Review about Dendrimers: Synthesis, Types, Characterization and Applications," vol. 4, 2015.

[25] R. Y. Patle and J. S. Meshram, "The advanced synthetic modifications and applications of multifunctional PAMAM dendritic composites," *React. Chem. Eng.*, vol. 7, no. 1, pp. 9–40, 2022, doi: 10.1039/D1RE00074H.

[26] B. Devadas, A. P. Periasamy, and K. Bouzek, "A review on poly(amidoamine) dendrimer encapsulated nanoparticles synthesis and usage in energy conversion and storage applications," *Coordination Chemistry Reviews*, vol. 444, p. 214062, Oct. 2021, doi: 10.1016/j.ccr.2021.214062.

[27] H. Karimipour, A. Shahbazi, and V. Vatanpour, "Fouling decline and retention increase of polyethersulfone membrane by incorporating melamine-based dendrimer amine functionalized graphene oxide nanosheets (GO/MDA)," *Journal of Environmental Chemical Engineering*, vol. 9, no. 1, p. 104849, Feb. 2021, doi: 10.1016/j.jece.2020.104849.

[28] W.-P. Zhu, J. Gao, S.-P. Sun, S. Zhang, and T.-S. Chung, "Poly(amidoamine) dendrimer (PAMAM) grafted on thin film composite (TFC) nanofiltration (NF) hollow fiber membranes for heavy metal removal," *Journal of Membrane Science*, vol. 487, pp. 117–126, Aug. 2015, doi: 10.1016/j.memsci.2015.03.033.

[29] G. Li, L. Shen, Y. Luo, and S. Zhang, "The effect of silver-PAMAM dendrimer nanocomposites on the performance of PVDF membranes," *Desalination*, vol. 338, pp. 115–120, Apr. 2014, doi: 10.1016/j.desal.2014.02.001.

[30] Z. Xu, S. Gu, D. Rana, T. Matsuura, and C. Q. Lan, "Chemical precipitation enabled UF and MF filtration for lead removal," *Journal of Water Process Engineering*, vol. 41, p. 101987, Jun. 2021, doi: 10.1016/j.jwpe.2021.101987.

[31] Z. Li, D. Rana, Z. Wang, T. Matsuura, and C. Q. Lan, "Synergic effects of hydrophilic and hydrophobic nanoparticles on performance of nanocomposite distillation membranes: An experimental and numerical study," *Separation and Purification Technology*, vol. 202, pp. 45–58, Aug. 2018, doi: 10.1016/j.seppur.2018.03.032.

[32] S. Singh, K. C. Khulbe, T. Matsuura, and P. Ramamurthy, "Membrane characterization by solute transport and atomic force microscopy," *Journal of Membrane Science*, vol. 142, no. 1, pp. 111–127, Feb. 1998, doi: 10.1016/S0376-7388(97)00329-3.

[33] I. Noda, T. Tsuge, and M. Nagasawa, "The intrinsic viscosity of polyelectrolytes," *J. Phys. Chem.*, vol. 74, no. 4, pp. 710–719, Feb. 1970, doi: 10.1021/j100699a005.

[34] C. Sun and X. Feng, "Enhancing the performance of PVDF membranes by hydrophilic surface modification via amine treatment," *Separation and Purification Technology*, vol. 185, pp. 94–102, Sep. 2017, doi: 10.1016/j.seppur.2017.05.022.

[35] G. Vitola, R. Mazzei, E. Fontananova, and L. Giorno, "PVDF membrane biofunctionalization by chemical grafting," *Journal of Membrane Science*, vol. 476, pp. 483–489, Feb. 2015, doi: 10.1016/j.memsci.2014.12.004.

[36]R. Wang, Y. Duan, and X. Xiong, "Preparation of hydrophilic poly(vinylidene fluoride) membrane by in-situ grafting of N-vinyl pyrrolidone via a reactive vapor induced phase separation procedure," *Journal of Polymer Science*, vol. 59, no. 20, pp. 2284–2294, 2021, doi: 10.1002/pol.20210446.

[37] P. Huo, C.-T. Zhong, and X.-P. Xiong, “Tailoring Morphology of PVDF-HFP Membrane via One-step Reactive Vapor Induced Phase Separation for Efficient Oil-Water Separation,” *Chin J Polym Sci*, vol. 39, no. 5, pp. 610–619, May 2021, doi: 10.1007/s10118-021-2527-x.

[38] R. Müller, C. Laschober, W. W. Szymanski, and G. Allmaier, “Determination of Molecular Weight, Particle Size, and Density of High Number Generation PAMAM Dendrimers Using MALDI−TOF−MS and nES−GEMMA,” *Macromolecules*, vol. 40, no. 15, pp. 5599–5605, Jul. 2007, doi: 10.1021/ma062599e.

[39] A. R. Madureira, C. I. Pereira, A. M. P. Gomes, M. E. Pintado, and F. Xavier Malcata, “Bovine whey proteins – Overview on their main biological properties,” *Food Res Int*, vol. 40, no. 10, pp. 1197–1211, Dec. 2007, doi: 10.1016/j.foodres.2007.07.005.

[40] K.-I. Shimazaki and K. Sukegawa, “Chromatographic Profiles of Bovine Milk Whey Components by Gel Filtration on Fractogel TSK HW55F Column,” *Journal of Dairy Science*, vol. 65, no. 11, pp. 2055–2062, Nov. 1982, doi: 10.3168/jds.S0022-0302(82)82461-2.

[41] Z. Adamczyk, A. Bratek, B. Jachimska, T. Jasiński, and P. Warszyński, “Structure of Poly(acrylic acid) in Electrolyte Solutions Determined from Simulations and Viscosity Measurements,” *J. Phys. Chem. B*, vol. 110, no. 45, pp. 22426–22435, Nov. 2006, doi: 10.1021/jp063981w.

[42] C. Darko, *An Experimental Approach of Introducing Polymer Crystallization to Students using Diblock Copolymer Thin Films*. 2018. doi: 10.17632/hry2mscm54.1.

[43] M. Liu, S. Thijssen, W. E. Hennink, J. Garssen, C. F. van Nostrum, and L. E. M. Willemsen, “Oral pretreatment with β-lactoglobulin derived peptide and CpG co-encapsulated in PLGA nanoparticles prior to sensitizations attenuates cow’s milk allergy development in mice,” *Front Immunol*, vol. 13, p. 1053107, 2022, doi: 10.3389/fimmu.2022.1053107.

[44] J. Lee *et al.*, “Protein fouling in carbon nanotubes enhanced ultrafiltration membrane: Fouling mechanism as a function of pH and ionic strength,” *Separation and Purification Technology*, vol. 176, pp. 323–334, Apr. 2017, doi: 10.1016/j.seppur.2016.10.061.

[45] H. He, W. Jing, W. Xing, and Y. Fan, “Improving protein resistance of α-Al_2O_3

membranes by modification with POEGMA brushes," *Applied Surface Science*, vol. 258, no. 3, pp. 1038–1044, Nov. 2011, doi: 10.1016/j.apsusc.2011.08.121.

[46] M. Hartinger, H.-J. Heidebrecht, S. Schiffer, J. Dumpler, and U. Kulozik, "Milk Protein Fractionation by Means of Spiral-Wound Microfiltration Membranes: Effect of the Pressure Adjustment Mode and Temperature on Flux and Protein Permeation," *Foods*, vol. 8, no. 6, Art. no. 6, Jun. 2019, doi: 10.3390/foods8060180.

[47] R. Gayatri *et al.*, "Preparation and Characterization of PVDF–TiO_2 Mixed-Matrix Membrane with PVP and PEG as Pore-Forming Agents for BSA Rejection," *Nanomaterials*, vol. 13, no. 6, Art. no. 6, Jan. 2023, doi: 10.3390/nano13061023.

Chapter 6. Engineering Polyvinylidene Fluoride Membranes Using Charge Tunable Dendrimer Polyamidoamine to Enable Microporous Membranes for Protein Separation

The content of this chapter has been published in: Separation and Purification Technology, Volume 354, Part 4, 2025, 128887, ISSN 1383-5866. Doi: 10.1016/j.seppur.2024.128887.

Abstract

Dendrimers are structurally precise molecules, whose peripheral layer provides ample sites for anchoring functional groups of different charges and charge densities. This characteristic renders them capability of providing numerous target functional groups on the surface of filtration membranes when modified by dendrimers. Consequently, there has been a growing interest in dendrimer-modified membranes. In this study, we investigated the engineering of polyvinylidene fluoride (PVDF) membranes using polyamidoamine (PAMAM) dendrimers anchoring different functional groups to tune the charges and charge density of membrane to enable microporous membranes for separation of charged macromolecules. PVDF membranes were functionalized by grafting PAMAM-G3.0 (generation 3) dendrimers with amine groups onto their surfaces and internal surfaces of membrane pores. Subsequently, the peripheral functional groups of dendrimers on the membranes were replaced by carboxyl groups, quaternary ammonium groups, or sulfonic acid groups for charges of different nature and densities. Surface chemical properties, electrical properties, and morphology were characterized using various techniques, including attenuated total reflectance Fourier-transform infrared (ATR-FTIR) spectroscopy, X-ray photoelectron spectroscopy (XPS), scanning electron microscopy (SEM), and

surface zeta potential measurement. The filtration performance of both PVDF and modified membranes was evaluated using polyethylene oxide (PEO), polyacrylic acid (PAA), and whey protein filtration. Among the modified membranes, the G3PA membranes, with carboxyl functional groups, exhibited the most effective whey protein separation performance. The whey protein rejection and permeate flux of the G3PA membranes were 79% and 30.3 LMH, respectively. As a comparison, the whey protein rejection and permeate flux of the pristine PVDF membranes were 58.9% and 15.3 LMH, respectively.

Acronyms and Symbols

Abbreviation

1,3-PS	1,3-propane sultone
ATR-FTIR	attenuated total reflectance-Fourier transform infrared
BSA	bovine serum albumin
CMC	carboxymethyl chitosan
DMAc	*N*, *N*-dimethylacetamide
EDA	ethylenediamine
EPTAC	glycidyltrimethylammonium chloride
FESEM	field-emission scanning electron microscope
HT	hydrotalcite
MA	methyl acrylate
MPD	*m*-phenylenediamine
MWCO	molecular weight cutoff
NIPS	non-solvent induced phase separation
PAMAM	polyamidoamine
PAA	polyacrylic acid
PAN	polyacrylonitrile
PC	polycarbonate

PDA	polydopamine
PEG	polyethylene glycol
PEO	polyethylene oxide
PES	polyethersulfone
PPI	polypropylene
PVDF	polyvinylidene fluoride
RO	reverse osmosis
SEM	scanning electron microscopy
TMC	trimesoyl chloride
XPS	X-ray photoelectron spectroscopy

Nomenclature

A	effective area of the membrane
A_{sample}	area of the membrane sample during porosity measurement
$c_{i,f}$	concentration of the feed
$c_{i,p}$	concentration of the permeate
l	thickness of the dry membrane sample
R_i	rejection of solute i
t	filtration time
v	volume of the permeate

w_d	weight of the dry membrane sample
w_w	weight of the wet membrane sample
ε	bulk porosity
ρ_b	density of n-butanol

6.1. Introduction

Membrane filtration technology finds widespread application across various fields owing to its high separation efficiency, selectivity, and minimal or zero chemical usage. Pressure-driven membranes operate by obstructing molecules larger than the membrane pore size through steric hindrance. Membranes with different pore sizes can thus segregate molecules based on their molecular size or weight. Consequently, by choosing membranes with appropriate pore sizes, membrane filtration can be deployed across a broad spectrum of separation scenarios. For example, reverse osmosis (RO) membranes effectively separate NaCl from water, widely employed in ultrapure water production [1]. Microfiltration membranes, typically featuring pore sizes ranging from 0.05 to 10 μm, are extensively utilized for removing fine particles or bacteria from solutions [2].

Polyvinylidene fluoride (PVDF) boasts excellent chemical resistance, thermal stability, aging resistance, and high mechanical strength [3], [4], making it a preferred material for fabricating filtration membranes. Over the past decade, there has been a notable surge in research efforts focusing on PVDF membranes. In 2014, the number of articles related to PVDF membranes was less than 500. However, by 2020, this figure had surpassed 700 [5]. Surface modification of PVDF membranes can significantly enhance filtration performance, resulting in higher rejection of target molecules, increased permeate flux, and improved anti-fouling properties. Such modifications render PVDF membranes applicable across a diverse range of separation systems. For instance, Bubela et al. grafted carboxyl-functionalized Fe_3O_4 nanoparticles onto PVDF membranes to augment permeability and anti-fouling properties, leading to a 100% increase in pure water flux for the modified membranes [6]. Similarly, Fan et al. observed that PVDF membranes with *in-situ* grown MnO_2 nanorods exhibited superior anti-fouling properties in bovine serum albumin (BSA) filtration [7]. Zhang et al. applied a quaternized chitosan cross-linked layer onto PVDF-

SiO_2 membranes to amplify the positive charge on the membrane surface. This resulted in an increase in the rejection of BSA from 63.97% for PVDF-SiO_2 membranes to 81.59% for the membrane coated with quaternized chitosan cross-linking. Remarkably, the permeate flux only decreased by 27.1% [8].

Dendrimers are star-burst-like polymers, first synthesized by Tomalia et al. in 1984 [9]. They boast a highly branched and well-defined molecular architecture, affording numerous sites for anchoring functional groups. Both the interior and the peripheral layers of dendrimers can be precisely engineered with different functional groups, enabling a high degree of control over their chemical and physical properties [10]. This distinction in properties between the peripheral layer and interior allows dendrimers to encapsulate nanoparticles or molecules, such as drugs and catalysts, inside their structure [11]. These unique properties have spurred extensive research in various fields, including drug delivery, gene delivery, sensors, and catalysis [12]. As a low-cost and easy-to-synthesize dendrimer, polyamidoamine (PAMAM) dendrimers are widely used in many fields including filtration membrane modification. PAMAM dendrimers provide a large number of reactive sites due to the presence of a high density of amine groups on its periphery layer [13]. The amine groups of PAMAM dendrimers can be easily converted to other functional groups through chemical reactions. Therefore, a large number of functional groups of choice can be anchored on the filtration membranes by the grafting of PAMAM dendrimers. The peripheral functional groups of PAMAM could be replaced with other functional groups to render membrane surfaces tailored polarity, hydrophilicity, charge nature (+/-), and charge density. Consequently, they can significantly impact the performance of filtration membranes, such as anti-fouling ability, permeability, and rejection of inorganic and organic ions. For instance, Qiu et al. [14] investigated the different functional groups of PAMAM dendrimer on the performance of NF membranes for metal ion removal. They found that NF membranes with PAMAM dendrimers possessing strongly positive

functional groups, e.g., quaternary ammonium, exhibited the highest rejection of divalent metal cations. Conversely, NF membranes with PAMAM dendrimers possessing strongly negative functional groups, sulfonic acid groups, showed the highest rejection of divalent anions. We hypothesize that a similar approach could be applied to the engineering of microporous membranes to introduce tailored charges (+/-) and charge densities to enable microporous membranes for the separation of charge macromolecules that are much smaller than the membrane pores to elevated fluxes, antifouling performance.

There are three methods to immobilize dendrimers on filtration membranes: blending, coating, and grafting. In the blending approach, dendrimers are added to the casting solution of membranes as additives, altering the membranes' hydrophilicity or influencing their formation process. Blending is a straightforward method that significantly enhances membrane performance without requiring additional treatment. For instance, Borgohain et al. incorporated PAMAM dendrimers and hydrotalcite (HT) into carboxymethyl chitosan (CMC) membranes, increasing the CO_2/N_2 selectivity from 49 to 312 during CO_2/N_2 gas separation [15]. Algarra et al. embedded thiol polypropylenimine (DAB-3-$(SH)_{16}$) dendrimers in cellulosic membranes and observed enhancement in membrane elasticity and anti-penetration properties against Pb^{2+}, Cd^{2+}, and Hg^{2+} [16].

According to the coating method, the dendrimers are coated or deposited on the surface of membranes. To strengthen the dendrimer layer, methods such as polymerization (where the dendrimer acts as the monomer), cross-linking, or heating are employed [17]. The dendrimer or dendrimer layer adheres to the membranes through electrostatic or van der Waals forces during coating [18]. Numerous studies have explored coating dendrimers onto membranes. For instance, Savariar et al. coated polypropylene imine (PPI) dendrimers onto polycarbonate (PC) membranes by adsorbing polyacrylic acid (PAA) onto the pore walls of the membrane via simple filtration. Subsequently, PPI dendrimers were electrostatically

adsorbed onto the PAA layer by filtration through the PAA/PC membrane [19]. Zhang et al. developed an interfacial polymerization method to coat PAMAM dendrimers. In their approach, PAMAM dendrimers were embedded within the polyamide layer formed by the interfacial polymerization of *m*-phenylenediamine (MPD) and trimesoyl chloride (TMC) [20]. Dopamine showed promise as a chemical for coating dendrimers onto membranes. A thin, robust polydopamine (PDA) layer was formed through automatic oxidative polymerization at a membrane surface and served as a selective layer as well as providing the sites for dendrimer grafting [14], [21].

In grafting methods, dendrimers are immobilized onto membranes via covalent bonds. Since most membranes cannot directly react with dendrimers, pretreatments such as UV irradiation, plasma treatment, or chemical treatment are required before grafting dendrimers. For example, Li et al. pretreated PVDF membranes with a mixture of KOH and $KMnO_4$ solutions, then reacted TMC on the membrane to provide grafting sites for dendrimer immobilization. Subsequently, they immobilized PAMAM dendrimers, in which Ag nanoparticles are encapsulated, by connecting the dendrimers with the acyl chloride groups of TMC [22]. Wei et al. sequentially immobilized PAA layers, SiO_2 layers, TMC layers, and PAMAM dendrimers onto PVDF membranes. These modified PVDF membranes exhibited excellent water permeability and separation efficiency during oil-water separation [23]. Zhang et al. proposed an interesting method for grafting dendrimers onto membranes. They first immobilized the core of the dendrimer, ethylenediamine (EDA), onto hollow fiber membranes, and then synthesized the dendrimer layer by layer on the membranes [24]. Sun et al. used PVDF membranes modified with PAMAM dendrimers to adsorb Cu^{2+} ions from water, achieving a maximum adsorption capacity of 153.8 mg/g [25]. Zhang et al. enhanced the maximum adsorption capacities for Cu^{2+}, Ni^{2+}, and Cd^{2+} to 155.19 mg/g, 124.28 mg/g, and 125.55 mg/g, respectively, by modifying PVDF membranes with hyperbranched polyamidoamine-palygorskite (PAMAM-Pal) [26].

In a previous study [27], we grafted PAMAM dendrimers onto PVDF membranes treated with a KOH isopropanol solution. The solution can fully immerse the PVDF membranes, allowing the alkaline to act on both the interior surfaces of membrane pores and the membrane surface. Consequently, the PAMAM dendrimer was able to be immobilized on both the interior and surface of the membranes in the subsequent grafting step to introduce charges onto these surfaces. As a result, the rejection of negatively charged Polyacrylic acid from 0% to 14.4%, proving the hypothesis that introducing charges onto membrane surface and pores could enable the separation of charged macromolecules using membranes of pore radii much larger than their dynamic radii. It was further demonstrated that the rejection of whey proteins was increased from 58.9% by the pristine PVDF membrane to 98.8% by the modified membrane, pointing to the great potential of such membranes for commercial applications. However, the pretreatment of the PVDF membranes using KOH isopropanol solution showed two disadvantages: (1) the membrane became fragile; and (2) the permeate fluxes were several times lower than the pristine PVDF membranes due to the formation of double carbon bonds (-C=C-) in the membrane matrices, which might result in breakup of some of the polymer carbon backbones. We further hypothesize that by using KOH aqueous solution for PVDF membrane pretreatment, the modification will be limited to the exterior surface of the membrane and therefore retain the integrity and strength of the membrane matrices and pore structures and hence avoid severely impacting the fluxes.

In this research, to test the aforementioned hypotheses, we used KOH aqueous solution for the pretreatment of the PVDF membrane to limit the functionalization and therefore the grafting of PAMAM dendrimers onto the exterior surfaces of membranes only since the aqueous solution of KOH cannot immerse the hydrophobic PVDF membrane. The peripheral functional groups of the dendrimers were then replaced with carboxyl groups, quaternary ammonium groups, or sulfonic acid groups to render the membranes with varied

charge and charge density. These membranes were then characterized and evaluated for the filtration of PAA, PEO, and whey proteins. Results indicate that appropriate modifications of membrane exterior surfaces could significantly improve both the rejection of charged macromolecules including PAA and whey proteins and permeate fluxes while preserving the mechanical strength of the membrane.

6.2. Experimental

6.2.1. Materials

The host polymer of membranes, PVDF, Kynar® 740 (Pellet, M_w = 410 kDa), was kindly supplied by Arkema Inc. (Philadelphia, PA). The pore former agent, polyethylene glycol (PEG) (M_w = 1 kDa), and the solvent for casting solution, anhydrous *N*, *N*-dimethylacetamide (DMAc) with a purity of 99.8% were purchased from Sigma-Aldrich Inc. (St. Louis, MO). Potassium hydroxide, methanol with a purity of 99.5%, and isopropanol with a purity of 99.5% were purchased from Sigma-Aldrich Inc. The ethylenediamine (EDA), with a purity of 99%, and methyl acrylate (MA), with a purity of 99% for PAMAM dendrimer synthesis were purchased from Sigma-Aldrich Inc. (St. Louis, MO). The 35 wt% PAA (M_w = 100 kDa) aqueous solution, polyethylene oxide (PEO) (M_w = 100 kDa), and whey protein for filtration were purchased from Sigma-Aldrich Inc. (St. Louis, MO). Barium chloride, hydrochloric acid, iodine, and potassium iodide for PEO concentration analysis were purchased from Sigma-Aldrich Inc. (St. Louis, MO). The Bradford Reagent for whey protein analysis was purchased from Sigma-Aldrich Inc. (St. Louis, MO). The PAA (M_w = 450 kDa), and sodium nitrate for surface zeta potential measurement were purchased from Sigma-Aldrich Inc. (St. Louis, MO). n-butanol with a purity of 99.5% for bulk porosity measurement was purchased from Sigma-Aldrich Inc. (St. Louis, MO). Glycidyltrimethylammonium chloride (EPTAC) with a purity of 90%,

and 1,3-propane sultone (1,3-PS) with a purity of 98% for functional group modification of PAMAM dendrimer were purchased from Sigma-Aldrich Inc. (St. Louis, MO).

6.2.2. PAMAM dendrimer synthesis

In this study, PAMAM generation 3.0 (PAMAM-G3.0) dendrimers were synthesized using the methods outlined in Chapter 5. The PAMAM dendrimer synthesis employed the divergent method, involving sequential Michael and amidation reactions starting from the EDA core [9], [28], [29]. The resulting products and intermediates underwent purification via vacuum distillation to remove residual MA or EDA. The final product manifested as a pale-yellow syrup-like substance at 120℃, solidifying at room temperature. The molecular formula is depicted in Figure 6.1.

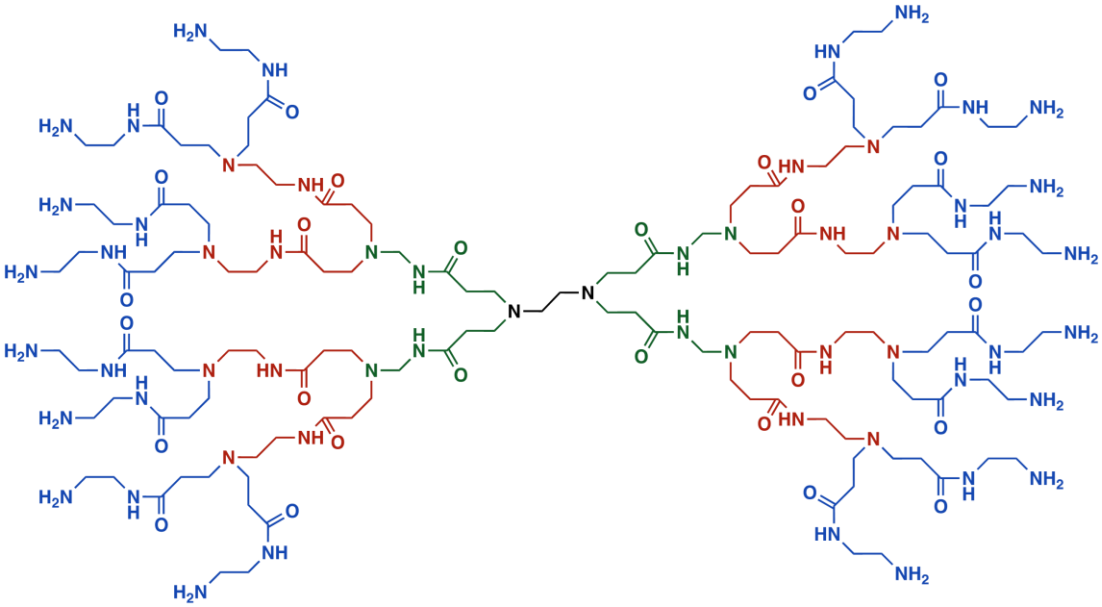

Figure 6.1 Chemical structure of PAMAM-G3.0 dendrimer.

6.2.3. Membrane fabrication

In this study, the PVDF membrane was fabricated using the non-solvent phase separation (NIPS) method, which was mentioned in Chapter 3. The casting solution used for

membrane fabrication consisted of 82 wt% DMAc, 15 wt% PVDF, and 3 wt% PEG.

6.2.4. Alkaline pretreatment of PVDF membranes

Alkaline pretreatment is a prerequisite before PAMAM dendrimer grafting. The PVDF membrane underwent the treatment with a 10 M KOH aqueous solution at 80°C for 30 minutes. Due to the hydrophobic nature of the PVDF membrane and its lower density compared to the KOH aqueous solution, the membrane could float on alkaline aqueous solution. The membrane was positioned with its selective layer facing downward in the KOH aqueous solution during the pretreatment. Care was taken so that the membrane floated at the top of the solution without any air bubbles between the selective surface and the solution. The KOH aqueous solution was stirred using a magnetic stir bar at 80 rpm throughout the process. After alkaline pretreatment, the membrane was cooled down by immersion in room temperature ethanol. Subsequently, the membrane underwent two ethanol washes followed by two deionized water washes to remove any residual chemicals, preparing it for subsequent modification with PAMAM dendrimer and filtration processes. The membranes treated with alkaline were labeled as Alk.

6.2.5. Grafting PAMAM dendrimer on membranes

PAMAM generation 3.0 (PAMAM-G3.0) dendrimers were immobilized on alkaline-pretreated PVDF membranes via the grafting method. The alkaline-pretreated (Alk) membranes were immersed in a methanol solution containing 2.5 wt% PAMAM-G3.0 and 0.5 M KOH, under vigorous stirring for 24 hours at 10°C. Subsequently, the membranes underwent two washes with ethanol and two washes with deionized water. The PAMAM-G3.0 grafted membranes were labeled as G3.0. The peripheral groups of PAMAM dendrimers on the surface of the membrane were converted from amine groups to carboxyl

groups, quaternary ammonium groups, or sulfonic acid groups using the following steps.

Carboxyl groups

To convert the peripheral groups of PAMAM dendrimer on membranes from amine groups to carboxyl groups, the G3.0 membranes were immersed in a 50 wt% MA methanol solution at 10℃ under stirring at 80 rpm for 24 hours. Then, the membranes underwent three washes with ethanol and were dried at room temperature. This reaction resulted in the presence of ester groups on the dendrimer surface of the membranes. Subsequently, the membranes were immersed in a 0.5 M NaOH aqueous solution at room temperature for 30 minutes to hydrolyze the ester groups into carboxyl groups. The membranes were then washed three times with deionized water and dried at room temperature. This modified membrane was labeled as G3PA.

Quaternary ammonium groups

To convert the amine groups to quaternary ammonium groups, the G3.0 membranes were immersed in a mixture of 0.1296 g EPTAC and 4 mL MeOH and under stirring at 50℃ for 6 hours at a speed of 80 rpm. Afterward, the membranes underwent three washes with ethanol and were dried at room temperature. The resulting membranes with quaternary ammonium groups were labeled as G3TAC.

Sulfonic acid groups

To convert the amine groups to sulfonic acid groups, the G3.0 membranes were immersed in a methanol solution containing 0.1044 g 1,3-PS and 0.5 M KOH under stirring at 50℃ for 6 hours at a speed of 80 rpm. Then, the membranes underwent three washes with ethanol and were dried at room temperature. The resulting membranes with sulfonic acid groups

were labeled as G3PS.

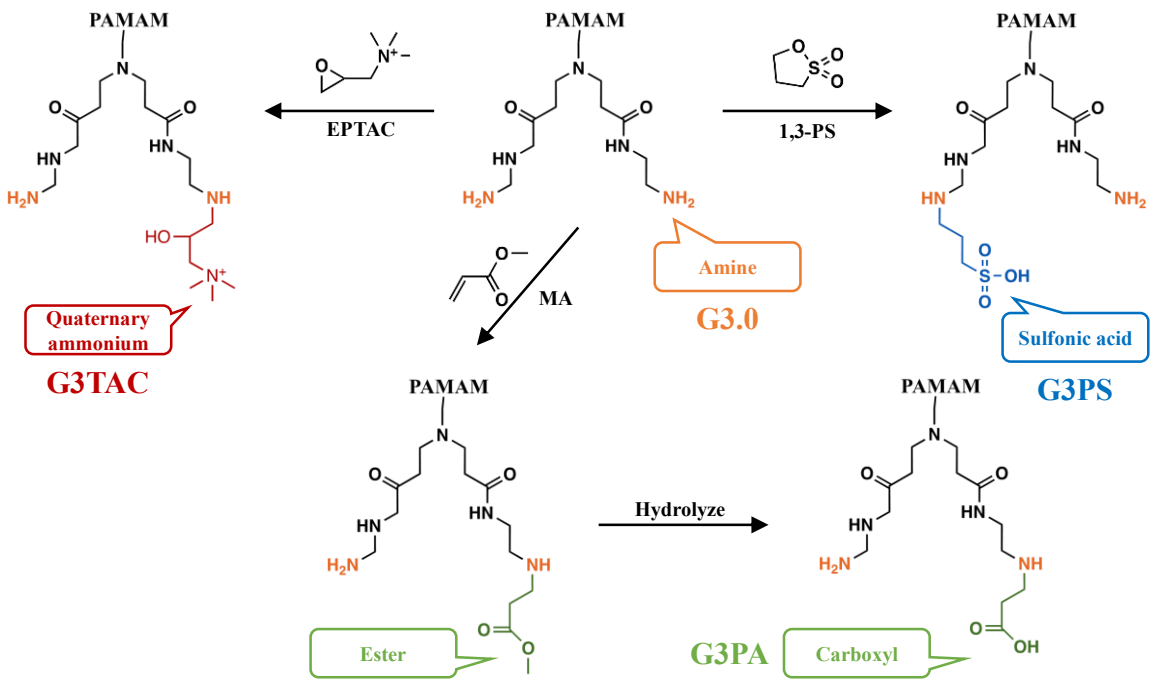

Figure 6.2 Sketch of process transferring functional groups of PAMAM dendrimer on PVDF membranes from amine groups to quaternary ammonium groups or sulfonic acid groups.

Indeed, amine groups and quaternary ammonium groups impart weak and strong positive charges to the membranes, respectively. Conversely, carboxyl groups and sulfonic acid groups confer weak and strong negative charges to the membranes, respectively.

6.2.6. Membrane filtration

A dead-end filtration setup was utilized to assess the filtration performance, following the methodology outlined in our previous research [30]. In this setup, the membrane is situated beneath the feed chamber, which holds 200 mL of the feed solution. The membrane, with an effective area of 0.00159 m^2, is positioned at the bottom of the feed chamber. The entire process is conducted at room temperature. An operating pressure of 60 psig (4.14 bar) is maintained using nitrogen gas supplied from a cylinder.

Two dissolvable polymer solutions, PAA and PEO, each with a concentration of 100 ppm, were subjected to filtration to investigate the separation mechanism during macromolecule separation. To ensure the accuracy of the experiment, 10 mL of permeate was discarded before sample collection. Then, continue the filtration until collecting 10 mL of permeate as a sample for subsequent analysis. All filtration tests were carried out in triplicate using three new coupons fabricated from different batches. The flux of the membranes was calculated using Equation (6-1) [30], as shown below.

$$Flux = \frac{v}{t \cdot A} \tag{6-1}$$

Where v is the volume (0.010 L) of the permeate, t (hour) the time required to collect 0.010 L of permeate, and A the effective area of the membrane (m^2).

The polymer and the whey protein rejection R_i were calculated by Equation (6-2) [30] below.

$$R_i = \frac{c_{i,f} - c_{i,p}}{c_{i,f}} \times 100\% \tag{6-2}$$

Where $c_{i,f}$ and $c_{i,p}$ are the concentration of the feed and permeate respectively.

The solute concentrations both in feed and permeate were determined by UV-Vis spectrophotometry, which were discussed in Chapter 3. The filtration performance of PVDF and modified membranes was examined under the natural pH of each feed solution. The pH of the whey protein and PEO feed solutions was approximately 6, while the pH of the PAA feed solution was around 4. Pure water filtration and whey protein filtration of commercial membranes were conducted under the same operational conditions as those for the homemade membranes.

6.2.7. Membrane characterization

ATR-FTIR

The chemical properties on the membrane's surface were analyzed using attenuated total reflectance-Fourier transform infrared (ATR-FTIR) spectroscopy, employing the Agilent Tech-Cary 630 spectrometer (Agilent, Canada).

XPS

The chemical properties on the surface of the membranes were quantified using X-ray photoelectron spectroscopy (XPS) technology. This analysis was performed using a Kratos Axis Nova spectrometer (Kratos Analytical, Ltd., UK) equipped with an Al X-ray source.

SEM

The morphology of the membrane's top surface and cross-section was investigated using scanning electron microscopy (SEM) on a JSM-7500F field-emission scanning electron microscope (FESEM) from JEOL, Japan. The details of surface and cross-section SEM measurements were in Chapter 3. Subsequently, the surface porosity and average pore size were analyzed using Image J software. The pore size here is the diameter of the pore.

Contact angle

The water contact angle of the membrane samples was measured using the sessile drop method with the VCA Optima Surface Analysis System (AST Product, Inc., Billerica, MA, US) at room temperature. A 1 μL deionized water droplet was carefully placed on the surface of the dry sample to measure the contact angle. Measurements were taken at 5 random spots on the sample, and the average value was reported.

Bulk porosity

The bulk porosity of the membrane was determined using the wet-dry method [31], which was mentioned in Chapter 3. The bulk porosity of the membranes (ε) can be calculated using Equation (6-3) [31].

$$\varepsilon = \frac{w_w - w_d}{A_{sample} \cdot l \cdot \rho_b} \quad (6\text{-}3)$$

Where w_w and w_d are the weight (g) of the wet and dry sample, respectively. A_{sample} is the area of the sample (cm^2), l is the thickness (cm) of the dry sample and ρ_b is the density (g/cm^3) of n-butanol, which is 0.81 $g \cdot cm^{-3}$ at 25℃. Three samples were used for the measurement and the average value was reported.

Surface zeta potential

The surface charge characteristics of the membranes were analyzed through surface zeta potential testing, utilizing the surface zeta potential cell (ZEN1020), an accessory kit for the Zetasizer Nano Z (Malvern Panalytical, Worcestershire, UK). The details of surface zeta potential measurement were mentioned in Chapter 3.

6.3. Results and discussion

6.3.1. Membrane characterization

Morphology

Figure 6.3 presents cross-sectional SEM images of PVDF membranes, and the membranes grafted by PAMAM dendrimers with different functional groups, such as amine groups

(G3.0), carboxyl groups (G3PA), quaternary ammonium groups (G3TAC), and sulfonic acid groups (G3PS). The PVDF membranes have a thickness of 33 μm and consist of a finger-like layer and a sponge-like layer. The finger-like layer is located on the side of the membranes with the selective layer, and the thickness ratio of the finger-like layer to the sponge-like layer is approximately 3:2. The modified membranes, including alkaline-treated and dendrimer-grafted membranes, exhibit similar cross-sectional morphology to PVDF membranes, indicating that the modifications do not impact the internal structure of the membrane matrix.

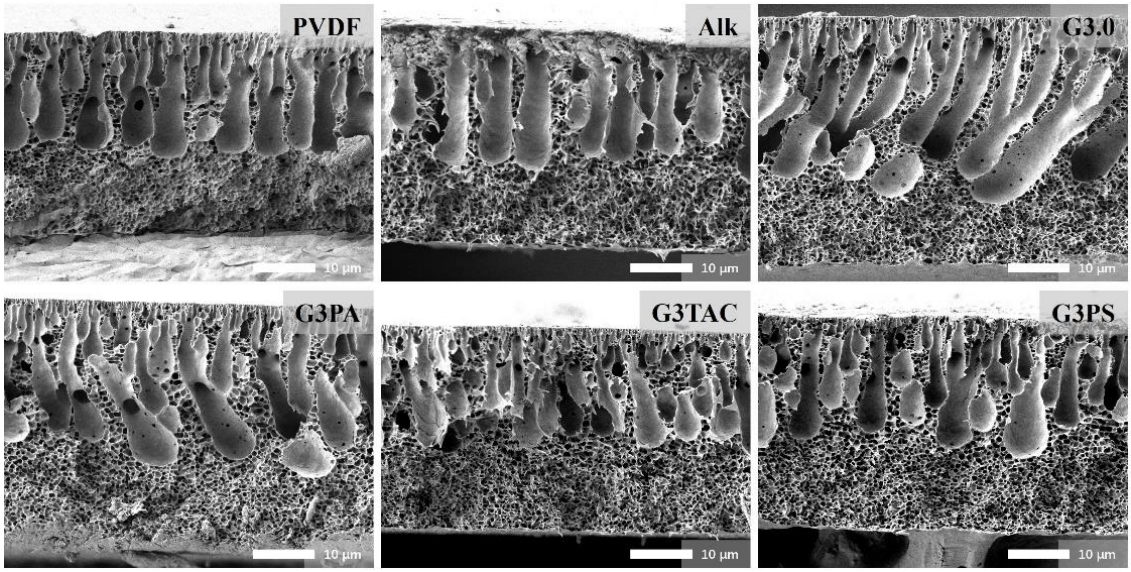

Figure 6.3 Cross-sectional SEM images of the PVDF membranes (PVDF), alkaline treated (Alk), and PAMAM dendrimer with different functional groups modified membranes.

The influence of alkaline treatment on the surface morphology of the membranes (Alk) is indeed significant, as depicted in Figure 6.4. Initially, the surface of the PVDF membranes exhibits uniformly distributed pores. However, after alkaline treatment, there is a noticeable enlargement of pores on the surface. This alteration can be attributed to the etching effect of the alkaline solution.

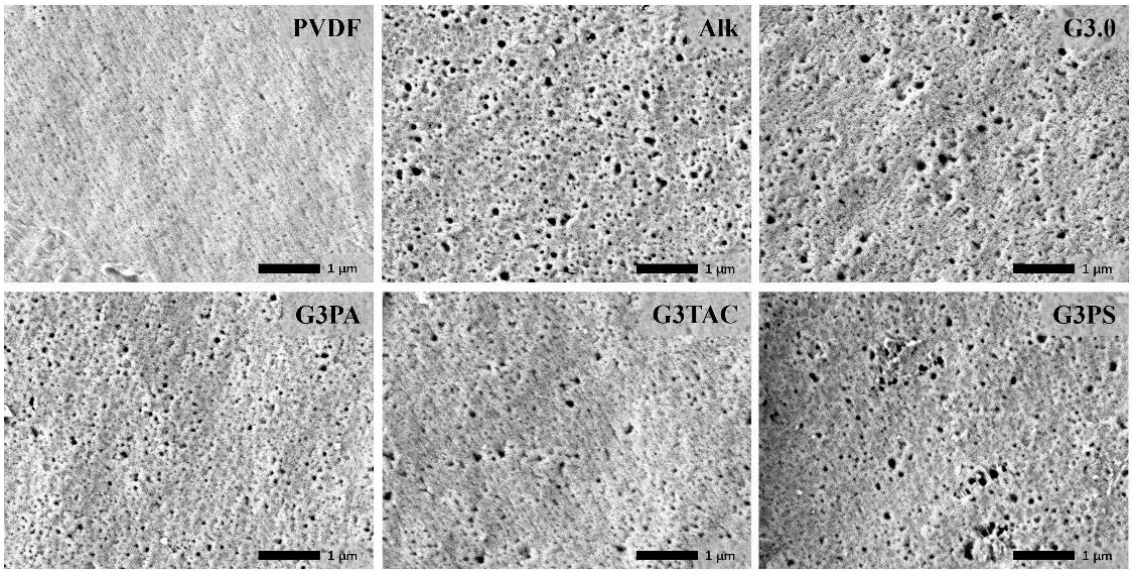

Figure 6.4 Surface SEM images of the PVDF membranes, alkaline treated, and PAMAM dendrimer with different functional groups modified membranes.

Based on the surface SEM images of the membranes, the surface porosity, and the average pore size were determined using Image J software and the results are listed in Table 6.1. As shown in Table 6.1, the PVDF membranes have a bulk porosity of 78% and a surface porosity of 1.7%. However, due to the alkaline etching during alkaline treatment, the surface porosity of the membranes (Alk) dramatically increased to 9.7%, and the average pore size increased from 34.8 nm to 81.2 nm. Additionally, since the alkaline treatment only affected the surface of the membranes, the bulk porosity of the membranes did not experience a significant change.

The morphology of the membranes did not undergo significant changes after grafting PAMAM dendrimers or converting the functional groups of dendrimers to carboxyl groups, quaternary ammonium groups, and sulfonic acid groups. The G3.0 membranes exhibited a bulk porosity of 77% and a surface porosity of 9.3%, similar to that of Alk membranes. However, the average pore size increased from 81.2 nm to 106.8 nm. This increase in pore size may be attributed to the presence of 0.5 M KOH in the dendrimer grafting solution,

leading to alkaline etching and enlargement of pore size during dendrimer grafting. The different processes for modifying the functional groups showed varying influences on porosity and pore size. For instance, converting G3.0 membranes to G3PA membranes resulted in a decrease in bulk porosity, surface porosity, and average pore size to 63%, 6.0%, and 56.4 nm, respectively. The decrease in bulk porosity and surface porosity is due to the swelling effect of MA on the membrane, during the functional group converting step. On the other hand, converting G3.0 membranes to G3TAC membranes only led to a decrease in surface porosity and average pore size to 3.1% and 51.6 nm, respectively. Lastly, converting to G3PS membranes only resulted in a decrease in bulk porosity to 64%.

Table 6.1 Bulk porosity, surface porosity, and the average pore size of the PVDF membranes, and modified membranes.

Membrane	Bulk porosity (%)	Surface porosity (%)	Average pore diameter (nm)
PVDF	78 ± 2	1.7 ± 0.2	34.8 ± 1.6
Alk	76 ± 1	9.7 ± 0.2	81.2 ± 1.8
G3.0	77 ± 3	9.3 ± 0.3	106.8 ± 2.4
G3PA	63 ± 2	6.0 ± 0.1	56.4 ± 0.6
G3TAC	74 ± 1	3.1 ± 0.1	51.6 ± 0.4
G3PS	64 ± 2	8.5 ± 0.2	107.6 ± 1.8

Surface chemical properties

Figure 6.5 illustrates the ATR-FTIR absorption difference between the top surface and the bottom surface of the PVDF and the modified membranes. The top surface of the membrane refers to the surface on the selective layer side of the membranes, which underwent further treatment with the alkaline solution and PAMAM dendrimer. All the modified membranes exhibit peaks above the baseline (red dashed line) at 1180 cm^{-1} and 1400 cm^{-1}. These peaks correspond to the stretching vibrations of the C-F bond [32] and the asymmetrical bending vibration of the C-H bonds [33], respectively. The peaks at 1180

cm^{-1} and 1400 cm^{-1} are above the baseline indicating a reduction in C-F bonds and C-H bonds on the modified surface.

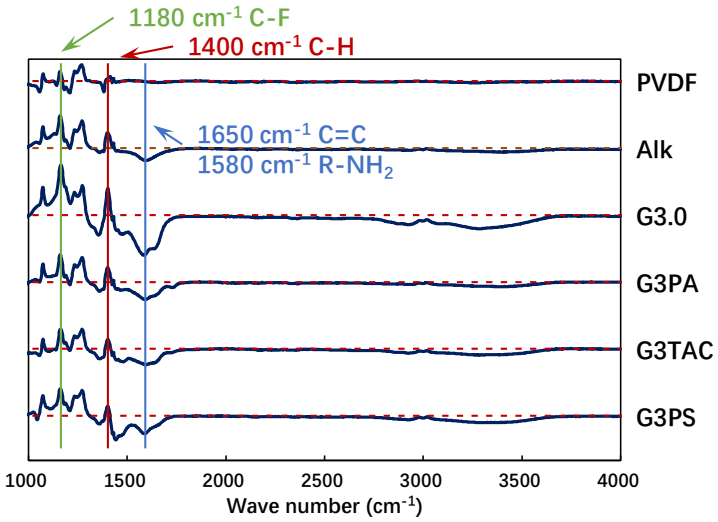

Figure 6.5 ATR-FTIR adsorption difference between the top surface and the bottom surface of the PVDF and the modified membranes. The peak above the baseline (red dashed line) indicates that this peak of the top surface is stronger than the peak of the bottom surface. Correspondingly, the peak below the baseline indicates that the peak of the top surface is weaker than the peak of the bottom surface.

Additionally, the absorption peak at 1650 cm^{-1} is attributed to the stretching vibrations of the C=C bond [34]. The peak at 1650 cm^{-1}, below the baseline, observed for the modified membranes suggests an increase in C=C bonds. Furthermore, the absorption peak of R-NH_2 (amine groups) is typically observed at 1580 cm^{-1} [35], which is close to the absorption peak of the C=C bond. Therefore, the peak of G3.0, G3PA, G3TAC, and G3PS membranes around 1650 cm^{-1}, which is below the baseline, may also be caused by the presence of amine groups. To differentiate whether the absorption peak around 1600 cm^{-1} is caused by C=C or amine groups, further XPS analysis is required.

The surface element composition of the membranes is presented in Table 6.2, as analyzed from the XPS spectrum (Figure 6.6). In PVDF membranes, the oxygen composition is 0.6

at%. The presence of oxygen detected on the surface of the PVDF membranes is attributed to the residual pore former agent PEG. The carbon-fluorine ratio on the surface of PVDF membranes is 0.93, slightly lower than 1, possibly due to defects in the PVDF molecules. For Alk membranes, the fluorine composition on the surface is 4.2 at%, indicating the removal of many fluorine atoms during alkaline treatment. Additionally, the oxygen composition increases from 0.6 at% to 21.3 at%, suggesting the introduction of abundant oxygen-containing groups, such as hydroxide groups and carboxyl groups, on the membrane surface.

Table 6.2 Membrane surface elemental composition of PVDF and modified membranes.

Membrane	Element composition (at%)				
	C 1s	N 1s	O 1s	F 1s	S 1s
PVDF	47.9	0.0	0.6	51.5	0.0
Alk	74.5	0.0	21.3	4.2	0.0
G3.0	73.3	5.5	18.1	3.1	0.0
G3PA	72.9	5.1	19.9	2.1	0.0
G3TAC	70.5	6.3	19.5	3.8	0.0
G3PS	69.7	2.8	21.2	5.2	1.1

Furthermore, the nitrogen composition increases from 0 at% for PVDF and Alk membranes to 5.5 at% for G3.0 membranes. This increase provides evidence that PAMAM dendrimers were successfully grafted onto the surface of the membranes. The mechanism of grafting PAMAM dendrimer on alkaline treated PVDF membranes was discussed in our previous research. Briefly, the alkaline treatment introduced the hydroxyl groups on the surface of PVDF membranes [22]. The amine group of PAMAM dendrimer formed a C-O-N structure with a hydroxyl group on membranes during dendrimer grafting.

Converting G3.0 membranes to G3PA membranes resulted in a decrease in nitrogen composition to 5.1 at%, as the introduction of carboxyl groups increases the carbon and oxygen composition on the membrane surface. Extra nitrogen atoms were introduced on

the surface of the membranes, by converting the functional groups of dendrimers on the surface to quaternary ammonium groups. Consequently, the introduction of quaternary ammonium groups increases the nitrogen composition from 5.5 at% to 6.3 at%. Furthermore, there is 1.1 at% sulfur detected on the surface of G3PS membranes, indicating the presence of sulfonic acid groups immobilized on the membranes. Notably, the nitrogen composition of G3PS membranes is 2.8 at%, significantly lower than that of G3.0 membranes. This suggests that the treatment with 1,3-PS solution caused parts of the PAMAM dendrimer to peel off from the membrane surface.

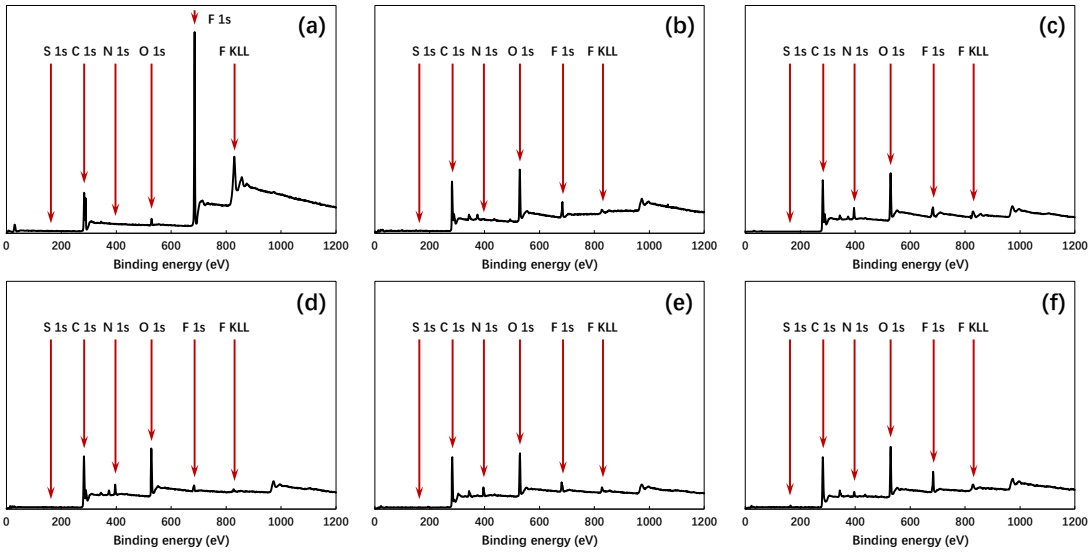

Figure 6.6 XPS full survey spectra of the PVDF (a), Alk (b), G3.0 (c), G3PA (d), G3TAC (e), and G3PS (f) membranes.

Surface hydrophilicity of membranes

The contact angles of the PVDF and modified membranes are shown in Figure 6.7. The PVDF membrane exhibited the highest contact angle, measuring at 77.8°. The alkaline treatment introduced numerous hydrophilic hydroxyl and carboxyl groups to the membrane, causing the contact angle to decrease to 52.6°. The following dendrimer grafting introduced amine groups causing a further contact angle decrease to 29.5°. The G3.0 and G3PS

membranes have the lowest contact angle. The contact angle of the G3PA membrane is approximately equal to that of the Alk membrane because the functional groups of dendrimers on the G3PA membranes are carboxyl groups, which are the same groups on the Alk membranes. The G3TAC membranes, with quaternary amine functional groups, have a contact angle of 39.8°.

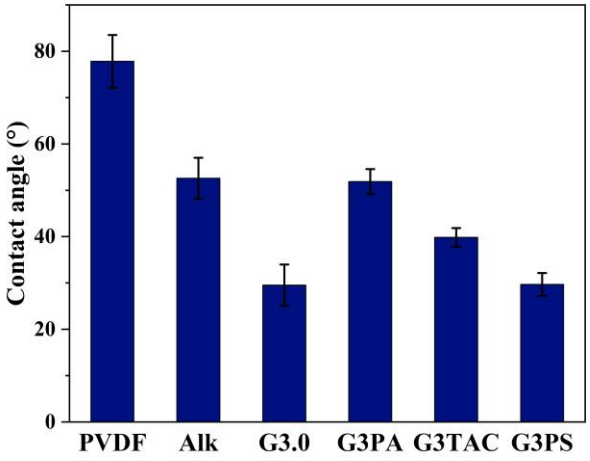

Figure 6.7 Contact angle of the PVDF membranes, alkaline treated, and PAMAM dendrimer with different functional groups modified membranes.

Surface zeta potential of membranes

Figure 6.8 illustrates the surface zeta potential of both the PVDF membranes and the modified membranes. The surface zeta potential exhibited a rapid decrease followed by reaching a plateau stage with an increase in pH. Initially, the surface zeta potential of the PVDF membranes measures at -41.5 mV at pH 6. After the alkaline treatment, there was a slight reduction in the surface zeta potential to -43.1 mV (for Alk membranes), attributed to the formation of carboxyl groups during the alkaline treatment process. Following the grafting of PAMAM-G3.0 dendrimer, positively charged amine groups were introduced, resulting in an increase in the surface zeta potential to -42.4 mV. Notably, the alkaline-treated membranes contain numerous negatively charged carboxyl groups, which counteract the positive charge of the amine groups. Consequently, the membranes continue

to exhibit a negative potential even after dendrimer grafting.

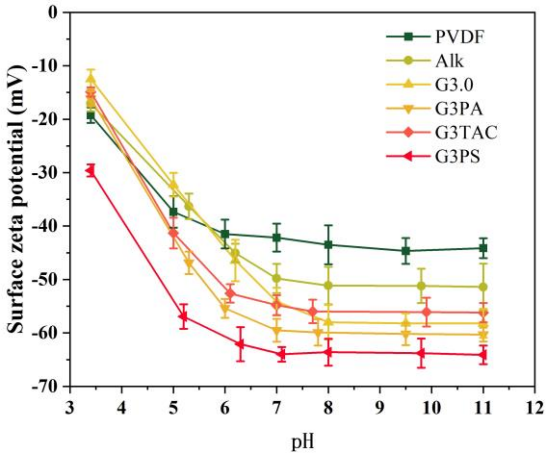

Figure 6.8 Surface zeta potential of the PVDF membranes, alkaline treated, and PAMAM dendrimer with different functional groups modified membranes.

The G3PA membranes, featuring negative functional groups, exhibited a smaller surface zeta potential (-55.4 mV) compared to the zeta potential of Alk or G3.0 membranes. Remarkably, the G3PS membranes, possessing strong negatively charged sulfonic groups, demonstrate the lowest surface zeta potential (-60.7 mV) at pH 6. Despite the strong positively charged quaternary ammonium groups present in G3TAC membranes, the membranes displayed a lower surface zeta potential than Alk membranes at pH 6. The surface zeta potential of G3.0 membranes decreased more rapidly as pH increased from 6 to 8. At pH 8, G3.0 membranes exhibited a lower surface zeta potential than G3TAC membranes. Similarly, membranes grafted with dendrimer exhibited abundant negatively charged carboxyl groups, which counteract the positive charge from quaternary ammonium groups. Consequently, G3TAC membranes displayed a negative surface zeta potential. Although the surface zeta potential of all membranes is negative, the magnitude of the surface zeta potential correlates with the charge intensity of functional groups on the membrane when the surface zeta potential reaches a plateau stage (pH > 8). For example, the order of surface zeta potential for dendrimer-grafted membranes is G3TAC (strong

positive) > G3.0 (weak positive) > G3PA (weak negative) > G3PS (strong negative). Notably, PVDF and Alk membranes exhibited a larger surface zeta potential than all dendrimer-grafted membranes.

6.3.2. Filtration performance of membranes

Figure 6.9 illustrates the pure water flux (a), permeate flux, and rejection of PEO (b), PAA (c), and whey protein (d) by PVDF and modified membranes. Initially, the pure water flux of the PVDF membranes was 274.1 LMH. Following alkaline treatment, the pure water flux increased to 577.8 LMH (for Alk membranes), marking a 2.1-fold increase compared to the PVDF membrane's pure water flux. G3.0 membranes exhibited a flux of 576.0 LMH, approximately equal to the flux of Alk membranes, whereas G3PA and G3TAC membranes experienced a decrease in flux to around 487 LMH. G3PS membranes demonstrated the lowest pure water flux at 424.5 LMH. The increase in pure water flux for Alk and G3.0 membranes is attributed to the increase in surface porosity. Specifically, the surface porosity of Alk and G3.0 membranes, which is 9.7% and 9.3%, respectively, is 5.6 times higher than PVDF membranes' surface porosity. This elevation in surface porosity reduced flow resistance as water traversed the membrane surface, consequently boosting pure water flux. Conversely, the decrease in pure water flux for G3PA, G3TAC, and G3PS membranes is attributed to a decrease in surface porosity. Although G3TAC membranes possess a smaller surface porosity (3.1%) compared to G3PA membranes (6.0%), their pure water flux remains approximately the same. This observation suggests that the decrease in both surface and bulk porosity contributes to the reduction in pure water flux. Notably, G3PA membranes exhibit a lower bulk porosity (63%) than G3TAC membranes (74%), resulting in higher flow resistance as water traversed the membrane matrix, thus maintaining similar water flow resistance across the membranes.

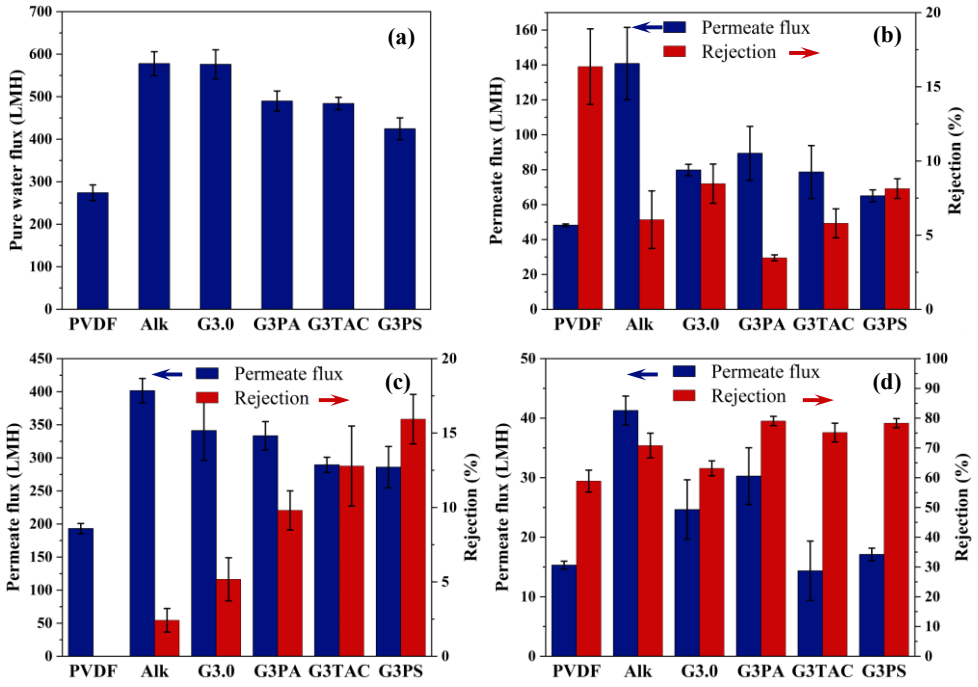

Figure 6.9 Pure water flux (a), permeate flux and rejection of PEO (b), PAA (c), and whey protein (d) of PVDF, alkaline treated and dendrimer grafted membranes.

PEO

PEO is electrically neutral in aqueous solutions and therefore does not interact with charged membranes. Consequently, PEO rejection serves as an indicator of membrane pore size distribution. As depicted in Figure 6.9 (b), PVDF membranes exhibited the highest PEO rejection at 16.4% and the lowest permeate flux at 48.2 LMH, suggesting that PVDF membranes possess the smallest pore size. The descending order of PEO rejection among the membranes is as follows: PVDF (Rejection: 16.4%) > G3.0 (8.5%) > G3PS (8.1%) > Alk (6.0%) ≈ G3TAC (5.8%) > G3PA (3.5%). Typically, a larger pore size should correspond to lower PEO rejection. However, based on SEM image analysis (Table 6.1), the average pore size exhibits the following ascending order: PVDF (34.8 nm) < G3TAC (51.6 nm) < G3PA (56.4 nm) < Alk (81.2 nm) < G3.0 (106.8 nm) ≈ G3PS (107.6 nm). Interestingly, G3.0 and G3PS membranes, despite having larger pore sizes, exhibited greater PEO rejection compared to Alk, G3TAC and G3PA membranes. This discrepancy

suggests that factors beyond pore size and surface porosity influence permeate flux during PEO filtration.

PAA

From Figure 6.9 (c) the increasing order of PAA separation is PVDF(0%) < Alk(2.4%) < G3.0(5.2 %) < G3PA (9.8%) < G3TAC(12.8%) < G3PS(15.9%). On the other hand, from Figure 6.8, the decreasing order of zeta potential at pH 7 is PVDF > Alk > G3.0 > G3TAC > G3PA > G3PS. A correlation is found between the order of PAA separation and that of zeta potential, i.e. the PAA separation increases and the zeta potential decreases, which seems reasonable considering the electrostatic repulsion, since PAA is negatively charged, while the negative charge of the membrane increases as zeta potential decreases. There is however a notable exception of G3TAC, whose position was shifted from before G3PA of zeta potential to behind G3PA of separation, despite the presence of the positively charged quaternary amine in G3TAC, which is expected to decrease PAA separation. One of the plausible explanations for this shift is that the positively charged groups at the membrane surface adsorb negatively charged PAA, forming a negatively charged layer on the membrane surface as illustrated in Figure 6.10 (a). This layer acts as a barrier, preventing PAA from entering membrane pores through electrostatic repulsion. Figure 6.9 (c) also shows that the flux is inversely correlated to the PAA separation, and its pattern is more like that of pure water permeation.

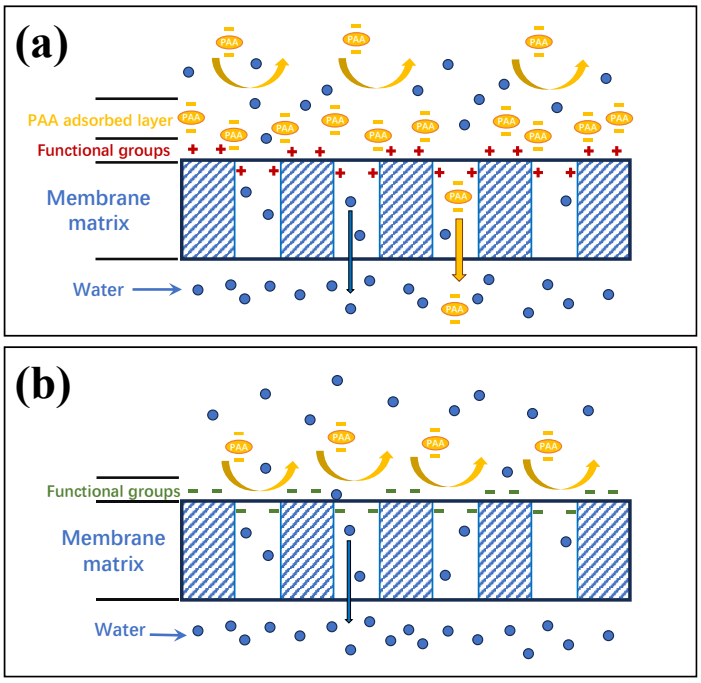

Figure 6.10 PAA separation mechanism by (a) membranes with positively charged functional groups on the surface, and (b) membranes with negatively charged functional groups on the surface

Whey protein

From Figure 6.9 (d) the whey separation is in the increasing order of PVDF (58.9%) < G3.0 (63.1%) < Alk (70.8%) < G3TAK (75.2%) ≤ G3SP (78.3%) ≤ G3PA (79.0%). The most notable change from the order in PAA separation is the exchange of the position of G3.0 and Alk. (Although the positions of G3PA and G3SP were also exchanged, the difference in their separations was less than 1% which is in an error range.) Interestingly, the shift of G3.0 to the lower separation was accompanied by the lowering of the permeate flux (It is now even lower than G3PA.), suggesting a higher degree of concentration polarization that contributed to the decrease of whey protein separation as well as flux.

6.3.3. Whey protein filtration performance of commercial membranes

Table 6.3 reveals the whey protein filtration performance of various commercial

membranes under the same operational conditions as homemade membranes. ST membranes, featuring a molecular weight cutoff (MWCO) of 10 kDa, exhibit the highest whey protein rejection at 98.7%. However, their permeate flux is a modest 4.2 LMH. V4 membranes, with an MWCO of 70 kDa, boast a similar rejection rate of 98% but offer a higher permeate flux of 14 LMH, about 3.3 times that of ST membranes. MW membranes, with an MWCO of 50 kDa, achieve a permeate flux of 33.7 LMH, nearly matching the flux of G3PA membranes. However, their whey protein rejection stands at 62.1%, 16.9% lower than rejection of G3PA membranes. Homemade PVDF membranes exhibit a rejection rate of 58.9%, slightly lower than that of MW membranes, yet their permeate flux is merely half that of MW membranes. Post-modification, the permeate flux of G3PA membranes escalates to the level of MW membranes while maintaining a higher whey protein rejection rate. This suggests that grafting generation 3 PAMAM dendrimers with carboxyl groups onto PVDF membrane surfaces significantly enhances both rejection and permeate flux.

Table 6.3 Pure water flux, whey protein rejection, and permeate flux of some commercial membranes.

Manufactory	Commercial name	Membrane material	Pore size /MWCO [a]	Pure water flux (LMH)	Whey protein filtration	
					Rejection	Permeate flux (LMH)
Microdyn Nadir™	MV020	PVDF	0.2 μm	24544.8	26.0%	1053.8
	MP005	PES [b]	0.05 μm	4140.0	56.3%	115.8
Synder™	V4	PVDF	70 kDa	23.4	98.0%	14.0
GE Osmonics™	MW	PAN [c]	50 kDa	442.7	62.1%	33.7
Synder™	MK	PES	30 kDa	35.8	92.8%	8.2
Synder™	ST	PES	10 kDa	13.8	98.7%	4.2

[a] Pore size and MWCO data are provided by the manufactory

[b] PAN: polyacrylonitrile

[c] PES: polyethersulfone

6.3.4. Comparison of dendrimer grafting at membrane surface only and both at surface and inside pores of membrane

In our previous study, we grafted generation 3 PAMAM dendrimers with peripheral amine groups both at the surface and inside of the KOH-isopropanol pretreated PVDF membrane. This process involved immersing the PVDF membrane in KOH isopropanol solution, allowing the alkaline solution to react both at the membrane surface and inside the membrane pores. Consequently, PAMAM dendrimers were grafted throughout the membranes.

Table 6.4 Comparison of surface and interior PAMAM dendrimer grafting membranes and the surface PAMAM dendrimer grafting membranes; Alk, G3.0 and G3PA represent alkaline treated membranes, PAMAM with amine groups and PAMAM with carboxyl groups grafted membranes.

	Surface and interior PAMAM grafting [27]			Surface PAMAM grafting (this work)		
	Alk	G3.0	G3PA	Alk	G3.0	G3PA
Alkaline treatment time (min)	1			30		
Alkaline treatment temp. (℃)	60			80		
KOH conc. (M)	0.5			10		
Contact angle (°)	57.7±1.3	48.9±1.5	57.4±1.8	52.6±4.4	29.5±4.5	51.9±2.7
Pore diameter (nm)	39.2±0.3	41.7±0.3	38.6±0.2	81.2±1.8	106.8±2.4	56.4±0.6
Surface porosity (%)	2.5±0.3	2.8±0.1	2.5±0.1	9.7±0.2	9.3±0.3	6.0±0.1
Bulk porosity (%)	71±1	67 ± 3	61 ± 2	76 ± 1	77 ± 3	63 ± 2
C composition (at%)	59.6	57.6	63.7	74.5	73.3	72.9
N composition (at%)	0	7.6	4.2	0	5.5	5.1
O composition (at%)	14.1	13.7	10	21.3	18.1	19.9
F composition (at%)	26.3	21	22.2	4.2	3.1	2.1
Pure water flux (LMH)	115.7±20.3	92.3±8.7	60.6±4.3	577.8±28.0	576.0±34.3	489.8±23.6
Whey protein rejection (%)	97.3±2.2	95.7±4.3	98.8±0.3	70.8±4.2	63.1±2.5	79.0±1.6
Whey permeate flux (LMH)	5.6±2.2	3.1±1.1	2.3±0.4	41.3±2.4	24.6±5.0	30.3±4.8

In this work, we exclusively grafted generation 3 PAMAM dendrimers with peripheral amine groups onto the surface of PVDF membranes by pretreating with KOH aqueous solution. As the aqueous solution cannot penetrate the pores of the hydrophobic PVDF membranes, the alkaline treatment is confined to the membrane surfaces. As shown in Table 6.4, this difference in treatment methods results in distinct outcomes. Because the KOH aqueous treatment only impacts the surface of the membranes and does not impact the inside of the membranes, it has little influence on the strength of the membranes. With aqueous solution treatment, PVDF membranes are subjected to a stronger alkaline treatment, leading to increased removal of fluorine and introduction of more oxygen-containing active functional groups. For instance, membranes treated with KOH aqueous solution exhibited, by XPS, a fluorine composition of 4.2 at% and an oxygen composition of 21.3 at%, compared to 26.3 at% fluorine and 14.1 at% oxygen by the isopropanol treatment. Moreover, aqueous solution treatment significantly enhances surface porosity, increasing it by a factor of 4.7, while having no impact on bulk porosity, which is crucial for membrane flux. However, alkaline treatment with aqueous solution necessitates higher KOH concentration, treating temperature, and duration. For instance, isopropanol treatment requires 0.5 M KOH, a treating temperature of 60℃, and 1 minute, whereas aqueous solution treatment demands 10 M KOH, 80℃, and 30 minutes.

The difference between the modification at the surface only and at the surface and inside the membrane is also manifested in the filtration performance. In our previous study, dendrimer grafting was allowed both at the surface and inside the membrane. As a result, the whey protein rejection was 95.7% for PAMAM-G3.0 grafted and 98.8% for PAMAM-G3PA (with carboxyl group) grafted membranes. The permeate flux of those two membranes was 3.1 LMH and 2.3 LMH, respectively. Thus, these membranes could achieve very high whey protein rejections due to the electrostatic repulsion occurring both at the membrane surface and in the membrane pore, but the permeate fluxes were low. For

the membranes, grafted dendrimer only at the surface, the whey protein rejection was 63.1% for the G3.0 and 79% for the G3PA membrane, respectively. The permeate flux of those two membranes was 24.6 LMH and 30.3 LMH, respectively. Thus, the whey protein separation was lowered by the surface only modification, but the flux increased remarkably.

6.4. Conclusions

In this research, PAMAM dendrimers were successfully grafted onto the surface of PVDF membranes. The surface porosity of the membranes was enlarged approximately 5.7 times through alkaline pretreatment, while the modification did not significantly impact bulk porosity. Additionally, all modifications led to a decrease in the zeta potential and contact angle on the membrane surface. Specifically, G3PS membranes exhibited the lowest surface zeta potential and contact angle, measuring at -60.7 mV (at pH 6) and 29.5°, respectively.

The PEO rejection of all modified membranes was lower than that of the PVDF membranes due to pore size enlargement. These modified membranes demonstrated the ability to separate PAA, a task unachievable by PVDF membranes, as their pore size is smaller compared to the modified ones. The increase in PAA rejection correlated with the decrease in the surface zeta potential of the membranes, suggesting that electrostatic exclusion enhances the separation of charged PAA molecules. This electrostatic interaction also proved effective at the macro-molecular level, such as with proteins.

In this work, modification led to an increase in both the whey protein separation and permeate flux of the membranes. The membranes with the best whey protein separation performance are G3PA membranes. Compared with the pristine PVDF membrane, the G3PA increased the permeate flux by 98%, while the separation increased from 58.9 % of

the pristine PVDF membrane to 79.0 % of G3PA. As a comparison, the MW membrane of GE Osmonics™, whose permeate flux, 33.7 LMH, is similar to that of the G3.5 membranes, only has a whey rejection of 62.1%. Moreover, it should be noted that only one type of homemade PVDF membrane was used in this study. A better performance of whey protein filtration could be expected by optimizing the properties of the PVDF membrane to be used for modification.

Results of this study, in comparison to that of the previous study, as discussed in Section 6.3.4, indicate that introducing appropriate charged functional groups onto both the exterior and intraporous surfaces is more efficient in terms of enhancing the rejection of membranes for charged macromolecules while modifying the exterior surfaces only helps to preserve the mechanical strength of membrane and elevates permeate fluxes.

6.5. References

[1] V. Vatanpour and A. Sanadgol, "Surface modification of reverse osmosis membranes by grafting of polyamidoamine dendrimer containing graphene oxide nanosheets for desalination improvement," *Desalination*, vol. 491, p. 114442, Oct. 2020, doi: 10.1016/j.desal.2020.114442.

[2] R. Singh, "Introduction to Membrane Technology," in *Membrane Technology and Engineering for Water Purification*, Elsevier, 2015, pp. 1–80. doi: 10.1016/B978-0-444-63362-0.00001-X.

[3] Z. Cui, N. T. Hassankiadeh, Y. Zhuang, E. Drioli, and Y. M. Lee, "Crystalline polymorphism in poly(vinylidenefluoride) membranes," *Progress in Polymer Science*, vol. 51, pp. 94–126, Dec. 2015, doi: 10.1016/j.progpolymsci.2015.07.007.

[4] Z. Cui, E. Drioli, and Y. M. Lee, "Recent progress in fluoropolymers for membranes," *Progress in Polymer Science*, vol. 39, no. 1, pp. 164–198, Jan. 2014, doi: 10.1016/j.progpolymsci.2013.07.008.

[5] D. Zou and Y. M. Lee, "Design strategy of poly(vinylidene fluoride) membranes for

water treatment," *Progress in Polymer Science*, vol. 128, p. 101535, May 2022, doi: 10.1016/j.progpolymsci.2022.101535.

[6] H. Bubela, V. Konovalova, J. Kujawa, I. Kolesnyk, A. Burban, and W. Kujawski, "Enhancing of transport parameters and antifouling properties of PVDF membranes modified with Fe3O4 nanoparticles in the process of proteins fractionation," *Separation and Purification Technology*, vol. 325, p. 124573, Nov. 2023, doi: 10.1016/j.seppur.2023.124573.

[7] K. Fan, J. Su, Z. Zeng, J. Hu, H. Yang, and Z. Hou, "Anti-fouling and protein separation of PVDF-g-PMAA@MnO_2 filtration membrane with in-situ grown MnO_2 nanorods," *Chemosphere*, vol. 286, p. 131756, Jan. 2022, doi: 10.1016/j.chemosphere.2021.131756.

[8] R. Zhang *et al.*, "Surface modification of PVDF membranes with quaternized chitosan for selective separation of negatively charged polysaccharides – exemplified with heparin," *Journal of Environmental Chemical Engineering*, vol. 11, no. 5, p. 110666, Oct. 2023, doi: 10.1016/j.jece.2023.110666.

[9] D. A. Tomalia *et al.*, "A New Class of Polymers: Starburst-Dendritic Macromolecules," *Polym J*, vol. 17, no. 1, pp. 117–132, Jan. 1985, doi: 10.1295/polymj.17.117.

[10] M. V. Walter and M. Malkoch, "Simplifying the synthesis of dendrimers: accelerated approaches," *Chem. Soc. Rev.*, vol. 41, no. 13, pp. 4593–4609, Jun. 2012, doi: 10.1039/C2CS35062A.

[11] B. Devadas, A. P. Periasamy, and K. Bouzek, "A review on poly(amidoamine) dendrimer encapsulated nanoparticles synthesis and usage in energy conversion and storage applications," *Coordination Chemistry Reviews*, vol. 444, p. 214062, Oct. 2021, doi: 10.1016/j.ccr.2021.214062.

[12] T. Baig, J. Nayak, V. Dwivedi, A. Singh, and P. K. Tripathi, "A Review about Dendrimers: Synthesis, Types, Characterization and Applications," vol. 4, 2015.

[13] A. T. Yasir, A. Benamor, A. H. Hawari, and E. Mahmoudi, "Poly (amido amine) dendrimer based membranes for wastewater treatment – A critical review," *Chemical Engineering Science*, vol. 273, p. 118665, Jun. 2023, doi: 10.1016/j.ces.2023.118665.

[14] Z.-L. Qiu *et al.*, "Ionic Dendrimer Based Polyamide Membranes for Ion Separation,"

ACS Nano, vol. 15, no. 4, pp. 7522–7535, Apr. 2021, doi: 10.1021/acsnano.1c00936.

[15] R. Borgohain and B. Mandal, "Thermally stable and moisture responsive carboxymethyl chitosan/dendrimer/hydrotalcite membrane for CO_2 separation," *Journal of Membrane Science*, vol. 608, p. 118214, Aug. 2020, doi: 10.1016/j.memsci.2020.118214.

[16] M. Algarra, M. I. Vázquez, B. Alonso, C. M. Casado, J. Casado, and J. Benavente, "Characterization of an engineered cellulose based membrane by thiol dendrimer for heavy metals removal," *Chemical Engineering Journal*, vol. 253, pp. 472–477, Oct. 2014, doi: 10.1016/j.cej.2014.05.082.

[17] O. Karatas, R. Keyikoglu, N. Atalay Gengec, V. Vatanpour, and A. Khataee, "A review on dendrimers in preparation and modification of membranes: progress, applications, and challenges," *Materials Today Chemistry*, vol. 23, p. 100683, Mar. 2022, doi: 10.1016/j.mtchem.2021.100683.

[18] D. J. Miller, D. R. Dreyer, C. W. Bielawski, D. R. Paul, and B. D. Freeman, "Surface Modification of Water Purification Membranes," *Angewandte Chemie International Edition*, vol. 56, no. 17, pp. 4662–4711, 2017, doi: 10.1002/anie.201601509.

[19] E. N. Savariar, M. M. Sochat, A. Klaikherd, and S. Thayumanavan, "Functional Group Density and Recognition in Polymer Nanotubes," *Angew. Chem. Int. Ed.*, vol. 48, no. 1, pp. 110–114, Jan. 2009, doi: 10.1002/anie.200804136.

[20] W.-P. Zhu, J. Gao, S.-P. Sun, S. Zhang, and T.-S. Chung, "Poly(amidoamine) dendrimer (PAMAM) grafted on thin film composite (TFC) nanofiltration (NF) hollow fiber membranes for heavy metal removal," *Journal of Membrane Science*, vol. 487, pp. 117–126, Aug. 2015, doi: 10.1016/j.memsci.2015.03.033.

[21] H. Wang, C. Wu, Z. Wei, C. Li, and Q. Liu, "Surface chemistry, topology and desalination performance controlled positively charged NF membrane prepared by polydopamine-assisted graft of starburst PAMAM dendrimers," *RSC Adv.*, vol. 6, no. 6, pp. 4673–4682, 2016, doi: 10.1039/C5RA25047A.

[22] G. Li, L. Shen, Y. Luo, and S. Zhang, "The effect of silver-PAMAM dendrimer nanocomposites on the performance of PVDF membranes," *Desalination*, vol. 338, pp. 115–120, Apr. 2014, doi: 10.1016/j.desal.2014.02.001.

[23] C. Wei *et al.*, "Fabrication of pH-Sensitive Superhydrophilic/Underwater Superoleophobic Poly(vinylidene fluoride)- *graft* -(SiO_2 Nanoparticles and PAMAM Dendrimers) Membranes for Oil–Water Separation," *ACS Appl. Mater. Interfaces*, vol. 12, no. 16, pp. 19130–19139, Apr. 2020, doi: 10.1021/acsami.9b22881.

[24] Q. Zhang, N. Wang, L. Zhao, T. Xu, and Y. Cheng, "Polyamidoamine Dendronized Hollow Fiber Membranes in the Recovery of Heavy Metal Ions," *ACS Appl. Mater. Interfaces*, vol. 5, no. 6, pp. 1907–1912, Mar. 2013, doi: 10.1021/am400155b.

[25] H. Sun *et al.*, "Preparation of PAMAM modified PVDF membrane and its adsorption performance for copper ions," *Environmental Research*, vol. 204, p. 111943, Mar. 2022, doi: 10.1016/j.envres.2021.111943.

[26] X. Zhang *et al.*, "Preparation of PVDF/Hyperbranched-Nano-Palygorskite Composite Membrane for Efficient Removal of Heavy Metal Ions," *Polymers*, vol. 11, no. 1, Art. no. 1, Jan. 2019, doi: 10.3390/polym11010156.

[27] Z. Xu *et al.*, "Polyamidoamine (PAMAM) dendrimer surface grafting polyvinylidene fluoride (PVDF) membranes to enable microporous membranes for protein separation," *Reactive and Functional Polymers*, doi: Under review after major revision.

[28] V. Gupta and S. Nayak, "Dendrimers: A Review on Synthetic Approaches," *J App Pharm Sci*, pp. 117–122, 2015, doi: 10.7324/JAPS.2015.50321.

[29] R. Y. Patle and J. S. Meshram, "The advanced synthetic modifications and applications of multifunctional PAMAM dendritic composites," *React. Chem. Eng.*, vol. 7, no. 1, Art. no. 1, 2022, doi: 10.1039/D1RE00074H.

[30] Z. Xu, S. Gu, D. Rana, T. Matsuura, and C. Q. Lan, "Chemical precipitation enabled UF and MF filtration for lead removal," *Journal of Water Process Engineering*, vol. 41, p. 101987, Jun. 2021, doi: 10.1016/j.jwpe.2021.101987.

[31] Z. Li, D. Rana, Z. Wang, T. Matsuura, and C. Q. Lan, "Synergic effects of hydrophilic and hydrophobic nanoparticles on performance of nanocomposite distillation membranes: An experimental and numerical study," *Separation and Purification Technology*, vol. 202, pp. 45–58, Aug. 2018, doi: 10.1016/j.seppur.2018.03.032.

[32] N. Daems, S. Milis, R. Verbeke, A. Szymczyk, P. P. Pescarmona, and I. F. J.

Vankelecom, “High-performance membranes with full pH-stability,” *RSC Adv.*, vol. 8, no. 16, pp. 8813–8827, Feb. 2018, doi: 10.1039/C7RA13663C.

[33] A. Qin, X. Li, X. Zhao, D. Liu, and C. He, “Engineering a Highly Hydrophilic PVDF Membrane via Binding TiO_2 Nanoparticles and a PVA Layer onto a Membrane Surface,” *ACS Appl. Mater. Interfaces*, vol. 7, no. 16, Art. no. 16, Apr. 2015, doi: 10.1021/acsami.5b00978.

[34] A. Bottino, G. Capannelli, O. Monticelli, and P. Piaggio, “Poly(vinylidene fluoride) with improved functionalization for membrane production,” *Journal of Membrane Science*, vol. 166, no. 1, pp. 23–29, Feb. 2000, doi: 10.1016/S0376-7388(99)00253-7.

[35] P. Salehian and T.-S. Chung, “Thermally treated ammonia functionalized graphene oxide/polyimide membranes for pervaporation dehydration of isopropanol,” *Journal of Membrane Science*, vol. 528, pp. 231–242, Apr. 2017, doi: 10.1016/j.memsci.2017.01.038.

Chapter 7. Effects of Polyamidoamine Dendrimer Immobilization on Protein Separation of PVDF Membrane: Mathematical Analysis by Donnan Steric Pore Model with Dielectric Exclusion (DSPM-DE)

Abstract

The immobilization of polyamidoamine (PAMAM) dendrimers on polyvinylidene fluoride (PVDF) membranes significantly enhances their performance in protein separation processes. This study investigates the impact of these modifications on membrane properties, including permeate flux and the rejection of polyacrylic acid (PAA) and whey protein. Discrepancies between the calculated and measured pore radii were observed using polyethylene oxide (PEO) filtration data and the Donnan steric pore model with dielectric exclusion (DSPM-DE) model. It was found that the presence of charged functional groups within membrane pores affects electrostatic interactions, leading to dielectric exclusion and enhanced solute rejection. The surface charge density of the modified membranes increased with pH, with sulfonic acid groups contributing to higher charge densities at lower pH levels. The Donnan potential of a membrane is influenced by several factors, including pore size, volume charge density, and the functional groups present on the membrane. Theoretical modeling using the DSPM-DE model provided insights into the separation mechanisms, revealing deviations between experimental and calculated results while effectively explaining improvements in flux and rejection rates.

Acronyms and Symbols

Abbreviation

ATR-FTIR	attenuated total reflectance-Fourier transform infrared
BSA	bovine serum albumin
CNTs	carbon nanotubes
DMAc	*N, N*-dimethylacetamide
DSPM-DE	Donnan steric pore model with dielectric exclusion
EDA	ethylenediamine
FESEM	field-emission scanning electron microscope
GO	graphene oxide
MA	methyl acrylate
NF	nanofiltration
PAA	polyacrylic acid
PAMAM	polyamidoamine
PEG	polyethylene glycol
PEO	polyethylene oxide
PVDF	polyvinylidene fluoride
SEM	scanning electron microscope
UF	ultrafiltration

Nomenclature

c_i	concentration of solute *i*
$c_{i,p}$	concentration of solute *i* in permeate phase
$c_{i,f}$	concentration of solute *i* in the feed phase
D	diffusivities
$D_{i,\infty}$	diffusion efficient of solute *i* in the bulk solution
e	electronic charge
F	Faraday constant
J_i	solute flux
J_v	solvent flux
$K_{i,a}$	advection hindrance factors
$K_{i,d}$	diffusion hindrance factors
k	Boltzmann constant
L_e	effective membrane thickness
M	molecular weight of the polymer
N_A	Avogadro number
ΔP	hydraulic pressure difference across the membrane
R	ideal gas constant
R_i	rejection of the solute *i*
R_{lim}	limiting rejection

r_p	radius of the membrane pore
r_s	Stokes radius of the solute
T	temperature
ΔW_i	change of solvation energy (energy barrier)
X	effective volume charge density
x	position along the thickness direction of the membrane
z_i	valance of the solute *i*
δ	thickness of the membrane active layer
ε_0	dielectric constant of vacuum
ε_b	dielectric constant of solvent in bulk
ε_p	dielectric constant of solvent in membrane pore
ζ	surface zeta potential of the membrane
$[\eta]$	intrinsic viscosity of the polymer
η_w	water dynamic viscosity
λ_i	ration of r_s and r_p
$\Delta\pi$	osmotic pressure difference between feed and permeate phase
σ	membrane surface charge density
$\phi(x)$	electrical potential at position x along the membrane pore
$\varphi_{DE,i}$	dielectric exclusion factor
$\varphi_{S,i}$	steric exclusion factors

$\Delta\psi_{\mathrm{D}}$	Donnan potential across two interfaces

7.1. Introduction

With the growing demand for separation efficiency and precision in modern industry, membrane separation technology has received increasing attention. Membrane filtration technology offers numerous advantages, such as high separation quality, no phase change during separation (excluding membrane distillation and evaporation), low energy consumption, high separation efficiency, simplicity of operation, and environmental friendliness. Membrane separation plays a crucial role in the removal of heavy metal ions, organic contaminants, and protein separation [1].

Among various membrane materials, polyvinylidene fluoride (PVDF) membranes are favored for their excellent mechanical strength, chemical resistance, and thermal stability. However, their hydrophobic nature and susceptibility to fouling limit their applications [1]. To address these challenges, research on enhancing the hydrophilicity and surface charge modification of PVDF membranes has gained increasing attention. Despite these advancements, understanding and predicting the separation performance of modified PVDF membranes, especially for charged solutes, remains complex. Various methods for improving PVDF membranes have been proposed, such as blending [2], surface grafting [3], and surface coating [3]. Researchers have also explored modifying PVDF membranes with novel materials like MXene [4], [5], carbon nanotubes (CNTs) [6], [7], [8], [9], metal-organic frameworks (MOFs) [10], [11], graphene oxide (GO) [12], [13], SiO_2 nanoparticles [14], and TiO_2 nanoparticles [15]. Polyamidoamine (PAMAM) dendrimers are highly branched polymers with a spherical structure and numerous surface functional groups (such as amino and carboxyl groups) [16], [17]. Modifying PVDF membranes with PAMAM dendrimers can significantly enhance the hydrophilicity of the membranes and introduce charged groups to the surface. This modification improves the water flux, separation capability, and antifouling performance of the membranes. For example, in our previous

research, the PVDF membrane whose surface is modified by PAMAM-G3 dendrimer with carboxyl groups, increases the rejection of whey protein by 34%, while simultaneously improving the permeate flux by 98% [18].

In models describing the ultrafiltration (UF) membrane separation process, most consider solute convection and diffusion transport. Few models take into account the electrostatic interactions between the membrane and the solute. The Donnan steric pore model with dielectric exclusion (DSPM-DE) is developed to describe and predict the transport behavior of ions and molecules in the nanofiltration (NF) membrane separation process [19]. This model combines charge exclusion (Donnan effect), size exclusion (Steric effect), dielectric exclusion, and the influence of the potential distribution within membrane pores. It provides a theoretical foundation for understanding and optimizing the separation performance of NF membranes. DSPM-DE model is based on the Nernst-Planck equation, taking into account advection, diffusion, convection, and electromigration effects on solute molecules. To simplify the process and facilitate analysis, the DSPM-DE model makes the following assumptions. (1) Only consider the effect of the active layer, ignore the influence of the support layer. (2) The pores in the active layer are the cylinder pores of uniform size. (3) The concentration gradient of the solute crossflow direction is ignored. Only consider the dimension that is vertical with the interface of the membrane. (4) All the solutes are assumed as spheres with Stokes radius. (5) The solution is dilute, so the interaction between the solutes and solutes is ignored. (6) The dielectric constant of solvent (water) inside the membrane pore is assumed to be spatially constant. (7) The volume charge density inside the membrane is uniform. (8) The membrane and interfaces of the membrane are electro-neutrality. (9) The system is at a steady state [19].

In this study, we used the DSPM-DE model to explore the separation performance of PVDF membranes and modified membranes. We aim to evaluate the separation performance of

PVDF membranes and modified membranes by combining experimental data with theoretical modeling and to interpret the results using the DSPM-DE model. Through this approach, we aim to elucidate the impact of PVDF membrane modification on its ability to separate charged solutes, as well as to clarify the separation process and mechanisms of charged solute molecules using charged UF membranes.

7.2. Experimental

7.2.1. Materials

The PVDF host polymer for membranes (Kynar® 740, M_w = 410 kDa) was supplied by Arkema Inc. (Philadelphia, PA). The pore-forming agent, polyethylene glycol (PEG, M_w = 1 kDa), and the casting solution solvent, anhydrous *N, N*-dimethylacetamide (DMAc, 99.8% purity), were purchased from Sigma-Aldrich Inc. (St. Louis, MO). Other chemicals from Sigma-Aldrich Inc. included potassium hydroxide, methanol (99.5% purity), isopropanol (99.5% purity), ethylenediamine (EDA, 99% purity), and methyl acrylate (MA, 99% purity) for PAMAM dendrimer synthesis. A 35 wt% polyacrylic acid (PAA) aqueous solution (M_w = 100 kDa), polyethylene oxide (PEO) (M_w = 100 kDa), whey protein, and bovine serum albumin (BSA) for filtration were also obtained from Sigma-Aldrich. For PEO concentration analysis, barium chloride, hydrochloric acid, iodine, and potassium iodide were used. The Bradford Reagent for whey protein analysis.

7.2.2. Membrane fabrication

In this study, the PVDF membrane was fabricated using the non-solvent phase separation (NIPS) method, which is mentioned in Chapter 3. The casting solution used for membrane fabrication consisted of 82 wt% DMAc, 15 wt% PVDF, and 3 wt% PEG.

7.2.3. Membrane modification

The PAMAM dendrimer was immobilized on a PVDF membrane pretreated with an alkaline solution. The details of PAMAM dendrimer immobilization are presented in our previous research [18], [20]. In brief, the PVDF membrane was pretreated with a 10 M KOH aqueous solution at 80℃ for 30 minutes. Since the aqueous solution cannot immerse and penetrate the PVDF membrane, the treatment only occurred on the surface. The pretreated membrane was then immersed in a methanol solution containing 2.5 wt% PAMAM-G5.0 dendrimer and 0.5 M KOH, under vigorous stirring for 24 hours at 10℃. This PAMAM dendrimer-grafted membrane was labeled as S-G5.0. The peripheral functional groups of the PAMAM dendrimer on the membranes were converted to carboxyl groups through subsequent reactions to produce different membranes. First, the S-G5.0 membranes were immersed in a 50 wt% MA methanol solution at 10℃ under stirring at 80 rpm for 24 hours to convert the PAMAM-G5.0 dendrimer to PAMAM-G5.5 dendrimer, which has ester peripheral functional groups. Subsequently, the membranes were immersed in a 0.5 M NaOH aqueous solution at room temperature for 30 minutes to hydrolyze the ester groups into carboxyl groups. This membrane was labeled as S-G5PA.

The S-G5+5.0 membrane is a membrane grafted with two layers of PAMAM-G5.0 dendrimer. To fabricate S-G5+5.0 membranes, the S-G5PA membranes were immersed in a methanol solution containing 2.5 wt% PAMAM-G5.0 and 0.5 M KOH, under vigorous stirring for 24 hours at 10℃. To produce the S-G5+5PA membranes the S-G5+5.0 membranes were treated with a 50 wt% MA methanol solution and subsequently hydrolyzed with a 0.5 M NaOH aqueous solution.

The PAMAM-G5.0 dendrimer for membrane modification was synthesized by the divergent method, which utilized sequential Michael and amidation reactions starting from

the EDA core [21], [22], [23].

Table 7.1 Modification conditions of different types of membranes.

Membrane	Functional groups	Alkaline treatment	1st layer of Dendrimer	2ed layer of Dendrimer
PVDF		NA		
O-Alk40 O-Alk50 O-Alk60	carboxyl carboxyl carboxyl	0.5 M KOH PrOH, 1 min at 40, 50 or 60℃	NA	
O-G3.0 O-G3PA	amine carboxyl	0.5 M KOH PrOH, 1 min at 60℃	PAMAM-G3.0	NA
S-Alk60	carboxyl	10 M KOH Water, 30 min at 80℃	NA	
S-G3.0 S-G3PA S-G3TAC S-G3PS	amine carboxyl quaternary amine sulfonic acid	10 M KOH Water, 30 min at 80℃	PAMAM-G3.0	NA
S-G5.0 S-G5.5	amine carboxyl	10 M KOH Water, 30 min at 80℃	PAMAM-G5.0	NA
S-G5+5 S-G5+5PA	amine carboxyl	10 M KOH Water, 30 min at 80℃	PAMAM-G5.0	PAMAM-G5.0

To compare the filtration performance of membranes, data of membranes from our previous study were cited [18], [20]. The information on the membranes discussed in this article is shown in Table 7.1. In the abbreviation for membrane names, the “O” stands for overall modification, which means both inside the membrane pore and the membrane surface were modified. The “S” stands for surface modification, which means only the membrane surface was modified. The “PA”, “TAC” and “PS” stand for the different peripheral functional groups of dendrimers immobilized on membranes, which means carboxyl, quaternary amine, and sulfonic acid, respectively. The overall modification of the membrane was achieved by immersing the PVDF membrane in an alkaline isopropanol solution. Since isopropanol can penetrate the PVDF membrane, the alkaline treatment occurs on both the surface and within the pores of the membrane. Consequently, in the

subsequent PAMAM grafting step, the PAMAM dendrimers are immobilized on both the surface and inside the pores of the membrane.

7.2.4. Membrane filtration

A dead-end filtration setup was used to evaluate filtration performance as described in our previous work [24]. The setup involved a 200 mL feed chamber with the membrane (0.00159 m^2) at the bottom. The process was conducted at room temperature with an operating pressure of 60 psig (4.14 bar) maintained using nitrogen gas. Two polymer solutions, PAA and PEO (100 ppm each), were filtered to study the separation mechanism. The feed concentration of whey protein for filtration is 100 ppm. To ensure accuracy, 10 mL of permeate was discarded before collecting a 10 mL sample for analysis. All filtration tests were carried out in triplicate using three new coupons fabricated in different batches. The flux of the membranes was calculated using Equation (7-1) [24], as shown below.

$$Flux = \frac{v}{t \cdot A} \tag{7-1}$$

Where v is the volume (0.010 L) of the permeate, t (hour) is the time required to collect 0.010 L of permeate, and A is the effective area of the membranes (m^2). The rejection was calculated by Equation (7-26), which is presented in section 7.2.6.

7.2.5. Membrane characterization

ATR-FTIR

The functional groups of the membrane's surface were determined by the attenuated total reflectance-Fourier transform infrared (ATR-FTIR) using the Agilent Tech-Cary 630 (Agilent, Canada) spectrometer. The membrane samples were washed with DI water and

dried before the measurement.

SEM

The morphology of the membrane's top surface was measured using a JSM-7500F field-emission scanning electron microscope (FESEM) from JEOL, Japan. The details of surface SEM measurements were mentioned in Chapter 3. The average pore size was determined by SEM image analysis through ImageJ software.

7.2.6. Modeling by DSPM-DE model

The DSPM-DE model describes the separation process of nanofiltration membranes, particularly the separation of charged ions by membranes with charged surfaces. The transport of solutes along the pores can be described by the extended Nernst-Planck Equation (7-2) [19].

$$J_i = -K_{i,d} \cdot D_{i,\infty} \cdot \frac{dc_i}{dx} + K_{i,a} \cdot c_i \cdot J_v - z_i \cdot c_i \cdot K_{i,d} \cdot D_{i,\infty} \cdot \frac{F}{R \cdot T} \cdot \frac{d\phi(x)}{dx} \qquad (7\text{-}2)$$

Where J_i and J_v are the solute flux and solvent (water) flux, respectively. $K_{i,a}$ and $K_{i,d}$ are the advection and diffusion hindrance factors, respectively. $D_{i,\infty}$ is the diffusion coefficient of solute *i* in the bulk solution. c_i and z_i are the concentration and valence of ion i. T is the temperature. F and R are the Faraday constant and the ideal gas constant, respectively. $\phi(x)$ is the electrical potential at position x along the membrane pore. The position x is 0 at the feed-membrane interface and δ at the permeate-membrane interface. The first term on the right side of the equation represents the diffusive flux of the solute caused by the concentration gradient. The second term represents the advective flux due to solvent flow. The third term describes the electro-migration caused by the potential gradient. $K_{i,a}$ can be calculated using the following empirical Equation (7-3) [25].

$$K_{i,a} = \frac{1+3.867\cdot\lambda_i-1.907\cdot\lambda_i^2-0.834\cdot\lambda_i^3}{1+1.867\cdot\lambda_i-0.741\cdot\lambda_i^2} \quad (7\text{-}3)$$

Where λ_i is the ratio of the radius of the solute, r_s, to the membrane pore, r_p. $K_{i,d}$ was calculated by the following empirical Equation (7-4) [25].

$$K_{i,d} = \begin{cases} \frac{1+1.125\lambda_i \ln\lambda_i-1.56\lambda_i+0.53\lambda_i^2+1.95\lambda_i^3-2.82\lambda_i^4+0.27\lambda_i^5+1.10\lambda_i^6-0.44\lambda_i^7}{(1-\lambda_i)^2}, & x \le 0.95 \\ 0.984\left(\frac{1-\lambda_i}{\lambda_i}\right)^{2.5}, & x > 0.95 \end{cases} \quad (7\text{-}4)$$

Average pore size of the membrane

For the uncharged solute, such as PEO, there is no electrostatic interaction between the solute and the membrane. The electro exclusion, including dielectric exclusion and Donnan exclusion, is absent, so the solute is rejected by the steric exclusion. Without considering the dielectric exclusion and Donnan exclusion. Equation (7-2) can be simplified to describe the rejection of solute *i* by the following Equation (7-5) [19].

$$R_i = 1 - \frac{c_{i,p}}{c_{i,f}} = 1 - \frac{K_{i,a}\cdot\varphi_{S,i}}{1-(1-K_{i,a}\cdot\varphi_{S,i})\cdot\exp\left(-\frac{J_v\cdot L_e}{D}\cdot\frac{K_{i,a}}{K_{i,d}}\right)} \quad (7\text{-}5)$$

Where R_i is the rejection of the solute i. $c_{i,p}$ and $c_{i,f}$ are the concentration of solute i in permeate phase and feed phase. The $\varphi_{S,i}$, and D are steric exclusion factors, and diffusivities, respectively. L_e is the effective membrane thickness. According to the Hagen-Poiseuille Equation (7-6), the effective membrane thickness is the function of the solvent flux and the radius of the membrane pore [19].

$$J_v = \frac{r_p^2\cdot(\Delta P-\Delta\pi)}{8\cdot\eta_w\cdot L_e} \quad (7\text{-}6)$$

Where ΔP is the hydraulic pressure difference across the membrane, $\Delta\pi$ is the osmotic pressure difference between the feed phase and permeate phase, and η_w is the water

dynamic viscosity. By measuring the pure water flux of the membrane at operating pressure, the effective membrane thickness could be written as a function of the average membrane pore size, by the Hagen-Poiseuille Equation (7-6).

With the operating pressure increase, the flux of the membrane will increase, and the advection will dominate the cross-membrane transport. Corresponding, the rejection will increase. When increasing the pressure to a certain value, the rejection will reach the limiting rejection, R_{lim}. Over the R_{lim} increase pressure does not help improve the flux, since any increase in advection transport is offset by an increase in concentration polarization and diffusion hindrance across the membrane. Therefore, Equation (7-5) can be written as Equation (7-7) [26], [27], [28].

$$R_{lim} = 1 - \frac{c_{i,p}}{c_{i,f}} = 1 - K_{i,a} \cdot \varphi_{S,i} \tag{7-7}$$

Based on simple geometric probability considerations, the probability of solute molecules entering the membrane pores, steric exclusion factor $\varphi_{S,i}$, can be calculated by the following Equation (7-8) [19].

$$\varphi_{S,i} = \begin{cases} \left(1 - \frac{r_s}{r_p}\right)^2, & for\ r_s < r_p \\ 0, & for\ r_s \geq r_p \end{cases} \tag{7-8}$$

Here, only the solutes that are smaller than the pore size can pass the membranes.

The PEO is electrically neutral in the aqueous solution. Therefore, the effect of steric rejection of membranes and the pore size of membranes was estimated by the rejection in PEO filtration. The Stokes radius of linear polymer, which is PEO and PAA here, can be calculated by Equation (7-9) [29].

$$r_s = 2.122 \times 10^{-8} \cdot (M \cdot [\eta])^{1/3} \quad (7\text{-}9)$$

Where r_s is the Stokes radius with the unit of cm, M is the molecular weight of polymer with the unit of g/mol, and $[\eta]$ is the intrinsic viscosity of the polymer, whose unit is dL/g. The intrinsic viscosity of PAA and PEO polymers can be calculated by Equations. (7-10) and (7-11).

For PAA [30],

$$[\eta] = 12.4 \times 10^{-4} \cdot M^{0.5} \quad (7\text{-}10)$$

For PEO [29],

$$[\eta] = 1.192 \times 10^{-4} \cdot M^{0.76} \quad (7\text{-}11)$$

The Stokes radius of PAA and PEO with molecular weight 100 kDa are 7.13 nm and 8.96 nm, based on Equations (7-9), (7-10) and (7-11). The diffusivities D of PAA and PEO can be calculated by Equation (7-12) [27].

$$D = \frac{k \cdot T}{6 \cdot \pi \cdot \eta_w} \times \frac{1}{r_s} \quad (7\text{-}12)$$

Where k is the Boltzmann constant. The diffusivity of PAA and PEO are 2.68×10^{-11} m^2/s and 3.37×10^{-11} m^2/s.

The Stokes radius and diffusivity of PEO were calculated by Equations (7-9), (7-11) and(7-12). The average pore size can be calculated by solving Equations (7-3), (7-4), (7-5), and (7-8), using PEO rejection and permeate flux data. By substituting the pure water flux data into Equation (7-6), the effective membrane thickness, L_e, in Equation (7-5) can be expressed as a function of average pore size r_p. If the flux of membrane is reaching

limiting flux, the average pore size can be calculated by limiting rejection of PEO, which is solving Equations (7-3), (7-7) and (7-8).

Dielectric exclusion

In the DSPM-DE model, the dielectric exclusion is represented by the dielectric exclusion factor, $\varphi_{DE,i}$, which is calculated by Equation (7-13) [19].

$$\varphi_{DE,i} = exp\left(-\frac{\Delta W_i}{k \cdot T}\right) \tag{7-13}$$

Where ΔW_i is the change of solvation energy (energy barrier), which is calculated by the Born model, i.e., Equation (7-14) [25].

$$\Delta W_i = \frac{z_i^2 \cdot e^2}{8 \cdot \pi \cdot \varepsilon_0 \cdot r_s} \cdot \left(\frac{1}{\varepsilon_b} - \frac{1}{\varepsilon_p}\right) \tag{7-14}$$

Where ε_0, ε_b and ε_p are the dielectric constant of vacuum, solvent in bulk, and solvent in membrane pore, respectively.

Membrane charge density

Before calculating Donnan exclusion, the volume charge density needs to be determined. If the charge in membrane pores is equal to the surface charge, the effective volume charge density X can be calculated by Equation (7-15) [31], [32].

$$X = \frac{2 \cdot \sigma}{r_p \cdot F} \tag{7-15}$$

Where σ is membrane surface charge density σ ($C \cdot m^{-2}$), which is calculated by the Gouy-Chapmann-Stern model, which is shown in Equation (7-16) [31], [32].

$$\sigma = \left\{2 \cdot \varepsilon_b \cdot \varepsilon_0 \cdot k \cdot T \cdot \sum_i^n c_i \cdot N_A \cdot \left[exp\left(\frac{z_i \cdot e \cdot \zeta}{k \cdot T}\right) - 1\right]\right\}^{0.5} \quad (7\text{-}16)$$

Where N_A is Avogadro's number, ζ is the surface zeta potential of the membrane, and e is the electronic charge.

Donnan exclusion

The Donnan exclusion factor $\varphi_{D,i}$ is calculated by Equation (7-17) [31].

$$\varphi_{\mathrm{D,i}} = \exp\left(-\frac{\mathrm{z_i \cdot e}}{\mathrm{k \cdot T}} \cdot \Delta\psi_{\mathrm{D}}\right) \quad (7\text{-}17)$$

Where $\Delta\psi_{\mathrm{D}}$ is the Donnan potential across two interfaces.

The ion *i* transport through the membrane can be expressed by Equation (7-2), which is mentioned in section 7.2.6. The solute flux J_i of ion *i* in Equation (7-2) can be expressed as Equation (7-18).

$$J_i = J_i \cdot \mathrm{c_{i,p}} \quad (7\text{-}18)$$

The potential gradient in Equation (7-2) can be expressed as Equation (7-19) [31], [33].

$$\frac{d\phi(x)}{dx} = \frac{\sum_{i=1}^{n} \frac{z_i \cdot Jv}{K_{i,d} \cdot D_{i,\infty}} \left(K_{i,c} \cdot c_i - c_{i,p}\right)}{\frac{F}{R \cdot T} \sum_{i=1}^{n} z_i^2 \cdot c_i} \quad (7\text{-}19)$$

Where $K_{i,c}$ is calculated by following the empirical Equation (7-20) [31].

$$K_{i,c} = 1 + 0.054 \cdot \lambda_{\mathrm{i}} - 0.988 \cdot \lambda_{\mathrm{i}}^2 + 0.441 \cdot \lambda_{\mathrm{i}}^3 \quad (7\text{-}20)$$

The system is electrically neutral, so the following equation holds [31].

Electrically neutral of feed side:

$$\sum_{i=1}^{n} z_i \cdot c_{i,f} = 0 \tag{7-21}$$

Electrically neutral of permeate side:

$$\sum_{i=1}^{n} z_i \cdot c_{i,p} = 0 \tag{7-22}$$

Electrically neutral inside the membrane pore:

$$\sum_{i=1}^{n} z_i \cdot c_i(x) + X(x) = 0 \tag{7-23}$$

The partitioning of ion *i* between the membrane and the feed phase is expressed as Equation (7-24) [31].

$$\frac{c_i(x=0)}{c_{i,f}} = \varphi_{s,i} \cdot \varphi_{DE,i} \cdot \varphi_{D,i} \tag{7-24}$$

The partitioning of ion *i* between the membrane and the permeate phase is expressed as Equation (7-25) [31].

$$\frac{c_i(x=\delta)}{c_{i,p}} = \varphi_{s,i} \cdot \varphi_{DE,i} \cdot \varphi_{D,i} \tag{7-25}$$

The rejection of the solute *i*, Equation (7-26), describes the relationship between the feed concentration $c_{i,f}$, and the permeate concentration, $c_{i,p}$, of solute i.

$$R_i = 1 - \frac{c_{i,p}}{c_{i,f}} \tag{7-26}$$

For PAA solution Equations (7-19) and (7-23) are written as Equations (7-27) and (7-28), respectively.

$$\frac{d\phi(x)}{dx} = \frac{\frac{z_{PAA}\cdot Jv}{K_{PAA,d}\cdot D_{PAA,\infty}}\cdot\left(K_{PAA,c}\cdot c_{PAA} - c_{PAA,p}\right) + \frac{z_H\cdot Jv}{K_{H,d}\cdot D_{H,\infty}}\cdot\left(K_{H,c}\cdot c_H - c_{H,p}\right)}{\frac{F}{R\cdot T}\cdot\left(z_{PAA}^2\cdot c_{PAA} + z_H^2\cdot c_H\right)} \tag{7-27}$$

$$c_H = \frac{z_{PAA}\cdot c_{PAA} + X(x)}{-z_H} \tag{7-28}$$

By using Equation (7-28) and replacing c_H by c_{PAA}, Equation (7-27) can be expressed as Equation (7-29).

$$\frac{d\phi(x)}{dx} = \frac{\frac{z_{PAA}\cdot Jv}{K_{PAA,d}\cdot D_{PAA,\infty}}\cdot\left(K_{PAA,c}\cdot c_{PAA} - c_{PAA,p}\right) + \frac{z_H\cdot Jv}{K_{H,d}\cdot D_{H,\infty}}\cdot\left(K_{H,c}\cdot\frac{z_{PAA}\cdot c_{PAA} + X(x)}{-z_H} - c_{H,p}\right)}{\frac{F}{R\cdot T}\cdot\left(z_{PAA}^2\cdot c_{PAA} - z_H\cdot z_{PAA}\cdot c_{PAA} - z_H\cdot X(x)\right)} \tag{7-29}$$

Equation (7-30) is obtained by arranging Equation (7-29).

$$\frac{d\phi(x)}{dx} = \frac{a\cdot c_{PAA} + \mathrm{b}}{\left(z_{PAA}^2 - z_H\cdot z_{PAA}\right)\cdot c_{PAA} - z_H\cdot X(x)}\cdot\frac{R\cdot T}{F} \tag{7-30}$$

Where *a* and *b* are expressed as Equations (7-31) and (7-32).

$$a = z_{PAA}\cdot J_v\cdot\left(\frac{K_{PAA,c}}{K_{PAA,d}\cdot D_{PAA,\infty}} - \frac{K_{H,c}}{K_{H,d}\cdot D_{H,\infty}}\right) \tag{7-31}$$

$$b = -\frac{J_v\cdot K_{H,c}\cdot X(x)}{K_{H,d}\cdot D_{H,\infty}} - \frac{z_{PAA}\cdot J_v\cdot c_{PAA,p}}{K_{PAA,d}\cdot D_{PAA,\infty}} - \frac{z_H\cdot J_v\cdot c_{H,p}}{K_{H,d}\cdot D_{H,\infty}} \tag{7-32}$$

Where z_H and z_{PAA} are 1 and -1 respectively. Equation (7-33) is obtained by substituting Equations (7-30) and (7-18) into Equation (7-2). Where solute *i* is PAA.

$$0 = -K_{PAA,d}\cdot D_{PAA,\infty}\cdot\frac{dc_{PAA}}{dx} + K_{PAA,a}\cdot c_{PAA}\cdot J_v - c_{PAA,p}\cdot J_v - z_{PAA}\cdot c_{PAA}\cdot K_{PAA,d}\cdot D_{PAA,\infty}\cdot\frac{a\cdot c_{PAA} + \mathrm{b}}{2\cdot c_{PAA} - X(x)} \tag{7-33}$$

Equation (7-34) can be obtained after rearranging.

$$K_{PAA,d} \cdot D_{PAA,\infty} \cdot \frac{dc_{PAA}}{dx} = -z_{PAA} \cdot K_{PAA,d} \cdot D_{PAA,\infty} \cdot c_{PAA} \cdot \frac{a \cdot c_{PAA} + b}{2 \cdot c_{PAA} - z_H \cdot X(x)} + K_{PAA,a} \cdot J_v \cdot c_{PAA} - c_{PAA,p} \cdot J_v \quad (7\text{-}34)$$

The Donnan potential, $\Delta\psi_D$, across the membrane can be calculated by solving Equations (7-17), (7-26) and (7-34), using PAA rejection and permeate flux data, with the boundary conditions, Equations (7-24) and (7-25).

7.3. Results and discussion

7.3.1. Morphology of membrane

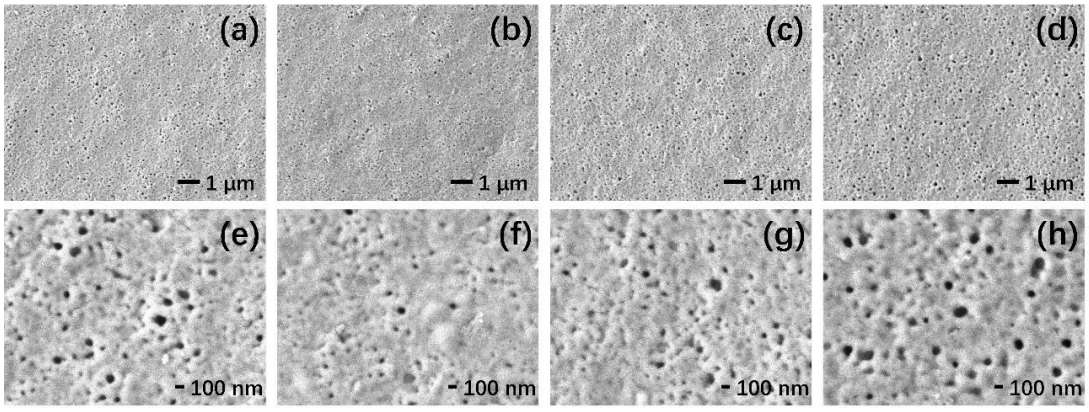

Figure 7.1 Surface SEM images of S-G5.0 ((a), (e)), S-G5PA ((b), (f)), S-G5+5.0 ((c), (g)), and S-G5+5PA ((d), (h)) membranes at different magnification, (a), (b), (c) and (d) are magnified 10,000 times, (e), (f), (g) and (h) are magnified 40,000 times.

Figure 7.1 shows the surface SEM images of S-G5.0, S-G5PA, S-G5+5.0, and S-G5+5PA membranes. The SEM images reveal that the pores of the modified membranes are predominantly circular. The pore size of the S-G5PA membrane is relatively small, whereas the pore size of the S-G5+5PA membrane is relatively large. The pore sizes of the S-G5.0 and S-G5+5.0 membranes are similar, lying between the pore sizes of the S-G5PA and S-G5+5PA membranes.

7.3.2. Membrane pore size

As discussed in section 7.2.6, the membrane average pore size was computed by solving Equations (7-3), (7-4), (7-5), and (7-8), using PEO rejection, and permeate flux data. In Equation (7-5), R_i and J_v are the PEO rejection and permeate flux in PEO filtration. The effective membrane thickness, L_e, in Equation (7-5) can be expressed as a function of average pore size r_p, by substituting the pure water flux data into Equation (7-6). The average pore size can be calculated by limiting rejection of PEO, by solving Equations (7-3), (7-7) and (7-8), when permeate flux is reaching limiting flux. In Equation (7-7), R_{lim} is the PEO rejection.

Table 7.2 Pure water flux, rejection & permeate flux of PEO filtration, measured pore radius and calculated pore radius of PVDF and overall modified membranes.

Membrane	Pure water flux (LMH) [18]	PEO-100 kDa [18]		Measured pore radius (nm) [18]	Calculated pore radius (nm)	
		Rejection (%)	Flux (LMH)		By R_i	By R_{lim}
PVDF	274.1	16.4	48.2	16.2	50.0	50.0
O-Alk40	211.4	26.9	22.2	18.8	36.1	36.2
O-Alk50	121.9	34.6	13.2	19.1	30.4	30.4
O-Alk60	115.7	55.1	17.0	19.6	21.2	21.2
O-G3.0	92.3	42.3	6.1	20.9	26.2	26.2
O-G3PA	60.6	46.8	5.0	19.3	24.2	24.2

The calculated pore radius of the membranes is listed in Table 7.2 (PVDF membranes and overall modified membranes) and Table 7.3 (surface modified membranes). As shown in Table 7.2 and Table 7.3, the pore radius calculated by rejection R_i using Equation (7-5) and limiting rejection R_{lim} using Equation (7-7), were almost the same. Even for the S-Alk60 membrane, which has the largest difference between the pore radius calculated by R_i and R_{lim}, the two values differ by only 0.5 nm. This indicates that the permeate flux was equal to or above the limiting flux, so the rejection of PEO reached the limiting

rejection.

Table 7.3 Pure water flux, rejection & permeate flux of PEO filtration, measured pore radius, and calculated pore radius of surface modified membranes (the pure water flux, PEO rejection, and PEO permeate flux are cited from our previous research).

Membrane	Pure water flux (LMH)	PEO-100 kDa		Measured pore radius (nm)	Calculated pore radius (nm)	
		Rejection (%)	Flux (LMH)		By R_i	By R_{lim}
S-Alk60	577.8	6.0	140.8	47.4	90.1	89.6
S-G3.0	576.0	8.5	79.8	47.8	74.2	74.2
S-G3PA	489.8	3.5	89.4	41.6	122.5	121.6
S-G3TAC	484.1	5.8	78.7	43.6	92.0	92.3
S-G3PS	424.5	8.1	65.0	59.8	75.8	75.6
S-G5.0	229.2	6.1	13.3	47.4	88.9	89.2
S-G5PA	266.7	10.4	6.8	37.7	65.6	65.7
S-G5+5.0	129.4	13.7	1.6	46.2	55.7	55.6
S-G5+5PA	332.0	6.7	26.6	58.5	85.2	85.3

The pure water flux, PEO filtration data and measured pore size of S-Alk60, S-G3.0, S-G3PA, S-G3TAC and S-G3PS membranes were obtained from [20].

The measured pore radius of PVDF membranes is 16.2 nm. However, the calculated pore radius is 50.0 nm (by R_i), which is 3.1 times the measured pore radius. The pore radius is calculated by R_i Equations (7-5), considering only the advection and diffusion transport and steric exclusion of the PEO solute. When calculating the pore radius of the membrane, all pores are simplified into standard, uniformly sized cylindrical structures, and the solute molecules are simplified into standard spheres. Then, using Equation (7-8), the steric exclusion factor is calculated based on the ratio of the cross-sectional areas of the membrane pores and the solute molecules. However, in reality, membrane pores are not uniformly sized. There is a distribution of pore sizes. When the range of pore size distribution is large, pores significantly larger than the average pore size could cause substantial PEO leakage, leading to a decrease in PEO rejection. As a result, the calculated pore radius may be larger than the pore radius obtained from SEM image analysis.

Additionally, during filtration, operating pressure can cause the pores to enlarge. When measuring with SEM images, there is no transmembrane pressure. Therefore, the pore radius obtained from SEM images tends to be smaller than the actual pore radius during filtration.

The same phenomenon is also observed in surface modified and overall modified membranes, where the calculated pore size (by R_i) is larger than the measured pore size. It is worth noticing that the pore walls of overall modified membranes contain charged functional groups. While the pore walls of PVDF membranes and surface modified membranes do not contain such charged functional groups inside the membrane pore. The enhancement of charges inside the membrane pores alters the effective dielectric constant within the pores. This change in the dielectric constant, due to enhanced charges in pores, affects the electric field distribution, typically leading to variations in the dielectric constant experienced by charged solutes at different locations, thereby altering the strength of the dielectric exclusion effect. Although PEO is an uncharged solute, it is still subject to the dielectric exclusion effect. The increased charge inside the pores enhances the dielectric constant of the solution within the pores, which in turn increases the repulsion of PEO molecules, which have a lower dielectric constant. Consequently, this results in higher PEO rejection. The increase in PEO rejection leads to a decrease in the calculated pore size.

During the overall alkaline treated membrane, the degree of reaction between the alkaline solution and the pore walls increases with rising treatment temperature. This results in more charged functional groups being introduced inside the pores, enhancing the charge inside the pores and increasing PEO rejection. Therefore, an increase in alkaline treatment temperature leads to a decrease in the ratio of calculated pore size to measured pore size. For example, this ratio for PVDF membranes is 3.1, whereas, for membranes treated with alkaline solutions at 40, 50, and 60°C, the ratios of calculated pore size to measured pore

size are 1.9, 1.6, and 1.1, respectively. There is no charge inside the pores of PVDF membranes. Therefore, as previously explained, the calculated pore size is much greater than the measured pore size for PVDF membranes.

7.3.3. Membrane charge density

Table 7.4 shows the surface charge density of PVDF and modified membranes, which were calculated by Equation (7-16) using the surface zeta potential of the membranes. The surface charge density of all the membranes increased with increasing pH. At pH 4, the surface charge density of PVDF membranes is 0.69 $mC \cdot m^{-2}$. Overall modification or surface modification has little effect on the surface charge density of the membranes, except for membranes grafted with sulfonic acid groups. For example, the surface charge density of overall modified membranes ranges from 0.60 $mC \cdot m^{-2}$ to 0.75 $mC \cdot m^{-2}$. The surface charge density of the surface modified membranes ranges from 0.54 $mC \cdot m^{-2}$ to 0.65 $mC \cdot m^{-2}$, except for S-G3PS membranes. The surface charge density of the S-G3PS membranes is 0.93 $mC \cdot m^{-2}$, which is obviously higher than that of other membranes. The functional groups of Alk, G3.0, G3PA, G3TAC, and G3PS membranes are carboxyl/hydroxyl (connected to the PVDF molecules), amine, carboxyl (connected to the dendrimer), quaternary ammonium, and sulfonic groups, respectively. At low pH values, the carboxyl groups on the membrane primarily exist in a non-ionized state. As the pH increases, these groups gradually lose protons and become negatively charged. Therefore, the ionization state of the membrane surface groups is controlled by the pH and their acid dissociation constants. When the pH is higher than the acid dissociation constants of the functional groups, these groups tend to lose protons and become negatively charged. When the pH is lower than the acid dissociation constants, the functional groups tend to absorb protons and become positively charged. The carboxyl and hydroxyl groups have relatively high acid dissociation constants, resulting in a low degree of ionization at pH 4. In contrast,

sulfonic acid groups have a lower acid dissociation constant, leading to significant ionization at pH 4. Therefore, the G3PS membrane exhibits a higher surface charge density at pH 4. It is worth noting that amine and quaternary ammonium groups are ionized and show positive charge at low pH. However, the O-G3.0, S-G3.0 and S-G3TAC membranes show negative surface zeta potential at pH 4. The possible reason is that the PVDF membrane required alkaline treatment, before PAMAM dendrimer grafting. The alkaline treated PVDF membranes have hydroxyl and carboxyl groups, leading to a negatively charged surface. After grafting, the loading rate of amine and quaternary ammonium groups are too low to offset the negative charge of the alkaline treated membranes. Therefore, the O-G3.0, S-G3.0 and S-G3TAC membranes show negative surface zeta potential at pH 4.

Table 7.4 Surface zeta potential and surface charge density of the PVDF and modified membranes.

Membrane	Surface zeta potential (mV) [18], [20]			Surface charge density ($mC \cdot m^{-2}$)		
	pH 4	pH 6	pH 8	pH 4	pH 6	pH 8
PVDF	-27.6	-41.3	-43.1	0.69	0.99	1.04
O-Alk60	-26.4	-49.6	-59.6	0.66	1.20	1.50
O-G3.0	-30.5	-51.2	-58.0	0.75	1.25	1.45
O-G3.5	-29.8	-52.2	-62.2	0.73	1.28	1.59
S-Alk60	-23.1	-43.1	-51.1	0.60	1.03	1.25
S-G3.0	-19.9	-44.1	-58.0	0.54	1.06	1.45
S-G3PA	-25.9	-55.4	-59.9	0.65	1.37	1.51
S-G3TAC	-24.8	-51.6	-56.0	0.63	1.26	1.39
S-G3PS	-38.7	-60.7	-63.6	0.93	1.54	1.64

The surface charge density of the modified membranes is significantly higher than that of the PVDF membrane at pH 6 and 8. For instance, the surface charge density of the PVDF membrane is 1.04 $mC \cdot m^{-2}$ at pH 8. The surface charge density of overall modified membranes ranges from 1.50 $mC \cdot m^{-2}$ to 1.59 $mC \cdot m^{-2}$ at pH 8. The surface modified membranes have a surface charge density ranging from 1.25 $mC \cdot m^{-2}$ to 1.64 $mC \cdot m^{-2}$. The

surface charge density increased by 50%, after overall modification, and increased by 20% to 60% by surface modification at pH 8.

Table 7.5 shows the volume charge density of the PVDF and modified membranes, calculated using Equation (7-15). The pore radius, calculated by R_i of Equation (7-5), was used for the volume charge density calculation. According to Equation (7-15), the volume charge density is related to both the surface charge density and the pore radius.

Table 7.5 Calculated volume charge density of PVDF and modified membranes.

Membrane	volume charge density (mol·m^{-3})		
	pH 4	pH 6	pH 8
PVDF	0.29	0.41	0.43
O-Alk60	0.65	1.18	1.47
O-G3.0	0.59	0.99	1.15
O-G3.5	0.63	1.09	1.36
S-Alk60	0.14	0.24	0.29
S-G3.0	0.15	0.30	0.41
S-G3PA	0.11	0.23	0.26
S-G3TAC	0.14	0.28	0.31
S-G3PS	0.25	0.42	0.45

The volume charge density of the PVDF membrane is 0.29 mol·m^{-3} at pH 4 and increases to 0.43 mol·m^{-3} as the pH rises to 8. For overall modified membranes, the volume charge density ranges from 0.59 mol·m^{-3} to 0.63 mol·m^{-3} at pH 4, and from 1.15 mol·m^{-3} to 1.47 mol·m^{-3} at pH 8. In contrast, the volume charge density of the surface modified membranes ranges from 0.11 mol·m^{-3} to 0.25 mol·m^{-3} at pH 4, and from 0.26 mol·m^{-3} to 0.45 mol·m^{-3} at pH 8. Despite the surface charge densities of these two types of membranes being similar, the volume charge density of the surface-modified membranes is much lower than that of the overall modified membranes. This is because the pore radius of the surface-modified membranes is significantly larger than that of the overall modified membranes, resulting in a substantially smaller volume charge density compared to the overall modified

membranes. Additionally, when calculating the pore radius of the membrane, the PEO rejection in overall modified membranes is affected by dielectric exclusion, resulting in a calculated pore radius that is smaller than the actual pore radius. This causes the calculated volume charge density to be higher than the actual volume charge density.

7.3.4. Donnan exclusion of membrane

The Donnan potential, $\Delta\psi_{\mathrm{D}}$, across the membrane can be calculated by solving Equations (7-17), (7-26) and (7-34), using PAA rejection and permeate flux data, with the boundary conditions, Equations (7-24) and (7-25). The pore radius, calculated using R_i of Equation (7-5), was utilized for Donnan's potential calculation. To simplify the calculations, the following assumptions were made: (1) The concentration of PAA in the feed phase remains constant throughout the filtration process. (2) The concentration polarization effect is neglected, so the feed concentration at the feed membrane interface, $c'_{PAA,f}$, is equal to the bulk concentration of feed, $c_{PAA,f}$. (3) The dielectric exclusion effect is neglected, implying $\varphi_{DE,i} = 1$.

Specifically, assume a guessing value of $c_{PAA}(x = 0)$ at feed membrane interface. Then use Runge-Kutta methods to calculate $c_{PAA}(x = \delta)$ at permeate membrane interface by Equation (7-34). The thickness of the membrane, δ, is equal to the effective thickness L_e, which is calculated by pure water flux and membrane pore radius through Equation (7-6).

The Runge-Kutta-Gill methods are a family of iterative methods used to solve ordinary differential equations (ODEs). Here, we use The Classical Fourth-Order Runge-Kutta-Gill Method (RKG4) to solve Equation (7-34), which is shown in the following [34]. First assume $y'(x) = f(x, y)$ and $y(x_0) = y_0$. Then the RKG4 method is given by the following set of equations. (1) Calculate the intermediate values (slopes) by Equations

(7-35), (7-36), (7-37) and (7-38).

$$k_1 = h \cdot f(x_n, y_n) \tag{7-35}$$

$$k_2 = h \cdot f(x_n + \frac{h}{2}, y_n + \frac{k_1}{2}) \tag{7-36}$$

$$k_3 = h \cdot f(x_n + \frac{h}{2}, y_n + \frac{1}{2} \cdot (-1 + \sqrt{2}) \cdot k_1 + (1 - \frac{\sqrt{2}}{2}) \cdot k_2) \tag{7-37}$$

$$k_4 = h \cdot f(x_n + h, y_n - \frac{\sqrt{2}}{2} \cdot k_2 + (1 + \frac{\sqrt{2}}{2}) \cdot k_3) \tag{7-38}$$

Update the solution by Equation (7-39).

$$y_{n+1} = y_n + \frac{h}{6} \cdot [k_1 + (2 - \sqrt{2}) \cdot k_2 + (2 + \sqrt{2}) \cdot k_3 + k_4] \tag{7-39}$$

Where h is the step size. k_1, k_2, k_3 and k_4 are the intermediate slopes. y_{n+1} is the estimated value of the solution at $x_{n+1} = x_n + h$. After using the RKG4 method solving Equation (7-34), the $c_{PAA}(x = \delta)$ is calculated. Verify that $c_{PAA}(x = 0)$ and $c_{PAA}(x = \delta)$ satisfy Equations (7-24) and (7-25) or not. If it is not satisfying, re-assume a new value to $c_{PAA}(x = 0)$ and calculate $c_{PAA}(x = \delta)$ by Equation (7-34). The number of steps was 1000 during the calculation. The PAA concentration distribution in the membrane is shown in Figure 7.2.

Table 7.6 lists the PAA rejection and permeate flux in PAA filtration, Donnan potential, $\Delta\psi_{\mathrm{D}}$ through the membrane, PAA concentration at feed-membrane, $c_{PAA}(x = 0)$, and permeate-membrane $c_{PAA}(x = \delta)$, interface.

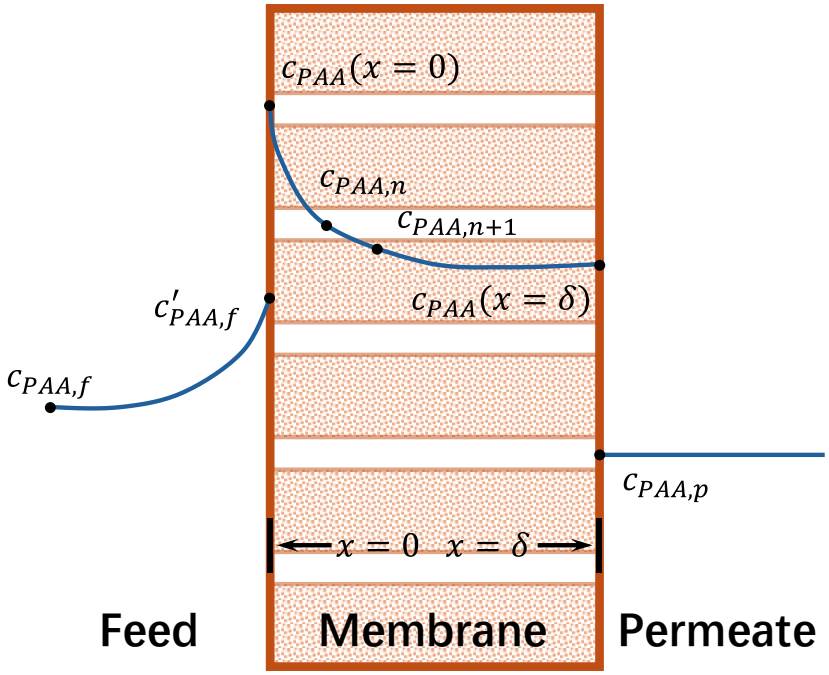

Figure 7.2 PAA concentration distribution along the membrane.

The Donnan potential through PVDF membranes is 3.28 V. It is worth noticing that the calculated Donnan potential of PVDF membranes is very high. It is against the common viewpoint that the PVDF membrane is electrically neutral in aqueous solution. Although our previous results suggest that PVDF membranes exhibit different zeta potential under different pH in solution, the specific reason why PVDF membranes show a high calculated positive Donnan potential under the current conditions remains unclear. For the O-G3.0 membrane, the Donnan potential is 3.43 V, which is higher than that of the PVDF membranes. This increase is due to the introduction of numerous positively charged amine functional groups on the O-G3.0 membranes. Except for the O-G3.0 membrane, the overall modifications decreased the Donnan potential. The Donnan potentials for the O-Alk60 and O-G3PA membranes, which both contain negatively charged groups, are -2.50 V and -3.16 V, respectively. Among all modified membranes, the O-G3PA membranes exhibit the lowest Donnan potential. The O-Alk60 and O-G3PA membranes have significantly lower Donnan potentials compared to surface-modified membranes, due to several factors. First,

the volume charge density of the O-Alk60 and O-G3PA membranes is much higher than that of the surface-modified membranes. For example, the volume charge densities of the O-Alk60 and O-G3PA membranes are 0.65 mol·m^{-3} and 0.63 mol·m^{-3}, respectively (Table 7.5). In contrast, the volume charge densities of the surface-modified membranes range between 0.11 mol·m^{-3} and 0.25 mol·m^{-3} (Table 7.5). Second, there are charged groups inside the pores of the overall modified membranes, leading to a significant dielectric exclusion effect within the membrane pores that cannot be neglected. However, to simplify the calculation of the Donnan exclusion, the dielectric exclusion effect was neglected. As a result, the computed Donnan exclusion effect is higher than the actual effect, leading to an overestimation of the Donnan potential. It is important to note that when using the DSPM-DE model to calculate the Donnan potential, the entire selective layer of the membrane is assumed to be charged. This means that the membrane's charge is considered uniform from the feed membrane interface ($x = 0$) to the permeate membrane interface ($x = \delta$), where (δ) equals the effective membrane thickness, L_e. However, for surface-modified membranes, the charges are concentrated in the PAMAM dendrimer layer on the surface. Measuring the thickness of this charged layer is challenging, and it is likely much smaller than the effective membrane thickness, L_e. As a result, the Donnan potential calculated using the DSPM-DE model for surface modified membranes may not accurately reflect the actual Donnan potential of the membrane.

The Donnan potential through the negatively charged S-Alk60 membrane is 0.53 V, which is unexpectedly positive. This may be due to errors in the PAA rejection results during the PAA filtration experiments. The Donnan potentials through the S-G3.0 and S-G3PA membranes are both -0.33 V, despite the differences in charged groups on their surfaces. One possible reason for this is that the pH of the PAA solution is low (pH 4), leading to a low degree of ionization of the carboxylate groups on the surface of the S-G3PA membrane, which results in a low Donnan potential. Additionally, the pore size of the S-G3PA

membrane (121.6 nm) is larger than that of the S-G3.0 membrane (74.2 nm), leading to a lower volume charge density in the S-G3PA membrane. However, the PAA rejection of the S-G3PA membrane is greater than that of the S-G3.0 membrane. This suggests that the carboxylic acid groups exert a stronger repulsive effect on PAA. The Donnan potential of the strongly positively charged S-G3TAC membrane is -0.87 V, which is lower than the Donnan potentials through the S-G3.0 and S-G3PA membranes, which have relatively weaker surface charges. The strongly negatively charged S-G3PS membranes exhibit the lowest Donnan potential among the surface-modified membranes, at -1.22 V. It is worth noting that although the Donnan potential of the O-G3PA membranes is -3.16 V, which is lower than that of the S-G3PS membranes at -1.22 V, the pore size of the O-G3PA membranes (24.2 nm) is smaller than that of the S-G3PS membranes (75.6 nm). However, the PAA rejection of the S-G3PS membranes (15.9%) is higher than that of the O-G3PA membranes (14.3%). This indicates that the charge intensity of functional groups on the membrane surface plays a more significant role in PAA separation.

Table 7.6 Rejection & permeate flux of PAA, calculated Donnan potential and PAA concentration at the feed membrane and permeate membrane interface of PVDF and modified membranes.

Membrane	PAA-100K (@ pH4) [18], [20]		Donnan potential $\Delta\psi_D$ (V)	$c_{PAA}(x=0)$ (M)	$c_{PAA}(x=\delta)$ (M)
	Rejection	Flux (LMH)			
PVDF	0.0%	193.1	3.28	1.92×10^{-4}	1.92×10^{-4}
O-Alk60	11.2%	65.7	-2.50	5.58×10^{-9}	4.96×10^{-9}
O-G3.0	0.0%	38.4	3.43	1.81×10^{-4}	1.81×10^{-4}
O-G3PA	14.3%	13.6	-3.16	1.99×10^{-9}	1.70×10^{-9}
S-Alk60	2.4%	401.5	0.53	2.05×10^{-6}	2.00×10^{-6}
S-G3.0	5.2%	341.2	-0.33	4.42×10^{-7}	4.20×10^{-7}
S-G3PA	9.8%	333.3	-0.33	4.55×10^{-7}	4.10×10^{-7}
S-G3-TAC	12.8%	289.5	-0.87	1.69×10^{-7}	1.47×10^{-7}
S-G3-PS	15.9%	285.9	-1.22	8.66×10^{-8}	7.28×10^{-8}

The PAA concentration in the feed bulk phase is 1×10^{-6} M. The PAA concentration at the

feed-membrane interface of PVDF membranes is 1.92×10^{-4} M, which is significantly higher than the concentration in the bulk solution. Due to absorption by the positively charged amine groups, the PAA concentration at the feed-membrane interface of S-G3.0 membranes is 1.81×10^{-4} M, which is also much higher than the bulk solution concentration. Except for the S-G3.0 and S-Alk60 membranes, the feed-membrane interface PAA concentrations of the modified membranes are lower than the bulk solution concentration due to repulsive interactions from the negative charges on the membranes. The feed-membrane interface PAA concentration of the S-Alk60 membrane is higher than the bulk solution concentration, which may be attributed to experimental errors during the PAA filtration experiment.

7.3.5. Filtration performance in whey protein separation

Table 7.7 lists the rejection and permeate fluxes for the S-G5.0, S-G5PA, S-G5+5.0, and S-G5+5PA membranes during the filtration of PAA, whey protein, and BSA (bovine serum albumin). In PAA filtration, the S-G5PA and S-G5+5PA membranes show the highest rejection, at 32.1% and 31.3%, respectively, whereas the amine group membranes (S-G5.0 and S-G5+5.0) exhibit lower rejections, at 20.0% and 7.6%, respectively. Regarding permeate flux, the S-G5+5PA membrane has the highest flux at 105.8 LMH, indicating that the double PAMAM layer with carboxyl groups significantly improves permeability. The S-G5.0 membrane also demonstrates a relatively high flux of 91.7 LMH. In contrast, the S-G5PA and S-G5+5.0 membranes have much lower permeate fluxes, at 47.9 LMH and 11.0 LMH, respectively. Carboxyl group modifications (S-G5PA and S-G5+5PA) enhance the rejection of PAA. The double PAMAM layer containing carboxyl group modification (S-G5+5PA) significantly enhances permeate flux during PAA filtration.

In whey protein filtration, the S-G5+5.0 membrane achieves the highest rejection at 92.9%,

followed closely by the S-G5.0 membrane with a rejection of 89.1%. The S-G5PA and S-G5+5PA membranes exhibit slightly lower rejections at 87.9% and 84.6%, respectively. In terms of permeate flux, the S-G5+5PA membrane maintains the highest flux at 6.7 LMH. The S-G5.0 and S-G5PA membranes have similar fluxes, both at 6.4 LMH, while the S-G5+5.0 membrane has the lowest flux at 2.8 LMH. For whey protein filtration, the membranes with amine group, S-G5.0 and S-G5+5.0, provide higher rejections.

Table 7.7 Rejection and permeate flux of single or PAMAM layer with amine or carboxyl groups modified membranes in PAA, whey protein, and BSA filtration.

Membrane	PAA		Whey		BSA	
	Rejection (%)	Flux (LMH)	Rejection (%)	Flux (LMH)	Rejection (%)	Flux (LMH)
S-G5.0	20.0	91.7	89.1	6.4	99.4	6.4
S-G5PA	31.3	47.9	87.9	6.4	99.9	5.3
S-G5+5.0	7.6	11.0	92.9	2.8	100.0	2.6
S-G5+5PA	32.1	105.8	84.6	6.7	99.4	4.2

In BSA filtration, all membranes exhibit very high rejection. The rejection of all membranes is over 99.4%. However, while the S-G5.0 and S-G5PA membranes have relatively higher fluxes, 6.4 LMH and 5.3 LMH, the S-G5+5PA membrane has a lower flux of 4.2 LMH, and the S-G5+5.0 membrane has the lowest flux at 2.6 LMH. This indicates that the double PAMAM layer with amine groups significantly reduces permeability. In BSA filtration, all membranes perform exceptionally well in terms of rejection, but double PAMAM layer modifications, especially with amine groups (S-G5+5.0), significantly reduce flux.

Therefore, amine group modifications generally provide high whey protein rejection but can significantly reduce flux when applied in double PAMAM layers. Carboxyl group modifications offer a good balance between rejection and permeate flux. Double PAMAM layer modifications not only have a minimal effect on protein rejection but may also lead

to a decrease in permeate flux compared to single PAMAM layer modifications.

Table 7.8 Rejection and permeate flux of PVDF, overall, and surface modified membranes in whey protein filtration.

Membrane [18], [20]	Whey protein filtration	
	Rejection (%)	Flux (LMH)
PVDF	58.9	15.3
O-Alk60	97.3	5.6
O-G3.0	95.7	3.1
O-G3PA	98.8	2.3
S-Alk60	70.8	41.3
S-G3.0	63.1	24.6
S-G3PA	79.0	30.3

Compared with our previous data, increasing the generation of PAMAM dendrimers for surface modification leads to higher whey protein rejection but a decrease in permeate flux. The whey protein rejection and permeate flux of PAMAM-G5.0 dendrimer modified membranes fall between those of PAMAM-G3.0 dendrimer surface modified membranes and PAMAM-G3.0 dendrimer overall modified membranes. This indicates that the filtration performance is still constrained by the selectivity-permeability trade-off principle.

7.4. Conclusions

In this study, we investigated the separation performance of pristine and modified PVDF membranes using the DSPM-DE model. The modifications involved grafting PAMAM dendrimers, which significantly improved the membrane properties. The results showed that the modified membranes exhibited increased permeate flux and enhanced rejection of PAA compared to the unmodified PVDF membranes. The PAMAM-G5.0 dendrimer modified membranes significantly increased whey protein rejection, while causing a substantial reduction in permeate flux.

Using PEO filtration data and the DSPM-DE model to calculate the pore radius of the membranes, it was found that the calculated pore radius was larger than the pore radius measured by SEM.

For the membranes with more charged functional groups inside the pores (charged pores), the PEO molecules experienced stronger dielectric exclusion during filtration, leading to increased PEO rejection. As a result, the calculated pore radius was closer to the pore radius measured by SEM. This indicates that, even though PEO is an electrically neutral molecule, it still experiences a certain degree of electrostatic interaction when passing through charged membrane pores.

The surface charge density of the membrane increases with pH rising. Due to the low acid dissociation constant of the sulfonic acid group, the S-G3PS membrane can achieve a relatively high surface charge density at lower pH levels, such as 0.93 $mC \cdot m^{-2}$ at pH 4. Introducing charged functional groups into the PVDF membrane significantly enhances the surface charge density, especially at higher pH values. The presence of charged functional groups within the membrane pores has a minimal effect on the surface charge density but greatly impacts the volume charge density. Membranes with charged functional groups inside the pores exhibit significantly higher volume charge density compared to membranes without such groups. Additionally, the modification process alters the pore size, with surface modified membranes having larger pore radii than those modified both on the surface and internally. Consequently, the volume charge density of surface-modified membranes is lower than that of membranes modified both on the surface and internally.

With the exception of the O-G3.0 and S-Alk60 membranes, membrane modifications significantly reduce the Donnan potential. Among these, overall modifications have the most substantial effect on lowering the Donnan potential. Higher volume charge densities

in O-Alk60 and O-G3PA membranes lead to lower Donnan potentials. The S-Alk60 membrane's positive Donnan potential (0.53 V) may be due to experimental errors, while S-G3.0 and S-G3PA membranes show -0.33 V, affected by the low pH of the PAA solution.

The analysis of UF membranes separating macromolecular solutes using the DSPM-DE model revealed certain discrepancies between the calculated and measured results. Experimental data, combined with theoretical modeling using the DSPM-DE model, elucidated the separation mechanisms and the impact of electrostatic interactions on membrane performance. The DSPM-DE model effectively explained the observed improvements in flux and rejection rates.

7.5. References

[1] G. Kang and Y. Cao, "Application and modification of poly(vinylidene fluoride) (PVDF) membranes – A review," *Journal of Membrane Science*, vol. 463, pp. 145–165, Aug. 2014, doi: 10.1016/j.memsci.2014.03.055.

[2] Y. Subasi and B. Cicek, "Recent advances in hydrophilic modification of PVDF ultrafiltration membranes – a review: part II," *Membrane Technology*, vol. 2017, no. 11, Art. no. 11, Nov. 2017, doi: 10.1016/S0958-2118(17)30233-1.

[3] Y. Subasi and B. Cicek, "Recent advances in hydrophilic modification of PVDF ultrafiltration membranes – a review: part I," *Membrane Technology*, vol. 2017, no. 10, Art. no. 10, Oct. 2017, doi: 10.1016/S0958-2118(17)30191-X.

[4] "Ultrathin 2D Ti_3C_2Tx MXene membrane for effective separation of oil-in-water emulsions in acidic, alkaline, and salty environment - ScienceDirect." Accessed: Jul. 16, 2024. https://www.sciencedirect.com/science/article/pii/S0021979719313931

[5] S. Chen, T. Wang, X. Zhuo, Y. Wang, and L. Wu, "PVDF mixed matrix membranes by incorporation of ionic liquid and MXene for enhancing permeation and antifouling performance," *Journal of Environmental Chemical Engineering*, vol. 10, no. 3, p. 108027, Jun. 2022, doi: 10.1016/j.jece.2022.108027.

[6] J. Zhao *et al.*, "Construction of a multi-layer protection of CS polymer brush grafted DA@CNTs coating on PVDF membrane for effective removal of dye effluent," *Journal of Hazardous Materials*, vol. 460, p. 132435, Oct. 2023, doi: 10.1016/j.jhazmat.2023.132435.

[7] S. Gholami, J. L. Llacuna, V. Vatanpour, A. Dehqan, S. Paziresh, and J. L. Cortina, "Impact of a new functionalization of multiwalled carbon nanotubes on antifouling and permeability of PVDF nanocomposite membranes for dye wastewater treatment," *Chemosphere*, vol. 294, p. 133699, May 2022, doi: 10.1016/j.chemosphere.2022.133699.

[8] S. Wu, K. Li, W. Shi, and J. Cai, "Chitosan/polyvinylpyrrolidone/polyvinyl alcohol/carbon nanotubes dual layers nanofibrous membrane constructed by electrospinning-electrospray for water purification," *Carbohydrate Polymers*, vol. 294, p. 119756, Oct. 2022, doi: 10.1016/j.carbpol.2022.119756.

[9] R. Zhou, D. Rana, T. Matsuura, and C. Q. Lan, "Effects of multi-walled carbon nanotubes (MWCNTs) and integrated MWCNTs/SiO_2 nano-additives on PVDF polymeric membranes for vacuum membrane distillation," *Separation and Purification Technology*, vol. 217, pp. 154–163, Jun. 2019, doi: 10.1016/j.seppur.2019.02.013.

[10] S. Shen, H. Li, Y. Shen, R. Bai, and G. Zhang, "Modification of PVDF membrane by post-modified NH_2-MIL-88B(Fe) showing improved permeability and oil/water separation performance," *Journal of Environmental Chemical Engineering*, vol. 11, no. 3, Art. no. 3, Jun. 2023, doi: 10.1016/j.jece.2023.109621.

[11] I. Gupta, E. T. Farinas, and S. Mitra, "Development of carbon nanotube-metal organic framework (MOF) hybrid antiviral microfiltration membrane," *Separation and Purification Technology*, vol. 315, p. 123766, Jun. 2023, doi: 10.1016/j.seppur.2023.123766.

[12] M. S. Sri Abirami Saraswathi, D. Rana, N. J. Kaleekkal, K. Divya, and A. Nagendran, "Investigating the efficacy of PVDF membranes customized with sulfonated graphene oxide nanosheets for enhanced permeability and antifouling," *Journal of Environmental Chemical Engineering*, vol. 8, no. 5, p. 104426, Oct. 2020, doi: 10.1016/j.jece.2020.104426.

[13] K. Ko, Y. Yu, M.-J. Kim, J. Kweon, and H. Chung, "Improvement in fouling resistance

of silver-graphene oxide coated polyvinylidene fluoride membrane prepared by pressurized filtration," *Separation and Purification Technology*, vol. 194, pp. 161–169, Apr. 2018, doi: 10.1016/j.seppur.2017.11.016.

[14] S. Ding, L. Zhang, Y. Li, and L. Hou, "Fabrication of a novel polyvinylidene fluoride membrane via binding SiO_2 nanoparticles and a copper ferrocyanide layer onto a membrane surface for selective removal of cesium," *Journal of Hazardous Materials*, vol. 368, pp. 292–299, Apr. 2019, doi: 10.1016/j.jhazmat.2019.01.065.

[15] Z. Li, D. Rana, Z. Wang, T. Matsuura, and C. Q. Lan, "Synergic effects of hydrophilic and hydrophobic nanoparticles on performance of nanocomposite distillation membranes: An experimental and numerical study," *Separation and Purification Technology*, vol. 202, pp. 45–58, Aug. 2018, doi: 10.1016/j.seppur.2018.03.032.

[16] R. Müller, C. Laschober, W. W. Szymanski, and G. Allmaier, "Determination of Molecular Weight, Particle Size, and Density of High Number Generation PAMAM Dendrimers Using MALDI−TOF−MS and nES−GEMMA," *Macromolecules*, vol. 40, no. 15, Art. no. 15, Jul. 2007, doi: 10.1021/ma062599e.

[17] T. Baig, J. Nayak, V. Dwivedi, A. Singh, and P. K. Tripathi, "A Review about Dendrimers: Synthesis, Types, Characterization and Applications," vol. 4, 2015.

[18] Z. Xu *et al.*, "Polyamidoamine dendrimer-modified polyvinylidene fluoride microporous membranes for protein separation," *Reactive and Functional Polymers*, p. 106021, Aug. 2024, doi: 10.1016/j.reactfunctpolym.2024.106021.

[19] R. Wang and S. Lin, "Pore model for nanofiltration: History, theoretical framework, key predictions, limitations, and prospects," *Journal of Membrane Science*, vol. 620, p. 118809, Feb. 2021, doi: 10.1016/j.memsci.2020.118809.

[20] Z. Xu, G. Ma, D. Rana, T. Matsuura, and C. Q. Lan, "Engineering polyvinylidene fluoride membranes using charge tunable dendrimer polyamidoamine to enable microporous membranes for protein separation," *Separation and Purification Technology*, vol. 354, p. 128887, Feb. 2025, doi: 10.1016/j.seppur.2024.128887.

[21]D. A. Tomalia *et al.*, "A New Class of Polymers: Starburst-Dendritic Macromolecules," *Polym J*, vol. 17, no. 1, pp. 117–132, Jan. 1985, doi: 10.1295/polymj.17.117.

[22] V. Gupta and S. Nayak, "Dendrimers: A Review on Synthetic Approaches," *J App*

Pharm Sci, pp. 117–122, 2015, doi: 10.7324/JAPS.2015.50321.

[23] R. Y. Patle and J. S. Meshram, "The advanced synthetic modifications and applications of multifunctional PAMAM dendritic composites," *React. Chem. Eng.*, vol. 7, no. 1, Art. no. 1, 2022, doi: 10.1039/D1RE00074H.

[24] Z. Xu, S. Gu, D. Rana, T. Matsuura, and C. Q. Lan, "Chemical precipitation enabled UF and MF filtration for lead removal," *Journal of Water Process Engineering*, vol. 41, p. 101987, Jun. 2021, doi: 10.1016/j.jwpe.2021.101987.

[25] N. Cevallos-Cueva, Md. M. Rahman, H. Hailu Kinfu, and V. Abetz, "Mass transport mechanism of nitrate selective nanofiltration membranes on the basis of the Donnan steric pore model with dielectric exclusion (DSPM-DE)," *Chemical Engineering Journal*, vol. 493, p. 152775, Aug. 2024, doi: 10.1016/j.cej.2024.152775.

[26] W. R. Bowen, A. W. Mohammad, and N. Hilal, "Characterisation of nanofiltration membranes for predictive purposes — use of salts, uncharged solutes and atomic force microscopy," *Journal of Membrane Science*, vol. 126, no. 1, pp. 91–105, Apr. 1997, doi: 10.1016/S0376-7388(96)00276-1.

[27] Y. Kiso, K. Muroshige, T. Oguchi, M. Hirose, T. Ohara, and T. Shintani, "Pore radius estimation based on organic solute molecular shape and effects of pressure on pore radius for a reverse osmosis membrane," *Journal of Membrane Science*, vol. 369, no. 1, pp. 290–298, Mar. 2011, doi: 10.1016/j.memsci.2010.12.005.

[28] O. Labban, C. Liu, T. H. Chong, and J. H. Lienhard V, "Fundamentals of low-pressure nanofiltration: Membrane characterization, modeling, and understanding the multi-ionic interactions in water softening," *Journal of Membrane Science*, vol. 521, pp. 18–32, Jan. 2017, doi: 10.1016/j.memsci.2016.08.062.

[29] S. Singh, K. C. Khulbe, T. Matsuura, and P. Ramamurthy, "Membrane characterization by solute transport and atomic force microscopy," *Journal of Membrane Science*, vol. 142, no. 1, pp. 111–127, Feb. 1998, doi: 10.1016/S0376-7388(97)00329-3.

[30] I. Noda, T. Tsuge, and M. Nagasawa, "The intrinsic viscosity of polyelectrolytes," *J. Phys. Chem.*, vol. 74, no. 4, pp. 710–719, Feb. 1970, doi: 10.1021/j100699a005.

[31] H. Zhang *et al.*, "Improving Ion Rejection of Conductive Nanofiltration Membrane

through Electrically Enhanced Surface Charge Density," *Environ. Sci. Technol.*, vol. 53, no. 2, pp. 868–877, Jan. 2019, doi: 10.1021/acs.est.8b04268.

[32] C. Labbez *et al.*, "A comparison of membrane charge of a low nanofiltration ceramic membrane determined from ionic retention and tangential streaming potential measurements," *Desalination*, vol. 147, no. 1, pp. 223–229, Sep. 2002, doi: 10.1016/S0011-9164(02)00539-8.

[33] A. Allagui, H. Benaoum, and O. Olendski, "On the Gouy–Chapman–Stern model of the electrical double-layer structure with a generalized Boltzmann factor," *Physica A: Statistical Mechanics and its Applications*, vol. 582, p. 126252, Nov. 2021, doi: 10.1016/j.physa.2021.126252.

[34] E. W. Weisstein, "Gill's Method." Accessed: Aug. 06, 2024. [Online]. Available: https://mathworld.wolfram.com/

Chapter 8. Conclusions

In this project, the process of protein separation using PAMAM dendrimer modified PVDF membranes was systematically studied. By selecting different KOH alkaline solutions, PAMAM was immobilized either on the surface of the PVDF membrane (treated with aqueous KOH) or simultaneously on both the surface and inside the pores of the PVDF membrane (treated with isopropanol KOH solution). The effects of different alkaline treatments on the surface properties of PVDF membranes and the filtration of whey protein or casein were also systematically investigated. Additionally, the DSPM-DE model was used to analyze the separation processes of PVDF membranes and PAMAM dendrimer-modified membranes.

At a feed pH of 10, alkaline treatment (isopropanol KOH solution) significantly increased the rejection of casein, and whey protein, without significantly altering membrane permeability. Under these conditions, the PVDF membrane showed a rejection of 76.4% for casein and 69.4% for whey protein, with permeate fluxes of 17.3 LMH and 17.7 LMH, respectively. After treatment with the alkaline solution at 60°C (Alk60 membrane from Chapter 3), the rejection for casein and whey protein increased to 88.5% and 80.4%, respectively, while the permeate fluxes remained largely unchanged at 17.5 LMH and 18.4 LMH.

The study on PAMAM dendrimer-modified PVDF membranes revealed that immobilizing PAMAM on both the surface and inside the pores of PVDF membranes significantly enhanced the rejection of whey protein but also notably reduced the permeate flux. After immobilizing generation 3 PAMAM dendrimer, with carboxyl functional groups, (G3PA membrane from Chapter 5), the rejection for whey protein increased from 58.9% (PVDF membrane) to 98.8%, while the permeate flux significantly decreased from 15.3 LMH

(PVDF membrane) to 2.3 LMH.

When PAMAM dendrimer was immobilized only on the surface of the PVDF membrane, the rejection for whey protein was moderately increased (whey protein rejection is less than when immobilized both on the surface and inside the pores), but due to the significant increase in surface porosity during alkaline treatment, the permeate flux of the membrane not only did not decrease but increased. After immobilizing generation 3 PAMAM dendrimer (with carboxyl functional groups) (G3PA membrane from Chapter 6), the rejection and permeate flux for whey protein increased to 79.0% and 30.3 LMH, respectively.

Analysis of PVDF membranes and modified membranes using the DSPM-DE model revealed that immobilizing PAMAM dendrimer on both the surface and inside the pores (overall modification) reduces pore size, while immobilizing PAMAM dendrimer only on the surface (surface modification) increases pore size. The surface charge density of the membranes increased significantly after modification. However, due to changes in pore size during modification, the volume charge density of the overall modified membranes is significantly higher than that of the surface-modified membranes, resulting in stronger Donnan potentials for the overall modified membranes.

Overall modification, which involves modifying both the membrane surface and interior, leads to decreased pore size and increased Donnan potential, significantly enhancing whey protein rejection. However, the reduced pore size also causes a significant decrease in permeate flux. In contrast, surface modification increases pore size and generates a negative Donnan potential, resulting in higher whey protein rejection and permeate flux. Nevertheless, due to the larger pore size, weaker Donnan potential, and absence of charges within the pores (leading to weaker dielectric exclusion), the whey protein rejection of

surface-modified membranes is lower than that of membranes modified both on the surface and interior.

For future research, the following are recommended:

1. Conduct protein separation tests using commercial PVDF membranes with surface PAMAM grafting. Previously, we applied bulk PAMAM grafting on commercial membranes but encountered issues: commercial PVDF UF membranes consist of a thin PVDF layer and a supporting layer of another polymer, which degraded during alkaline isopropanol treatment. This degradation produced suspended particles that blocked membrane pores, reducing both flux and mechanical strength. Surface-only PAMAM grafting on commercial PVDF membranes can avoid these issues. Additionally, commercial membranes generally offer good uniformity, stable pore size distribution, and high permeability. Thus, PAMAM surface-grafted membranes are expected to achieve higher permeate flux while maintaining similar rejection rates.

2. Conduct protein separation tests on commercial PVDF membranes with different pore sizes or MWCO after PAMAM surface grafting to identify the optimal pore size for effective protein separation.

3. Test the long-term stability of surface PAMAM-grafted membranes through extended filtration and backwashing to determine if PAMAM or other organic molecules are released over time.

4. Assess the crossflow filtration performance of surface PAMAM-grafted membranes for protein separation, focusing on protein rejection, permeate flux, and anti-fouling properties.

5. Use PEO molecules with different molecular weights in filtration tests to refine pore size

analysis using the DSPM-DE model. By combining SEM-measured pore size distribution data, incorporate the effects of membrane pore size distribution in the steric exclusion analysis within DSPM-DE.

6. Conduct PAA filtration under various feed pH levels. Altering the pH changes the charge intensities of PAA and the membrane, enabling analysis of how charge variations affect separation performance.

7. In DSPM-DE analysis, consider using the zeta potential of PAA in place of valency, as zeta potential may better reflect the charge characteristics of the solute.

8. In DSPM-DE analysis, measure the dielectric properties of the membranes and consider the dielectric effect during calculation. In this research, the effect of dielectric exclusion was ignored, to simplify the calculation. However, when calculating the pore size of the membrane through the filtration data of PEO, it was found that the dielectric effect inside the membrane pores has an impact on the rejection of the solute. It is important to consider the effect of dielectric interactions.

9. Systematically study intraporous modification of PVDF and other hydrophobic membranes using alkaline/alcohol/water ternaries while avoiding phase separation.